N/0002653--031-REV. 1

Response to External Peer Review Team Report for Corrective Action Unit 97: Yucca Flat/Climax Mine, Nevada National Security Site, Nye County, Nevada

Revision No.: 1

December 2016

UNCLASSIFIED

/s/ Joseph P. Johnston 12/08/2016
Joseph P. Johnston, Navarro CO Date

Prepared for U.S. Department of Energy under Contract No. DE-NA0002653.

Approved for public release; further dissemination unlimited.

Available for sale to the public from:

U.S. Department of Commerce
National Technical Information Service
5301 Shawnee Road
Alexandria, VA 22312
Telephone: 800.553.6847
Fax: 703.605.6900
E-mail: *orders@ntis.gov*
Online Ordering: *http://www.ntis.gov/help/ordermethods.aspx*

Available electronically at *http://www.osti.gov/bridge*

Available for a processing fee to U.S. Department of Energy and its contractors, in paper, from:

U.S. Department of Energy
Office of Scientific and Technical Information
P.O. Box 62
Oak Ridge, TN 37831-0062
Phone: 865.576.8401
Fax: 865.576.5728
Email: *reports@adonis.osti.gov*

Reference herein to any specific commercial product, process, or service by trade name, trademark, manufacturer, or otherwise, does not necessarily constitute or imply its endorsement, recommendation, or favoring by the United States Government or any agency thereof or its contractors or subcontractors.

Printed on recycled paper

N/0002653--031-REV. 1

RESPONSE TO EXTERNAL PEER REVIEW TEAM REPORT FOR CORRECTIVE ACTION UNIT 97: YUCCA FLAT/CLIMAX MINE, NEVADA NATIONAL SECURITY SITE, NYE COUNTY, NEVADA

Revision No.: 1
December 2016
Navarro
c/o U.S. DOE
P.O. Box 98952
Las Vegas, NV 89193-8952

Prepared for U.S. Department of Energy under Contract No. DE-NA0002653.

Approved for public release; further dissemination unlimited.

RESPONSE TO EXTERNAL PEER REVIEW TEAM REPORT FOR CORRECTIVE ACTION UNIT 97: YUCCA FLAT/CLIMAX MINE, NEVADA NATIONAL SECURITY SITE, NYE COUNTY, NEVADA

Approved by: /s/ Kenneth Rehfeldt Date: 12/08/2016

Kenneth Rehfeldt, UGTA Project Manager
Navarro

TABLE OF CONTENTS

List of Figures . . . iv
List of Tables . . . x
List of Acronyms and Abbreviations . . . xi
Executive Summary . . . ES-1

1.0 Introduction . . . 1-1

1.1 Approach to Addressing PRC Comments . . . 1-2

2.0 Key Uncertainties . . . 2-1

2.01 Review and Conservative Nature of the LCA Base-Case Model . . . 2-2
2.1 Uncertainty in Model Domain/Boundary Conditions . . . 2-6
2.1.1 Western Boundary . . . 2-6
2.1.2 Southern Boundary . . . 2-13
2.1.3 Northern Boundary . . . 2-15
2.1.4 Water Table Boundary and AA/VA Flow Direction . . . 2-23
2.1.5 Hydraulic Connection between Aquifers . . . 2-26
2.2 Model Calibration . . . 2-30
2.2.1 Poorly Posed Calibration . . . 2-30
2.2.2 Lack of Steady-State Head Data . . . 2-32
2.2.3 Use of Parameter Bounds . . . 2-40
2.2.4 Omission of Available Calibration Data . . . 2-43
2.2.5 Using the Jacobian to Determine Weights for Targets . . . 2-44
2.2.6 Field Measurements of Hydraulic Conductivity Not Honored in the Calibrated Model . . . 2-49
2.3 Uncertainty in Hydraulic Properties and Pathways . . . 2-53
2.3.1 Country Rock . . . 2-53
2.3.1.1 Limited Characterization of Aquifer Properties . . . 2-53
2.3.1.2 Model Permeabilities Inconsistent with Field Measurements . . . 2-55
2.3.1.3 Preferential Flow . . . 2-64
2.3.2 Faults . . . 2-66
2.3.3 Tuff Confining Unit . . . 2-73
2.3.4 Effective Porosity . . . 2-76
2.3.5 Potential for Flow of Surface Water into Fractures in the Alluvium . . . 2-77
2.3.6 Anisotropy and Preferential Flow in the Unsaturated Zone . . . 2-81
2.4 Source Term and Mass Flux to the LCA . . . 2-82
2.4.1 No Uncertainty Associated with the RST . . . 2-82
2.4.2 Uncertainties in Partition Factors Are Not Well Defined Particularly for Cavities in Carbonate Rock . . . 2-83
2.4.3 Water Flow into Cavities . . . 2-84
2.4.4 Uncertainty in the Exchange Volume Not Fully Captured . . . 2-86
2.4.5 Possible Chimney and Cavity Pathway to the LCA . . . 2-89
2.5 Transport . . . 2-97

TABLE OF CONTENTS (CONTINUED)

2.5.1 Values Used for Pu Retardation Are Not Well Supported and May Be Too High 2-97
2.5.2 Melt-Glass Dissolution Is Largely Neglected 2-103
2.6 Simulating Critical Observations 2-104
2.6.1 Field Measured ^{3}H Concentrations Are Not Simulated by the N-I (2013a) Model. 2-104
2.6.2 Crater-Infiltration Data Are Not Well Matched in the Model 2-110
2.6.3 Geochemical and Environmental Isotopes Not Fully Evaluated . . . 2-113
2.6.4 Interpretation of Temperature Data 2-121
2.6.5 Realistic Geologic Features 2-122
2.6.6 Other Sources of Data Are Available but Unused 2-123
2.7 Uncertainty Assessment 2-124
2.7.1 Current Evaluation Does Not Capture the 95th Percentile. 2-124
2.7.2 Expected Alternative Flow Models Were Not Included 2-127
2.7.3 Limited Number (100) of NSMC Realizations of the Flow Model Produced Parameter Value Combinations That Do Not Capture the 95th Percentile of Parameter Combinations That Lead to Rapid Transport 2-130
2.7.4 Limited Calibrated Flow Models Used to Evaluate Transport Uncertainty. 2-131
2.7.5 Limited Alternative Models Used to Evaluate Relevant Detonations 2-137
2.7.6 Limited Range of Transport Parameters Values Used to Evaluate Transport Uncertainty 2-140
2.7.7 Mesh Refinement Not Necessarily Conservative. 2-141
2.8 Unforeseen Uncertainties and the Need for Extended Peer Review. 2-146
2.8.1 New Concerns and Approaches Will Likely Arise 2-146
2.8.2 Climate Change 2-148
2.9 Location of Radionuclide Plumes—Recommendations for Monitor Wells and Testing/Sampling Programs during the CADD/CAP Stage 2-149
2.9.1 The Extent of Contamination Is Poorly Defined at Present 2-149
2.9.2 The Existing Observation Well Network Is Inadequate. 2-150

3.0 Comment Response Summary 3-1

4.0 References. 4-1

Appendix A - Additional Model Simulations of the AA/VA System To Evaluate the Effects of Alternative Parameter Sets and Conceptual Models on RN Transport to the LCA

A.1.0 Additional Model Simulations of the AA/VA System To Evaluate the Effects of Alternative Parameter Sets and Conceptual Models on RN Transport to the LCA A-1

A.2.0 References. A-17

TABLE OF CONTENTS (CONTINUED)

Appendix B - Analysis of Low-Level ^{3}H Observations and Possible Sources

B.1.0 Analysis of Low-Level ^{3}H Observations and Possible Sources B-1

B.1.1 TW-B B-1
B.1.2 WW-A. B-3
B.1.2.1 Hydraulic and Contaminant Data B-3
B.1.2.2 WW-A Model Calibration B-6
B.1.2.3 WW-A Model Domain B-7
B.1.2.4 3-D Transport Simulation with Particle Tracking B-8
B.1.3 WW-3 . . . . . B-11
B.1.3.1 WW-3 Pumping History and Water Levels B-12
B.1.3.2 WW-3 Pond B-13
B.1.3.3 ^{3}H Measurements at WW-3 . . . . . B-14
B.1.3.4 WW-3 Pond Model. B-20
B.1.3.5 WW-3 Pond Model Results B-21
B.1.4 UE-6d B-24
B.1.5 UE-6e B-27

B.2.0 References. B-29

LIST OF FIGURES

NUMBER	TITLE	PAGE
2-1	Point Locations and Calibrated Head Field at -1,000 m amsl and Steady-State Head Residuals for the Gridded Contour Model Calibration	2-9
2-2	Breakthrough Plots for LCA Flow Fields Investigating Western Boundary Uncertainty	2-11
2-3	Particle Travel Paths and Times for the Base-Case (upper left), 47 kg/s Northwest Recharge (upper right), and Gridded Contour-Point (center) Flow Fields	2-12
2-4	Time-Cumulative Probability of MCL Exceedance at 1,000 Years for the Transmissivity-Width Product Flux Constraint (left) and Total Influx Constraint (right) Flow Fields	2-14
2-5	95th Percentile Contaminant Boundary Ensemble at 50 Years	2-16
2-6	Transmissivity-Width Product Location and Simulated Transmissivity	2-18
2-7	Definition of Boundaries for the Yucca Flat LCA Model	2-20
2-8	Northern Flux vs. Particle Breakthrough for the NSMC Cases	2-22
2-9	Particle Travel Paths and Times for the Base-Case (left) and 1 kg/s (right) Flow Fields at 200 Years	2-23
2-10	Particle Locations for All SZ AA/VA Tests Colored (left) by the Number of Years since the Start of the Simulation (1961) and (right) by HSU	2-25
2-11	Particle Paths for All SZ AA/VA Tests That Have Particles That Reach the LCA Colored (left) by Years since the Start of the Simulation (1961) and (right) by HSU	2-26
2-12	SZ AA/VA Tests Categorized by Whether or Not Some Particles Reach the SZ LCA	2-27
2-13	Pre-development Hydraulic Head Contours and Flow Vectors in the Shallow AA/VA	2-28
2-14	Pre-development Heads in the SZ AA/VA Flow and Transport Model at a 500-m Elevation (left) and along the Lower Model Boundary (right)	2-29
2-15	Potentiometric Surface for the Base-Case (left) and Additional TCU/LCA Calibration Wells (right)	2-33

LIST OF FIGURES (CONTINUED)

NUMBER	TITLE	PAGE
2-16	Particle Travel Paths and Times for the Base-Case (left) and Additional Volcanic Confining Unit/Carbonate Aquifer Calibration Wells (right) Flow Fields	2-34
2-17	Breakthrough Plots for Base-Case and Additional TCU/LCA Calibration Wells Flow Fields	2-35
2-18	Simplified Hydrographs for Wells ER-6-1-2 and TW-D	2-37
2-19	Breakthrough Plots for LCA Flow Fields Investigating Alternative Interpretations of the LCA Pre-development Water Levels	2-39
2-20	Particle Breakthrough for the Base Case and the Case Considering Data Quality in the Steady-State Target Weights	2-48
2-21	Particle Travel Paths and Times for the Base-Case (left) and Expanded Parameter Range (right) Flow Fields	2-51
2-22	Particle Breakthroughs for the Base-Case and Calibration with Expanded Parameter Range Flow Fields	2-52
2-23	Comparison of Calibrated Base-Case Parameters for the LCA Model (N-I, 2013a, Table 5-11) with Pumping Scale Hydraulic Conductivity Measurements from Yucca Flat (SNJV, 2006b, Figure 6-19)	2-56
2-24	Faults Included in the Yucca Flat LCA Flow and Transport Model	2-57
2-25	Spatial Distribution of Pumping-Scale Hydraulic Conductivity Values for the LCA	2-59
2-26	LCA Model North–South Rezonation	2-60
2-27	Particle Travel Paths and Times for the Base-Case (upper left), North–South Subzones (upper right), and North–South Subzones with Specified Permeability (bottom) Flow Fields	2-63
2-28	Breakthrough Plots for Base-Case and Country Rock Subzones Flow Fields	2-64
2-29	Potentiometric Surface for the Base-Case (left) and the Case Including Only the Large Basin-Forming Faults (right)	2-73
2-30	Particle Travel Paths and Times for the Base-Case (upper left), Faults without Low-Permeability Cores (upper right), No Faults with Traces <3 km (lower left), and No Minor Faults (lower right) Flow Fields	2-74

LIST OF FIGURES (CONTINUED)

NUMBER	TITLE	PAGE
2-31	Breakthrough Plots for Base Case, Calibration without Low-Permeability Fault Cores, without Faults with Traces <3 km, and without Minor Faults	2-75
2-32	Cumulative Mass of ^{14}C Transported to the LCA for Alternative AA/VA System Models	2-77
2-33	Carpetbag Fault Scarp on June 18, 2014 (left); and on August 14, 2014, 10 days after the August 4, 2014, 100-Year Storm Event	2-79
2-34	Ponded Water in the U3fd (LAGUNA) (top) and U3kp (SEAMOUNT) (bottom) Craters on August 14, 2014, 10 Days after the August 4, 2014, Storm Event	2-80
2-35	Different Zones of Damage Produced by a Nuclear Explosion in Rock	2-87
2-36	Simulated Changes to the Permeability Field near the BILBY Detonation for the Breaching Scenario: (left) before the BILBY Detonation and (right) after the BILBY Detonation	2-90
2-37	Permeability Fields at the Bottom (left) and Top (right) of the TCU after the End of Testing (1992)	2-91
2-38	Location of Boundary "Breaches" (circles) (left) and the Volumes (right) around Tests Where Testing Effects Significantly Increased the Permeability	2-92
2-39	Close-up of Faults and Breaches (left) and Zones of Permeability Enhancement (right) in the North–Central Part of the SZ AA/VA Model	2-92
2-40	Location of the LCA Satellite Well (U-3cn 5) and the Post-Shot Well (U-3cn PS 2) Relative to the 2 R_c Exchange Volume of BILBY	2-93
2-41	Hydrographs of Hydraulic Head in the TCU at U-3cn PS 2 (top) and in the LCA at U-3cn 5 (bottom)	2-94
2-42	Well U-3cn PS 2 Raw RN Data (top) and ^{3}H Data Adjusted to the Time of Detonation (bottom)	2-95
2-43	Time-Cumulative (top) and 800-Year (bottom) Probability of MCL Exceedance for Base-Case (left) and Alternative Pu Sorption Case (right)	2-102
2-44	Pu Fractional Exceedance Volume for Base-Case and Alternate K_d Case	2-103
2-45	Monthly and Yearly Precipitation Record from the BJY Precipitation Station in Yucca Flat (top) and the Rolling 5-Year Average Annual Precipitation (bottom)	2-111

LIST OF FIGURES (CONTINUED)

NUMBER	TITLE	PAGE
2-46	Dolomite and Calcite Saturation Indices for Yucca Flat Area Groundwater (from SNJV, 2006a, Table 5-1) and Devils Hole	2-115
2-47	Relation between P_{CO2} and DIC for LCA Groundwater in and near Yucca Flat and at Devils Hole	2-117
2-48	Relationship between Mg^{2+} Concentration and Alkalinity (as HCO_3^-) in LCA Groundwater in and near Yucca Flat and at Devils Hole	2-119
2-49	Relation between Mg^{2+} Concentration and pH for LCA Groundwater in and near Yucca Flat and at Devils Hole	2-119
2-50	Particle Tracking Results Showing the Number of Particles Reaching the Southern Line of Demarcation for Simulations Based Upon the NSMC Flow Fields	2-126
2-51	Time-Cumulative Probability of MCL Exceedance for Base-Case (upper left), NSMC 1 Fast (upper right), NSMC 84 Fast (lower left), and Additional Steady-State Target Wells (lower right) Flow Fields	2-134
2-52	Time-Cumulative Probability of MCL Exceedance for North–South Subzones (upper left), 47 kg/s Northwest Recharge (upper right), Calibrated Northwest (lower left), and Quality Weighted Steady-State Targets (lower right) Flow Fields	2-135
2-53	Time-Cumulative Probability of MCL Exceedance for Faults without Low-Permeability Cores (upper left), No Faults with Trace Lengths <3 km (upper right), and No Minor Faults (lower center) Flow Fields	2-136
2-54	Time-Cumulative Probability of MCL Exceedance for Base-Case (upper left), Increased Longitudinal Dispersivity (upper right), and Increased Dispersivity for All Components (lower center) Flow Fields	2-142
2-55	Calibrated Parameters for the Base-Case Level 2 and Level 3 Meshes	2-144
2-56	Calibrated Head Field in the LCA for the Base-Case Level 2 (left) and Level 3 (right) Meshes	2-145
2-57	Particle Travel Paths and Times for the Base-Case Level 2 (left) and Level 3 (right) Meshes	2-146
2-58	Percentage of Particle Breakthrough in 1,000 Years near the Model's Southern Boundary for the 30 Detonations within 3 R_c of the SZ LCA	2-147

LIST OF FIGURES (CONTINUED)

NUMBER	TITLE	PAGE
2-59	Base-Case Breakthrough for the Level 2 and 3 Meshes	2-147
A-1a	Scatterplots Showing Simulated versus Measured Heads along with the One-to-One Line and Calculated r^2 Values	A-3
A-1b	Scatterplots Showing Simulated versus Measured Heads along with the One-to-One Line and Calculated r^2 Values	A-4
A-1c	Scatterplots Showing Simulated versus Measured Heads along with the One-to-One Line and Calculated r^2 Values	A-5
A-2a	Histograms of Error (measured minus simulated heads, in meters) for 24 Simulations	A-6
A-2b	Histograms of Error (measured minus simulated heads, in meters) for 24 Simulations	A-7
A-2c	Histograms of Error (measured minus simulated heads, in meters) for 24 Simulations	A-8
A-3a	Simulated (blue circles) and Measured (black circles) Hydraulic Heads through Time at Well TW-7	A-9
A-3b	Simulated (blue circles) and Measured (black circles) Hydraulic Heads through Time at Well TW-7	A-10
A-3c	Simulated (blue circles) and Measured (black circles) Hydraulic Heads through Time at Well TW-7	A-11
A-3d	Simulated (blue circles) and Measured (black circles) Hydraulic Heads through Time at Well TW-7	A-12
A-4	Plot Showing the Fraction of Particles Reaching the LCA from SZ Sources (solid circles) and UZ Sources (open circles) as a Function of the Calibration Correlation Coefficient	A-14
A-5	Spatial Plot of Head Residuals (measured minus simulated) as a Function of Time for Model Run SET3_7 (r^2 = 0.97)	A-16
B-1	^{3}H Measurements at TW-B Relative to the PRESIDIO Detonation	B-2
B-2	Estimated Annual Water Withdrawals from WW-A in Gallons (from Elliott and Moreo, 2011)	B-4

LIST OF FIGURES (CONTINUED)

NUMBER	TITLE	PAGE
B-3	Measured Water Levels at WW-A in Meters Above Mean Sea Level	B-4
B-4	Measured ^{3}H Concentrations at WW-A	B-6
B-5	Relation between the Cap of a Sphere and a Disk of an Equivalent Volume	B-8
B-6	Simulated Particle Breakthrough Curves at the Pumping Well (WW-A) as a Function of Elapsed Time since the HAYMAKER Detonation (June 27, 1962)	B-10
B-7	Annual Water Withdrawals from WW-3 between 1952 and 1970 (from Elliott and Moreo, 2011)	B-11
B-8	Water-Level Changes at WW-3	B-12
B-9	Elliptical Pond Near WW-3 That Was Used for Water Supply	B-13
B-10	Schematic of the Model Domain Showing Locations of Interest WW-3 and UE-6d	B-20
B-11	Model Results of the Water Pressure at WW-3 for Scenarios 1 (a) and 2 (b)	B-22
B-12	Simulated Migration of the Wetting Front ($\theta = 1$) for Scenarios 1 (a) and 2 (b)	B-23
B-13	Simulated Migration of ^{3}H to WW-3 for Scenario 1 (left) and Scenario 2 (right)	B-24
B-14	Water-Level Changes at Well UE-6d	B-25
B-15	Location of Nearby Nuclear Detonations to Wells UE-6d and WW-3	B-27

LIST OF TABLES

NUMBER	TITLE	PAGE
ES-1	Responses to YF/CM PRC Comments	ES-3
2-1	Summary of Simulations Investigating Western Boundary Uncertainty	2-10
2-2	Summary of Simulations Investigating Alternative Interpretations of the LCA Pre-development Water-Levels Uncertainty	2-38
2-3	Water-Level Uncertainty for LCA Model Steady-State Calibration Targets	2-46
2-4	LCA Model Country Rock Permeability Bounds Estimated from Pumping Test Scale Measurements and Calibrated Values	2-51
2-5	Geometric Average Permeability of Pumping Test Data Located within LCA Model Subzones	2-61
2-6	Summary of Simulations Investigating Country Rock Permeability and Zonation Uncertainty	2-62
2-7	Summary of Simulations Investigating Alternative Fault Conceptualizations	2-67
2-8	Pu Concentration Observations at Locations within or near the SZ LCA	2-99
2-9	Example Initial Cavity Concentration for Pu	2-101
2-10	Carbonate Rock Matrix K_d and Fracture R_d Distributions for Pu	2-101
2-11	Groundwater ^{3}H Data Measured since the PRC Initiation	2-108
2-12	Model Parameters Most Strongly Correlated with Particle Breakthrough	2-139
2-13	Recommended Non-exhaustive List of Testing and Sampling Programs To Better Characterize Key Pathways That Control the Contaminant Boundary	2-152
B-1	Parameter Values Used in Particle Tracking Simulations for WW-A	B-9
B-2	^{3}H Measurements at WW-3	B-14
B-3	^{3}H Measurements at WW-C-1	B-15
B-4	^{3}H Measurements at UE-6d	B-26
B-5	^{3}H Measurements from UE-6e	B-28

LIST OF ACRONYMS AND ABBREVIATIONS

General Acronyms and Abbreviations

2-D	Two dimensional
3-D	Three dimensional
acre-ft/yr	Acre feet per year
amsl	Above mean sea level
asl	Above sea level
atm	Atmosphere
bgs	Below ground surface
BJY	Buster Jangle
CADD	Corrective action decision document
CAI	Corrective action investigation
CAP	Corrective action plan
CAU	Corrective action unit
CDF	Cumulative distribution function
CR	Closure report
DL	Detection limit
DoD	U.S. Department of Defense
DOE	U.S. Department of Energy
DVRFS	Death Valley Regional Flow System
ECDF	Empirical cumulative distribution function
EOI	Effective open interval
FEHM	Finite Element Heat and Mass Transfer
FFACO	*Federal Facility Agreement and Consent Order*
ft	Foot
ft/day	Feet per day
ft^3/day	Cubic feet per day
FY	Fiscal year
g/cm^3	Grams per cubic centimeter
gpm	Gallons per minute
HFM	Hydrostratigraphic framework model
HST	Hydrologic source term

LIST OF ACRONYMS AND ABBREVIATIONS (CONTINUED)

HSU	Hydrostratigraphic unit
IAEA	International Atomic Energy Agency
InSAR	Interferometric Synthetic Aperture Radar
K	Hydraulic conductivity
k	Permeability
ka	Thousand years
K_d	Distribution coefficient
kg/s	Kilograms per second
km	Kilometer
km^2	Square kilometer
km/yr	Kilometers per year
K-S	Kolmogorov-Smirnov
kt	Kiloton
LANL	Los Alamos National Laboratory
LLNL	Lawrence Livermore National Laboratory
m	Meter
m^2	Square meter
m/day	Meters per day
m/yr	Meters per year
Ma	Million years ago
MCL	Maximum contaminant level
MDL	Minimum detection limit
Mgal	Million gallon
mg/L	Milligrams per liter
mi	Mile
mL/g	Milliliters per gram
mm	Millimeter
mm/yr	Millimeters per year
MPa	Megapascal
MWAT	Multiple-well aquifer test
NA	Not available
NAD	North American Datum

LIST OF ACRONYMS AND ABBREVIATIONS (CONTINUED)

NDEP	Nevada Division of Environmental Protection
N-I	Navarro-Intera, LLC
NNSA/NFO	U.S. Department of Energy, National Nuclear Security Administration Nevada Field Office
NNSS	Nevada National Security Site
NSMC	Null Space Monte Carlo
OTA	Office of Technology Assessment
Pa	Pascal
pCi/L	Picocuries per liter
P_{CO2}	Partial pressure of carbon dioxide
PRC	Peer Review Committee
r^2	Coefficient of determination
R_c	Cavity radius
R_d	Retardation factor
RMS	Root mean square
RN	Radionuclide
RST	Radiological source term
SAE	Supplemental analysis and evaluation
SDWA	*Safe Drinking Water Act*
SNJV	Stoller-Navarro Joint Venture
SZ	Saturated zone
TD	Total depth
UGTA	Underground Test Area
UR	Use restriction
USGS	U.S. Geological Survey
UTM	Universal Transverse Mercator
UZ	Unsaturated zone
WL	Water level
YF/CM	Yucca Flat/Climax Mine
°C	Degrees Celsius

LIST OF ACRONYMS AND ABBREVIATIONS (CONTINUED)

Stratigraphic, Geologic, Hydrostratigraphic, and Hydrogeologic Unit Abbreviations and Symbols

AA	Alluvial aquifer
AA/VA	Alluvial aquifer/volcanic aquifer
ATCU	Argillic tuff confining unit
LCA	Lower carbonate aquifer
LCA3	Lower carbonate aquifer thrust plate
LTCU	Lower tuff confining unit
OSBCU	Oak Spring Butte confining unit
TCU	Tuff confining unit
TM-LVTA	Timber Mountain lower vitric-tuff aquifer
TSA	Topopah Spring aquifer
UCCU	Upper clastic confining unit
VA	Volcanic aquifer

LIST OF ACRONYMS AND ABBREVIATIONS (CONTINUED)

Symbols for Elements and Compounds

C	Carbon
Ca	Calcium
$CaCO_3$	Calcite
$CaMg(CO_3)_2$	Dolomite
Cl	Chlorine
CO_2	Carbon dioxide
CO_3	Carbonate
Cs	Cesium
DIC	Dissolved inorganic carbon
H	Hydrogen
^3H	Tritium
H_2O	Water
HCO_3	Bicarbonate
I	Iodine
Mg	Magnesium
Ni	Nickel
Np	Neptunium
O	Oxygen
OH^-	Hydroxide
Pu	Plutonium
Sr	Strontium
Tc	Technetium
U	Uranium
$\delta^{13}C$	Delta carbon-13

EXECUTIVE SUMMARY

The Underground Test Area (UGTA) Corrective Action Unit (CAU) 97, Yucca Flat/Climax Mine (YF/CM), in the northeast part of the Nevada National Security Site (NNSS) requires environmental corrective action activities to assess contamination resulting from underground nuclear testing. These activities are necessary to comply with the UGTA corrective action strategy defined in Appendix VI, Revision No. 4, of the *Federal Facility Agreement and Consent Order* (FFACO) (1996, as amended). The *Phase I Flow and Transport Model Document for Corrective Action Unit 97: Yucca Flat/Climax Mine, Nevada National Security Site, Nye County, Nevada* (N-I, 2013a) was developed and subjected to an external peer review as required by the corrective action investigation (CAI) stage of the UGTA strategy. The YF/CM Peer Review Committee (PRC) raised a number of questions and provided recommendations for supplemental analyses (in the *External Peer Review Team Report for Corrective Action Unit 97: Yucca Flat/Climax Mine, Nevada National Security Site, Nye County, Nevada* [N-I, 2015]).

The purpose of this document is to provide responses to the PRC recommendations addressing the uncertainties identified by the PRC so that sufficient confidence in the contaminant boundary forecasts is established to advance to the Corrective Action Decision Document (CADD)/Corrective Action Plan (CAP) stage and initiate model evaluations. The PRC summarized their concerns and recommendations, and presented discussions of each of these uncertainties in their report (N-I, 2015). The U.S. Department of Energy (DOE), National Nuclear Security Administration Nevada Field Office (NNSA/NFO) responses are summarized in Table ES-1.

In the process of responding to the comments and recommendations, the YF/CM modeling team reanalyzed existing data and models, ran new models recommended by the PRC, drilled three new wells (ER-2-2, ER-3-3, and ER-4-1), and sampled additional wells. The new wells were drilled near deeply buried, large-yield detonations (ER-2-2 and ER-4-1) or near faults (ER-2-2 and ER-3-3) to investigate the extent of contamination associated with tests near the lower carbonate aquifer (LCA) or faults. No new detections of elevated tritium (^{3}H) concentrations in the LCA were observed in the resampled wells or in the LCA during drilling of the three new wells, supporting the observation that ^{3}H contamination of the LCA is of limited areal extent and that simulations documented in the Phase I flow and transport model document (N-I, 2013a) adequately bound radionuclide (RN) transport.

The overall conclusion from this effort is that the original YF/CM flow and transport models documented in the Phase I flow and transport model document conservatively bounded the contaminant migration in YF/CM, and that the new models recommended by the PRC did not lead to the development of credible transport scenarios with different transport pathways or contamination over a larger spatial extent.

Table ES-1
Responses to YF/CM PRC Comments
(Page 1 of 27)

#	Recommendation	Focus of the Concern	Summary of Response
2.1.1 Western Boundary			
1	Expand the model domain to include Rainier Mesa and use head and perched spring data from that area for calibration.	This uncertainty focuses on the model prediction that flow direction in some areas of the western part of the system is northerly, which the PRC states is opposite to the direction presented in the conceptual model and opposite to the flow simulated by the regional model of the Death Valley Regional Flow System (DVRFS).	Model studies were conducted to show that recharge from Rainier Mesa does not influence the transport model results. The alternate model studies included (1) applying a fixed amount of flow from Rainier Mesa into northwestern Yucca Flat, (2) treating this flow as a calibration target, (3) penalizing the model for northward flow in this area, and (4) using as calibration targets pseudo-points based on the Fenelon et al. (2012) conceptual model. These simulations led to less-extensive transport results compared to the base-case model and further did not eliminate the northerly flow in the northwestern part of the model. Hence, there is no benefit in extending the western model domain or in using head and perched spring data from that area.
2.1.2 Southern Boundary			
2	Extend model domain to the south to capture contaminant boundaries that extend beyond the current model domain.	The concern under this uncertainty is that some simulations predict the southern extent of the contaminant boundary to fall beyond the model domain.	It is not necessary to extend the southern model boundary because simulations that reach the boundary are known to be conservative, and reduction of the contaminant boundary extent is anticipated during model evaluation (CADD/CAP) as the conservative models are either refined or removed from the ensemble. The contaminant boundaries associated with this model are known to be conservative for the following reasons: (1) recent estimates of the water flux through the high-permeability corridor are considerably less (~20 kilograms per second [kg/s]) than that estimated for the base-case model (~148 kg/s); (2) although contamination is forecasted, it is not observed in the LCA wells (e.g., U-3cn 5, ER-7-1, and UE-7nS) located in the high-permeability eastern corridor along pathways that impacted the southern boundary; (3) although ^{3}H above its *Safe Drinking Water Act* (SDWA) maximum contaminant level (MCL) (CFR, 2015) is forecasted, it is not observed above the minimum detection limit (MDL) (1,500 to 1,800 picocuries per liter [pCi/L]) in the LCA in the three new wells (ER-2-2, ER-3-3, and ER-4-1); and (4) carbon-14 (^{14}C) data suggest longer travel times. An example simulation using the 20 kg/s flux produced a contaminant boundary well north of the southern model boundary. Hence, the current southern boundary is sufficient.

Table ES-1
Responses to YF/CM PRC Comments
(Page 2 of 27)

#	Recommendation	Focus of the Concern	Summary of Response
2.1.3 Northern Boundary			
3	Investigate inflow from the north with multi-well aquifer testing and water sampling.	The concern under this uncertainty is that significant flow from the north is possible and could be an important factor in RN transport out of Yucca Flat.	Recent reanalysis of the ER-6-1 multiple-well aquifer test (MWAT) data (Halford, 2012 and 2016) and historically reported results (Winograd and Thordarson, 1975; Harrill et al., 1988) indicate that the current base-case model overestimates flow from the north. Alternate models with lower flux constraints reduce the northern flux significantly, leading to a reduction in the southern extent of the contaminant boundary. Hence, the current understanding of the northern boundary flux is sufficient and an MWAT in the north is unnecessary.
2.1.4 Water Table Boundary and AA/VA Flow Direction			
4	Contour simulated water levels in the AA/VA, compare with available data and include the resulting uncertainty in flux to the LCA in future modeling.	This concern is that it is difficult to determine the simulated groundwater flow direction in the shallow aquifer from the information presented, especially with regard to flow toward faults. Present-day flow directions can differ from those indicated by the pre-development hydraulic heads estimated in Fenelon et al. (2012) due to the effects of nuclear testing.	As requested, a contour map of simulated pre-testing hydraulic heads (with inferred flow directions) was developed and compared to pre-development heads and flow directions shown in Fenelon et al. (2012). The modeled heads differ from the Fenelon et al. (2012, Plate 3) pre-development heads and flow directions. The strongest hydraulic gradients in the alluvial aquifer/volcanic aquifer (AA/VA) flow system are downward to the LCA, which are not evident in map view. Flow directions depend on whether faults are assumed to be permeable. The saturated zone (SZ) AA/VA system model assumes faults are permeable through the tuff-confining unit (TCU) and, therefore, water and RNs enter the LCA at many places in the model. The Fenelon et al. (2012) conceptual model assumes that faults serve no hydrologic role other than to offset aquifers. In their conceptualization, groundwater and RNs from the alluvium and tuffs reach the LCA only where alluvial aquifers (AAs) and volcanic aquifers (VAs) are offset across faults. The SZ AA/VA model is based on a scenario more conducive for transport to the LCA and is therefore sufficient.

Table ES-1
Responses to YF/CM PRC Comments
(Page 3 of 27)

#	Recommendation	Focus of the Concern	Summary of Response
2.1.5 Hydraulic Connection between Aquifers			
5	Evaluate uncertainty in flux to the LCA associated with the inconsistency of the boundary between the LCA and AA/VA models. Couple the AA/VA and LCA models and use all the head data within the combined multi-aquifer system for calibration.	This uncertainty concerns the use of loose coupling between the AA/VA and the LCA models, and the possible resulting underestimation of recharge to the LCA model.	It is not necessary to couple the AA/VA and LCA models to develop a combined multi-aquifer system model. The modeling team does not agree with the premise of the comment that the SZ AA/VA and SZ LCA models are inconsistent. Consistency in heads between the SZ AA/VA system model and the SZ LCA model was enforced by applying steady-state heads from the LCA model to the base of the SZ AA/VA model along faults. Small increases in LCA heads that might have occurred due to testing induced overpressures in the tuffs contribute little uncertainty to the overall downward gradient dominated by the overpressures in the tuff and can be justifiably ignored, as demonstrated by sensitivity studies presented in Appendix I of N-I (2013), which examined the effect of ignoring hydraulic transients in the LCA due to testing in the shallower tuffs and alluvium. In conclusion, joint calibration of the AA/VA and LCA models (development of a combined multi-aquifer system model) is not necessary.
2.2.1 Poorly Posed Calibration			
6	Expand the model domain to couple the aquifer systems, extend the domain to the groundwater divide to the west, include more target data from the available dataset as well as through additional data collection, and simplify the parameterization.	This uncertainty focuses on the fact that the LCA model optimization is underconstrained with respect to the number of adjustable parameters in the model.	Extending the LCA model domain to include AA/VA is not necessary, because the number of parameters to be estimated and the number of observations used for parameter estimation remain unchanged whether the models are fully coupled or loosely coupled through their common boundary conditions. There is no advantage to a coupled model with extended LCA model domain to include AA/VA because of the greater structural complexity represented by a coupled model with extended LCA model domain to include AA/VA, the increased refinement needed for high-gradient zones, and the increased number of unknown parameters. In addition, the base-case model presented in N-I (2013) is more conservative with respect to transport forecasts than an alternate model that includes the additional wells recommended by the PRC (N-I, 2015, Section 6.2.1). The alternate case did not calibrate as well, and the added calibration targets led to a contaminant boundary more northerly than the N-I (2013) transport model. Therefore, no further action is needed to address this recommendation.

Table ES-1
Responses to YF/CM PRC Comments
(Page 4 of 27)

#	Recommendation	Focus of the Concern	Summary of Response
2.2.2 Lack of Steady-State Head Data			
7	Calibrate a coupled model of the aquifers, include more calibration targets, resurvey the well heads to ensure accuracy of the targets, and completely represent the data that were used to develop steady state targets in the residual analysis.	The focus of this uncertainty is that steady-state heads from different wells are not concurrent; they are sparse, affected by detonations, and many come from sections with long well screens.	There is no need to couple the SZ AA/VA and SZ LCA (see Responses #5 and #6). The current land surface accuracy for the Yucca Flat LCA wells is generally less than 1 foot (ft) and is much smaller than the hydraulic head changes across Yucca Flat that are ~50 ft (Fenelon et al., 2012). Alternative approaches to represent head data variability led to transport results that were not more extensive than those for the N-I (2013) transport models. The alternate models included (1) using mean water levels calculated by the U.S. Geological Survey (USGS), (2) using multiple steady-state targets to encompass temporal variability, (3) using pseudo-points to honor head contours reported in Fenelon et al. (2012), and (4) using weights based on data quality. Therefore, no further action is needed under this recommendation.
2.2.3 Use of Parameter Bounds			
8	Reduce the number of parameters through re-parameterization, remove bounds from the parameters, include more calibration targets, and adjust the model conceptualization and construction if the estimated parameter values are not reasonable.	This uncertainty addresses the concern that placing bounds on parameters during an estimation process can lead to models that are not realistic or that underpredict transport.	The conceptual flow model and parameter bounds documented in N-I (2013) were carefully determined and are consistent with available flow system information. The effects of reducing the number of adjustable parameters with respect to fault properties was explored (see Response #19). These model studies supplemented with current estimates of water flux (Halford, 2016) through Yucca Flat and RN data demonstrate that the base-case model (N-I, 2013) does not underpredict transport (see Response #2). Hence, it is not necessary to further address this recommendation.
2.2.4 Omission of Available Calibration Data			
9	Include as many calibration targets as possible (also use multiple targets at individual locations for the steady state calibration to incorporate the transient nature of the data into the steady state calibration uncertainty), include hydrogeologic features to facilitate a fit to those targets, and present residuals related to all of the measurements. Critically review all available calibration data.	The concern raised is that there are head measurements available from some wells that were not used in the LCA calibration.	Several alternate models were developed to evaluate this recommendation as follows: (1) including the additional wells recommended by the PRC, (2) using multiple targets at locations with transient water levels not associated with anthropogenic activities, and (3) assigning weights based on data quality. The alternate models did not lead to transport in excess of the base case. Hence, further addressing this recommendation is not necessary.

Table ES-1
Responses to YF/CM PRC Comments
(Page 5 of 27)

#	Recommendation	Focus of the Concern	Summary of Response
2.2.5 Using the Jacobian to Determine Weights for Targets			
10	Determine weights by evaluating the quality of the target data based on well construction and measurement procedures.	This uncertainty was focused on determining target weights from data quality rather than mathematical constructions.	The base-case model is more conservative than the alternate model using calibration weights. The modeling team performed a critical review of the LCA water-level data quality. The LCA model was recalibrated using the temperature corrected data and steady-state calibration weights that consider data quality. This alternate model achieved a poorer calibration and forecasted a contaminant boundary more northerly than the current base case. Hence, it is not necessary to further address this recommendation.
2.2.6 Field Measurements of Hydraulic Conductivity Not Honored in the Calibrated Model			
11	After estimating parameters without bounds, compare the values to equivalent field values; if they are unreasonable, adjust the model conceptualization and/or construction.	This uncertainty was motivated by the fact that estimated parameter values do not match all the field measurements.	The base-case model takes into account the available hydraulic conductivity data. Great care has been exercised in choosing the underlying conceptual flow model, and in setting bounds on parameters that are plausible and consistent with the available information. Small-scale hydraulic conductivity estimates are expected to display more variability than volume-averaged estimates needed on a larger scale. In response to PRC comments regarding spatial distribution of hydraulic conductivity measurements, an LCA model was recalibrated using rezonation of the SZ LCA, which divided the three north–south zones into northern and southern components. This model achieved poorer calibration than the base case and also forecasted less transport. The suggested alternatives have been adequately addressed, and model conceptualization and/or construction does not require adjustment.

Table ES-1
Responses to YF/CM PRC Comments
(Page 6 of 27)

#	Recommendation	Focus of the Concern	Summary of Response
2.3.1.1 Limited Characterization of Aquifer Properties			
12	Conduct MWATs in the central and western parts of Yucca Flat.	This uncertainty concerns the scale dependence of hydraulic conductivity measurements.	A model simulation was created that expanded bounds on country rock and fault permeability to encompass the measured values and allow larger values to be assigned during calibration. This model achieved poorer calibration than the base case and forecasted less transport. During the drilling of three new wells (ER-2-2, ER-3-3, and ER-4-1) within the central part of Yucca Flat, water levels in the neighboring wells that were instrumented did not show any responses to the drilling activities. Additionally, water pumping rates out of these wells have been below 100 gallons per minute (gpm). These observations support the conceptual model of permeabilities being lower at least in the neighborhood of each well. Because the LCA in the central and western parts of the basin did not respond to the 2004 ER-6-1-2 MWAT, calibrated permeabilities in this part of the basin were constrained solely by steady-state heads, which indicate west-to-east flow in this part of the basin. Consequently, the calibrated permeabilities reflect the lower west–east permeability across the faults and fractures, which have a dominant north–south orientation. Matching the observed hydraulic head data in the western and central portions of Yucca Flat required the model to select lower permeability values than those for the eastern portion. Further, majority of the source locations are not in these portions of the basin—if tests within 3 R_c of the top of LCA are considered, only 9 out of 39 locations lie within central and western Yucca Flat. Hence, refining parameter measurements for those portions of Yucca Flat will lead to relatively small gains in reducing the uncertainty in the contaminant forecasts.
2.3.1.2 Model Permeabilities Inconsistent with Field Measurements			
13	Use available hydraulic properties data to delineate permeability zones in the model. Honor the measured hydraulic conductivities. Reevaluate the choice of the “fast” scenario.	This uncertainty is focused on the apparent mismatch between the permeability values used in the model versus pumping-scale data.	Pumping tests tend to select the higher-permeability zones and do not necessarily represent large-scale averages. The alternate flow models considering a north–south subdivision of the country rock, and those with expanded permeability bounds, do not calibrate to the data as well as the base-case model, and forecast less southern extent for the contaminant boundary compared to the base case. The issue has been adequately addressed through additional modeling, and it is not necessary to modify the base-case model.

Table ES-1
Responses to YF/CM PRC Comments
(Page 7 of 27)

#	Recommendation	Focus of the Concern	Summary of Response
2.3.1.3 Preferential Flow			
14	Thoroughly evaluate existing data for indications of karst and install new wells to investigate for karst. If karst features cannot be ruled out, include alternative models that have continuous high hydraulic conductivity pathways from the northern to the southern end of Yucca Flat and passing through source zones.	This uncertainty addresses local-scale permeable pathways in the country rock.	Available subsurface and outcrop evidence, as well as hydrogeologic reasoning, indicates that extensive solution channels that could provide basin-scale transport pathways in Yucca Flat do not exist. Although karst features have been observed sporadically in boreholes (e.g., identified by a drop in the drill string while deepening Well UE-10j and later confirmed with video logs) and outcrops, karst features are relatively rare in the extensive limestone outcrops exposed in the surrounding mountain blocks, and an integrated set of saturated solution channels throughout the Yucca Flat basin is unlikely. Hence, karst is not believed to have created extensive permeable pathways in Yucca Flat, and further work suggested in this recommendation is not necessary.
2.3.2 Faults			
15	Extend the range of permeability considered for modeling faults well above the highest measured value and include alternative models without impermeable fault cores.	This uncertainty focuses on flow and transport through faults, and includes several sub-comments that are addressed in Responses #15 through #19.	Extrapolating small discrete measurements over an entire fault zone spanning a potentially 36-kilometer (km) feature is not realistic, and cannot be reconciled with the observed gradient and realistic flow rates through the LCA within Yucca Flat. Permeabilities from cross-hole response are more representative of large scale values and are used for bounding parameter distributions. An alternate model without low-permeability fault cores resulted in slightly greater transport to the southern boundary—12% of the cases considered in the probabilistic transport analysis using the alternate models reached the southern boundary of the model as compared to 10% for the base case. As discussed under Response #2, these models are known to be conservative, incorporating north–south fluxes far greater than the current estimates. Hence, it is not necessary to extend the range of permeabilities beyond the values already considered in the base-case model.
16	Assign increased permeability to the material that is currently simulated as country rocks near major faults in the analysis of uncertainty.	This uncertainty focuses on flow and transport through faults, and includes several sub-comments that are addressed in Responses #15 through #19.	This recommendation is implicitly included in the model. The grid spacing at the explicitly simulated faults in a direction perpendicular to the fault plane in the current model is 125 meters (m); thus, 125 m of country rock on each side of the fault center is included in the volume that is assigned damage zone properties. Hence, further work suggested in this recommendation is not necessary.

Table ES-1
Responses to YF/CM PRC Comments
(Page 8 of 27)

#	Recommendation	Focus of the Concern	Summary of Response
17	Explore greater fault permeability in the AA/VA model, and characterize AA/VA fault behavior.	This uncertainty focuses on flow and transport through faults, and includes several sub-comments that are addressed in Responses #15 through #19.	The LCA transport results were not significantly impacted by alternate AA/VA models including a wide range of lateral permeabilities with an upper bound of 5×10^{-12} square meters (m^2), as well as incorporating breaching scenarios. Other modeling cases were run such as one in which the entire RN inventory from eight key tests was initially placed directly into the LCA to simulate the effects of breaching scenarios (N-I, 2013). These cases did not significantly impact the contaminant boundary even though the models assumed that significant amounts of ^3H from deeply buried tests are initially distributed in the LCA. Available data do not support the type of breaching proposed by PRC. The three new wells drilled in Yucca Flat (ER-2-2, ER-3-3, and ER-4-1) targeted detonations within a few cavity radii (R_c) (estimated based on the maximum yields reported in NNSA/NFO [2015] and the equation in Pawloski [1999]) of faults to determine the impact of faults on transport to the LCA. The absence of ^3H in the LCA in these wells indicates that nearby faults were not significant transport pathways to the LCA, in spite of their proximity to the working points. Hence, it is not necessary to extend the range of permeabilities considered in the AA/VA model or to further characterize fault behavior.
18	Evaluate the contaminant boundary using an alternative flow model in which all faults in the volcanic rocks serve as permeable pathways to the LCA.	This uncertainty focuses on flow and transport through faults, and includes several sub-comments that are addressed in Responses #15 through #19.	As discussed for Response #17, the LCA transport results were not significantly impacted by alternate AA/VA models including a wide range of lateral fault permeabilities, or by incorporating breaching scenarios. Therefore, no further action is needed under this recommendation.
19	Include an alternative model which has no or many fewer minor faults; this may require allowing flow and transport to occur between the AA/VA and LCA via the TCU in addition to the major faults.	This uncertainty focuses on flow and transport through faults, and includes several sub-comments that are addressed in Responses #15 through #19.	See Responses #17 and #18. The alternate models did not significantly increase transport compared to the base-case model. Hence, further work suggested in this recommendation is not necessary.

Table ES-1
Responses to YF/CM PRC Comments
(Page 9 of 27)

#	Recommendation	Focus of the Concern	Summary of Response
2.3.3 Tuff Confining Unit			
20	Evaluate the uncertainty in the contaminant boundary due to flow across the TCU that is not impermeable, but rather honors the available data on hydraulic properties of the TCU.	This uncertainty focuses on the process of flow across the TCU.	Interruption of the lateral continuity of the TCU by faults, and in certain model scenarios by local vertical pathways to the LCA created by the force of the nuclear detonations (the "breaching scenario"), is already incorporated in the SZ AA/VA conceptual models documented in N-I (2013). A wide range of lateral permeabilities (10^{-17} to 10^{-12} m^2)—consistent with available Yucca Flat-specific TCU hydrologic testing data—were assumed or calibrated (N-I, 2013, Figure 4-12). The upper limit of this range has been extended to 5×10^{-12} m^2 in model runs in response to the PRC comments. Three breaching cases that allow transport across the lower boundary in non-faulted locations have already been run (N-I, 2013). In these breaching cases, hydrofracturing along the lower TCU boundary was allowed and, if this occurred, the rock was assigned high permeability (10^{-12} m^2) and low porosity (0.01) between the detonation and the LCA. These model runs did not significantly impact the contaminant boundary. Moreover, the available ^3H data from large-yield, deeply buried detonations such as BILBY, CALABASH, STRAIT, and WAGTAIL indicate that the type of breaching proposed by the PRC does not occur. Hence, further work suggested in this recommendation is not necessary.
21	Develop new data and field testing to determine the lateral continuity of the TCU as an effective hydraulic barrier to vertical transport.	This uncertainty focuses on the process of flow across the TCU.	The SZ AA/VA model alternatives considered the possibility that nuclear testing created fracture pathways to the top of the LCA (N-I, 2013, Section 4.0). This so-called breaching hypothesis was investigated by the new wells drilled into the LCA near the CALABASH, STRAIT, and WAGTAIL detonations. Two of the wells (ER-2-2 near CALABASH and ER-3-3 near WAGTAIL) also investigated whether faults were significant transport pathways for TCU-hosted detonations to the LCA. No ^3H was detected above the MDL (1,500 to 1,800 pCi/L) in the LCA water produced during drilling, indicating that the transport pathways hypothesized by the PRC do not exist at these wells (ER-2-2, ER-3-3, and ER-4-1). Hence, further work suggested in this recommendation is not necessary.

Table ES-1
Responses to YF/CM PRC Comments
(Page 10 of 27)

#	Recommendation	Focus of the Concern	Summary of Response
2.3.4 Effective Porosity			
22	Evaluate uncertainty in the contaminant boundary due to effective fracture porosity of the TCU.	This uncertainty is motivated by lack of sufficient data regarding effective porosity in the TCU.	The base-case model presented in N-I (2013) is sufficiently conservative. Damage zones or chimneys in the TCU were assumed to have a fracture porosity of 0.01. In response to PRC comments, additional simulations were run with an assumed fracture porosity of 5×10^{-04} to assess potential significance of continuous fracture networks on simulated RN fluxes to the LCA. These simulations indicated that the breakthrough of ^{14}C and other long-lived RNs to the LCA is smaller when fracture flow combined with fracture-matrix diffusion is considered, but that there may be some earlier breakthrough of ^{3}H compared with the base case. However, because the contaminant boundary is defined by ^{3}H initially emplaced within the LCA, the effect of some early ^{3}H breakthrough from the TCU is not expected to alter the range of N-I (2013) contaminant boundaries. Hence, further work suggested in this recommendation is not necessary.
2.3.5 Potential for Flow of Surface Water into Fractures in the Alluvium			
23	Model faults as local zones of preferential flow through the unsaturated and saturated alluvium. Gather field data to ascertain the degree to which fissures contribute to enhanced local recharge.	This uncertainty concerns open fractures and faults at the surface that could act as conduits for flow of surface water to water table.	Most of these surface cracks generated by nuclear testing have since become sealed due to infilling by sediments and from weathering, but as indicated by recent photos in Appendix C of the PRC report (N-I, 2015), there are isolated areas along major faults where infilling of these cracks is incomplete. Field observations of these open surface cracks taken before and after the August 4, 2014, storm suggest that these cracks have not been areas of preferential water movement during runoff events. The practice during the nuclear testing period was to avoid major fault zones, so if preferential flow into these areas were to occur, it would pass between detonations and would not be available to flow into craters that formed above the detonations elsewhere. Hence, further work suggested in this recommendation is not necessary.

Table ES-1
Responses to YF/CM PRC Comments
(Page 11 of 27)

#	Recommendation	Focus of the Concern	Summary of Response
2.3.6 Anisotropy and Preferential Flow in the Unsaturated Zone			
24	Determine the maximum depth of recent infiltration along possible flow pathways to detonation cavities at craters with high rates of recharge.	This uncertainty is motivated by concerns about preferential infiltration from crater bottoms.	This issue was determined to be a low priority because unsaturated zone (UZ) detonations did not contribute significantly to the contaminant boundary. Roughly 90% of UZ detonations are above the SZ AA/VA model, and the 10% that are above the SZ LCA are in the extreme northern end of the basin. This means that regardless of crater infiltration rates and wetting front velocity, the contaminant boundary will be defined by other, more deeply buried detonations further downgradient. Hence, further work to address this recommendation is not necessary.
2.4.1 No Uncertainty Associated with the RST			
25	Include uncertainties in radiologic source term (RST) in modeling.	This uncertainty focuses on the RST.	RST uncertainty, as documented in Bowen et al. (2001), has been explicitly incorporated in the source term via screening analyses documented in Appendix C of N-I (2013). Source term uncertainty has already been examined to varying degrees in each of the three model types (UZ, SZ AA/VA, and SZ LCA models) through uncertainty analysis in melt-glass partitioning factors, exchange volume size, alternate conceptual models (constant mass or constant concentration), and inventory uncertainty. The RST uncertainty approach used in the screening analysis, with the exception of melt glass dissolution, was also used in determining initial LCA model inventories for the detonations with initial inventories within the SZ LCA. Comparison of unclassified and classified R_c, inventory, and yield for the 39 deep tests likely to impact the contaminant boundary has been completed. The results showed that R_c is generally smaller than unclassified estimates based on maximum yield, thus reducing the number of tests intersecting the SZ LCA (cavity dimension based on maximum announced yield identified in NV-209-REV 16 [NNSA/NFO, 2015] and Equation 1 in UCRL-ID-136003 [Pawloski, 1999]). The initial source term concentrations and the total inventory deposited in the SZ LCA are not substantially impacted. These results were presented to the Nevada Division of Environmental Protection (NDEP) on June 5, 2015. The results suggest that the contaminant boundary would not be greatly impacted if classified source terms had been used. Hence, further work suggested in this recommendation is not necessary.

Table ES-1
Responses to YF/CM PRC Comments
(Page 12 of 27)

#	Recommendation	Focus of the Concern	Summary of Response
2.4.2 Uncertainties in Partition Factors Are Not Well Defined Particularly for Cavities in Carbonate Rock			
26	Develop support for partition factors used.	This uncertainty concerns the partition factors appropriate for modeling the concentration of RNs in cavities in silicic as well as carbonate rocks.	The International Atomic Energy Agency (IAEA) RN partitioning recommendations were developed using a combination of underground nuclear test data from the NNSS, Mururoa/Fangataufu, and other underground nuclear testing locations (IAEA, 1998a, b, and c); and hence are consistent with data from the NNSS. Supporting work on partitioning factors for tests detonated in carbonate rock were performed by the UGTA Activity, including extensive work done on NASH and KANKAKEE debris (Carle et al., 2008). The partition factors are consistent with observations and do not need to be revised.
2.4.3 Water Flow into Cavities			
27	Measure and monitor enhanced-recharge-driven transport in and below detonation craters.	This uncertainty addresses the hydraulic properties beneath detonation cavities in the TCU and the potential for rapid transport.	There is no need to further characterize, measure, or monitor enhanced, recharge-driven transport below detonation craters near UZ-hosted tests. Roughly 90% of the UZ detonations were located above the SZ AA/VA domain, which provides additional barriers to RN transport to the SZ LCA. The effectiveness of the SZ AA/VA system as a barrier to RN migration from the UZ to the SZ LCA was demonstrated in N-I (2013) by comparing RN fluxes with and without the UZ RN fluxes present. The results in both cases were the same. The 10% of the UZ-hosted detonations that lie directly above the SZ LCA occur in the northern parts of the LCA model (NASH, HANDCAR, KANKAKEE) or are monitored by a nearby well that shows no evidence of RN transport (BOURBON). Therefore, because a considerable amount of work has already been done to demonstrate that these sources do not impact the contaminant boundary, additional crater studies are not considered necessary.

Table ES-1
Responses to YF/CM PRC Comments
(Page 13 of 27)

#	Recommendation	Focus of the Concern	Summary of Response
2.4.4 Uncertainty in Exchange Volume Not Fully Captured			
28	Extend the uncertainty analysis to include exchange volumes of at least 5 R_c.	The concern of this uncertainty is that fracturing associated with nuclear detonations could extend further than that included in the model.	The general configuration of detonation-altered zones and properties described in Appendix C of N-I (2013) are largely based on information compiled in the Office of Technology Assessment (OTA) report (OTA, 1989). The exchange volume is related to the size of the damage zone, but is also related to volatility and molecular weight of the RNs comprising the hydrologic source term (HST) and whether the exchange volume is located in a saturated or unsaturated environment. N-I (2013) used Yucca Flat specific data and HST modeling (Tompson, 2008) as well as cavity data from the RAINIER and CHANCELLOR detonations to estimate RN-specific exchange volumes. Only ^{14}C has a maximum exchange volume size of 5 R_c within the SZ, and the initial concentration of ^{14}C is only slightly above the SDWA MCL (CFR, 2015) assuming a 1 R_c exchange volume (N-I, 2012, Figure 2-6). Using a 5 R_c for ^{14}C would lower the initial concentration below the MCL. Using the recommended 5 R_c exchange volume for all detonations and all RNs would create lower initial concentrations that are most likely unrealistic and would impart an additional element of non-conservatism. ^{3}H measurements and water production rates observed during drilling of Wells ER-2-2, ER-3-3, and ER-4-1 have indicated that the TCU is largely uncontaminated and unfractured at distances of 2.5 to 3 R_c from the working point (based on the maximum announced yield of the nearby tests). This indicates that the exchange volumes used in N-I (2013) are adequate for contaminant boundary calculations.

Table ES-1
Responses to YF/CM PRC Comments
(Page 14 of 27)

#	Recommendation	Focus of the Concern	Summary of Response
2.4.5 Possible Chimney and Cavity Pathways to the LCA			
29	Expand the uncertainty analysis to include a greater range of permeability enhancement assigned to the damage zone. Where possible, consider using shot holes to test field permeability of the damage zones.	This uncertainty addresses the size of the exchange volume and damage zone associated with an underground test.	Historical studies with air injection and gas tracers have been used to characterize cavities and chimneys in the TCU at Rainier Mesa (Peterson et al., 1977a and b, and 1978). Because the rocks are partially water-filled, estimated air-permeabilities and porosities are minimum estimates of the single-phase values. The results indicated that the air-permeabilities were on the order of 8 to 150 Darcies (roughly 8×10^{-12} to 1.5×10^{-10} m^2) in the upper parts of the chimney above the injection hole, and sometimes much less (0.001 to 12 Darcies, roughly 10^{-15} to 1.2×10^{-11} m^2) in the lower part of the chimney that included the cavity region. Air-filled porosity (accessible void volume) was on the order of 0.09 to 0.17. For comparison, the average air permeability of the surrounding media was estimated to be about 1 Darcy (roughly 10^{-12} m^2) in the vitric tuff and 0.001 to 0.36 Darcies (10^{-15} to 3.6×10^{-13} m^2) in the adjacent undamaged zeolitic rocks. The chimney/cavity systems, therefore, had enhanced permeability relative to the surrounding rock. Low water production rates and lack of measured ^3H during drilling of the three new wells in Yucca Flat (ER-2-2, ER-3-3, and ER-4-1) indicated lack of enhanced permeability near and below the working point. Drilling results indicate little to no transport into the LCA from the nearby underground tests. This supports the conclusion that damage zone permeability does not produce significant vertical transport in the region surrounding deeply buried large underground tests near the interface with the LCA, or faults that intersect the LCA. Further work suggested in this recommendation is not necessary.
2.5.1 Values Used for Pu Retardation Are Not Well Supported and May Be Too High			
30	Decrease Pu K_d values used for modeling. Collect more data to understand Pu retardation, and further evaluate existing data.	This uncertainty is associated with the concern that the sorption coefficient distributions used in the transport model for plutonium (Pu) may not be sufficiently conservative.	To address this recommendation, the range of Pu distribution coefficient (K_d) values for the LCA was decreased from 900 to 10,000 milliliters per gram (mL/g) to 0.76 to 1,096 mL/g (Sutton, 2009). Although Pu contamination for the reduced K_d case was more extensive, the effect was insignificant because the contaminant boundary remained dominated by ^3H. Hence, further work suggested in this recommendation is not necessary.

Table ES-1
Responses to YF/CM PRC Comments
(Page 15 of 27)

#	Recommendation	Focus of the Concern	Summary of Response
2.5.2 Melt-Glass Dissolution Is Largely Neglected			
31	Include melt-glass dissolution in UZ models. Consider additional processes affecting cavity-debris behavior in the LCA, and include an instant-release case.	This uncertainty concerns the initial inventory assigned to each detonation and melt-glass dissolution.	This uncertainty is considered a low priority that does not require further analysis. Melt-glass dissolution in the UZ is not important to contaminant transport because dry conditions follow the detonation, and the wetting front from crater infiltration will not arrive until long after melt glass has cooled (in some cases, hundreds of years). Significant glass dissolution occurs only at elevated temperatures, and transport of liberated Pu due to glass dissolution is limited by sorption and filtration of colloids (Zavarin et al., 2015). Additionally, UZ detonations were shown in N-I (2013) to be secondary to other detonations for defining the contaminant boundary, so late-time melt-glass dissolution would have only a minor impact. The parametric uncertainties associated with calculating the HST for the SZ LCA included inventory uncertainty and melt-glass partition fractions. The inventory uncertainty varied from a factor of 0.1 to 10 depending on the RN group (i.e., residual ^{3}H, activation products, fission products, or unspent fuel), and melt-glass fractions varied from 0 to 100% depending on the RN. The uncertainty associated with initial inventory and melt-glass partition factors is much larger than the total expected melt-glass dissolution, and immediately releasing a small percentage of the RNs incorporated in melt-glass to the LCA will not significantly change the contaminant boundary. Hence, further work suggested by this recommendation is not necessary.

Table ES-1
Responses to YF/CM PRC Comments
(Page 16 of 27)

#	Recommendation	Focus of the Concern	Summary of Response
2.6.1 Field Measured ^{3}H Concentrations Are Not Simulated in the N-I (2013) Model			
32	Simulate sub-regions of the model with smaller mesh size and more particles to understand mismatches.	This uncertainty focuses on the non-zero levels of ^{3}H concentrations detected in Wells ER-2-1, UE-6e, UE-6d, TW-B, and WW-A.	Past ^{3}H detections in the SZ AA/VA system and LCA were explained with a combination of modeling and groundwater sampling. Since the completion of N-I (2013), several wells have been resampled (ER-6-2, UE-7nS, WW-3, WW-2, ER-2-1, UE-6d, UE-6e, and TW-B). Five of these wells (ER-2-1, ER-6-2, TW-B, UE-6d, and UE-6e) were identified by the PRC as of special concern (N-I, 2013, Table 6-4) based on previous ^{3}H measurements. The ^{3}H detected at WW-A is attributed to RN migration from the HAYMAKER detonation induced by pumping from WW-A while functioning as a water-supply well. The ^{3}H detected in ER-2-1 samples is consistent with contaminated water moving outward from an initial exchange volume of 4 R_c or less (two SZ detonations are within a lateral distance of 4.1 R_c from ER-2-1). Sampling wells with anomalous historical results has been completed and the results explained. Wells UE-6d, UE-6e, and TW-B are currently below the low-level detection limit (~2 pCi/L), indicating that past ^{3}H occurrences, although unexplained, were not the leading edges of a contaminant plume. Hence, further work suggested by this recommendation is not necessary.
33	Incorporate processes that could lead to observed lateral transport of ^{3}H in the AA/VA.	This uncertainty focuses on the non-zero levels of ^{3}H concentrations detected in Wells ER-2-1, UE-6e, UE-6d, TW-B, and WW-A.	The ^{3}H detected at WW-A was the result of 27 years of pumping for water supply, a factor that induced ^{3}H migration from the HAYMAKER test ~0.5 km away from WW-A. Even this explanation required the presence of hydrodynamic dispersion in the alluvium, in addition to pumping. Wells UE-6d, UE-6e, and TW-B are currently below the low-level detection limit (~2 pCi/L), indicating that past ^{3}H occurrences, although unexplained, were not the leading edges of a contaminant plume. Hence, further work suggested by this recommendation is not necessary.

Table ES-1
Responses to YF/CM PRC Comments
(Page 17 of 27)

#	Recommendation	Focus of the Concern	Summary of Response
34	Evaluate whether timing of sampling or nature of completion of non-detect wells may be such the ^3H occurrences were missed.	This uncertainty focuses on the adequacy of sampling locations and frequency in the LCA.	Sampling frequency and completion depth intervals relative to potential contamination sources were examined. Near-field wells such as ER-7-1, UE-7nS, and U-3cn 5 tended to have shallow completion depths in the LCA and relatively frequent measurements, so that transient RN fluxes to the LCA from the overlying tuffs were likely to be observed if they occurred. These wells all have measured ^3H concentrations that are slightly above to below detection, indicating that RN movement from the nearby tests to the LCA was at most very minor. Far-field wells such as WW-C, WW-C-1, TW-D, UE-1q, and ER-6-1 also have shallow completion depths, and in most cases had near-yearly sample collection. These wells have experienced only very low levels of ^3H over many decades. The samples from these far-field wells are presently free of measurable ^3H, confirming that the southern half of Yucca Flat basin is uncontaminated. Hence, further work under this recommendation is not necessary.
35	Gather field data to define the current extent of contamination, then adjust the model to better represent the field system.	This uncertainty focuses on the adequacy of sampling locations and frequency in the LCA.	Since the completion of N-I (2013), several wells have been resampled (ER-6-2, UE-7nS, WW-3, WW-2, ER-2-1, UE-6d, UE-6e, and TW-B). Five of these wells (ER-2-1, ER-6-2, TW-B, UE-6d, and UE-6) were identified by the PRC as of special concern (N-I, 2013, Table 6-4) based on previous ^3H measurements. Additionally, three new wells (ER-2-2, ER-3-3, and ER-4-1) were drilled near deeply buried, large-yield detonations (ER-2-2 and ER-4-1) or near faults (ER-2-2 and ER-3-3) to investigate the extent of contamination associated with tests near the LCA or faults. No new detections of elevated ^3H concentrations in the LCA were observed in the resampled wells or in the LCA during drilling of the three new wells, although elevated ^3H (~10 million pCi/L) was observed in the Tertiary volcanics above the TCU at ER-2-2 (within 2 R_c of the CALABASH test). Hence, further work under this recommendation is not necessary.

Table ES-1
Responses to YF/CM PRC Comments
(Page 18 of 27)

#	Recommendation	Focus of the Concern	Summary of Response
2.6.2 Crater-Infiltration Data Are Not Well Matched in the Model			
36	Ensure that the crater-recharge model is conservative.	This uncertainty addresses the rate of surface flux into the UZ by enhanced recharge through craters.	The differences between the long-term (1,000-year) infiltration rates estimated for the HYRAX, LAGUNA, and BYE craters in N-I (2013, Table E-1) and independent estimates calculated by the reviewers or published in the open literature from field data result from the fact that the observations were performed during a time period of higher than normal precipitation, which biases the observed data above the long term trend. Hence, further work under this recommendation is not necessary.

Table ES-1
Responses to YF/CM PRC Comments
(Page 19 of 27)

#	Recommendation	Focus of the Concern	Summary of Response
2.6.3 Geochemical and Environmental Isotope Not Fully Evaluated			
37	Justify the choice of initial chloride concentrations. Explain differences in interpretations of ^{14}C in the Yucca Flat and Ash Meadows LCA flow systems. Avoid interpreting ages from dissolved organic carbon-14 data.	This uncertainty addresses the interpretation of ^{36}Cl and ^{14}C data.	The assumption that the chloride concentration of LCA recharge is ~7 milligrams per liter (mg/L) is based on the mean chloride concentration of dozens of tunnel seeps in tuffs at Rainier Mesa. The use of this value in recharge to the LCA in Yucca Flat is reasonable in that water in the tuffs at Rainier Mesa (a regional recharge area) has undergone no or minimal chloride leaching (as in the LCA) or evaporative enrichment after discharge (as do perched spring data). Furthermore, the use of 7 mg/L to correct the LCA samples that appear to have been affected by halite dissolution allows for a range in $^{36}Cl/Cl$ ratios similar to those measured in packrat middens between 10,000 and 40,000 years ago (a range that is neither too high or too low) and which matches the temporal variations in the packrat midden data (Kwicklis and Farnham, 2014). While this does not prove the use of 7 mg/L is correct, it is at least internally consistent with the ranges and timing of $^{36}Cl/Cl$ variations estimated from the packrat midden data. Three explanations for possible higher rates of isotope exchange in the Devils Hole flow system compared with Yucca Flat are as follows: (1) Flow in the Devils Hole system experiences more vertical variations due to faults and stratigraphic offsets, and undergoes a larger range of temperature and pressure variations that would promote calcite dissolution and re-precipitation. (2) Degassing of carbon dioxide (CO_2) under atmospheric conditions at Devils Hole promotes deposition of fine-grained, porous calcite, with which later groundwater then interacts. (3) Dolomite dissolution, combined with calcite precipitation, effectively serves as a carbon isotope exchange mechanism. None of these processes that potentially occur at Devils Hole apply to the LCA in Yucca Flat. Hence, further work under this recommendation is not necessary.

Table ES-1
Responses to YF/CM PRC Comments
(Page 20 of 27)

#	Recommendation	Focus of the Concern	Summary of Response
2.6.4 Interpretation of Temperature Data			
38	Explain temperature at the water table, use temperature data to inform calibration of the coupled flow model, and incorporate water fluxes indicated by temperature data into determination of the contaminant boundary.	This uncertainty concerns the interpretation of temperature data in the Yucca Flat area.	Further work as suggested in this recommendation will not reduce the model uncertainty. The work to explain groundwater temperature patterns is described in detail in Appendix H of N-I (2013). From the data and associated models, it was interpreted that drainage from the AA/VA might be occurring near the major basin-bounding faults, consistent with the groundwater ^{14}C age distribution in the LCA. The possible range of groundwater inflow from the north was limited to 0 to 50 kg/s based on temperature profiles from Wells UE-10j and ER-8-1. The temperature data support recent assessments of small basin-wide fluxes and slow travel times as indicated by inorganic ^{14}C data. Further work under this recommendation is not necessary.
2.6.5 Realistic Geologic Features			
39	Incorporate more realistic geologic features as computational capabilities, software, and data improve.	This uncertainty addresses geological simplifications incorporated in the hydrostratigraphic model.	The base case model and the alternate conceptualizations presented in Responses #11 through #21, #42, and #44 encompass these uncertainties.
2.6.6 Other Sources of Data Are Available but Unused			
40	Review and use data from surrounding DOE and DOD facilities to further constrain water levels, boundary fluxes, and estimates of hydraulic properties. Among other approaches discussed in previous sections of this report, the peer review team recommends building confidence in the Yucca Flat model by using the Yucca Flat modeling approach to simulate single-test detonations outside Yucca Flat in similar geological units where there has been groundwater monitoring (e.g., the 40-kt RULISON test in 1969 in Colorado, the 200- to 1,000-kt FAULTLESS test in 1968 in central Nevada, or the 12-kt SHOAL test in 1963 in northern Nevada).	This uncertainty addresses sources of data from outside the CAU area that could potentially be used in the conceptual model.	All available data that may be used to constrain water levels within Yucca Flat, including data from surrounding DOE and U.S. Department of Defense (DoD) facilities, were evaluated and applied where applicable. The uniqueness of the different testing environments makes direct extrapolation of the results of offsite nuclear testing to Yucca Flat inappropriate. Hence, further work under this recommendation is not necessary. Due to the uniqueness of the different testing environments, direct extrapolation of the results of offsite nuclear testing is unlikely to add new insights to the processes already included in the Yucca Flat flow and transport model.

Table ES-1
Responses to YF/CM PRC Comments
(Page 21 of 27)

#	Recommendation	Focus of the Concern	Summary of Response
2.7.1 Current Evaluation Does Not Capture the 95th Percentile			
41	Generate flow models that represent combinations of values from the upper end of their parameter distributions and explore whether calibration is successful.	This uncertainty addresses the perception that some of the extreme parameter values may not be sampled in the uncertainty analysis.	The uncertainty analysis in N-I (2013) and the alternate models presented in the response to the PRC comments together provide reasonable bounds for plausible transport scenarios. Several examples where parameters were manually changed to investigate the impact to the model are already presented (Responses #15 through #19). It is not reasonable to manually pick the upper end of multiple distributions simply to enhance the transport prediction. Using biased sampling of transport parameters may result in unrealistic predictions and misallocation of monitoring or remediation resources. Hence, further work under this recommendation is not necessary.
2.7.2 Expected Alternative Flow Models Were Not Included			
42	Include alternative flow models with fast flow fields from many detonation locations.	This uncertainty addresses the concern that some of the alternate conceptual models were not included in the uncertainty analysis.	The LCA model has already appropriately included fast path cases. As demonstrated by the Null Space Monte Carlo (NSMC) analysis (N-I, 2013), and also discussed in Responses #8 and #13, a wide range of parameter combinations were simulated, each matching observed water-level observations. As reported in Response #44, several additional fast path cases as well as particle starting locations at 39 detonations within 3 R_c of the saturated LCA (based on the maximum of the announced yield range [NNSA/NFO, 2015] and the equation published in Pawloski [1999]) were considered. The PRC identified 10 alternative cases they felt should be simulated; reasonable transport models based on these recommendations did not lead to significantly higher contaminant transport than the base case, or led to cases that did not match observed water levels and were not acceptable alternatives. Hence, further work under this recommendation is not necessary.
2.7.3 Limited Number (100) of NSMC Realizations			
43	Employ the approach described in Section 6.7.1 of N-I (2015) to capture fast flow fields without excessive numbers of simulations.	This uncertainty addresses the possibility that the effect of most permeable pathways was not captured by the range of uncertainty used in the model.	Fast flow path cases that produced more extensive transport, did not match observed water levels in the basin, and therefore are not acceptable alternatives. For example, the LCA model recalibrations specifying large faults as a high-permeability features produced faster transport than the base case, but were largely unsuccessful in matching steady-state heads in western Yucca Flat. Hence, further work under this recommendation is not necessary.

Table ES-1
Responses to YF/CM PRC Comments
(Page 22 of 27)

#	Recommendation	Focus of the Concern	Summary of Response
2.7.4 Limited Calibrated Flow Models Used to Evaluate Transport Uncertainty			
44	Include more fast flow field models coupled with transport parameter values from the end of the distribution that enhances transport.	This uncertainty addresses the concern that the model did not include continuous high-conductivity pathways.	The modeling team disagrees with the approach proposed by the PRC that transport parameters be hand-drawn from parts of the distribution that maximizes transport. Biased sampling of conservative parameters creates unreasonable transport cases and results in extremely unlikely predictions above the 95th percentile. Using such unlikely predictions may result in misallocation of monitoring and/or remediation resources. A set of 39 possible contaminant sources (all detonations within 3 R_c of the SZ LCA) was used to identify alternate fast flow fields for transport uncertainty evaluation. Ten alternate model cases were selected for transport and contaminant boundary calculations in the LCA. These results along with LCA ^3H concentrations obtained from drilling Wells ER-2-2, ER-3-3, and ER-4-1, and the lower basin flux data (Halford, 2016) support the conclusion that the transport parameters distributions used to develop the contaminant boundary ensemble (N-I, 2013) adequately bound the range of uncertainty.
2.7.5 Limited Alternate Models Used to Evaluate Relevant Detonations			
45	Include more flow fields in the uncertainty evaluation with bias to capture the 95th percentile, and include all sources with enhanced transport.	This uncertainty focuses on the concern that some potentially important contaminant sources were excluded from the model.	This uncertainty was addressed using particle tracking studies followed by developing a contaminant boundary forecast for the particle track case with the largest total particle breakthrough at the southern boundary. Particle tracking studies included the 39 detonations within 3 R_c of the SZ LCA and the 83 NSMC flow fields that achieved an acceptable calibration from N-I (2013). The percentage of particles arriving near the model's southern boundary within 1,000 years varied from 13 to 82%. The 95th percentile contaminant boundary for the simulation with the largest total particle breakthrough was similar to that for the base case. Further work in the direction suggested in this recommendation is not necessary.

Table ES-1
Responses to YF/CM PRC Comments
(Page 23 of 27)

#	Recommendation	Focus of the Concern	Summary of Response
2.7.6 Limited Range of Transport Parameters Values Used to Evaluate Transport Uncertainty			
46	Include Pu isotopes with combinations of lower K_d values and higher mass in the source term, expand the evaluated uncertainty range of matrix diffusion, and include higher values of dispersivity.	This uncertainty addresses the concern that the ranges considered in the model for some of the transport parameters were not sufficiently wide.	Alternative transport simulations using reduced Pu K_ds for the LCA matrix, reduced Pu retardation factors (R_d) for the LCA fractures, and increased dispersivity values did not lead to transport in excess of the base case. Reducing the range of Pu LCA matrix K_ds from the 900 to 10,000 mL/g values used for contaminant boundary calculations (N-I, 2013) to 0.76 to 1,096 mL/g (Sutton, 2009) produced more extensive Pu contamination; but because the contaminant boundary remained dominated by ^{3}H, the impact to the contaminant boundary was insignificant. Increased dispersivity resulted in more diffuse transport and a wider contaminant boundary with less MCL exceedances near the model's southern boundary compared to the base case. Larger Pu mass in the source term is not consistent with known concentrations in near-field samples or with published literature (Responses #25 and #26). Use of higher dispersivity values did not result in contaminant boundaries substantially different from those calculated in the base case. Further work suggested in this recommendation is not necessary.
2.7.7 Mesh Refinement Not Necessarily Conservative			
47	Evaluate higher level meshes to determine definitively the mesh-refinement level for which there is no change in the contaminant boundary.	This uncertainty focuses on the effects of the mesh size on model predictions.	Comparison of calibrated transport model results for 125-m spacing (Level 2 mesh) and 62.5-m spacing (Level 3 mesh) demonstrates that while transport from some locations was enhanced, transport from other locations was reduced; and the overall particle paths and travel times do not change significantly with mesh refinement. Further work in the direction suggested in this recommendation is not necessary.

Table ES-1
Responses to YF/CM PRC Comments
(Page 24 of 27)

#	Recommendation	Focus of the Concern	Summary of Response
2.8.1 New Concerns and Approaches Will Likely Arise			
48	Engage external experts in periodic peer review.	This uncertainty is motivated by a desire for UGTA to employ external reviewers more frequently throughout the life of the project.	All UGTA Activity products are reviewed by a pre-emptive review committee that includes experts in a variety of fields (e.g., geology, radiochemistry, and hydrology) and an ex officio NDEP member. Additional reviewers are added as necessary. This committee is highly knowledgeable regarding the YF/CM CAU and different aspects of the flow and transport model. New contractors are introduced throughout the life of each CAU and, therefore, bring new perspectives to the work. The current process of using internal pre-emptive reviews with a final external peer review meets the requirements of the FFACO (1996, as amended) and will not be changed.
2.8.2 Climate Change			
49	Evaluate whether long-term climate change and associated extreme weather events would have a significant impact on transport of radionuclides.	This uncertainty addresses the concern that the climate may change radically over the 1,000-year time frame of concern.	A preliminary assessment indicates that the U.S. Southwest will experience warmer and drier conditions. If true, then current models are already conservative. By continued execution of the UGTA strategy (FFACO, 1996 as amended), any such assessment of regional scale climate change will occur when monitoring indicates a need for this action.

Table ES-1
Responses to YF/CM PRC Comments
(Page 25 of 27)

#	Recommendation	Focus of the Concern	Summary of Response
2.9.1 The Extent of Contamination Is Poorly Defined at Present			
50	Determine the bounds of contaminant migration in both the AA/VA and LCA.	This uncertainty focuses on the need to define the bounds of contaminant migration.	Since the completion of N-I (2013), eight wells have been resampled (ER-2-1, ER-6-2, TW-B, UE-6d, UE-6e, UE-7nS, WW-2, and WW-3). Five of these wells (ER-2-1, ER-6-2, TW-B, UE-6d, and UE-6) were identified by the PRC as of special concern (N-I, 2013, Table 6-4) based on previous ^{3}H measurements. Additionally, three new wells (ER-2-2, ER-3-3, and ER-4-1) were drilled near deeply buried, large-yield detonations (ER-2-2 and ER-4-1) or near faults (ER-2-2 and ER-3-3) to investigate the extent of contamination associated with tests near the LCA or faults. No new detections of elevated ^{3}H concentrations in the LCA were observed in the resampled existing wells or in samples collected while drilling the three new wells. This supports the observation that ^{3}H contamination of the LCA is of limited areal extent and that simulations documented in N-I (2013) adequately bound RN transport. Contamination in the AA/VA is generally limited to a few R_c around the working point (as observed during drilling of ER-2-2), except near WW-A, where 27 years of pumping for water supply induced migration toward the pumping well; in the LCA, no wells have ^{3}H concentration that exceed the MCL (20,000 pCi/L), except for the U-2ce (NASH) satellite well, which appears to be in an isolated thrust block of the lower carbonate aquifer thrust plate (LCA3). This supports the observation that ^{3}H contamination of the LCA is of limited areal extent and that simulations documented in N-I (2013) adequately bound RN transport.

Table ES-1
Responses to YF/CM PRC Comments
(Page 26 of 27)

#	Recommendation	Focus of the Concern	Summary of Response
2.9.2 The Existing Observation Well Network Is Inadequate			
51	Conduct a comprehensive formal review of existing data quality, and maintain a groundwater monitoring program designed to evaluate model uncertainties and delineate contaminant boundaries.	This uncertainty addresses the well network necessary to determine the extent of contamination.	Continued execution of the UGTA strategy (FFACO, 1996 as amended) and implementation of the NNSS Integrated Sampling Plan (NNSA/NFO, 2014) will continue to address this comment. Sampling plan implementation will ensure samples are collected routinely and that the results are annually evaluated for quality and consistency with the conceptual models of flow and transport (N-I, 2013). ^{3}H concentration maps are presented in the Annual Site Environmental reports and will also be presented in UGTA Annual Sampling reports. A summary of RN detections in the SZ AA/VA and LCA domains spanning five decades in some cases was included in Tables 4-45 and 4-46 and as Appendix D in N-I (2013). In addition, numerous historical reports have been identified to help constrain permeability variations in the vicinity of underground nuclear tests, including those that involve post-shot holes. Selection and placement of monitoring wells is the focus of the final stage of the UGTA strategy (FFACO, 1996 as amended), the Closure Report (CR) stage, and not the CAI or CADD/CAP stages. No further actions are therefore necessary to address this recommendation.

Table ES-1
Responses to YF/CM PRC Comments
(Page 27 of 27)

#	Recommendation	Focus of the Concern	Summary of Response
52	General locations for new wells, aquifer tests, and sampling during the CADD/CAP stage, including samples from existing wells, are recommended in Section 5.9.2.	This uncertainty addresses the well network necessary to determine the extent of contamination.	Execution of the UGTA strategy (FFACO, 1996 as amended) and implementation of the NNSS Integrated Sampling Plan (NNSA/NFO, 2014) will continue to address this comment. Since the completion of N-I (2013), eight wells have been resampled (ER-2-1, ER-6-2, TW-B, UE-6d, UE-6e, UE-7nS, WW-2, and WW-3). Five of these wells (ER-2-1, ER-6-2, TW-B, UE-6d, and UE-6) were identified by the PRC as of special concern (N-I, 2015, Table 6-4) based on previous ^{3}H measurements. Additionally, three new wells (ER-2-2, ER-3-3, and ER-4-1) were drilled near deeply buried, large-yield detonations (ER-2-2 and ER-4-1) or near faults (ER-2-2 and ER-3-3) to investigate the extent of contamination associated with tests near the LCA or faults and to provide hydraulic data in the central parts of the basin that were not hydraulically stressed by the ER-6-1-2 MWAT in 2004. No new detections of elevated ^{3}H concentrations in the LCA were observed in the resampled existing wells or in samples collected during drilling the three new wells. This supports the observation that ^{3}H contamination of the LCA is of limited areal extent and that simulations documented in N-I (2013) adequately bound RN transport.

Note: Cavity dimension based on maximum announced yield identified in NV-209-REV 16 (NNSA/NFO, 2015) and Equation 1 in UCRL-ID-136003 (Pawloski, 1999).

REFERENCES

Bowen, S.M., D.L. Finnegan, J.L. Thompson, C.M. Miller, P.L. Baca, L.F. Olivas, C.G. Geoffrion, D.K. Smith, W. Goishi, B.K. Esser, J.W. Meadows, N. Namboodiri, and J.F. Wild. 2001. *Nevada Test Site Radionuclide Inventory, 1951–1992,* LA-13859-MS. Los Alamos, NM: Los Alamos National Laboratory.

CFR, see *Code of Federal Regulations.*

Carle, S.F., M. Zavarin, Y. Sun, and G.A. Pawloski. 2008. *Evaluation of Hydrologic Source Term Processes for Underground Nuclear Tests in Yucca Flat, Nevada Test Site: Carbonate Tests*, LLNL-TR-403485. Livermore, CA: Lawrence Livermore National Laboratory.

Code of Federal Regulations. 2015. Title 40 CFR, Part 141, "National Primary Drinking Water Regulations." Washington, DC: U.S. Government Printing Office.

FFACO, see *Federal Facility Agreement and Consent Order*.

Federal Facility Agreement and Consent Order. 1996 (as amended March 2010). Agreed to by the State of Nevada; U.S. Department of Energy, Environmental Management; U.S. Department of Defense; and U.S. Department of Energy, Legacy Management. Appendix VI, which contains the Underground Test Area Strategy, was last modified June 2014, Revision No. 5.

Fenelon, J.M., D.S. Sweetkind, P.E. Elliott, and R.J. Laczniak. 2012. *Conceptualization of the Predevelopment Groundwater Flow System and Transient Water-Level Responses in Yucca Flat, Nevada National Security Site, Nevada*, Scientific Investigations Report 2012-5196. Reston, VA: U.S. Geological Survey.

Halford, K., U.S. Geological Survey. 2012. Personal communication to A. Tompson (LLNL) regarding groundwater flow estimates for the Yucca Flat/Climax Mine CAU, 9 October. Carson City, NV.

Halford, K., U.S. Geological Survey. 2016. Personal communication to S. Kelkar (Navarro/HGL) regarding UGTA-YF, MWAT analysis, 3 March. Carson City, NV.

Harrill, J.R., J.S. Gates, and J.M. Thomas. 1988. *Major Groundwater Flow Systems in the Great Basin Region of Nevada, Utah and Adjacent States*. Hydrological Investigation Atlas HA-694-C, scale 1:1,000,000. Denver, CO: U.S. Geological Survey.

IAEA, see International Atomic Energy Agency.

International Atomic Energy Agency. 1998a. *The Radiological Situation at the Atolls of Mururoa and Fangataufa, Technical Report, Volume 3: Inventory of Radionuclides Underground at the Atolls,* IAEA-MFTR-3. In "Proceedings of an IAEA Conference, Vienna, 30 June – 3 July." Vienna, Austria.

International Atomic Energy Agency. 1998b. *The Radiological Situation at the Atolls of Mururoa and Fangataufa, Technical Report, Volume 4: Releases to the Biosphere of Radionuclides from Underground Nuclear Weapons Tests at the Atolls*, IAEA-MFTR-4. In "Proceedings of an IAEA Conference, Vienna, 30 June – 3 July." Vienna, Austria.

International Atomic Energy Agency. 1998c. *The Radiological Situation at the Atolls of Mururoa and Fangataufa, Technical Report, Volume 6: Dose due to Radioactive Materials Present in the Environment or Released form the Atolls*, IAEA-MFTR-6. In "Proceedings of an IAEA Conference, Vienna, 30 June – 3 July." Vienna, Austria.

Kwicklis, E., and I. Farnham. 2014. "Testing the ^{14}C Ages and Conservative Behavior of Dissolved ^{14}C in a Carbonate Aquifer in Yucca Flat, Nevada (USA), Using ^{36}Cl from Groundwater and Packrat Middens." In *Hydrogeology Journal,* Vol. 22(6): pp. 1359–1381.

N-I, see Navarro-Intera, LLC.

NNSA/NFO, see U.S. Department of Energy, National Nuclear Security Administration Nevada Field Office.

Navarro-Intera, LLC. 2013. *Phase I Flow and Transport Model Document for Corrective Action Unit 97: Yucca Flat/Climax Mine, Nevada National Security Site, Nye County, Nevada*, Rev. 1, N-I/28091-080. Las Vegas, NV.

Navarro-Intera, LLC. 2015. *External Peer Review Team Report for Corrective Action Unit 97: Yucca Flat/Climax Mine, Nevada National Security Site, Nye County, Nevada*, Rev. 0, N-I/28091-091. Las Vegas, NV.

OTA, see U.S. Congress, Office of Technology Assessment.

Pawloski, G.A. 1999. *Development of Phenomenological Models of Underground Nuclear Tests on Pahute Mesa, Nevada Test Site—BENHAM and TYBO*, UCRL-ID-136003. Livermore, CA: Lawrence Livermore National Laboratory.

Peterson, E., P. Lagus, and K. Lie. 1977a. *Summary of the DINING CAR Tracer-Gas Chimney Pressurization Studies,* SSS-R-77-3185. Prepared for the Defense Nuclear Agency. La Jolla, CA: Systems, Science and Software.

Peterson, E., P. Lagus, and K. Lie. 1977b. *Summary of the MING BLADE Tracer-Gas Chimney Pressurization Studies,* SSS-R-78-3535; DNA 4491T. Prepared for the Defense Nuclear Agency. La Jolla, CA: Systems, Science and Software.

Peterson, E., P. Lagus, and K. Lie. 1978. *Summary of the MIGHTY EPIC Tracer-Gas Pressurization Studies,* SSS-R-78-3542; DNA 4492T. Prepared for the Defense Nuclear Agency. La Jolla, CA: Systems, Science and Software.

Sutton, M. 2009. *Review of Distribution Coefficients for Radionuclides in Carbonate Minerals.* LLNL-SR-415700. Livermore, CA: Lawrence Livermore National Laboratory.

U.S. Congress, Office of Technology Assessment. 1989. *The Containment of Underground Nuclear Explosions,* OTA-ISC-414. Washington, DC: U.S. Government Printing Office.

U.S. Department of Energy, National Nuclear Security Administration Nevada Field Office. 2014. *Nevada National Security Site Integrated Groundwater Sampling Plan,* Rev. 0, DOE/NV--1525. Las Vegas, NV.

U.S. Department of Energy, National Nuclear Security Administration Nevada Field Office. 2015. *United States Nuclear Tests, July 1945 through September 1992,* DOE/NV--209-REV 16. Las Vegas, NV.

Winograd, I.J., and W. Thordarson. 1975. *Hydrogeologic and Hydrochemical Framework, South-Central Great Basin, Nevada-California, with Special Reference to the Nevada Test Site*, Professional Paper 712-C. Washington, DC: U.S. Geological Survey.

Zavarin, M., P. Zhao, C. Joseph, J. Begg, M. Boggs, Z. Dai, and A. B. Kersting. 2015. *Hydrothermal Alteration of Glass from Underground Nuclear Tests: Formation and Transport of Pu-Clay Colloids at the Nevada National Security Site,* LLNL-TR-671402. Livermore, CA: Lawrence Livermore National Laboratory.

1.0 INTRODUCTION

The Yucca Flat/Climax Mine (YF/CM) flow and transport document (N-I, 2013a) presented the ensemble of contaminant boundary forecasts required in Section 3 of Appendix VI of the *Federal Facility Agreement and Consent Order* (FFACO) (1996, as amended). Following the FFACO process, an external peer review of this document and supporting data was completed by the YF/CM Peer Review Committee (PRC) over a one-year period during fiscal year (FY) 2014 and FY 2015, and was reported in *External Peer Review Team Report for Corrective Action Unit 97: Yucca Flat/Climax Mine, Nevada National Security Site, Nye County, Nevada*, Rev. 1 (N-I, 2015).

The remaining step in the CAI stage is the determination by the Nevada Division of Environmental Protection (NDEP) on whether the model is acceptable for completing the Corrective Action Investigation (CAI) stage and initiating the Corrective Action Decision Document (CADD)/Corrective Action Plan (CAP) stage of the strategy (FFACO, 1996 as amended).

To support NDEP's decision, the YF/CM PRC made the following statement (N-I, 2015; p. 5-1):

> *The peer review team commends the N-I team for its efforts in using limited data to model the fate of radionuclides in groundwater at Yucca Flat. Recognizing the key uncertainties and related recommendations discussed in Section 6.0 of this report, the peer review team has concluded that DOE is ready for a transition to model evaluation studies in the CADD/CAP stage.*

The PRC qualified the recommendation to move from the CAI stage into the CADD/CAP stage of the Underground Test Area (UGTA) strategy with the caveat that the uncertainties and associated recommendations identified in the PRC report (N-I, 2015) be carefully addressed during the CADD/CAP stage. The purpose of this document is to address each PRC recommendation so that sufficient confidence in the contaminant boundary forecasts is established to advance to the CADD/CAP stage and initiate model evaluations. The U.S. Department of Energy (DOE), National Nuclear Security Administration Nevada Field Office (NNSA/NFO) responses, summarized in Table ES-1, include supporting data, illustrative examples, and additional field data and modeling studies when applicable. Supplemental analyses carefully address the uncertainties noted by the PRC,

and demonstrate that the YF/CM model provides fundamental understanding and appropriately bounds the uncertainties in the forecast of radionuclide (RN) migration. The PRC summarized their key concerns and recommendations in a table (N-I, 2015, Table ES-1), and presented discussions of each of these uncertainties (N-I, 2015, Section 6.0). The modeling team presents a summary of their responses in Table ES-1, followed by detailed discussion of each in Section 2.0 of this document (the corresponding subsections in Section 2.0 are noted in the shaded rows in Table ES-1). The headings of the subsections in Section 2.0 are selected to be identical to the subsection headings in Section 6.0 of the YF/CM PRC report (N-I, 2015).

Throughout this document, including the appendices, any cavity dimension information (e.g., radius) for detonations where the yield remains classified is derived as follows:

- Based on the maximum yield listed in *United States Nuclear Tests, July 1945 through September 1992,* DOE/NV--209-REV 16 (NNSA/NFO, 2015).
- Calculated using Equation (1) from *Development of Phenomenological Models of Underground Nuclear Tests on Pahute Mesa, Nevada Test Site—BENHAM and TYBO,* UCRL-ID-136003 (Pawloski, 1999).

Equation (1) from Pawloski (1999) is included in Section 2.5.1 of this document.

1.1 Approach to Addressing PRC Comments

The external PRC report (N-I, 2015) touched on many aspects of the flow and transport models developed for YF/CM (N-I, 2013a) and on the adequacy of the supporting datasets (SNJV, 2006a and b; SNJV, 2007) and monitoring networks (NNSA/NFO, 2014). Given the diversity of the issues and concerns they raised, it is inevitable that the modeling team would agree with some comments and recommendations, but not with others. For some of the issues raised by the PRC, the team acknowledges the technical validity of the comment but argues that no action is required because of the overall insensitivity of the contaminant boundary calculations to that particular aspect of the model. That is to say, whereas the PRC comments focused on uncertainties in the model, the team considers both model *uncertainty* and model *sensitivity* in their responses. This latter position recognizes that not all uncertainties identified by the PRC matter equally. Several years of modeling the combined unsaturated zone (UZ), saturated zone (SZ) alluvial aquifer/volcanic aquifer (AA/VA), and SZ lower carbonate aquifer (LCA) systems have produced considerable insight into which aspects of the overall flow and transport system—and which detonations or classes of

detonations—tend to define the contaminant boundaries. The PRC chose not to take advantage of the insights already developed through modeling to prioritize their comments, which if left unclarified by the modeling team would have resulted in a highly unfocused and inefficient set of activities on the part of the team and the UGTA Activity. For example, the need to better characterize the extent of contamination in the LCA by drilling new wells and resampling old wells where low-level tritium (^{3}H) may have been detected decades ago has been a high priority for the UGTA Activity since the peer review was conducted. However, better understanding of the RN release mechanisms from unsaturated, carbonate-rock hosted detonations in the northern part of the basin was identified as technically interesting but ultimately low-impact activity, given the higher sensitivity of the contaminant boundaries to other tuff-confining unit (TCU)-hosted detonations close to the LCA further south in the basin.

During the course of the PRC review and the development of the accompanying report (N-I, 2015), the modeling team pointed out that many of the contaminant boundaries reported in N-I (2013a), could already be demonstrated to overestimate the extent of contaminations based on comparisons with existing RN data from monitoring wells, or through velocity estimates based on naturally occurring carbon-14 (^{14}C) measurements, among other arguments. Considerable insight into the YF/CM flow and transport system has been obtained via the models documented in N-I (2013a) and in this document. The original set of models documented in the N-I (2013a) was intended to explore a broad range of parameters and conceptual models to increase the likelihood that the true contaminant boundary would lie within the ensemble of contaminant boundaries. The intention was that the broad range of calculated outcomes could then be narrowed by comparing models with existing data or by collecting additional data in the model evaluation phase of the CADD/CAP stage.

In instances where the modeling team believed that the concerns of the PRC could be efficiently investigated with existing models or with simple new models, the team ran these simulations to explore the impact of the suggested parameter changes or conceptual models recommended by the PRC. However, this does not imply that the team endorses the proposed approach or parameter set; in many cases, these models were run solely to provide objective evidence that even with a much different set of model parameters or conceptual models, the response of the flow and transport system is robust enough that the simulated outcomes based on these hypothesized parameters or concepts are similar to those already presented in N-I (2013a).

2.0 KEY UNCERTAINTIES

The YF/CM PRC identified what they believed to be key uncertainties associated with the YF/CM flow and transport model and made recommendations on how to address these uncertainties (N-I, 2015). This section provides the NNSA/NFO response to the PRC recommendations. The numbering of the section titles below mimics Section 6.0 and Appendix H of the PRC report. For example, Section 2.1.1 corresponds to the Section H.6.1.1 from the external peer review document section titles. For each section and subsection, a few sentences in the beginning summarize the subject area of uncertainty, followed in italics by the corresponding recommendation from Appendix H, and then the response to the recommendation by the modeling team. The response to each uncertainty consists of a leading summary paragraph followed, where appropriate, by more detailed discussions. Activities conducted in response to the PRC recommendations included new model runs; new field data analysis; and inclusion of a few older data that address the perceived shortcomings of the original flow and transport models, and explore the impact of the uncertainty on the contaminant boundary extent (N-I, 2013a).

The modeling team has compared solute transport and travel velocities for alternate conceptualizations against those from the base-case model. In some cases, the 95th percentile contaminant boundaries were compared. However, in order to minimize the computational burden, a comparison between models was performed in some cases using advective particle tracking by releasing 500 particles at each of the 39 sources (located at 39 underground tests within 3 cavity radii [R_c] of the SZ LCA) and counting the number of particles crossing an east–west line near the southern model boundary. The particle tracking was run for 1,000 years using non-sorbing and non-decaying particles. The porosity used in the particle tracking was assumed to be 0.0045, which is the mode of country rock fracture porosity used for the SZ LCA transport modeling in N-I (2013a). This number of particles is a measure of the advective particle transit times from source locations to the boundary for a selected value of porosity, but does not include transport mechanisms such as diffusion, dispersion, sorption, or radioactive decay. Care must be exercised when interpreting the particle breakthrough as a surrogate for the 1,000-year contaminant boundary calculations; slower transport prior to 200 years is significant for the contaminant boundary because ^{3}H is largely removed by radioactive decay after 200 years.

A drilling campaign was conducted in Yucca Flat to drill three wells, each in the vicinity of a medium- to large-yield nuclear detonation deeply buried near the LCA. The locations of these wells were selected to investigate the hydraulic properties of the alluvium, the tuff and LCA, the size and geometry of the exchange volume, RN transport mechanisms within and between the tuffs and the LCA, and the degree of RN contamination in the LCA near the detonations (Kwicklis, 2015). Preliminary information from these wells demonstrates that the YF/CM base-case flow and transport models (N-I, 2013a) are conservative and is used to address several PRC comments.

2.01 Review and Conservative Nature of the LCA Base-Case Model

The model-forecast contaminant boundary for the YF/CM Corrective Action Unit (CAU) is controlled by the extent of contamination calculated for the LCA and, accordingly, the majority of the PRC comments were in regards to the LCA. This section describes the LCA model base case and conservative nature of the base case. The philosophy adopted for the Phase I LCA groundwater flow model was to be conservative in the modeling assumptions when they are likely to affect the forecast extent and magnitude of RN transport, especially when data are sparse or may be subject to alternative interpretations. The goal of the LCA modeling was to develop a range of reasonable groundwater flow fields that reproduce the observed steady-state and transient water-level observations and do not underrepresent the possible extent of contaminant migration. Given this goal, overestimating the transport was acceptable to the modeling team for the CAI stage.

The basic assumptions of the Phase I LCA groundwater model are as follows: (1) The properties are homogeneous within a geologic feature or permeability zone. (2) Each model fault contains three hydraulic zones: a central gouge zone (fault core) and two damage zones on either side of the central gouge zone. (3) The faults are expected to have much greater permeability parallel to their strike and low permeability perpendicular to their strike because of the presence of higher permeability in the fault damage zone and low permeability in the fault core zones. (4) The flow system is in steady state. (5) The spatial resolution of permeability contrasts is limited to the grid scale analyzed, which has a minimum spacing of about 125 meters (m). (6) The spatial distribution of vertical recharge is as identified in the UZ and SZ AA/VA system models, and in the Death Valley Regional Flow System (DVRFS) model in areas of the LCA not directly overlain by either of these two models.

Uncertainty exists in all aspects of the LCA flow model. Significant structural uncertainty exists in the hydraulic continuity of the LCA in the northern portion of the Yucca Flat basin as well as

vertical/lateral influx into the model study area. The calibration of the LCA flow model used both the steady-state heads and transient drawdowns observed during the ER-6-1-2 multiple-well aquifer test (MWAT) to support estimation of the boundary fluxes and permeability of the faults and the LCA country rock. The base-case calibration conservatively assumed that there is hydraulic continuity in the LCA in the northern portion of the Yucca Flat basin, and the calibrated northern boundary fluxes were found to range from about 50 to about 400 kilograms per second (kg/s) (with the base-case value of 130 kg/s). The total fluxes into the model were found to range from about 150 kg/s to about 500 kg/s (with the base-case value of 268 kg/s).

The northern boundary flux in the existing literature ranges from less than 1 kg/s (Winograd and Thordarson, 1975) to more than 1,000 kg/s (Pohlmann et al., 2007). Lateral flow and local recharge have been estimated as 1,000 acre feet per year (acre-ft/yr) (40 kg/s) (Harrill et al., 1988) or less (Winograd and Thordarson, 1975). For the base-case model calibration, the upper limits for this boundary were set at 500 kg because the entire discharge in the Ash Meadows basin (which includes contribution from several other sub-basins in addition to Yucca Flat) is estimated to be between 700 and 820 kg/s (Laczniak et al., 1999).

Uncertainty of the boundary fluxes has decreased since the Phase I flow and transport modeling was performed. The large fluxes in the literature are primarily based on the large-scale DVRFS model (Belcher et al., 2004). The large flux values from the DVRFS model have been acknowledged as being erroneous for application to the smaller-scale Yucca Flat Phase I model (Halford, 2009). Fenelon et al. (2016) estimated an annual recharge volume of 1,200 acre-ft/yr (47 kg/s) for the Yucca Flat hydrographic area using the Maxey-Eakin method. Halford (2016) used the Maxey-Eakin regional water-budget tool from Fenelon et al. (2016, Appendix B), and estimated a minimum and maximum recharge of 700 and 1,500 acre-ft/yr (27 and 59 kg/s) to the Yucca Flat hydrographic area. This range of recharge is generally consistent with previously published regional water budgets and conceptual models of relative water availability (Winograd and Thordarson, 1975; Harrill et al., 1988). Fenelon et al. (2016) report Yucca Flat sub-basin discharge of about 1,000 acre-ft/yr. The Phase I flow and transport model (N-I, 2013a) likely overestimates the total flow and groundwater velocity through the Yucca Flat LCA primarily by overestimating the boundary fluxes.

Considerably lower flux values than those reported for the base case (N-I, 2013a) model have resulted from the reanalysis of the results of ER-6-1-2 MWAT conducted in 2004 (SNJV, 2005a). Formal

documentation of the reanalysis of ER-6-1-2 MWAT (Halford, 2009, 2012, and 2016) is being planned as a specific uncertainty reduction activity during the CADD/CAP stage. The flux through the high-transmissivity eastern corridor of Yucca Flat between Wells ER-7-1 and ER-6-1-2 was estimated to be approximately 19 kg/s (Halford, 2016), or about 10 times lower than the simulated boundary flux of 189.6 kg/s that was calculated to flow through the same part of the LCA in the base-case model documented in N-I (2013a). Based on flow directions provided in Plate 4 of Fenelon et al. (2012), this flux represents the following: (1) the combined inflow through the northwestern part of the basin from Rainier Mesa, and through or beneath the Eleana Range on the west; (2) flow from the north through Climax Stock and associated contact-metamorphosed zones as well as faulted slivers of LCA; (3) flow through the clastic rocks of the Half-Pint range on the northeast and east; and (4) and drainage from the shallow alluvium and volcanic rocks. Because the gradient of 8.3×10^{-05} ft/ft between ER-7-1 and ER-6-1-2 in this corridor has less than a 5 percent coefficient of variation, the dominant uncertainty is associated with the transmissivity-width product ($0.7 \times 10^{+09}$ cubic feet per day [ft^3/day]), which could differ by a factor of 2, leading to an estimated uncertainty range in flux of 9.5 to 38 kg/s. This limit on flux through the high-transmissivity eastern corridor suggests that several models documented in N-I (2013a)—including the base case and many Null Space Monte Carlo (NSMC) results with northern boundary fluxes greater than 50 kg/s—are unrealistic. Preliminary simulations using these realistic flux values (see Section 2.1.2) led to 95 percentile contaminant boundary forecasts that were well north of the southern boundary of the model. These new preliminary models will be explored more fully during the model evaluation phase of the CADD/CAP stage.

Another set of observations that demonstrates the conservatism of the contaminant boundaries in the current ensemble of contaminant boundaries given in N-I (2013a) is the near-field measurements of ^{3}H, ^{90}Sr, and ^{137}Cs measured in groundwater at the NASH satellite Well UE-2ce over several decades. NASH was a 39-kiloton (kt)-yield test detonated on January 19, 1967, in the unsaturated LCA3 about 2.6 R_c above the water table (NNSA/NFO, 2015; N-I, 2013a, Table B-1). The UE-2ce well is 183 m south of the NASH working point; was intermittently pumped between 1977 and 1984, and again in 2008; and was bailed at other times. The RN recovery data from Well UE-2ce show that although ^{3}H exceeded more than 1,000 times its maximum contaminant level (MCL) during pumping, ^{90}Sr and ^{137}Cs never exceeded their MCL, despite being estimated to be more than 10^{+05} times their MCL in the carbonate source term (N-I, 2013a, Figure 2-6). This suggests that ^{90}Sr and ^{137}Cs are attenuated by sorption in the field, which significantly slows their migration relative to ^{3}H. Therefore, contaminant

boundaries calculated on the assumption that ^{90}Sr and ^{137}Cs do not sorb in carbonate rock should be considered conservative.

Newly drilled Wells ER-2-2, ER-3-3, and ER-4-1—located within 2.5 to 3 R_c of the CALABASH, WAGTAIL, and STRAIT detonations (cavity dimensions based on maximum announced yield [NNSA/NFO, 2015] and Equation 1 in Pawloski [1999])—were observed during drilling to have ^3H concentrations below the minimum detection limit (MDL) (1,500 to 1,800 picocuries per liter [pCi/L]) in the LCA, despite either being within 2 R_c of the SZ LCA (STRAIT) or within 2 R_c of faults (WAGTAIL and CALABASH). These observations, combined with a reexamination of ^3H and head data from the BILBY post-shot well (U-3cn PS 1) and satellite well (U-3cn 5), indicate the exchange volume radius beneath large-yield, deeply buried tests is less than 2 R_c, and that permeable fracture pathways created by the detonations themselves do not extend 2 R_c or more beneath the working points of these detonations. The ^3H concentrations below the MDL (1,500 to 1,800 pCi/L) in the LCA beneath the STRAIT detonation—and the evidence that no ^3H plume is present at ER-3-3 despite being downgradient of scores of deeply buried detonations near the Yucca fault (including seven within 2 R_c of the SZ LCA [cavity dimensions based on maximum announced yield (NNSA/NFO, 2015) and Equation 1 in Pawloski (1999)])—together confirm the generality of the BILBY observations that the TCU is an effective barrier that prevents most, if not all, radioactivity from reaching the LCA. Thus the use of $3R_c$ in determining the potential contaminant sources to LCA is likely conservative.

In the current document, the “base-case” model reported in N-I (2013a) is used as a representative case with which other models and associated flow and transport results can be compared. The base case is one of the several models that are consistent with the hydrologic observations pertaining to Yucca Flat but is not presumed or inferred to be the “best” or “most reasonable” flow model. It is simply the model against which other models based on different assumptions are compared.

2.1 Uncertainty in Model Domain/Boundary Conditions

2.1.1 Western Boundary

This uncertainty focuses on the model prediction that flow direction in some areas of the western part of the system is northerly, which the PRC states is opposite to the direction presented in the conceptual model and opposite to the flow simulated by the regional model of the DVRFS.

PRC Recommendation: The peer review team recommends inclusion of the Rainier Mesa area in the model and use of head data from that area as calibration targets (including the semi-perched springs that reflect saturated groundwater heads) to improve the representation of the flow field and build confidence in model predictions.

RESPONSE: This uncertainty is addressed effectively by conducting several model studies investigating the influence of recharge from the Rainier Mesa area (the northwest boundary flux in this model) on the results of the transport model. It was found that these simulations led to less extensive transport results compared to the base case but did not eliminate the northerly flow in the northwestern part of the model. These modeling studies are discussed below.

One of the concerns expressed by the PRC (N-I, 2015, Section 6.1.1) was that the direction of flow in some areas of the western part of the flow model is to the north, which is opposite to the direction presented in the regional model of the DVRFS. It is important to note that both the model simulations (N-I, 2013a, Figure 5-47) and the hand-drawn contours of the available head data (Fenelon et al., 2012, Plate 4) indicate that the overall flow direction is west to east in the western half of the Yucca Flat basin. However, some local north–south flow is not a contradiction to this large-scale picture, because regional models use a large-scale representation of the flow system, while local models represent smaller-scale processes that often reflect more variability and heterogeneity. The occurrence of a localized northerly component of flow is consistent with the Yucca Flat well data in the west–central portion of the model domain. Well data control the outcome of the parameter estimation process with respect to the calibrated flow field. For example, comparison of the heads at Wells UE-10j (2,416 feet [ft]) and WW-2 (2,417 ft) in the northern portion of the model with Wells TW-D (2,427 ft) and UE-1q (2,426 ft) in the central portion of the model indicates a northerly head gradient.

The water levels in the VA units surrounding Yucca Flat to the west, north, and northeast are much higher than those in the LCA of the central portion of Yucca Flat. In the northwest, Well ER-12-2 in

the upper clastic confining unit (UCCU) has heads higher than 4,528 ft, and White Rock Spring (a perched spring) has head above 4,800 ft. To the north, Climax Stock areas have heads in the range of 4,800 to 5,000 ft above sea level (asl). To the northeast, heads in the UCCU are 3,900 ft asl (UE-15d WW) to 4,300 ft asl (UE-15j). However, the LCA wells in the northern portion of the model (i.e., UE-10j, WW-2) and UCCU/LCA wells (i.e., UE-10 ITS5) have heads in the range of 2,400 to 2,500 ft. The distances between the higher and lower head areas are about 1 to 3 miles (mi), indicating hydraulic gradients in the range of 0.1 to 0.3. However, within the northern part of LCA—between UE-10j with a head of about 2,416 ft, and U-7a with a head of approximately 2,480—the gradient is 8×10^{-04}, or 100 to 200 times lower. This is consistent with the conceptual model that the northern portion of Yucca Flat is surrounded by low-permeability rocks (UCCU) that even with higher heads limit the total amount of water that can flow into the northern—and, by way of similar argument—western, and eastern portions of Yucca Flat. Very little water flow is expected within or on top of the UCCU as evidenced by the four Effinger wells located in the small breach in the Eleana Range where the Rainier Mesa and Tippipah Highways meet and pass into the Area 12 Camp. The four Effinger wells were all dry, suggesting no perched or flowing water at the alluvium/Eleana contact in the breach area (Moore, 1962).

Several flow model simulations were developed to clarify how the northwestern boundary condition impacts the occurrence of northerly flow in the model. One set of simulations considered the influence of flow across the northwestern boundary adjacent to Rainier Mesa (a no-flow boundary in the base-case model because of the presence of the UCCU). The original no-flow approximation was relaxed and replaced by a flux boundary that is constrained by estimated recharge rates on the eastern side of Rainier Mesa. Another set of simulations sought to increase flow across the major faults (Carpetbag, Topgallant, and Yucca), thus increasing easterly flow and reducing local northerly and southerly gradients by using flow direction as a calibration target in western Yucca Flat. Lastly, simulations were performed using head data extrapolated from the U.S. Geological Survey (USGS) Scientific Investigations Report 5196 (Fenelon et al., 2012) as calibration targets. Note that these simulations and others discussed throughout this document examine the influence of alternate interpretations of the data on RN transport and do not represent a change in the base model.

The simulations are as follows:

1. *Northwest recharge as the total net infiltration (47 kg/s) occurring in the area east of the Eleana range divide and west of the LCA model's western boundary.* The net infiltration rates were extracted from the Rainier Mesa Infilv3 model (N-I, 2013b). The value of 47 kg/s represents an upper limit of the possible recharge from the area east of the Eleana range topographic divide. In this area, the UCCU has an eastern dip toward Yucca Flat. While this value is higher than the estimate of total flow from the eastern part of Yucca Flat, such as the 19 kg/s estimate based on the MWAT data (Halford, 2016), it is being used here as an upper bound on the recharge available from the west.

2. *Northwest recharge estimated during the calibration process by scaling the total recharge extracted from the Rainier Mesa Infilv3 model while maintaining the same relative spatial recharge distribution as the 47 kg/s case listed in (1) above.* Note: Estimating the northwest recharge as a calibration parameter produced a low recharge value of 0.72 kg/s.

3. *Considering flow direction as a calibration parameter.* The northerly flow component in the LCA model primarily occurs within the LCA central and the Carpetbag fault zones. The velocity in each node within these zones is evaluated and, if a northern flow component is present, an error term is calculated that penalizes the objective function.

4. *Using gridded points created from the LCA head contours from USGS Scientific Investigations Report 5196 (Fenelon et al., 2012).* The gridded data were exported on a uniform 4-kilometer (km) grid in areas of less than 0.003 gradient and on a 1-km grid in areas of greater than 0.003 gradient, thereby providing 201 calibration points to enforce the conceptual model in Fenelon et al. (2012). Figure 2-1 illustrates the location of the points and calibrated head field. The figure also shows the head residuals (black numbers) at the observation wells.

To assess the effect of alternate flow models on transport, particle tracking originating from the 39 tests identified to have exchange volumes within 3 R_c of the SZ LCA was run on each of the calibrated flow fields described above using the parameters and procedures described in N-I (2013a). The particle tracking was run for 1,000 years using non-sorbing and non-decaying particles. The porosity was assumed to be 0.0045, which is the mode of country rock fracture porosity used for the SZ LCA transport modeling in N-I (2013a). The percentage of particles crossing a hypothetical east–west fence at northing 4,090,000 m (4.5 km north of the LCA model's southern boundary) provides an integrated estimate of the number of particles transferred across the entire LCA model domain along the particle pathways, as a percentage of the total number of particles from all source locations. These results do not represent RN transport because the important attenuation mechanisms of radioactive decay, sorption, and matrix diffusion are not simulated.

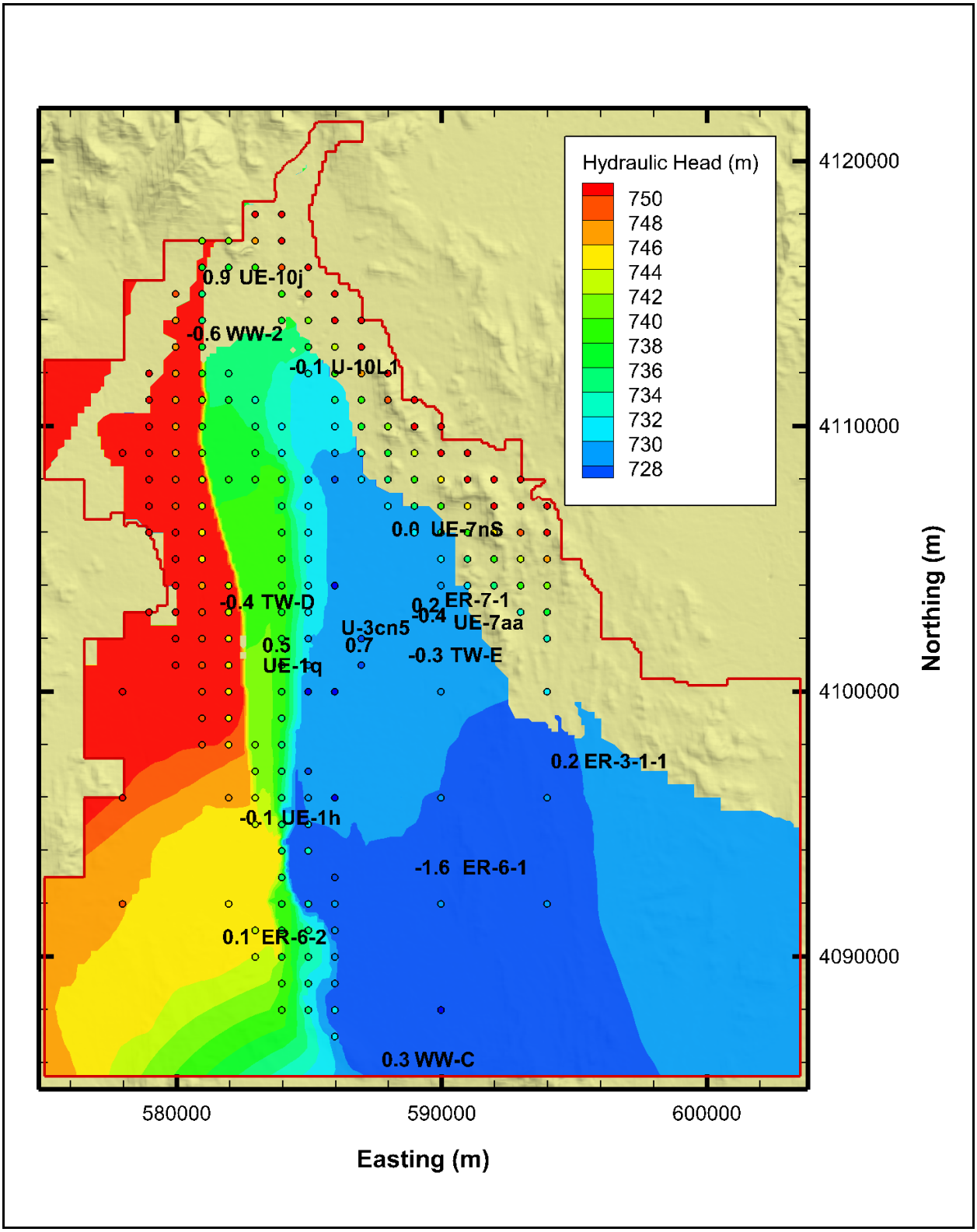

Figure 2-1
Point Locations and Calibrated Head Field at -1,000 m amsl and Steady-State Head Residuals for the Gridded Contour Model Calibration
Note: Head residuals at observation wells are shown in black.

Table 2-1 summarizes the results for recalibrated models evaluating the western boundary compared to the base case. An objective function value of 20.0 or smaller was selected to determine whether LCA model recalibrations are acceptable and realistic compared to the observation data. An objective function of 20.0 approximately translates to a root mean square (RMS) error that is 5 percent of the range in steady-state heads and ER-6-1-2 MWAT drawdowns. Using this criterion, all simulations produce acceptable calibrations.

Table 2-1
Summary of Simulations Investigating Western Boundary Uncertainty [a]

Simulation	Objective Function	Percentage of Particle Breakthrough within 1,000 Years	Calibration Summary
Base case	1.15	64	• This is a baseline metric to evaluate the influence of alternate flow simulations.
Fixed 47 kg/s northwest boundary recharge. Note that this value represents the upper limit of recharge expected from Rainier Mesa.	1.16	79	• Northern flow in western Yucca Flat is still present. • There is increased transport from western Yucca Flat eastward toward Yucca fault. • Particles from NASH will reach Area 6 in southern Yucca Flat within 1,000 years. • Total particle breakthrough is moderately increased compared to the base case.
Calibrated northwest boundary recharge (0.72 kg/s)	1.18	69	• Northern flow in western Yucca Flat is still present. • Total particle breakthrough is slightly increased compared to the base case.
Flow direction calibration	11.6	63	• Northward flow in LCA central and Carpetbag fault zones is still present. • Transport is essentially the same as the base case. • There is increased objective function due to model trade-offs between matching heads in southwest Yucca Flat wells and conceptual model requirements to reduce the northerly flow.
Calibration using gridded contour-points	6.78	35	• Northern flow in western Yucca Flat is still present. • Heads are higher in western Yucca Flat compared to the base case. • Transport is much slower due to reduced total flow through the model (128 kg/s) compared to the base case (268 kg/s) and decreased LCA east zone country rock permeability compared to the base case.

[a] Note that the percent particle breakthrough reflects only advective transport, without the effects of attenuation mechanisms such as radioactive decay, matrix diffusion and sorption.

Figure 2-2 illustrates breakthrough curves for the flow fields investigating western boundary uncertainty. Among these simulations, the recalibrations using a fixed 47 kg/s recharge and gridded-contour points have distinctly different flow fields and transport behaviors compared to the base case (Figure 2-3). For the simulation including a 47 kg/s northwest boundary recharge, the transport from detonations located in western Yucca Flat is increased, and total particle breakthrough at 1,000 years is increased due to the additional recharge. For the simulation using gridded calibration points, the flow and transport primarily occurs in faults, and total particle breakthrough is approximately one-half of that from the base case. This is because the LCA east country rock permeability is reduced approximately 2 orders of magnitude, and total flux into the model is reduced by a factor of 2. (Section 2.7.4 presents the contaminant boundaries from additional flow fields that are used to evaluate transport uncertainty.) The southern extent of the contaminant boundary for the 47 kg/s northwest recharge flow field is not significantly different from the base case because the majority of the YF/CM detonations are located in east–central Yucca Flat. The transport for the gridded contour-point case is slower compared to the base case.

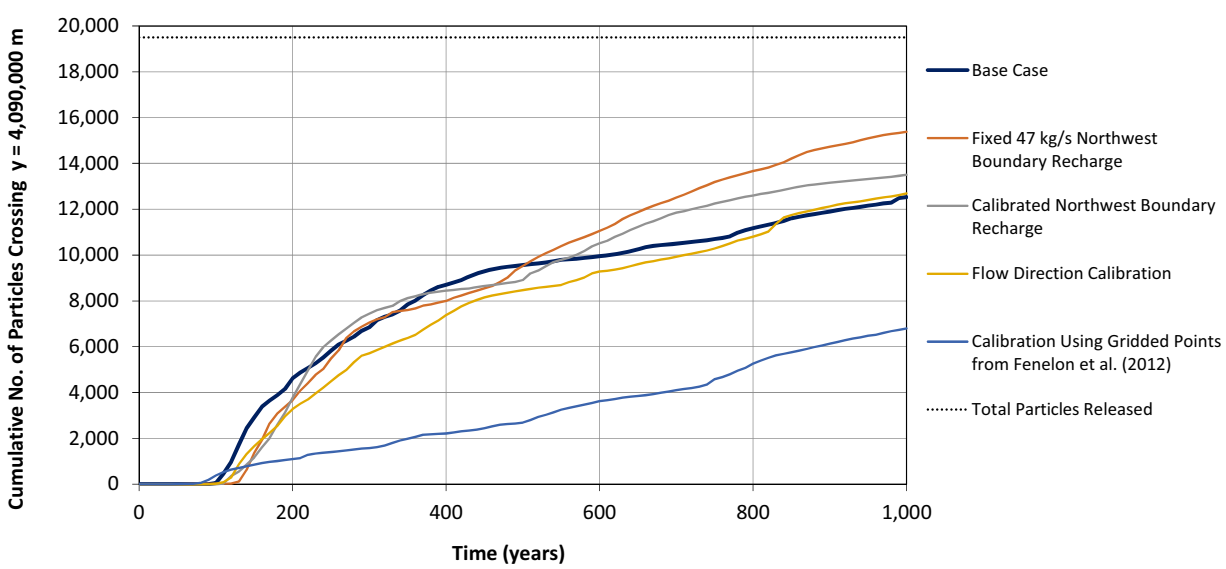

Figure 2-2
Breakthrough Plots for LCA Flow Fields Investigating Western Boundary Uncertainty

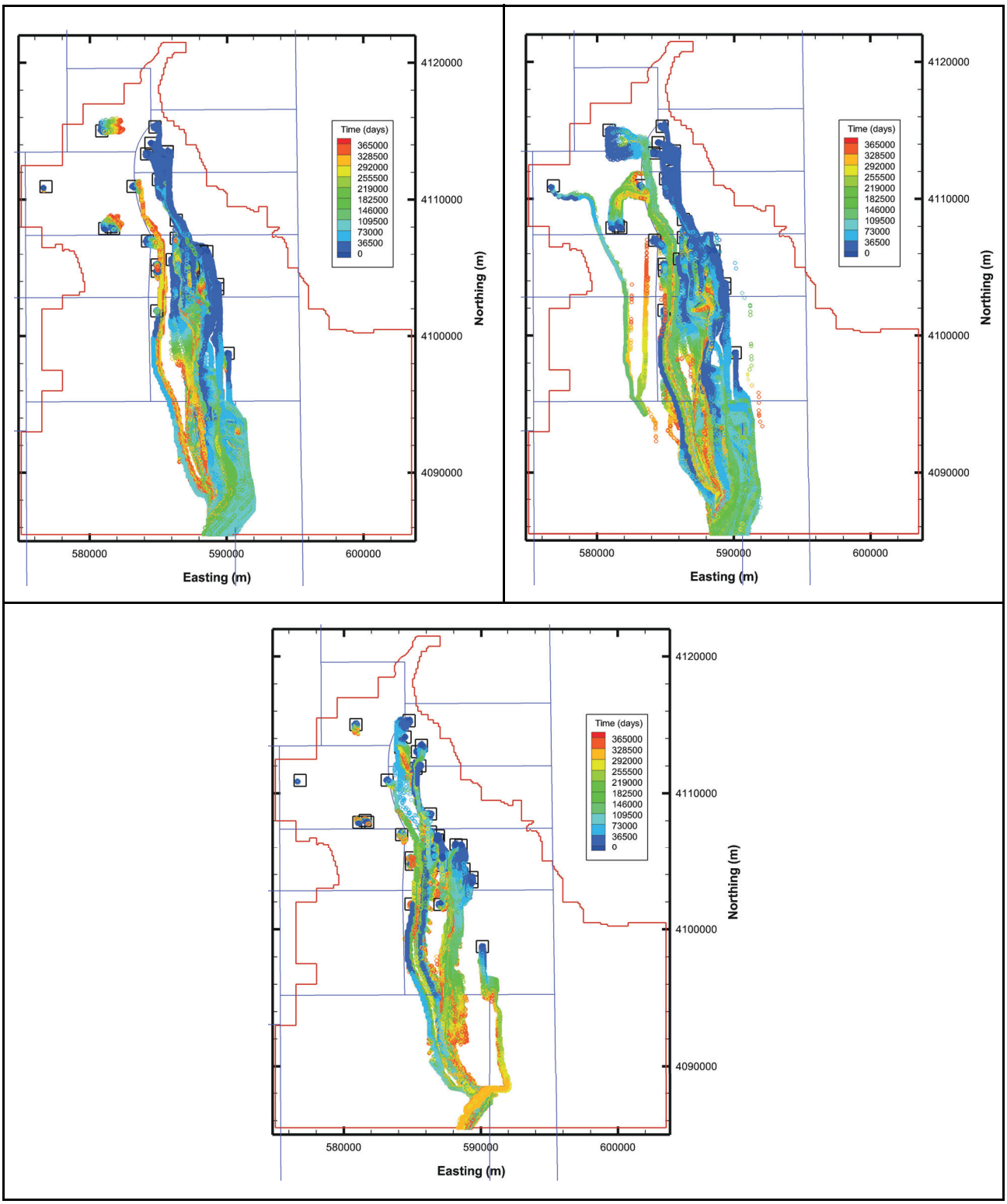

Figure 2-3
Particle Travel Paths and Times for the Base-Case (upper left), 47 kg/s Northwest Recharge (upper right), and Gridded Contour-Point (center) Flow Fields

In summary, the results of four scenarios for the western boundary show that the forecast contaminant boundary is within the uncertainty bounds determined from the models presented in N-I (2013a). The northward flow in north–central Yucca Flat is imposed by the calibration data and the conceptual model of the LCA as being permeable and homogeneous in large north–south-oriented zones. The higher observed heads in the southern LCA central zone compared to the northern LCA central zone generate the northward flow.

2.1.2 Southern Boundary

The concern under this uncertainty is that some simulations predict the southern extent of the contaminant boundary to fall beyond the model domain.

PRC Recommendation: The peer review team recommends that to better delineate the full extent of the contaminant boundary, future model simulations should extend the domain farther to the south to capture all areas where there is greater than a 5 percent probability of exceeding the maximum contaminant level (MCL).

RESPONSE: The current southern model boundary is sufficient because, as discussed below, transport is overpredicted by those simulations where the southern boundary was impacted. This is supported by the absence of observed ^{3}H levels above the *Safe Drinking Water Act* (SDWA) MCL (CFR, 2015) (20,000 pCi/L) at the LCA wells in the high-permeability eastern corridor located along simulated pathways that impact the southern boundary (e.g., U-3cn 5, ER-7-1, and UE-7nS). The base-case model forecasts levels of ^{3}H above the MCL at these wells for the present date. Also, these wells were placed in the vicinity and downstream of detonation locations. The absence of contamination at these wells indicates that the existing LCA flow and transport models overpredict transport. This is consistent with the preliminary data from the Wells ER-2-2, ER-3-3, and ER-4-1 located beyond the western margin of the high-permeability eastern corridor, showing the absence of ^{3}H in water from the Yucca Flat LCA in concentrations that exceed the detection limit (DL) (1,000 to 1,500 pCi/L) of the screening method. Recent hydrological analyses support that the base-case model overestimates flow through Yucca Flat (Halford, 2012 and 2016; Fenelon et al., 2016). Two alternate flow models were calibrated using constraints derived from the recent hydrological analyses that limit the water flux through the model domain. The resulting time-cumulative probability of MCL exceedance in 1,000 years from transport calculations for these models is shown in Figure 2-4. The first model uses the constraint that the flux through the

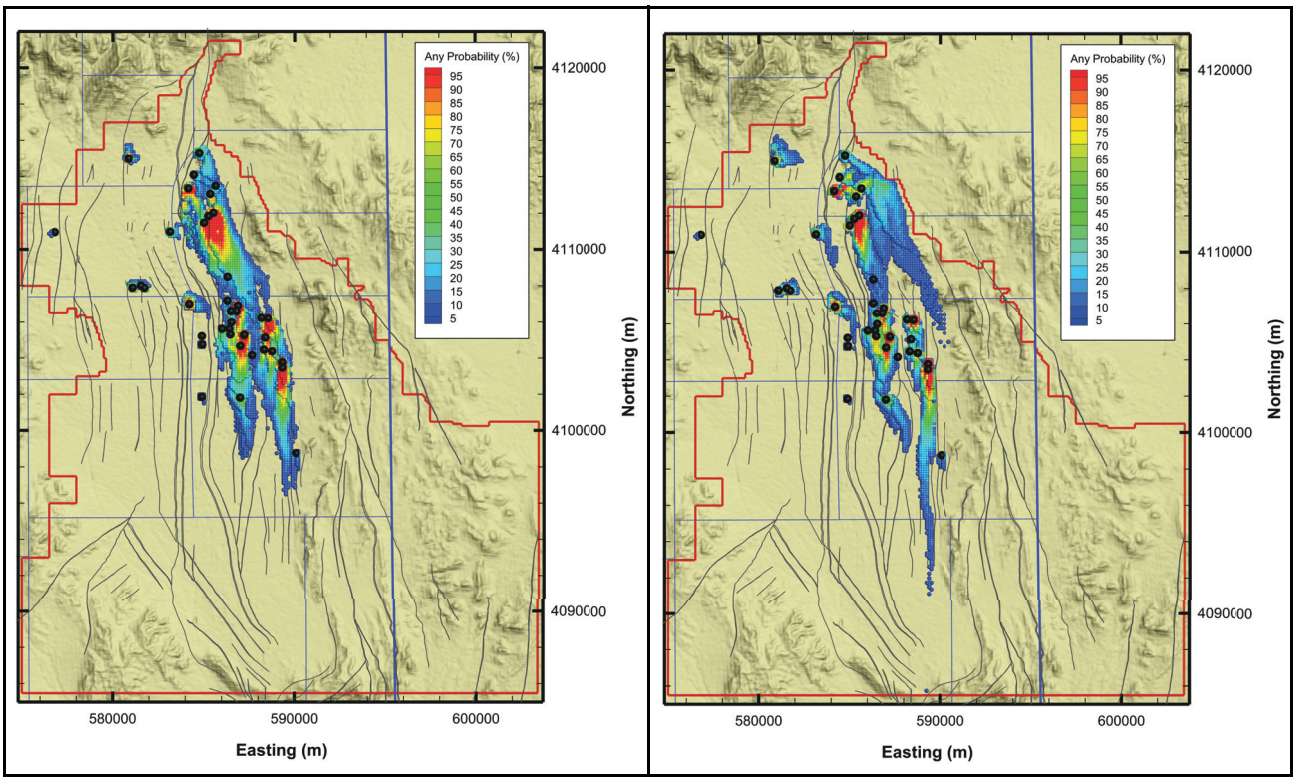

Figure 2-4
Time-Cumulative Probability of MCL Exceedance at 1,000 Years for the Transmissivity-Width Product Flux Constraint (left) and Total Influx Constraint (right) Flow Fields

high-transmissivity corridor through the eastern Yucca Flat is 20 kg/s (500 acre-ft/yr) (Halford, 2016); and the second model uses the constraint that the total inflow of water to the model is 40 kg/s (1,000 acre-ft/yr). Fenelon et al. (2016) report a Yucca Flat sub-basin discharge of about 1,000 acre-ft/yr. The objective functions achieved by the high-transmissivity corridor flux and total flux constraints were 9.1 and 21.2, respectively. These results demonstrate that an acceptable calibration can be achieved using much lower flux values than were used for the base-case model, but further model adjustments are needed to achieve the same degree of calibration that was achieved for the base case.

The horizontal to vertical anisotropy of the LCA country rock and faults was increased compared to the base case, suggesting the actively flowing thickness of the LCA needs to be reduced to match the steady-state head calibration targets with a reduced flux through the model. Both these models forecast 95th percentile contaminant boundaries to be well north of the southern boundary of the model. As noted in the PRC review comments, some transport realizations with the existing base-case

flow model indicate the potential for contaminants in excess of the SDWA MCLs to leave the southern boundary of the YF/CM CAU. However, even with the base-case flow model that is considered to have high flux values, the probability of this is generally less than 10 percent (N-I, 2013a). These realizations represent low-probability (less than 10 percent) cases using tails of the key transport parameters in combination with a flow model that is conservative. The alternative LCA flow model using a 1 kg/s northern boundary flux and the LCA transport models using either alternative strontium (Sr) and cesium (Cs) sorption coefficients, alternative fault damage zone fracture porosities, or alternative scale-dependent matrix diffusion do not result in contaminants in excess of the SDWA MCLs leaving the southern boundary of the model domain (N-I, 2013a).

Identification of initial use restriction (UR) boundaries is one of the regulatory decisions required at the beginning of the CADD/CAP stage. The modeling team believes that the present-day (50-year) contaminant boundary ensemble, which does not extend to the southern boundary (Figure 2-5), can be used to establish initial UR boundaries. Another required regulatory decision is to establish a regulatory boundary objective. The team believes that sufficient confidence exists in the understanding of RN transport from YF/CM tests to determine these objectives. Therefore, the team believes there is no need to extend the southern model boundary given the current understanding of the existing data and modeling results.

The models that predict MCL exceedance at the southern boundary are very conservative in terms of total flow through the LCA and grossly overpredict RN concentrations at observation locations. Less-conservative models, more in line with observed conditions within the LCA, do not forecast MCL exceedance at the model's southern boundary.

2.1.3 Northern Boundary

The concern under this uncertainty is that significant flow from the north is possible and could be an important factor in RN transport out of Yucca Flat.

PRC Recommendation: Multi-well hydraulic testing and water sampling at the northern Yucca Flat boundary should be undertaken to investigate inflow from the north, including the fracture/fault hydraulic properties of rocks that occur along the northern extension of the Boundary/Yucca fault across the topographic divide to the north (Climax Stock, LCA, contact-metamorphosed LCA, and overlying Tertiary volcanic rocks).

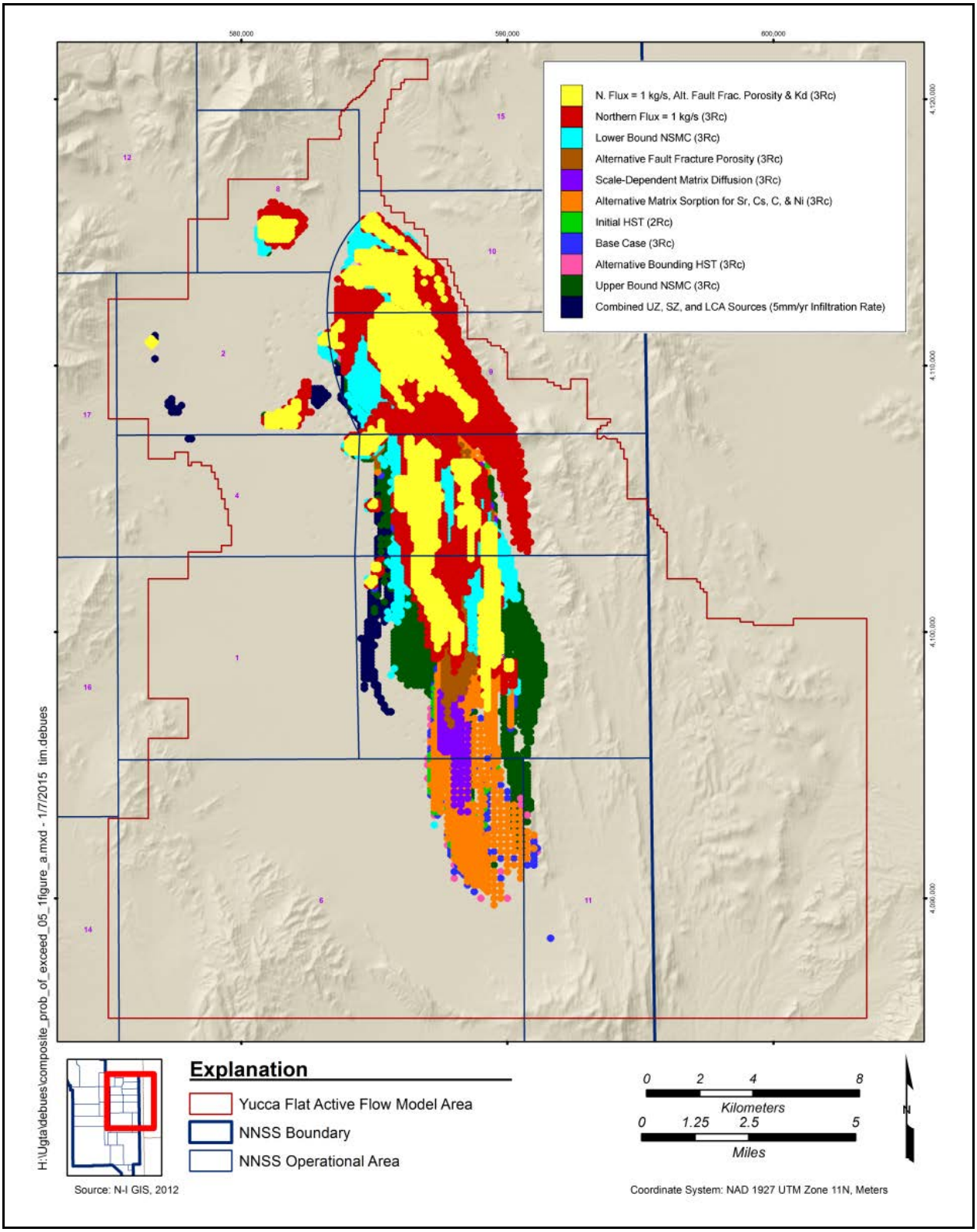

Figure 2-5
95th Percentile Contaminant Boundary Ensemble at 50 Years

RESPONSE: While fracture/fault hydraulic properties do impact the flux, the fully described concern in Section 6.1.3 of the PRC report (N-I, 2015) is focused on the flux through the northern boundary, and not the hydraulic properties of the fractures/faults alone. This uncertainty is effectively addressed by considering the basin-wide flux estimates (Fenelon et al., 2016) and more recent reanalysis of flux through Yucca Flat (Halford, 2012 and 2016) and alternate model studies detailed below.

The modeling team conducted a study to assess the sensitivity of the particle transport and breakthrough near the model's southern boundary to the northern flux. The team found that the breakthrough time at a demarcation line near the model's southern boundary was not sensitive to the northern flux for values in the range of 56 to 403 kg/s; however, if a low flux value of 1 kg/s were used, the particle transport was reduced compared to the base case using a value of 130 kg/s. These are discussed below.

Uncertainty in the lateral influx to the LCA from north of Yucca Flat was also identified by the modeling team in N-I (2013a, pp. 7–9). The NSMC analysis (N-I, 2013a) led to 83 simulations that met the criteria of acceptable calibration using observed steady-state water levels and the ER-6-1-2 MWAT drawdown data. The NSMC analysis resulted in different viable solution sets that each met the objective function criteria with regard to matching the calibration data. The northern boundary fluxes selected by the NSMC analysis were in the range of 56 to 403 kg/s, which is much larger than some of the flux estimations in the published literature—20 kg/s by Harrill et al. (1988) and 1 kg/s by Winograd and Thordarson (1975). The larger fluxes in the N-I (2013a) model were, in part, based on the DVRFS model (Belcher et al., 2004) that is on a much coarser scale than the YF/CM model and lacks the resolution to accurately define local flow conditions within Yucca Flat.

It is expected that better constraining the flux to the northern boundary will greatly reduce the estimates of total flow through Yucca Flat. An estimate of flow through Yucca Flat can be obtained from an analysis of the ER-6-1-2 MWAT. Using the observed water-level responses, the USGS estimated a transmissivity-width product of $0.7 \times 10^{+09}$ ft^3/day for the high-transmissivity eastern corridor in Yucca Flat (Halford, 2016). The hydraulic gradient in this area can be reliably estimated between Wells ER-7-1 and ER-6-1-2 (Figure 2-6) based on head measurements reported for the past six years (2010 to present) on the USGS website (USGS and DOE, 2016). Although the heads at the two wells have varied over time, the head difference between the wells is remarkably constant at

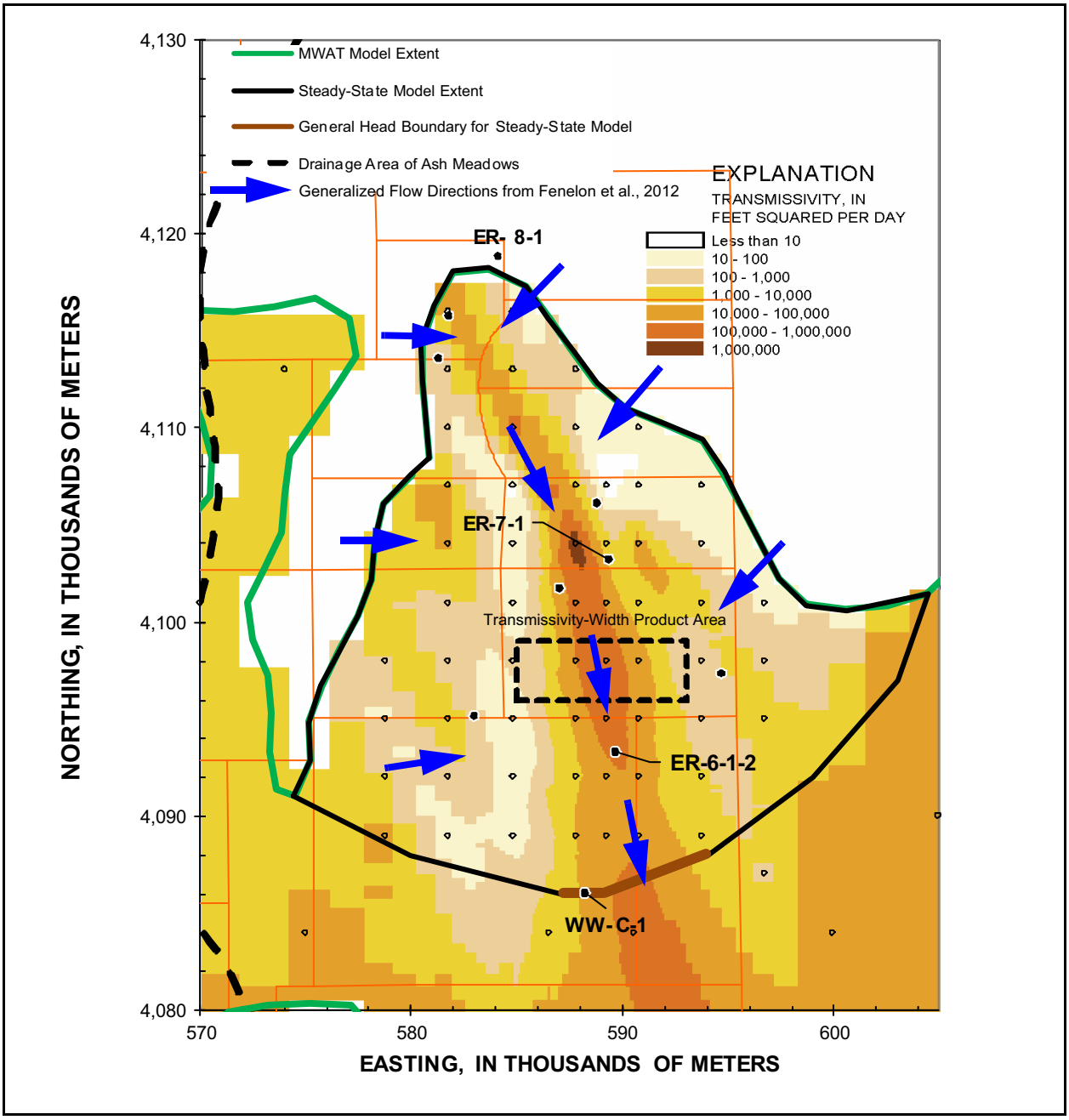

Figure 2-6
Transmissivity-Width Product Location and Simulated Transmissivity
Source: Modified from Halford, 2012

2.715 ft ± 0.11 ft (1 σ) when differences are calculated at similar times. Taking the distance between the wells of 32,674 ft (9,960 m), a gradient of 8.3×10^{-05} ft/ft is calculated.

Multiplying the transmissivity-width product and gradient gives $0.58 \times 10^{+05}$ ft^3/day, which is 490 acre-ft/yr (19 kg/s). This flux moving through the high transmissivity eastern corridor, which

based on Plate 4 of Fenelon et al. (2012), should capture the entire basin flow except for the eastern lateral flow south of ER-3-1, western lateral flow, and precipitation derived recharge in the southwest corner of the basin. Because flow converges in the eastern corridor, flux estimates should incorporate flow from the north, from Rainier Mesa, from most of the western boundary, through the northern Halfpint Range, and include most infiltration from the overlying AA/VA units. Because recharge from the southwest and lateral flow in the southeast do not flow through the testing areas further north, and because the primary interest concerns the groundwater flux that drives transport through the basin, including fluxes in the southwest and southeast corners of the basin is not necessary.

For comparison, the base-case calibration (N-I, 2013a, Table 5-10) calculates that 268 kg/s exits from the basin, which minus the southeast lateral flow (59.3 kg/s), western lateral flow (24.3 kg/s) and top western recharge (19.8 kg/s) yields 164.7 kg/s flowing through the eastern corridor, or roughly eight times that estimated above from the transmissivity-width product of 20 kg/s by Halford (2012) (Figure 2-7). As the calculation indicates, it is likely that the base-case flow and transport model overestimates the groundwater flux through Yucca Flat originating not only from the north but from all lateral flow directions.

To assess the impact of the northern flux on transport, particle tracking was run by releasing 500 particles at each of the 39 sources at the 39 underground tests within 3 R_c of the SZ LCA on each of the NSMC cases (with respect to the base-case calibration) and on the 1 kg/s alternative flow model described in N-I (2013a). The particle tracking was run for 1,000 years using non-sorbing and non-decaying particles. The porosity used in the particle tracking was assumed to be 0.0045, which is the mode of country rock fracture porosity used for the SZ LCA transport modeling in N-I (2013a). The number of particles that crossed the line of demarcation (northing of 409000 m) near the LCA model's southern boundary was counted and used to evaluate the effect of variable northern influx on transport. The particle tracks provide an integrated measure of advective velocity because no other processes such as decay, sorption, matrix diffusion, or dispersion were considered. The results were examined at incremental periods of 100 years up to 1,000 years.

Figure 2-8 illustrates the scatter plots of northern flux vs. percent of particle breakthrough at several time periods between 100 and 1,000 years.The interrelationship between northern flux and incremental particle breakthrough was investigated by calculating the correlation between particle breakthrough and northern flux; the absolute values ranged from a minimum of 0.02 to a maximum of

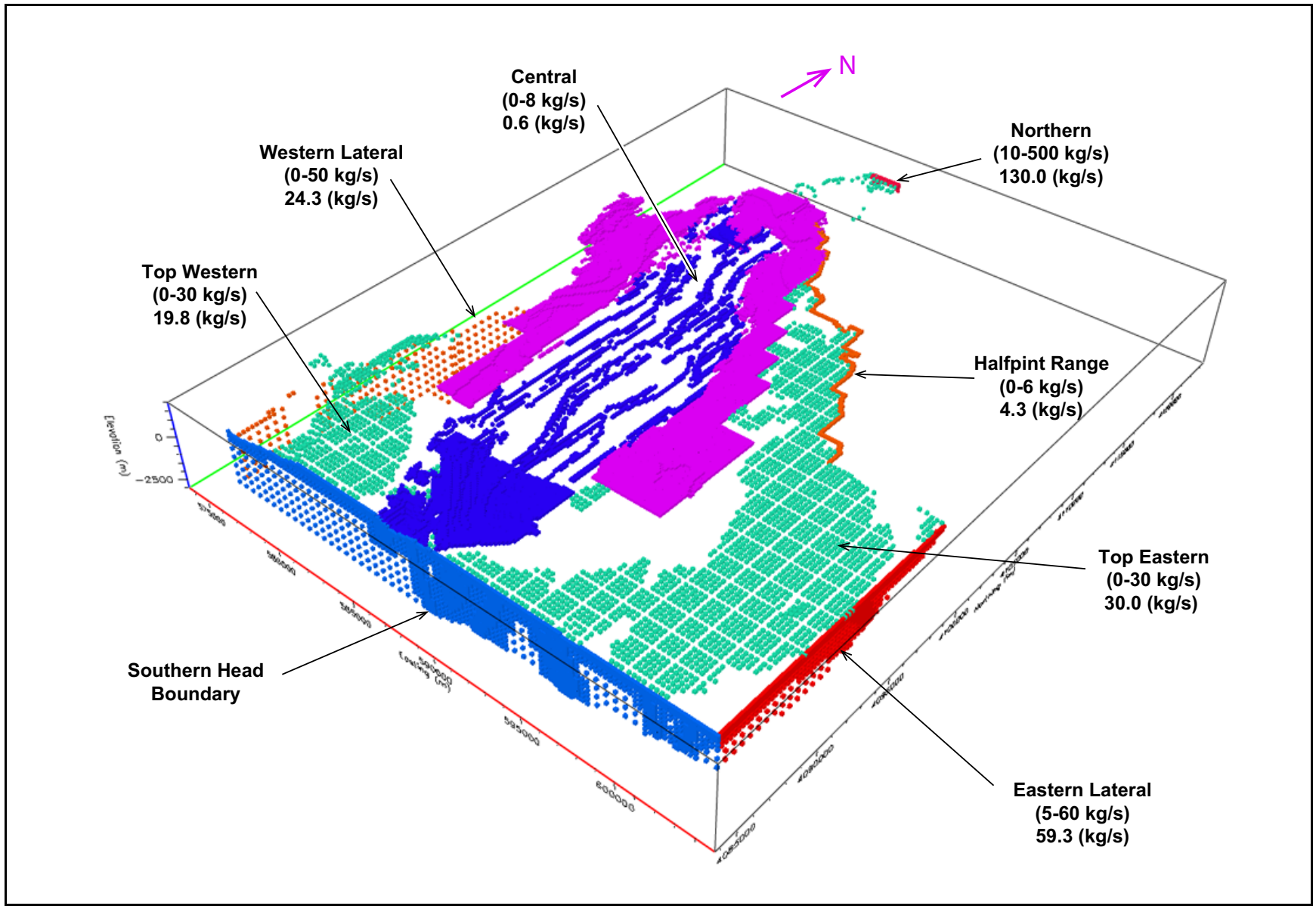

Figure 2-7
Definition of Boundaries for the Yucca Flat LCA Model
Source: N-I, 2013a, Figure 5-32

0.06, indicating the number of particles crossing the boundary is almost completely uncorrelated with the magnitude of the northern flux for the range of values considered in the NSMC analysis (56 to 403 kg/s). This result was surprising, as one would expect flux at a major inflow boundary to have a significant impact on transit times from the source locations to the boundary. Evidently, how flow is routed through the basin and how much flow moves through the areas with deeply buried tests is more important for particle transit times than the overall magnitude of flow through the model. It is the combination of flow through country rock and through the faults that provide a control on RN transport. For detonations located away from major faults, flow through the country rock must first transport RNs away from the source zones to faults before the preferential pathways provided by the faults move RNs through Yucca Flat.

The modeling team also performed a model analysis with the northern influx fixed at the lower value reported in the literature of 1.0 kg/s (Winograd and Thordarson, 1975). Comparing particle transport for this case against the base case (130 kg/s) indicates that transport is much smaller for the 1.0 kg/s case at shorter time scales (i.e., 100 or 200 years), which is more in line with expectations. ^{3}H is by far the largest contributor to the contaminant boundary forecast, and shorter time scales correspond to the time when ^{3}H concentrations are more likely to be above the MCL. Figure 2-9 illustrates particle paths and times after 200 years of advective transport. At 200 years, the base case has 24 percent of the particles reaching the model's southern boundary, and the 1 kg/s case has maximum particle travel only half the distance to model's southern boundary. The contaminant boundary illustrated in Figure 6-82 of N-I (2013a) indicates that, when the northern boundary flux rate is set to 1 kg/s, MCL exceedance does not occur at the LCA model's southern boundary. A northern flux value that is lower than the range considered in the NSMC analysis is consistent with Winograd and Thordarson (1975) and Harrill et al. (1988).

In conclusion, the current base-case value (130 kg/s) of the northern flux is likely an overestimate, and smaller values such as 1 kg/s would produce much less transport.

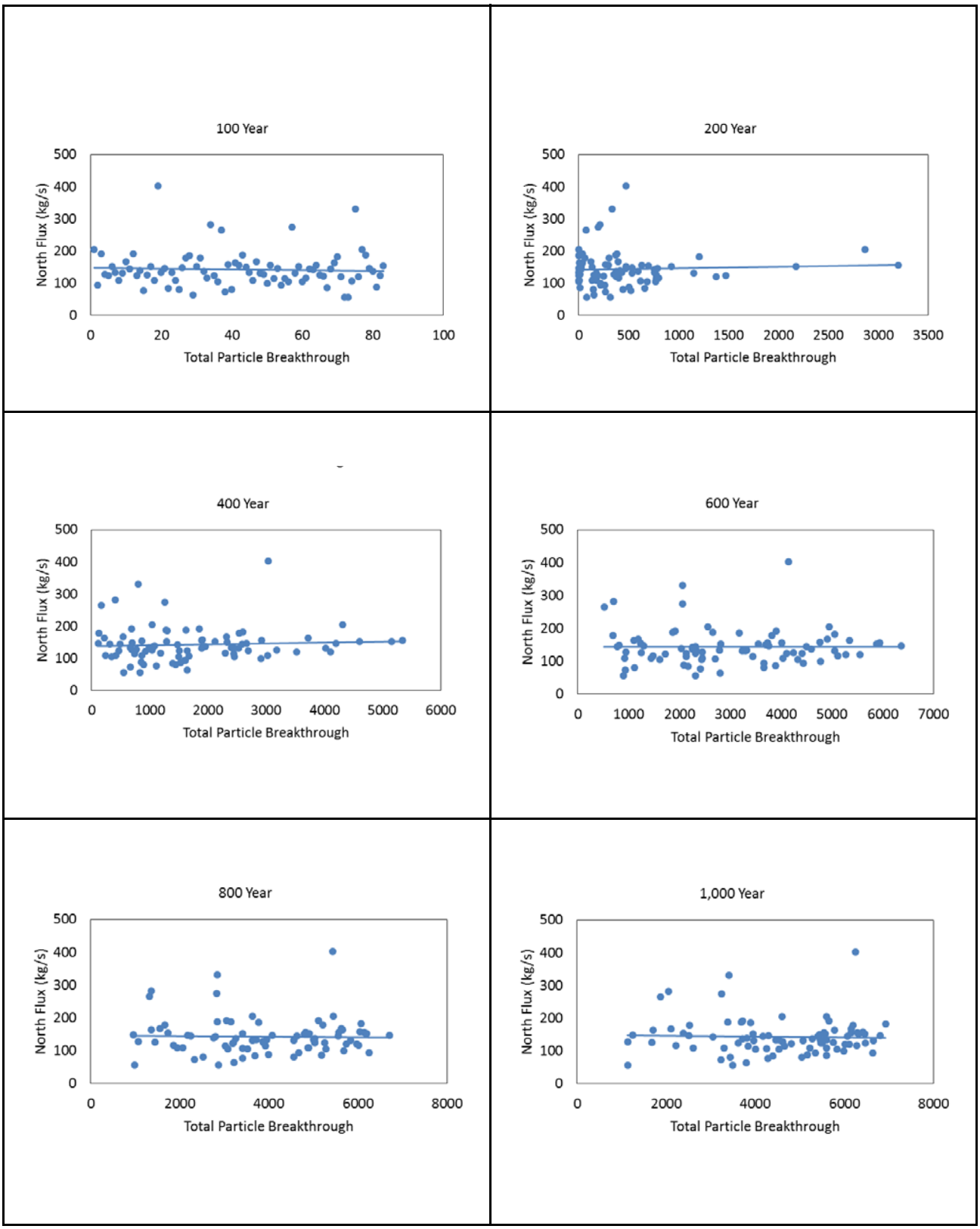

Figure 2-8
Northern Flux vs. Particle Breakthrough for the NSMC Cases

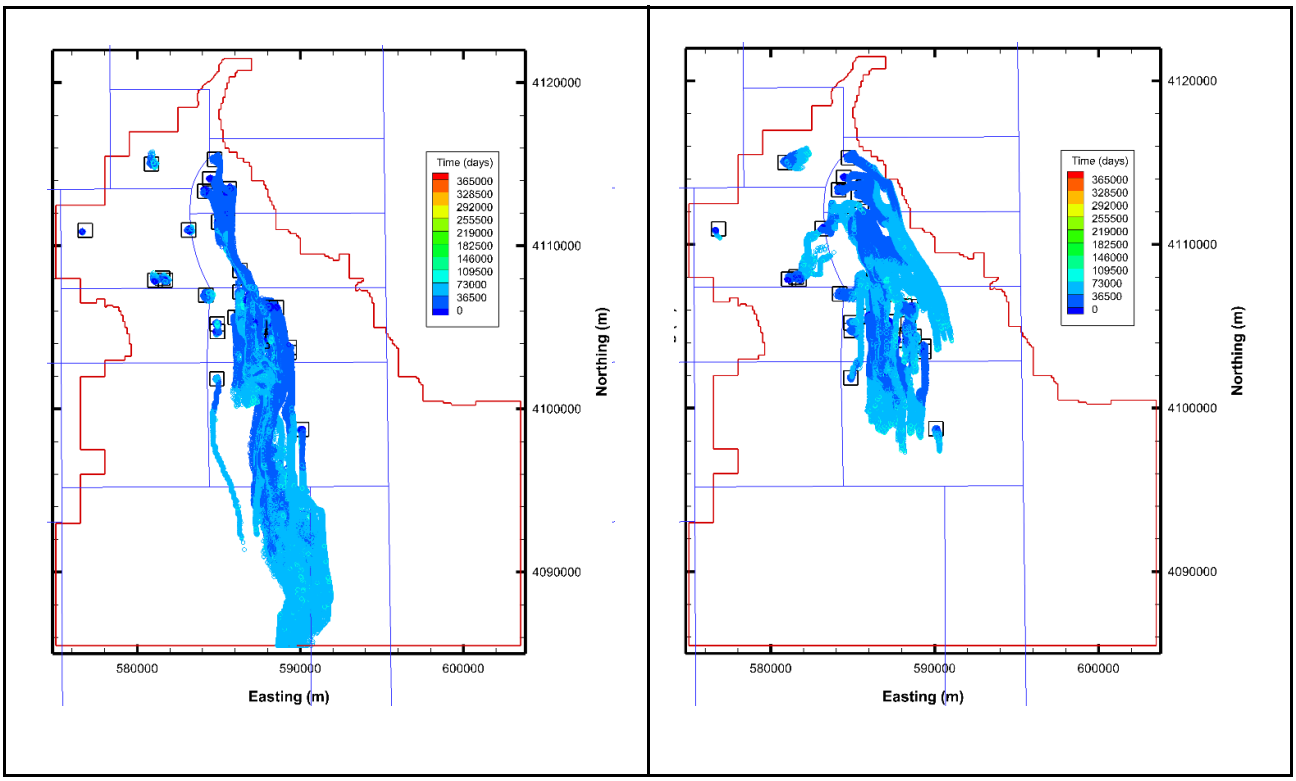

Figure 2-9
Particle Travel Paths and Times for the Base-Case (left) and 1 kg/s (right) Flow Fields at 200 Years

2.1.4 Water Table Boundary and AA/VA Flow Direction

The concern expressed in this uncertainty is that it is difficult to determine the direction of simulated groundwater flow in the shallow aquifer from the information presented, especially with regard to flow toward faults. Present-day flow directions can differ from those indicated by the pre-development hydraulic heads estimated in Fenelon et al. (2012) due to the effects of nuclear testing.

PRC Recommendation: The peer review team recommends contouring simulated water levels in the AA/VA system and comparing the simulated contours to the horizontal gradients and flow directions shown in Fenelon et al. (2012) and in Fig. 4-2 of N-I (2013a) to build confidence in the reasonableness of the predicted fluxes into the LCA. Given the poor quality of the available head data, especially due to its transient nature, the uncertainty associated with flux to the LCA resulting from uncertain spatially variable hydraulic heads and gradients in the AA/VA should be examined.

RESPONSE: As requested, the modeling team has developed a contour map of simulated pre-testing hydraulic heads (with inferred flow directions) to discuss the similarities and differences between this map and Fenelon et al. (2012). These pre-testing flow directions have been potentially altered, at least in the short term, because of the strong impact of nuclear tests on heads in the AA/VA during and after the testing period. Particle tracks during the 1,000-year simulations can be used to illustrate the complexity of the flow regime. The ensemble of simulations presented in N-I (2013a) explicitly consider uncertainty in flux to the LCA (both water flux and RN flux). For example, transient outflow of water from the volcanics to the LCA varies by over 3 orders of magnitude (N-I, 2013a, Table 4-12) due to changing assumptions about hydrostratigraphic unit (HSU) and fault permeability and testing effects, which in turn affect flow directions.

The modeling team has developed new particle tracks that illustrate integrated flow directions over the 1,000-period of transient flow (Figures 2-10 through 2-12). In Figure 2-10, representative tracks are shown from all sources in the AA/VA. In Figure 2-11, only the tracks from the sources with some particles that eventually exit to the LCA are shown. In each case, two plots are shown: one colored by travel time; the other colored to show paths along a fault, the TCU or other rock type. The delineation between these two types of sources is shown in Figure 2-12. Lateral flow toward fault zones is quite evident from these tracks. Also, north/south flow within fault zones occurs in some cases. There are a large number of tests in the central and northwestern portions of the domain containing only particles that never reach the LCA.

Although flow toward faults and subsequent drainage down faults to the LCA was part of the Fenelon et al. (2012) conceptual model, hydraulic contours and flow directions illustrated in Figure 2-13 assume that the primary function of faults is to compartmentalize aquifers. In contrast, the SZ AA/VA flow and transport model documented in N-I (2013a, Section 4.0) conceptualized faults as the dominant transport pathway between the tuffs and the LCA.

The pre-development flow directions conceptualized by Fenelon et al. (2012) display a complex pattern that reflects the offset or continuity of aquifers across faults, as represented in the Yucca Flat hydrostratigraphic framework model (HFM) (Figure 2-13). In contrast, the pre-testing head contours in the AA/VA flow model are generally smooth and indicate flow toward the southern end of the basin, consistent with the LCA heads that were imposed at the base of the SZ AA/VA system model (Figure 2-14). The intent was to ensure consistent hydraulic heads at the interface between the SZ

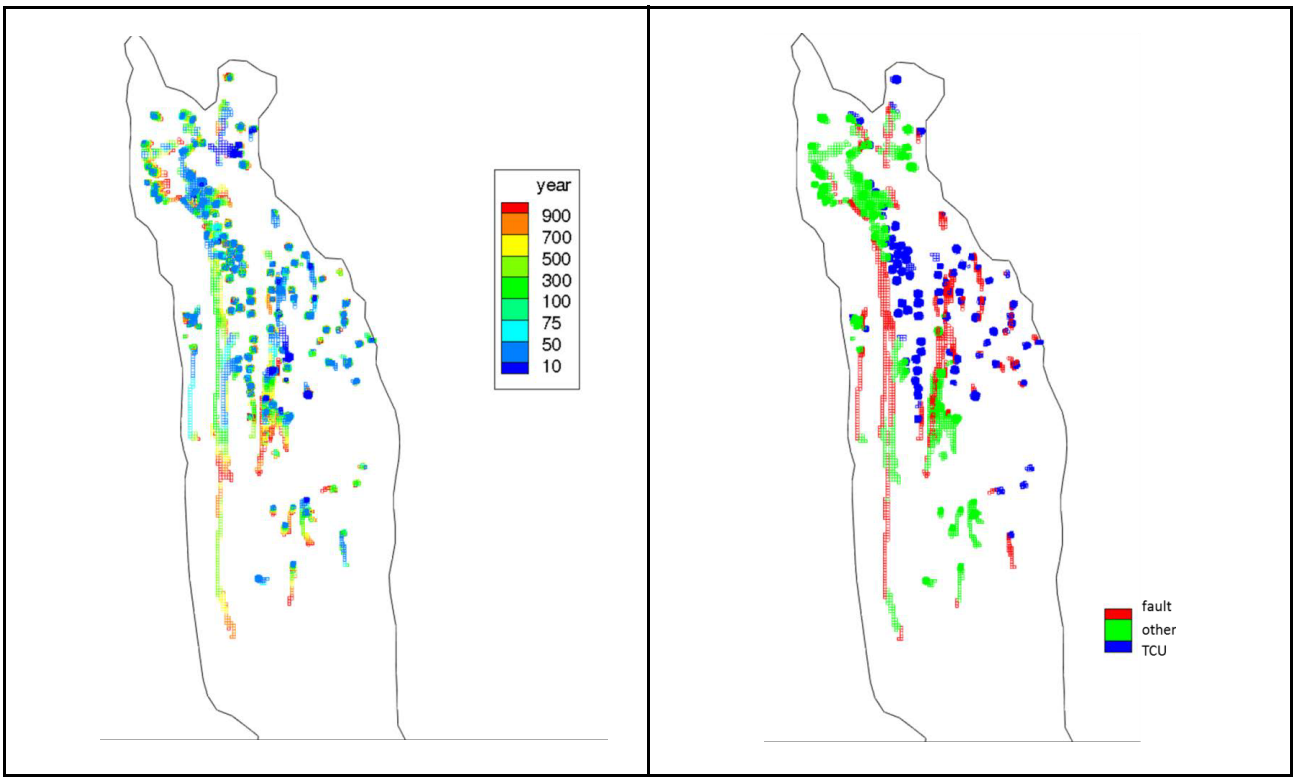

Figure 2-10
Particle Locations for All SZ AA/VA Tests Colored (left) by the Number of Years since the Start of the Simulation (1961) and (right) by HSU
Note: All tests included in the AA/VA model are shown.

AA/VA and SZ LCA models (N-I, 2013a, Section 4.3). As a result of this assumption, a few hydraulic heads in the southern part of the basin used by Fenelon et al. (2012) to infer northerly flow were poorly matched in the SZ AA/VA flow model. Some of the pre-development heads in the southern part of the basin were identified from complex hydrographs only after the modeling approach employed in the SZ AA/VA model had been implemented. Because there are only a few shallow UZ tests in the southern part of the basin in the vicinity of Yucca Lake, these differences in flow direction are expected to have little effect on RN migration. To compensate for differences in these models, a new well (ER-3-3) has been drilled near TW-7, which is where hydraulic heads are lowest (730.6 m) and the volcanic and carbonate aquifers are most likely to be juxtaposed across the Yucca fault. The LCA groundwater produced during drilling at ER-3-3 did not produce measurable ^{3}H (DL of approximately 1,500 pCi/L), indicating the hypothesized hydraulic connection near TW-7 is not currently a pathway for RN transport. The different conceptual models that underlie the shallow flow system interpretation of Fenelon et al. (2012) and the SZ AA/VA system model of N-I (2013a) have potentially significant impact regarding the RN flux to the LCA. In the Fenelon et al. (2012)

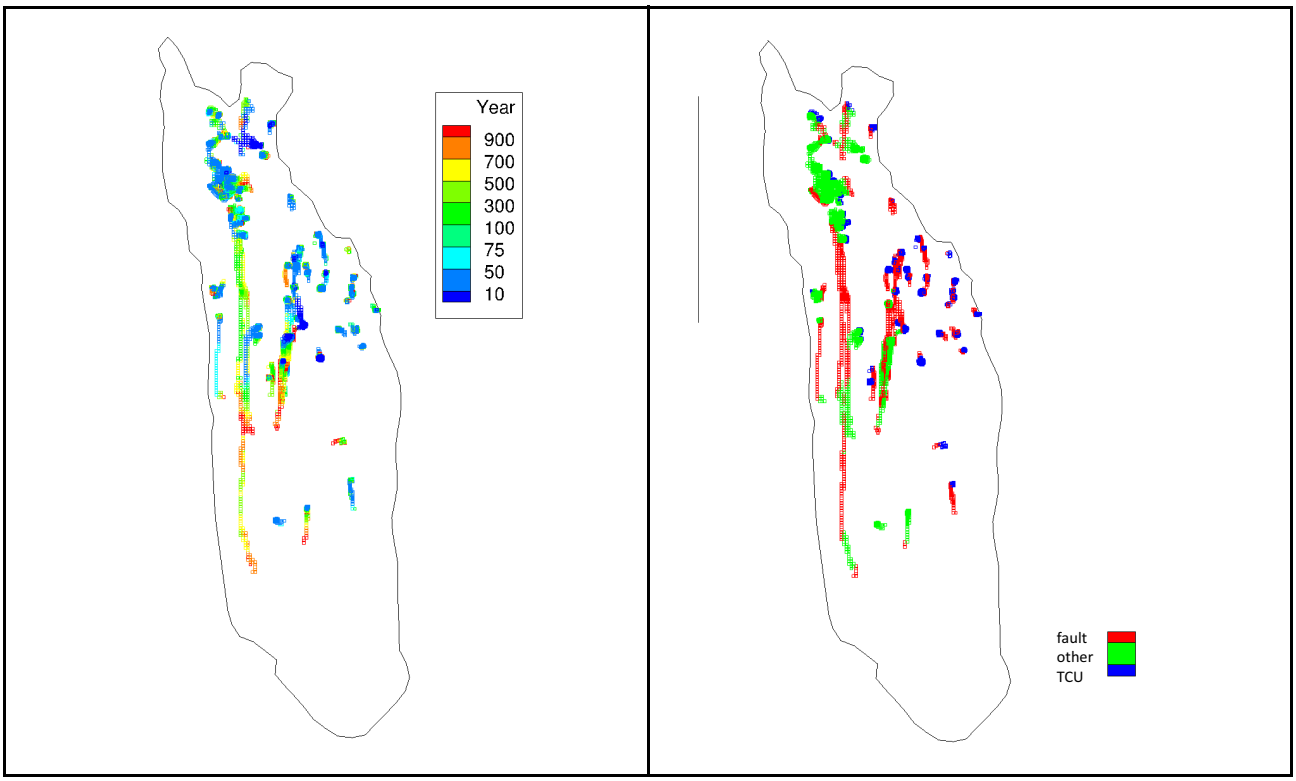

Figure 2-11
Particle Paths for All SZ AA/VA Tests That Have Particles That Reach the LCA Colored (left) by Years since the Start of the Simulation (1961) and (right) by HSU

conceptual model, RNs must travel long lateral distances before arriving at the single hydraulic connection between the tuffs and LCA near ER-3-3. The SZ AA/VA model is more conservative because RNs can reach the LCA after traveling laterally to the nearest fault and then downward.

In conclusion, no further work is warranted under this uncertainty.

2.1.5 Hydraulic Connection between Aquifers

This uncertainty concerns the use of loose coupling between the AA/VA and the LCA models, and the possible resulting underestimation of recharge to the LCA model.

PRC Recommendation: The PRC recommends that the uncertainty associated with the consistency of the upper boundary of the LCA model and the lower boundary of the AA/VA model be considered in future simulations of the contaminant boundary. One suggestion is to follow common convention for modeling multi-aquifer systems separated by an aquitard and model them together. This approach would ensure continuity of heads between aquifers where they are connected at the faults. The

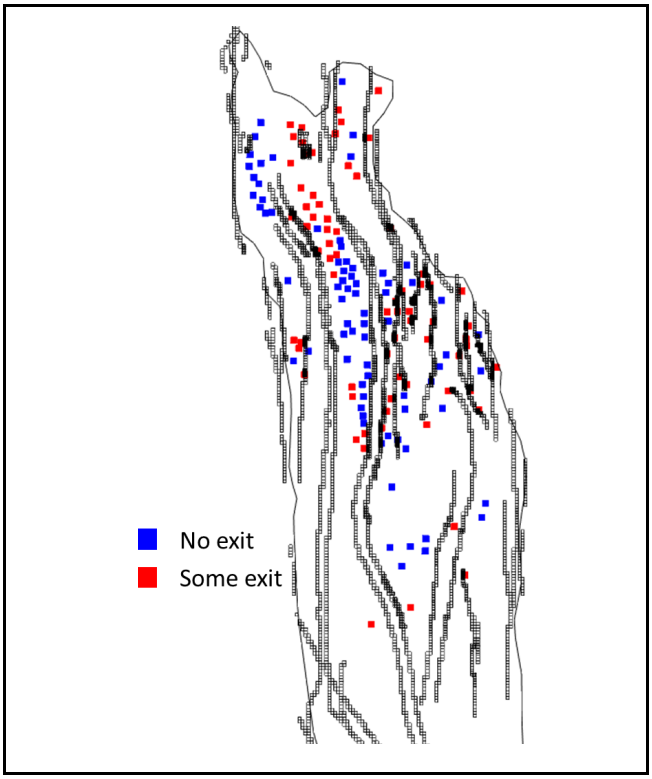

Figure 2-12
SZ AA/VA Tests Categorized by Whether or Not Some Particles Reach the SZ LCA

coupled model grid can be fairly coarse, at least much coarser than the decoupled models that were used for both flow and transport predictions of the contaminant boundary. Once the models are coupled, then all the head data within the combined multi-aquifer system can be used for calibration. The flux leaking into the LCA from the coarse-grid coupled aquifer model would help constrain further calibrations with the fine-grid flow and transport model. Use of the most recent USGS regional modeling (Faunt, 2012) for establishing head boundaries in the local-scale flow model of Yucca Flat is recommended.

RESPONSE: The modeling team agrees that the approach of using two SZ models, instead of an integrated model, provides incomplete feedback between the two models. However, the uncoupled models are an acceptable approximation because the overall downward gradient between the tuffs and the LCA is locally dominated in the testing areas by testing-induced overpressures associated with pore compression. Small changes in LCA heads due to test-induced drainage or natural recharge cycles do not significantly affect driving vertical gradients. Thus, the uncertainty regarding migration in the shallow aquifer and potential downward migration to the LCA is dominated by uncertainty in

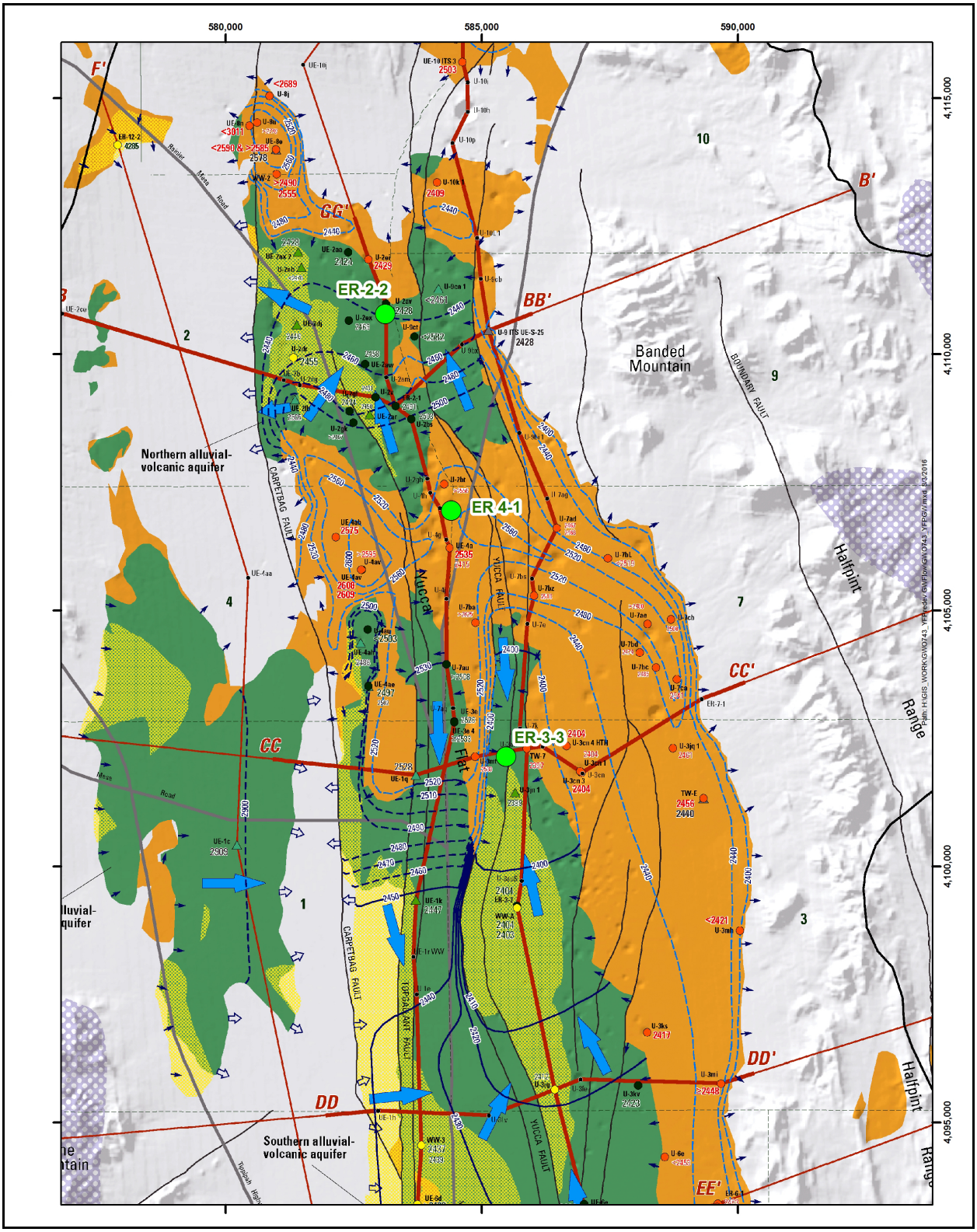

Figure 2-13
Pre-development Hydraulic Head Contours and Flow Vectors in the Shallow AA/VA
Source: Modified from Plate 3 of Fenelon et al., 2012

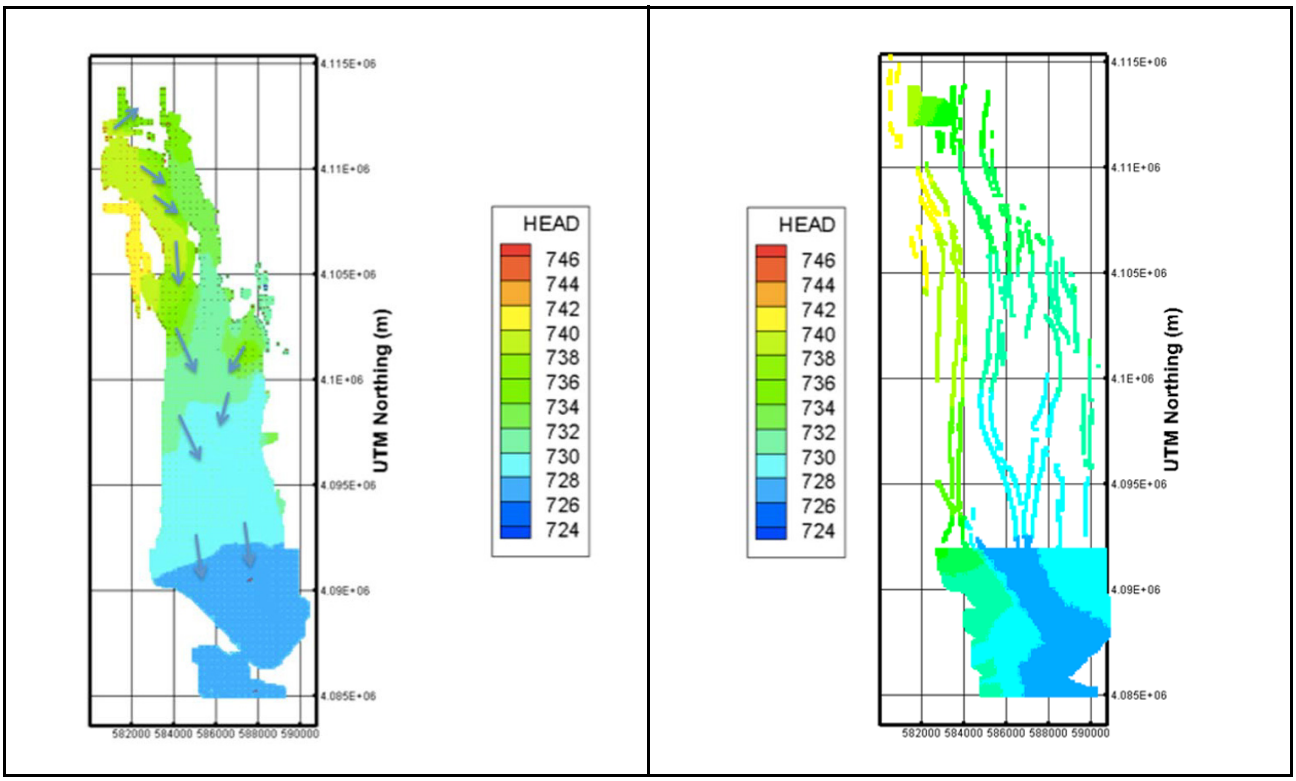

Figure 2-14
Pre-development Heads in the SZ AA/VA Flow and Transport Model at a 500-m Elevation (left) and along the Lower Model Boundary (right)

the shallow aquifer parameters and role of vertical flow along structural features like faults, and not by uncertainty in the hydraulic head values at the top of the LCA.

The three principal models developed for meeting the regulatory objectives—the UZ model (itself consisting of 12 separate grids), the SZ AA/VA model, and the SZ LCA model—each had specific requirements for grid and time-step resolution to represent model-specific processes and features. Consequently, a loose coupling of these models through integrated boundary conditions was necessary to make the problem computationally tractable. Considerable care was exercised in ensuring that boundary conditions and hydraulic properties were consistent across models for the different modeling scenarios, and that water and RN mass balance between model domains was maintained in both time and space. However, because the LCA transport model assumed steady-state flow, transient recharge events to the LCA arising from crater infiltration or enhanced drainage from pore compression associated with nuclear testing in the TCU were not explicitly modeled, and a long-term average recharge was applied at the top of the LCA. The effect of this approximation was evaluated with explicit transient flow modeling and particle tracking to demonstrate the

insignificance of the short term (decades-long) transients over the 1,000-year period of regulatory interest (N-I, 2013a, Appendix I). The evaluation showed that small amounts of vertical leakage in the center of the basin are quickly dissipated by the high-permeability LCA without significantly altering the hydraulic heads or flow directions. Therefore, the heads in the LCA can be reasonably approximated as constant and used to constrain the heads at the base of the SZ AA/VA system model, despite the relatively small head increases in the LCA over the past few decades. These head increases are seen throughout southern Nevada in the LCA and are most pronounced near the basin margins near possible recharge areas; thus, there is no evidence they are associated with nuclear testing.

In conclusion, joint calibration of the AA/VA and LCA models is not necessary.

2.2 Model Calibration

2.2.1 Poorly Posed Calibration

This uncertainty focuses on the fact that the LCA model optimization is underconstrained with respect to the number of adjustable parameters in the model.

PRC Recommendation: The peer review team recommends the problem be better posed by coupling the aquifers in one model; including more calibration targets (e.g., [1] AA/VA heads, [2] heads and springs east of the groundwater divide on Rainier Mesa, and [3] heads Fenelon identified as representative of the regional carbonate aquifer such as UE-8e, UE-10 ITS 3 (2160), UE-10bf, UE-10 ITS 5 before the measurement in 1972, U-7a, WW-C-1, and ER-3-1—this list provides examples and, as such, is not a compulsory nor comprehensive list); collecting additional calibration data via field activity; and simplifying the parameterization of the model.

RESPONSE: The modeling team has performed additional calibration studies using models designed to address the PRC recommendations stated above, and they found that the current base-case model is more conservative than the alternate models with respect to transport forecasts. These additional studies are summarized below.

The decision to model the SZ AA/VA and SZ LCA domains separately was motivated by (1) the need to have adequate grid and hydrostratigraphic resolution for transport calculations in both domains, and (2) the need to capture the highly transient nature of the AA/VA system following nuclear testing

without imposing the highly transient time-stepping requirements on the quasi-steady-state LCA flow system. These requirements still hold. Moreover, the number of parameters to be estimated and the number of observations used for parameter estimation remains unchanged whether the models are fully coupled or loosely coupled through their common boundary conditions, as currently represented. To the modeling team's knowledge, all reliable hydraulic head data within the existing SZ AA/VA and LCA models were used to inform the calibration; however, in some wells where the open or screened interval intersected multiple aquifers, the hydraulic heads could not always be unambiguously attributed to a single aquifer. Where the contributing aquifer was not clear, the data were omitted from the calibration of the base case.

Model recalibrations were conducted with the results showing that the base-case model is more conservative. The additional calibration wells identified by the PRC have been reviewed, and the wells that are likely representative of LCA water levels have been included as calibration targets. The PRC recommended that the following wells be included in the model calibration: ER-3-1, WW-C-1, U-7a, UE-8e, UE-10bf, UE-10 ITS 3, and UE-10 ITS 5. A description of each well identified by the PRC is as follows:

- **Well ER-3-1** is located in southeast Area 3 and is screened within the LCA. The water levels from this well were used in the model calibration presented in N-I (2013a).

- **Well WW-C-1** is located in southeast Area 6 approximately 30 m southeast of WW-C and is screened in the LCA. Well WW-C was used in the N-I (2013a) LCA model calibration and is approximately screened over the same depth interval as WW-C-1. Due to the close proximity of WW-C-1 to WW-C and the approximately equivalent water levels in both wells, including this well is equivalent to doubling the weight of the WW-C observation. This well was not included in the LCA model calibration presented in N-I (2013a) or recalibration presented here.

- **Well U-7a** is located in northwest Area 7 and is open to low-permeability volcanic rock and the LCA. Fenelon et al. (2012) considers the water level to be representative of the carbonate aquifer, and it was included in the LCA model recalibration.

- **Well UE-8e** is located in south–central Area 8 and has shallow and deep completions. Fenelon et al. (2010) identifies the deeper completion as being located in low-permeability volcanic rock and the LCA. The water level from the deep completion is 2,579 m, which is 162 m higher than the nearby well WW-2. Fenelon et al. (2012) considers the water level from this well as anomalous and does not use the data in the interpretation of groundwater flow directions. This well was not included in the LCA model calibration presented in N-I (2013a) or recalibration presented here.

- **Well UE-10bf** is located in the northwest corner of Area 10. This well is open to low-permeability volcanic rock and the LCA. Fenelon et al. (2012) considers this water level representative of carbonate aquifer. This well was included in the LCA model recalibration.

- **Well UE-10 ITS 3** is located in the northwest corner of Area 10 and has shallow and deep completions. The deeper completion is open to low-permeability volcanic rock and the LCA. Fenelon et al. (2012) considers this water level representative of carbonate aquifer. This well was included in the LCA model recalibration.

- **Well UE-10 ITS 5** is located in east–central Area 8 and is open to low-permeability volcanic rock and the LCA. Fenelon et al. (2012) considers this water level representative of carbonate aquifer. This well was included in the LCA model recalibration.

The LCA model was recalibrated using the additional four wells (U-7a, UE-10bf, UE-10 ITS 3, and UE-10 ITS 5). Figure 2-15 illustrates the potentiometric surfaces for the base case and additional TCU/LCA calibration wells. The LCA model recalibration achieved a higher objective function (18.9) compared to the base case (1.15) due to the four additional calibration targets. The highest residuals in steady-state heads were in the additional wells U-7a and UE-10bf. Figure 2-16 illustrates the particle locations and times for the base case and additional calibration wells at 1,000 years. Transport east of Yucca fault is slower with the added targets and spatial distribution of particles is more dispersed. Figure 2-17 illustrates the particle breakthrough for the base case and additional TCU/LCA wells. The transport of particles at the southern line of demarcation is lower during the first 700 years but is similar (64 percent) to the base case (66 percent) at 1,000 years. However, including the additional wells in the model calibration significantly decreased transport at shorter time periods, such as 100 or 200 years, which corresponds to the time when ^{3}H concentrations may be above the MCL (N-I, 2013a).

In conclusion, the model calibrated using additional targets does not lead to particle breakthrough that is significantly different from the N-I (2013a) base-case transport model at 1,000 years, and leads to decreased particle breakthrough at 200 years. No further work is warranted under this uncertainty.

2.2.2 Lack of Steady-State Head Data

The focus of this uncertainty is that steady-state heads from different wells are not concurrent, they are sparse, affected by detonations, and many come from sections with long well screens.

PRC Recommendation: The peer review team recommends calibrating a coupled model of the aquifers, including more calibration targets, resurveying the well heads to ensure both the accuracy

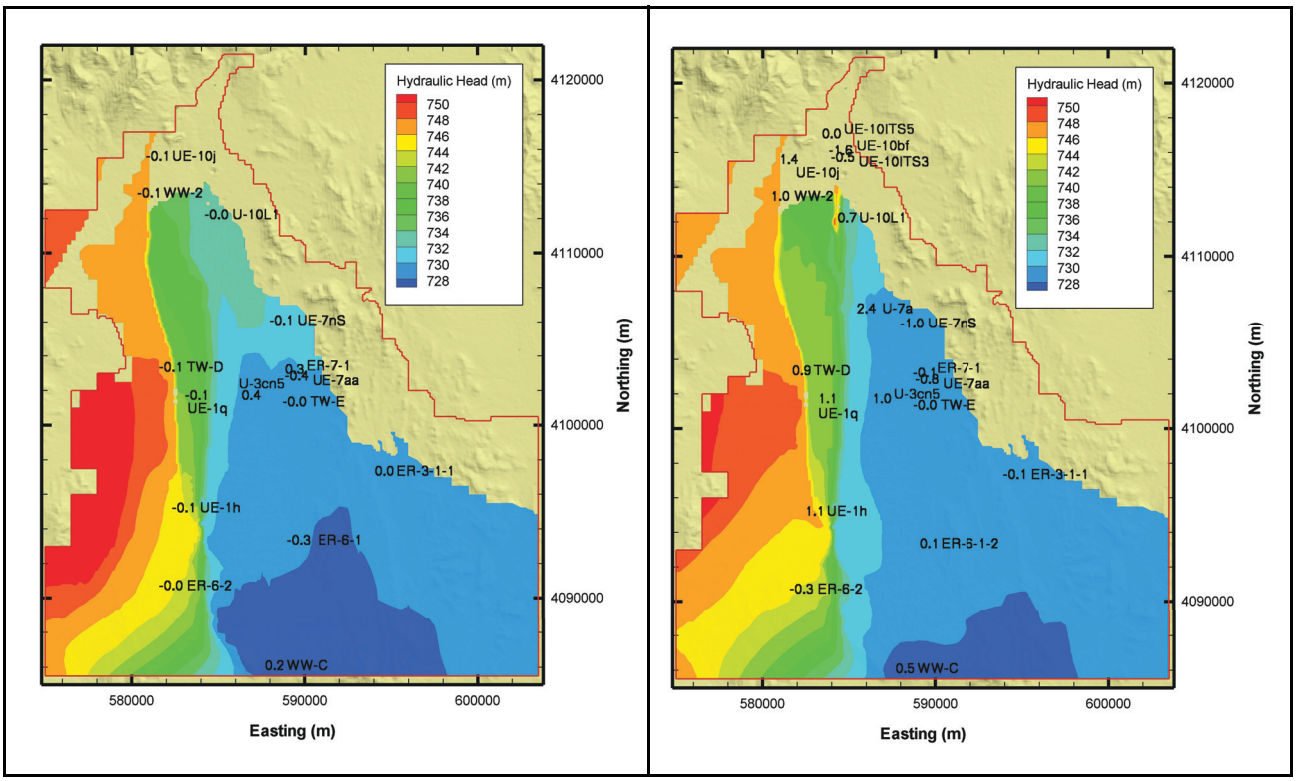

Figure 2-15
Potentiometric Surface for the Base-Case (left) and Additional TCU/LCA Calibration Wells (right)

of the targets and to determine whether the measuring point may have changed with time, as well as completely representing the data that were used to develop steady-state targets. To completely represent the data, use all the data points (with deviations due to recovery and measurement errors omitted) as targets, and present a residual at each location for every measurement that has been recorded over the years. This would provide a realistic representation of the difference between measured and simulated heads.

RESPONSE: The reasons for not coupling the models have been presented in the response to Section 2.1.5. Due to the greater complexity of the structure represented by a coupled model, the increased refinement needed for high-gradient zones, and the increased number of unknown parameters, there is no advantage to a coupled model.

The modeling team has performed additional studies using five alternate flow models to demonstrate how the alternative interpretations of the LCA pre-development water levels and variability in water

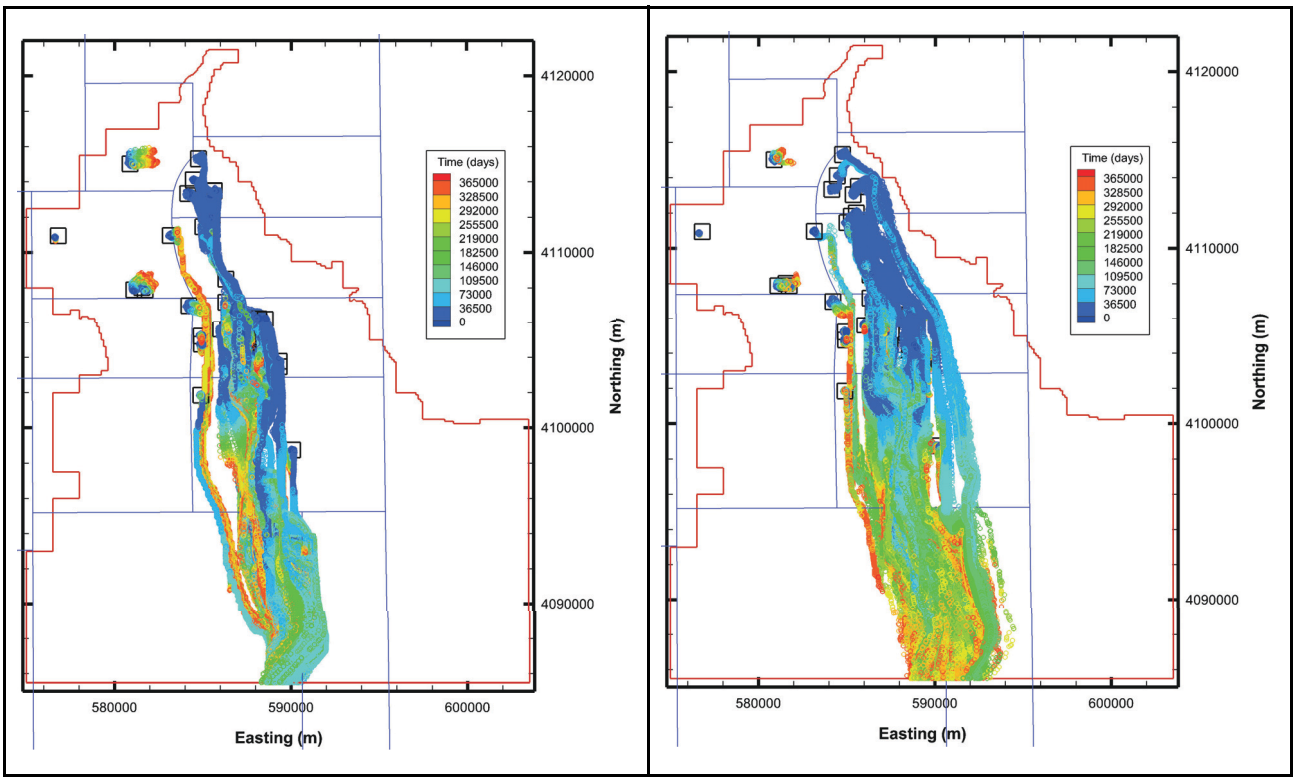

Figure 2-16
Particle Travel Paths and Times for the Base-Case (left) and Additional Volcanic Confining Unit/Carbonate Aquifer Calibration Wells (right) Flow Fields

levels affect flow and transport, and to show that particle breakthroughs for the alternate models are approximately equivalent to the base case. These additional studies are summarized below.

The well heads were resurveyed in 2003, so a relatively high level of confidence is associated with well head elevations.

Pre-development heads reported in Fenelon et al. (2012) that were not previously used in the calibration because of uncertainty in the contributing aquifer have been included in an LCA model recalibration, which is presented in Section 2.2.1. In the AA/VA model, all available data were used in the calibration, and because it was a transient model, no assumptions needed to be made regarding whether the data represented transient or steady-state conditions.

It should be noted that the “steady-state” head data available from individual wells are just as important as the MWAT data for model calibration. Parameter estimates are informed both by the steady-state head data and the MWAT data. While the problem is underconstrained, as is often the

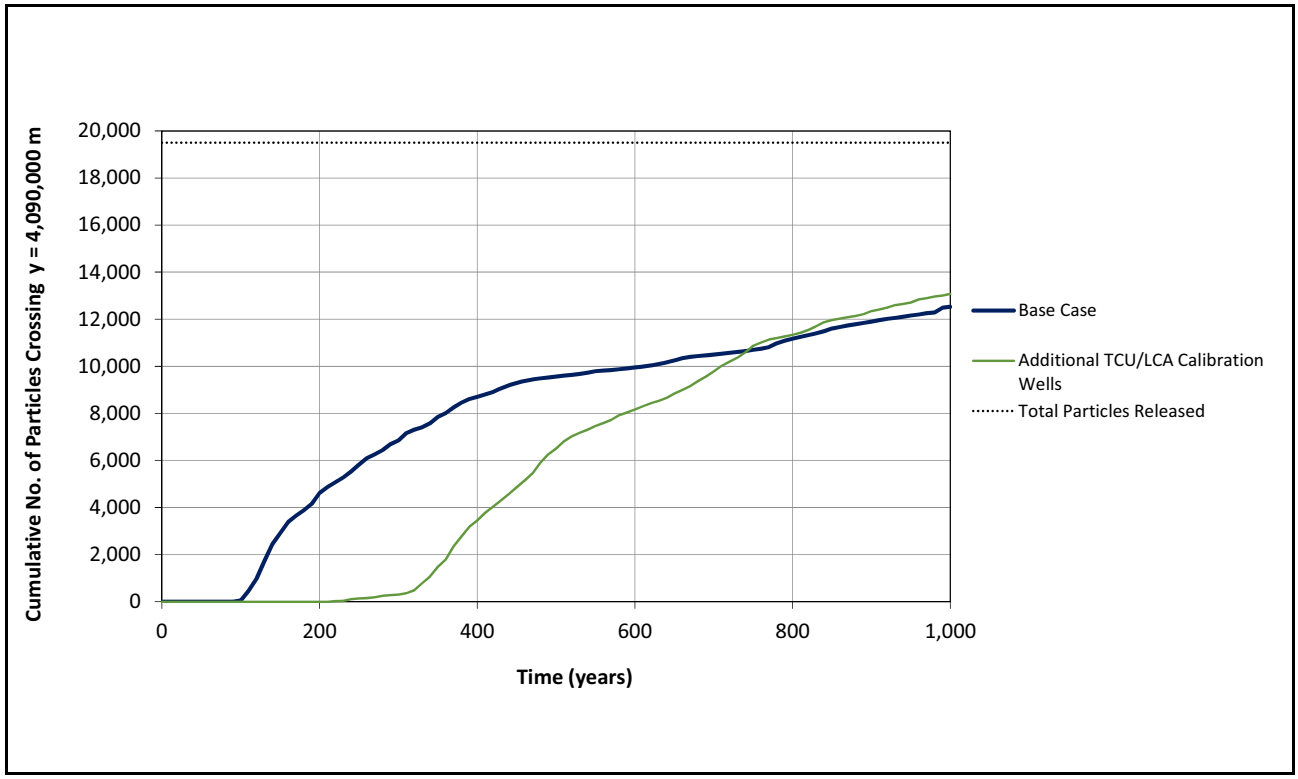

Figure 2-17
Breakthrough Plots for Base-Case and Additional TCU/LCA Calibration Wells Flow Fields

case in hydrological studies, the discussion of the NSMC results (N-I, 2013a) and the alternate model cases presented in this report demonstrates that the calibrated base-case flow model leads to conservative transport estimates.

Several additional data sources published by the USGS are available at this time. This material was not available at the time the LCA model was being developed because much of the work was completed prior to 2010. Although some of the additional data sources are discussed in N-I (2013a), the hydraulic head data was not directly used in the LCA model calibration. The additional data sources are as follows:

- *Groundwater Flow Systems at the Nevada Test Site, Nevada: A Synthesis of Potentiometric Contours, Hydrostratigraphy, and Geologic Structures*, USGS Professional Paper 1771 (Fenelon et al., 2010). This data source identified mean water in each well considered representative of predevelopment conditions.

- *Database of Groundwater Levels and Hydrograph Descriptions for the Nevada Test Site Area, Nye County, Nevada*, Data Series 533 (Elliott and Fenelon, 2013). This data source contains a

database of groundwater levels and hydrograph descriptions for the Nevada National Security Site (NNSS).

- *Conceptualization of the Predevelopment Groundwater Flow System and Transient Water-Level Responses in Yucca Flat, Nevada National Security Site, Nevada*, USGS Scientific Investigations Report 5196 (Fenelon et al., 2012). This data source presents a conceptualization of the predevelopment groundwater flow system and transient responses in Yucca Flat.

Several LCA model simulations have been developed that use alternative water-level data sources as calibration targets, including using multiple targets at locations with transient water levels not associated with anthropogenic activities. The impact to transport was assessed showing that the alternate models did not lead to significantly increased transport compared to the base case. The simulations developed to demonstrate how alternative interpretations of the LCA pre-development water levels and variability in water levels affect flow and transport are as follows:

1. ***Including the additional Wells U-7a, UE-10bf, UE-10 ITS 3, and UE-10 ITS 5.*** This recalibration is presented in Section 2.2.1.

2. ***Using mean water levels calculated by USGS Professional Paper 1771 (Fenelon et al., 2010) for the LCA model steady-state calibration targets.*** Most of the target water levels used in the N-I (2013a) analysis are within 0.3 m of Fenelon et al. (2010), but Well U-3cn 5 is different by approximately 2 m.

3. ***Using multiple steady-state calibration targets extracted from Data Series 533 (Elliott and Fenelon, 2013) that encompass the temporal variability of steady-state heads.*** Hydrographs for the 16 wells used in the N-I (2013a) calibration fluctuate up to 2.7 m over the periods of record. The hydrograph data for many of the target wells consist of hundreds of records and efficient model calibration required simplifying the hydrographs. The data were simplified by selecting a set of six water-level records from each hydrograph that capture the variability in the hydrograph data. Figure 2-18 illustrates typical simplified hydrographs for Wells ER-6-1-2 and TW-D. Each of the six water-level records at each well were treated as individual targets, thereby creating a residual that includes the water-level variability.

4. ***Using a grid of calibration targets created from the LCA head contours in USGS Scientific Investigations Report 5196 (Fenelon et al., 2012).*** This recalibration is presented in Section 2.1.1.

5. ***Considering data quality in the steady-state target weights.*** This recalibration is presented in Section 2.2.5.

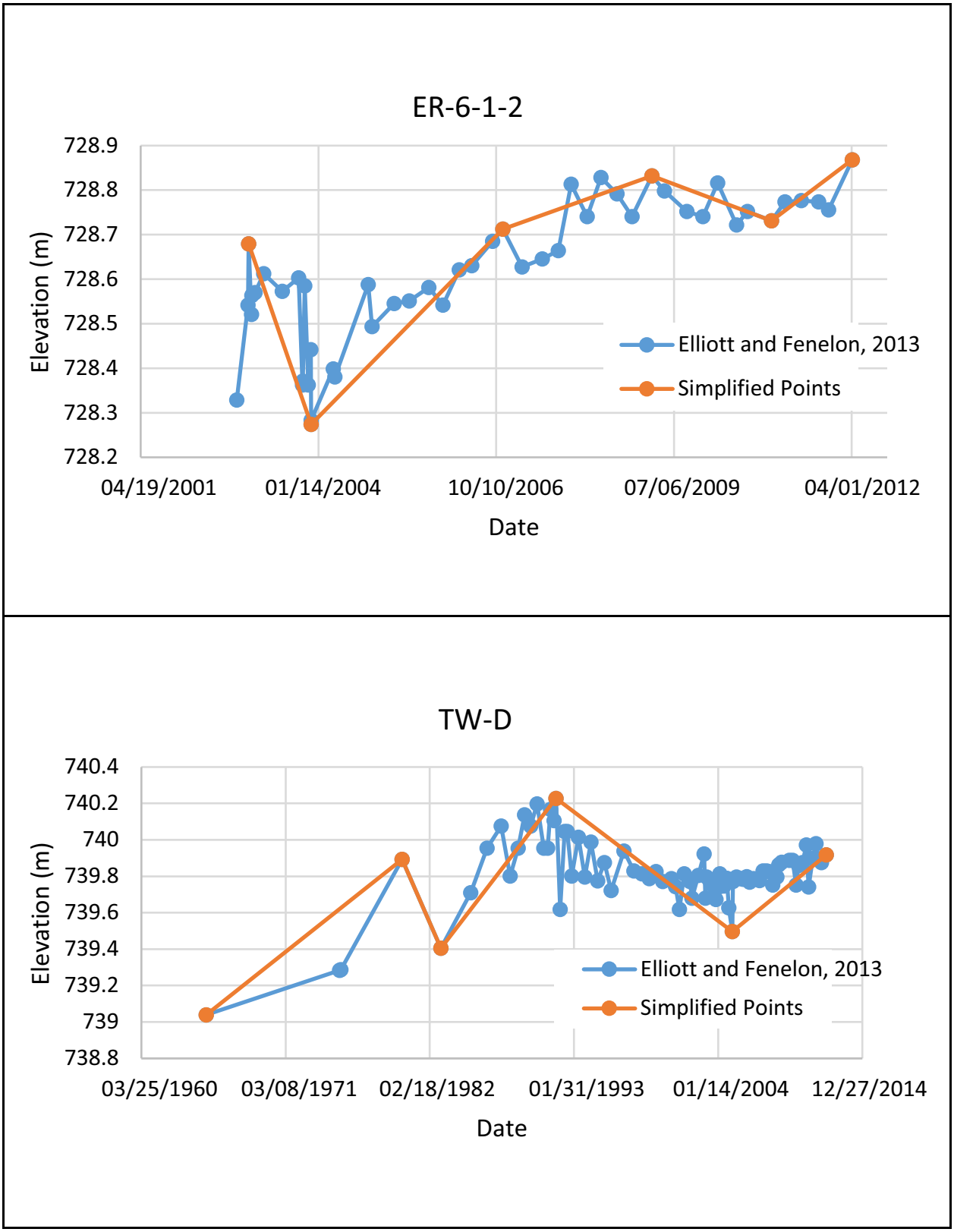

Figure 2-18
Simplified Hydrographs for Wells ER-6-1-2 and TW-D

Table 2-2 summarizes the model recalibration results evaluating uncertainty due to alternative interpretations of steady-state water levels. Figure 2-19 illustrates particle breakthroughs for the base case and the simulations investigating alternative interpretations of the LCA pre-development water levels. Care must be exercised when interpreting the particle breakthrough as a surrogate for the 1,000-year contaminant boundary calculations: slower transport prior to 200 years is significant for the contaminant boundary because ^{3}H is largely removed by radioactive decay after 200 years. Figure 2-19 shows that the base case predicts larger particle breakthrough than any alternate model considered here for up to 500 years.

Table 2-2
Summary of Simulations Investigating Alternative Interpretations of the LCA Pre-development Water-Levels Uncertainty
(Page 1 of 2)

Simulation	Objective Function (RMS)	Percentage of Particle Breakthrough within 1,000 Years	Calibration Summary
Base case	1.15	64	• This is a baseline metric to evaluate the influence of alternate flow simulations.
Additional Wells	18.9	66	• Particle breakthrough is similar to the base case. • Calibration is worse than the base case. • Two of the additional wells, U-7a and UE-10bf, have highest residuals. • Transport east of Yucca Flat is slower than the base case. • Particle transport at shorter time periods (i.e., 100 and 200 years) is slower than the base case.
Calibration targets from USGS Professional Paper 1771 [a]	6.71	63	• Flow field is very similar to the base case. • Highest residuals are generally at wells with calibration targets that have the largest deviation from the base case. • Particle transport in Yucca fault is slower compared to the base case. • Total particle breakthrough is similar to the base case.
Calibration targets from USGS Data Series 533 [b]	2.41	64	• Northern flow in western Yucca Flat is slightly increased. • Total particle breakthrough is similar to the base case.

Table 2-2
Summary of Simulations Investigating Alternative Interpretations of the LCA Pre-development Water-Levels Uncertainty
(Page 2 of 2)

Simulation	Objective Function (RMS)	Percentage of Particle Breakthrough within 1,000 Years	Calibration Summary
Contour-points	6.78	35	• Northern flow in western Yucca Flat is still present. • Heads are higher in western Yucca Flat compared to the base case. • Particle transport is much slower due to reduced total flow through the model (128 kg/s) compared to the base case (268 kg/s), and decreased LCA east zone country rock permeability compared to the base case.
Weights based on data quality	16.4	79	• Heads are lower in western Yucca Flat. • LCA east and Yucca fault permeability is higher compared to the base case. • Particle transport is faster compared to the base case.

[a] Fenelon et al., 2010
[b] Elliott and Fenelon, 2013

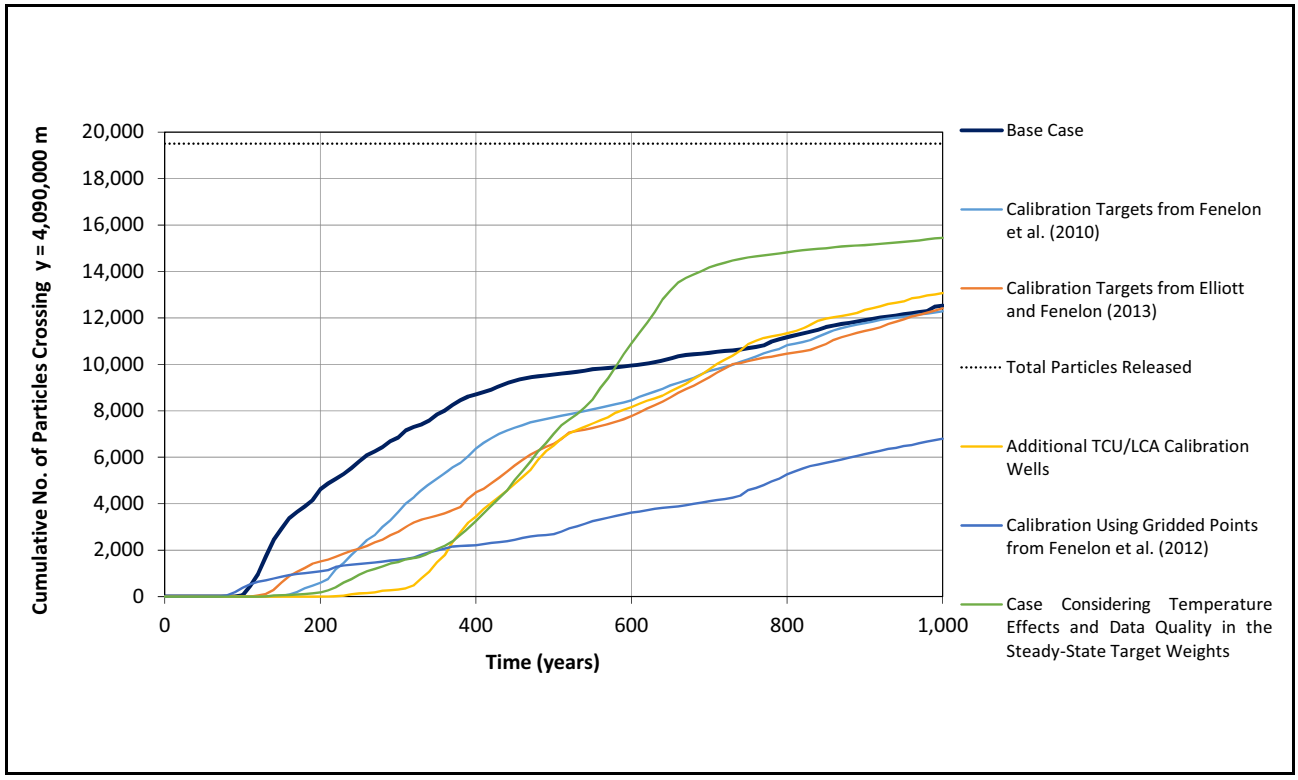

Figure 2-19
Breakthrough Plots for LCA Flow Fields Investigating Alternative Interpretations of the LCA Pre-development Water Levels

The 1,000-year particle breakthrough for the USGS Professional Paper 1771 (Fenelon et al., 2010), Data Series 533 (Elliott and Fenelon, 2013), and additional TCU/LCA wells cases are similar to the base-case LCA modeling presented in N-I (2013a); but the total particle breakthrough prior to 800 years is significantly less than the base case. The flow field for the calibration using gridded points from Fenelon et al. (2012) has significantly slower particle transport compared to the base case. The flow field considering temperature effects and data quality in the steady-state calibration targets has less particle breakthrough prior to 600 years, but increased total breakthrough at 1,000 years compared to the base case.

The PRC expressed concern that the original LCA model steady-state head data were selected from non-concurrent sections of the hydrographs, and that the water levels were intentionally selected to minimize the differences between observed and simulated heads, which may have overstated the degree of calibration achieved. The objective function obtained from the model calibrations using the targets provided by USGS Data Series 533 (Elliott and Fenelon, 2013) or USGS Professional Paper 1771 (Fenelon et al., 2010) may be a more complete representation of the degree of calibration that was actually achieved for the LCA model. However, the objective function using the revised dataset is only moderately higher and is still within the range of values considered acceptable (i.e., 1.15 for the base case and vs. 6.71 for the USGS Professional Paper 1771 case [Fenelon et al., 2010]).

In conclusion, calibrations using alternate steady-state head data produce models that have less particle breakthrough near the model's southern boundary prior to 500 years, indicating that the contaminant boundary—which is dominated by short-lived RNs like ^{3}H, ^{137}Cs, and ^{90}Sr—will be less extensive than the base-case model.

2.2.3 Use of Parameter Bounds

This uncertainty addresses the concern that placing bounds on parameters during an estimation process can lead to models that are not realistic or that underpredict transport.

PRC Recommendation: The peer review team recommends reducing the number of parameters through re-parameterization, removing bounds from the parameters, including more calibration targets, and adjusting the model conceptualization and construction if the estimated parameter values are not reasonable. Parameters should not be constrained for the calibration. The resulting estimated parameter values should be compared with equivalent values measured in the field.

Substantial differences between the parameter values estimated by the calibration and the values measured in the field are an indication that there is a problem with model conceptualization or construction, and such clues should be used to improve the model.

RESPONSE: The effects on the model calibrations using reduced numbers of adjustable parameters are reported for several cases in Section 2.3.2 in response to uncertainties related to fault properties. Additionally, Section 2.2.6 examines the sensitivity of the model calibration to less constrained permeability and notes the results that the calibrated permeabilities did not reach their expanded range. Objective function values achieved in these alternate calibrations were similar to or greater than that for the base case, and the particle transport was similar to or less than the base case for the alternate cases that achieved acceptable calibrations.

Calibrations using reduced number of parameters found that including small faults with trace lengths less than 3 km is not needed to calibrate the model; however, tying the parameters for larger faults (traces greater than 3 km) produced a poor calibration. These results indicate that including small faults overparameterized the model; however, it is necessary to individually parameterize the larger faults to produce an acceptable calibration. Faults having varying hydraulic properties are consistent with qualitative characterization of faults at the NNSS (Sweetkind and Drake, 2007; and Prothro et al., 2009) in that damage zones tend to scale with fault offset; damage zones associated with large-offset faults (greater than 100 m) are many tens of meters wide.

The modeling team agrees that improperly constraining parameters during the calibration is a poor practice. However, unconstrained parameter values are not beneficial because the results they produce may not be meaningful to the analysis, whereas properly constrained parameters can focus the modeling analysis on appropriate solutions. In particular, the correlation between flux boundary conditions and hydraulic conductivity requires placing bounds on the flux boundary conditions or hydraulic conductivity. Furthermore, properly constraining parameters is a way to provide a priori information based on measured data that are not otherwise incorporated in the model. Hence, great care has been exercised in choosing the underlying conceptual flow model and setting bounds on parameters to be wide while being consistent with the available information about the flow system.

Consider the upper bound on the permeability of faults, which is currently set to a value of 1×10^{-09} square meters (m^2). Some of the NSMC simulations derived from the base-case calibration and uncertainty analysis (N-I, 2013a) produced fault permeability values at the upper level. While the

upper level could be increased, it is not reasonable to do so. It has been more than 20 years since the cessation of underground nuclear testing at the NNSS. No radioactivity associated with underground testing has been detected in the wells located in the southern portion of the YF/CM CAU (wells south of U-3cn 5). Using the upper bound permeability value currently used in the LCA model of 1×10^{-09} m^2 (representing an unrealistically conservative case of a fault continuously open over the entire length of Yucca fault), a north–south hydraulic gradient in the LCA of 0.0008 (Section 2.1.1), and an effective porosity of 0.02 (2 percent) yields a velocity of about 35 meters per day (m/day) (about 13 kilometers per year [km/yr]). At that velocity, a particle could traverse the entire length of Yucca Flat (30 km) from UE-10j to WW-C in less than three years. This can be contrasted against travel time estimates of ^{14}C that range around 10,000 years through Yucca Flat (Kwicklis and Farnham, 2014). Clearly, the upper limit of fault permeability is already overly conservative. Making it even larger is not reasonable.

The highest pumping test scale measurement of hydraulic conductivity within the LCA of Yucca Flat is approximately 130 m/day (1.5×10^{-10} m^2) from WW-C (SNJV, 2006a).The highest measured hydraulic conductivity value within the LCA of Yucca Flat is approximately 4,200 m/day (5×10^{-09} m^2) from logging Well ER-6-1. The ER-6-1 well cluster is located in a faulted area of the LCA and the may be representative of highly conductive fault damage zones. This high value is close to the upper-bound permeability of faults but represents only a 30-ft interval out of 1,385 ft of logging in a single well (SNJV, 2005a, Table 2-4). Averaging the permeability over the entire logged interval reduces the value to 8.7×10^{-11} m^2. Clearly, a value of 1.0×10^{-09} as a large-scale-average fault permeability is already overly conservative. Making it even larger is not reasonable.

The calibrated base-case hydraulic conductivities for faults or country rock span the entire range of large-scale K_{sat} values measured in the LCA (roughly 10^{-03} to 10^{+02} m/day). Although higher values of K have been estimated from borehole flow logs, these small-scale values are not at the appropriate scale to include in the model and ignore the fact that closely spaced measurements can differ widely, confirming that these are due to local heterogeneities. The large-scale cross-hole drawdown data from the ER-6-1-2 MWAT that were used to help calibrate the LCA model provide more scale-appropriate datasets.

In conclusion, greatly increasing the LCA model parameter bounds beyond those used in N-I (2013a) or those used in the model recalibrations presented in this document is not useful. Realistic parameter

bounds are needed to prevent exploring unrealistic parameter space. Several model recalibrations were performed using reduced numbers of fault parameters (see Section 2.3.2). Parameterizing the minor faults (faults other than the large basin-forming faults) is not needed to calibrate the LCA model, but individually parameterizing the large faults is needed to calibrate the LCA model. It is not necessary to further address this recommendation.

2.2.4 Omission of Available Calibration Data

The concern raised is that there are head measurements available from some wells that were not used in the LCA calibration.

PRC Recommendation: The peer review team recommends using an expanded model domain and more calibration targets including those that do not fit the conceptual model of a flat potentiometric surface in the LCA. An attempt should be made to include features in the model that will generate heads similar to the targets. The residuals related to all of the measurements (excluding outliers that are likely errors and recovery conditions) should be presented. A critical review of all calibration data with respect to water levels, thermal effects, well completions, geophysical logs, and core and cuttings should be undertaken to clarify the conceptual model. Head data from all wells should be reevaluated to confirm the location of targets in the AA/VA/TCU/LCA, to determine whether each head measurement represents normal pressurization, and to assess whether the well completion is sufficient to ensure there is minimal communication between zones. If results of the reassessment are inconclusive, single-point piezometers should be installed in key areas as determined from the analysis.

RESPONSE: The modeling team performed a critical review of the LCA model steady-state calibration data and performed several alternative LCA model calibrations. The base case is conservative compared to the alternate models with respect to particle breakthrough at times prior to 600 years. All the models, except one, have similar or less particle breakthrough at 1,000 years. The case using data quality in the weights had 79 percent breakthrough at 1,000 years, but the objective function is high (16.4), indicating a poorer agreement with observations. These alternate simulations are documented in other sections including the following:

- Section 2.2.1 presents a review of the additional calibration wells identified by the PRC and a recalibration of the LCA model using the additional wells as calibration targets.

- Section 2.2.2 presents several LCA model simulations that use alternative water-level data sources to develop steady-state calibration targets, including using multiple targets at locations with transient water levels not associated with anthropogenic activities.
- Section 2.2.5 presents an analysis of LCA water-level data quality and correction of water levels for thermal effects. The LCA model was recalibrated using the temperature corrected data and steady-state calibration weights that consider data quality.

The conclusion was that particle breakthrough was similar to or less than the base case, except for the alternate model discussed in Section 2.2.5. For that model, the total particle breakthrough near the model's southern boundary within 1,000 years was larger (79 percent) than the base case (64 percent); however, particle breakthrough prior to 600 years is less than the base case, indicating that the contaminant boundary—which is dominated by short-lived RNs such as ^{3}H, ^{137}Cs, and ^{90}Sr—will be less extensive than the base-case model. Hence, it is not necessary to further address this recommendation.

2.2.5 Using the Jacobian to Determine Weights for Targets

This uncertainty was focused on determining target weights from data quality rather than mathematical constructions.

PRC Recommendation: The peer review team recommends determining weights for each target by evaluating the quality of the target data based on well construction and measurement procedures.

RESPONSE: The LCA model was recalibrated using the temperature-corrected data and steady-state calibration weights that consider data quality as described below. It was found that the current base-case model achieves a better calibration (1.15) than did the alternate model (16.4).

Original weights on steady-state and transient head observations reported in N-I (2013a) reflect the goal of having each data type influence the calibration. Alternative weighting schemes can be implemented based on observation data accuracy (i.e., weights are the inverse of the standard deviation of the measurements) to investigate the impact of weighting scheme (and measurement uncertainty) on parameter estimates. This approach will tend to de-weight observations made in the western part of the basin where natural transients have caused heads to increase over the last several decades. This also fits with the idea of using the greatest number of locations, appropriately weighted for uncertainty, to better constrain the model.

The modeling team performed a critical review of the LCA water-level data quality and a model calibration considering data quality in the steady-state head. The steady-state head data were reviewed to estimate a total uncertainty related to the following:

- Land surface accuracy
- Depth-to-water measurement accuracy
- Borehole deviation correction
- Barometric effects
- Variability in steady-state water levels due to recharge transients
- Water temperature effects

The predevelopment water levels reported by Fenelon et al. (2012) included an estimate of water-level measurement accuracy and land surface accuracy for each well. All Yucca Flat steady-state water-level measurements were accurate to within 1 ft. The water-level measurement and land surface uncertainties reported by Fenelon et al. (2012) are used for the depth-to-water and land-surface elevation uncertainty (Table 2-3).

Within the water levels reported by Fenelon et al. (2012), the errors caused by borehole deviation in the conversion from depth-to-water to water-level altitude are generally less than 0.5 ft. Where the errors are known to be larger, the measured water levels are corrected for borehole deviation (Elliott and Fenelon, 2013). The uncertainty associated with borehole deviation is assumed to be 0.5 ft for all wells.

Changes in barometric pressure can cause fluctuations in water levels of confined and semi-confined aquifers that are not a reflection of head changes in the aquifer, thus adding uncertainty in head measurements. Barometric pressure and water level are inversely related, and an increase of barometric pressure causes a decrease in water level. The barometric pressure changes are most pronounced when regional storms occur in the fall, winter, and spring seasons. Water-level modeling of distal well response pumping tests by N-I (2013a) determined that the fluctuations in water levels due to barometric effects are generally less than 1 ft during the fall, winter, and spring seasons. A 1-ft uncertainty is used to represent barometric effects on water-level elevations for all wells.

The uncertainty due to variability in steady-state water levels is estimated as the standard deviation of all water-level measurements. The water-level data from Elliott and Fenelon (2013), considered representative of predevelopment conditions, are used to determine the standard deviation for all water-level measurements at each well. Wells with limited data (insufficient number of measurements

Table 2-3
Water-Level Uncertainty for LCA Model Steady-State Calibration Targets

Land Surface Accuracy (ft)	Land Surface Accuracy Uncertainty (m)	Water-Level Measurement Accuracy Uncertainty (m)	Record Count	Standard Deviation (m)	Data Period (yr)	Temperature Corrected Average Water Altitude (m)	Temperature Correction (m)	Water-Level Variability Uncertainty (m)	Temperature Uncertainty (m)	Total Uncertainty (m)[a]
WW-C-1	0.30	0.30	17	0.48	36	726.6	--	0.48	1.5[b]	3.05
ER-6-2	0.30	0.03	78	0.50	17	746.2	0.2	0.50	--	1.30
ER-6-1	0.30	0.03	35	0.09	8	728.4	-0.2	0.09	--	0.88
UE-1h	0.30	0.03	69	0.51	44	745.2	1.5	0.51	--	1.30
ER-3-1-1	0.30	0.03	2	0.01	1	728.7	--	0.51[c]	1.5[b]	2.80
U-3cn 5	0.30	0.03	102	0.21	46	726.5	-1.6	0.21	--	1.00
TW-E	0.30	0.30	4	0.49	40	731.6	--	0.51[c]	1.5[b]	3.08
UE-1q	0.30	0.03	77	0.08	20	740.3	0.9	0.08	--	0.87
UE-7aa	0.30	0.30	8	0.56	2	729.7	--	0.56	1.5[b]	3.13
TW-D	0.30	0.03	80	0.19	47	739.9	0.1	0.19	--	0.98
ER-7-1	0.30	0.03	41	0.14	9	729.1	-0.3	0.14	--	0.93
UE-7nS	0.30	0.30	184	0.27	36	730.7	-0.1	0.27	--	1.34
U-10L-1	0.30	0.30	3	0.42	8	733.4	--	0.51[c]	1.5[b]	3.08
WW-2	0.30	0.03	73	0.31	19	737.4	0.7	0.31	--	1.10
UE-10j	0.30	0.03	61	0.22	15	736.7	0.1	0.22	--	1.02

[a] Total uncertainty for each well, calculated by adding the cells shaded in gray in the row for that well. Total uncertainty may vary from the summed total as a result of rounding. All wells have 0.30 m barometric effect and 0.15 borehole deviation uncertainty along with barometric effect and borehole deviation uncertainty.
[b] Temperature data not available for well; use the 95th percentile correction for all wells.
[c] Fewer than five-year monitoring period and five measurements; use the greater of 95th percentile standard deviation for all wells or well location standard deviation.

-- = Not applicable

or a short monitoring time period) have an uncertainty assigned to these wells that is taken from the 95th percentile of the standard deviations for all wells with sufficient data. Using the 95th percentile value of the standard deviations for wells with data conservatively estimates this uncertainty toward a large value. Wells with fewer than five measurements and/or a less than a five-year monitoring period were considered to have insufficient data.

Water temperatures affect the water levels by altering the density of the water column in the well and the length of the water column above the completion interval. The water level in a well with a higher temperature will be greater than the water level in a well with a lower temperature. The water-level data used for the steady-state calibration targets were not corrected for temperature effects (N-I, 2013a). Reiner (2007) provides groundwater temperature data for wells at and in the vicinity of the Nevada Test Site (NTS) during the years 2000 through 2006. The groundwater temperature profile data from Reiner (2007) were used to correct the Yucca Flat water levels. Correction of the Yucca Flat steady-state wells within the LCA for water temperature effects is possible because all wells are completed in the same aquifer with similar geothermal conditions, and most of the wells have a similar depth. The average water column temperature for the LCA steady-state calibration wells is approximately 37 degrees Celsius (°C). All wells with higher temperatures have the water levels adjusted down, as water has lower density at higher temperature, and wells with a lower temperature have water levels adjusted up. The wells without temperature data have an additional source of uncertainty that is the 95th percentile temperature correction value (1.5 m) for all wells with temperature data.

The steady-state water-level weights are proportional to the inverse of the total uncertainty for each well. The weight for each well is normalized by the sum of the weights for all the steady-state targets used in the base case. Normalizing the weights considering data quality by the total weight of the base-case weights ensures that weighting between the steady-state heads and ER-6-1 MWAT transient heads is the same as that used in the base case and facilitates direct comparison of the objective functions. Table 2-3 summarizes the water-level uncertainty for each steady-state calibration target.

The LCA model recalibration with temperature corrected water levels and weights considering data quality achieved a higher objective function (16.4) compared to the base case (1.15) primarily due to the temperature corrected water levels not being matched by the model. The temperature corrections at Wells U-3cn 5 and UE-1h are approximately equal to the residual at these wells. The availability of

temperature profile data at these wells also decreased the uncertainty and increased the weights compared to the other wells used in the steady-state calibration. Figure 2-20 illustrates the particle breakthroughs for the base case and calibration considering data quality flow fields. The total particle breakthrough near the model's southern boundary within 1,000 years was larger (79 percent) than the base case (64 percent), but particle breakthrough prior to 600 years is less than the base case. As discussed in Section 2.2.2, slower transport prior to 200 years is significant for the contaminant boundary because ^{3}H is largely removed by radioactive decay after 200 years.

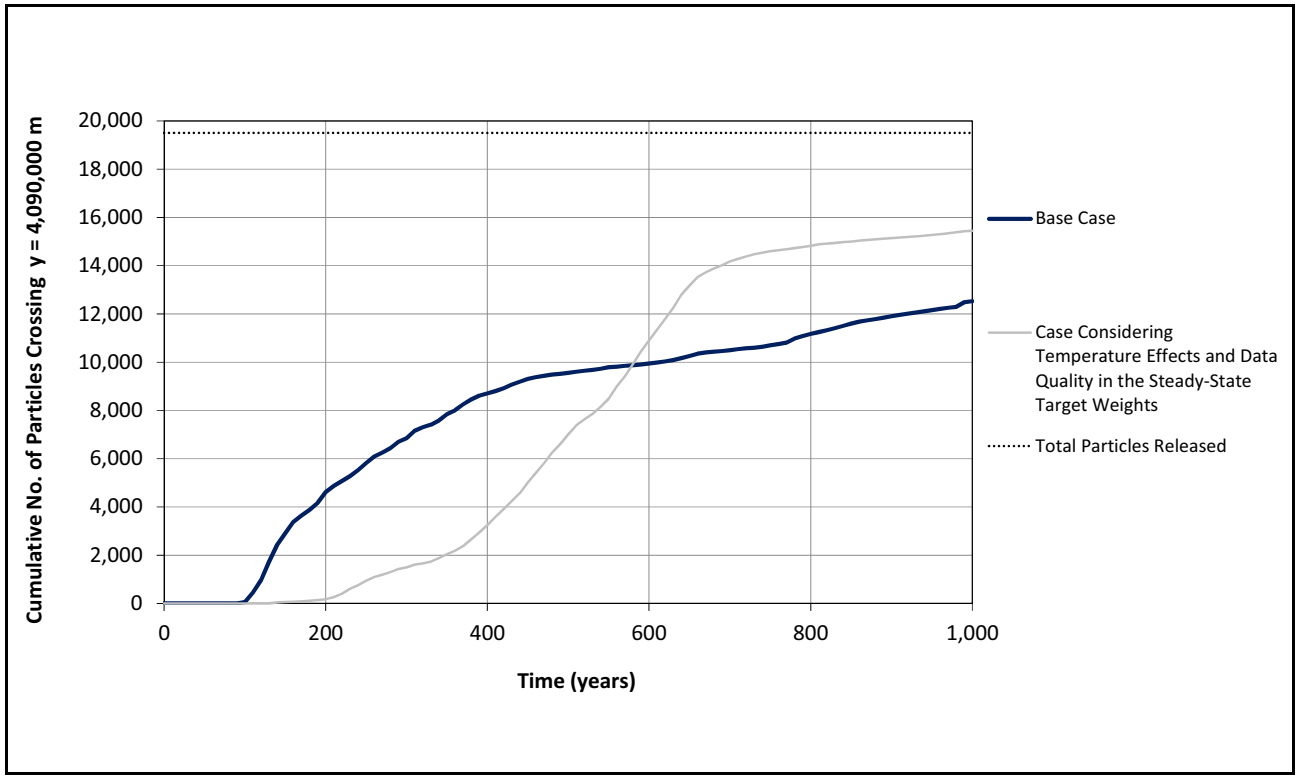

Figure 2-20
Particle Breakthrough for the Base Case and the Case Considering Data Quality in the Steady-State Target Weights

In conclusion, the overall pattern of transport for the alternate case is similar to the base case, but total particle breakthrough near the model's southern boundary within 1,000 years is larger (79 percent) than the base case (64 percent). Section 2.7.4 presents additional flow fields used to evaluate transport uncertainty and its effect on the contaminant boundary, which included this case. Although total particle breakthrough for this case is higher than the base case, the southern extent of the 95th percentile contaminant boundary is less than the base case.

2.2.6 Field Measurements of Hydraulic Conductivity Not Honored in the Calibrated Model

This uncertainty was motivated by the fact that estimated parameter values do not match all the field measurements.

PRC Recommendation: The peer review team recommends that parameters be estimated without bounds, and the estimated parameter values be compared with equivalent values measured in the field. Substantial differences between the parameter values estimated by the calibration and the values measured in the field are an indication that there is a problem with model conceptualization or construction. These clues should be used to improve the model. If the parameters are unreasonable, adjust the model conceptualization and/or construction.

RESPONSE: The modeling team agrees that improperly constraining parameters during the calibration is a poor practice. However, unconstrained parameter values are not beneficial because the results may not be meaningful. Parameter constraints are needed for realistic model calibration, and reaching these bounds is not a problem if they represent a realistic bounding estimate for the parameter. In particular, the correlation between flux boundary conditions and hydraulic conductivity requires placing bounds on the flux boundary conditions or hydraulic conductivity. Hence, great care has been exercised in choosing the underlying conceptual flow model and in setting bounds on parameters to be wide while being consistent with the available information about the flow system.

Small-scale hydraulic conductivity estimates from borehole flow logs or from single-well tests are naturally expected to display more variability than volume-averaged estimates produced by cross-hole responses to pumping. Large-scale properties (over hundreds or thousands of meters) appropriate for direct application in the LCA model are best defined from cross-hole responses to pumping, not conductivity estimates from single-well tests or borehole flow logs that represent local-scale conditions. This philosophy is reflected in the flow and transport document (N-I, 2013a) and remains the position of the modeling team. Bounds were placed on the possible range of permissible parameters so that the parameter estimation code PEST searched only for parameter combinations that were physically plausible. This is a valid approach when no specific data exist for a specific model feature but a range of values for similar features has been measured elsewhere. This approach was adopted by the modeling team, as documented in N-I (2013a), and remains a valid approach.

It should be noted that although the parameters estimated by PEST are given appropriate limits, the combined stresses on the system generated by the superimposed set of boundary conditions may cause one or several permeability terms to reach their limits. This is not seen as a problem, considering the reasonableness of the permeability limits. To examine the sensitivity of the LCA model calibration to less constrained permeability, the modeling team performed an LCA model calibration considering moderately expanded country rock and fault permeability bounds that are realistic when compared to field scale measurements. Scale dependence of permeability values is well recognized. For example, Geldon (2004) analyzed Yucca Mountain Project core, slug, single-well, and cross-hole pumping test scale data from the volcanic tuffs in the c-holes complex and the nearby CP basin, and noted a distinct effect of increasing hydraulic conductivity with test scale. Cross-hole hydraulic conductivity was found to be approximately a factor of 10 higher than the single well hydraulic conductivity for hydraulic conductivity values greater than 1 m/day.

Section 2.3.1.2 presents a review of Yucca Flat pumping scale measurements of hydraulic conductivity, and Section 2.3.2 presents a review of Well ER-6-1 hydraulic conductivity data, which are believed to be representative of a fault damage zone. These data were used to select expanded parameter ranges that encompass the measured hydraulic conductivity data recognizing that model or cross-hole scale permeability may be larger than the single well values.

In response to PRC comments regarding spatial distribution of hydraulic conductivity measurements, the modeling team also considered an LCA model recalibration using rezonation of the SZ LCA, which divided the three north–south zones into northern and southern components. As summarized in Table 2-4, the ranges of values for the southern zones were taken to be higher than the corresponding northern zones because the pump test hydraulic conductivities are generally higher in southern Yucca Flat compared to northern Yucca Flat. Table 2-5 (see Section 2.3.1.2) summarizes available Yucca Flat pump test permeability data). The LCA model rezonation is discussed in Section 2.3.1.2. The ranges of values for the fault parameters were also expanded to encompass the measured hydraulic conductivity data. The minimum permeability of all faults was lowered to 1.0×10^{-15} m^2, and the maximum permeability was increased to 1.0×10^{-09} m^2.

The LCA model recalibration achieved a higher objective function (9.5) compared to the base case (1.15) due to underpredicting steady-state heads in western Yucca Flat. Figure 2-21 illustrates particle locations and times for the base case and expanded parameter range fields. Transport from the

Table 2-4
LCA Model Country Rock Permeability Bounds Estimated from Pumping Test Scale Measurements and Calibrated Values

Model Zone	Initial Value (m^2)	Lower Bound (m^2)	Upper Bound (m^2)	Calibrated Value (m^2)
North LCA east	4.41×10^{-12}	1.0×10^{-15}	1.0×10^{-10}	1.49×10^{-12}
South LCA east	4.41×10^{-12}	1.0×10^{-14}	1.0×10^{-09}	2.93×10^{-12}
North LCA central	1.69×10^{-13}	1.0×10^{-15}	1.0×10^{-10}	4.25×10^{-14}
South LCA central	1.69×10^{-13}	1.0×10^{-14}	1.0×10^{-09}	6.07×10^{-14}
North LCA west	1.22×10^{-13}	1.0×10^{-15}	1.0×10^{-10}	1.23×10^{-13}
South LCA west	1.22×10^{-13}	1.0×10^{-14}	1.0×10^{-09}	7.14×10^{-14}

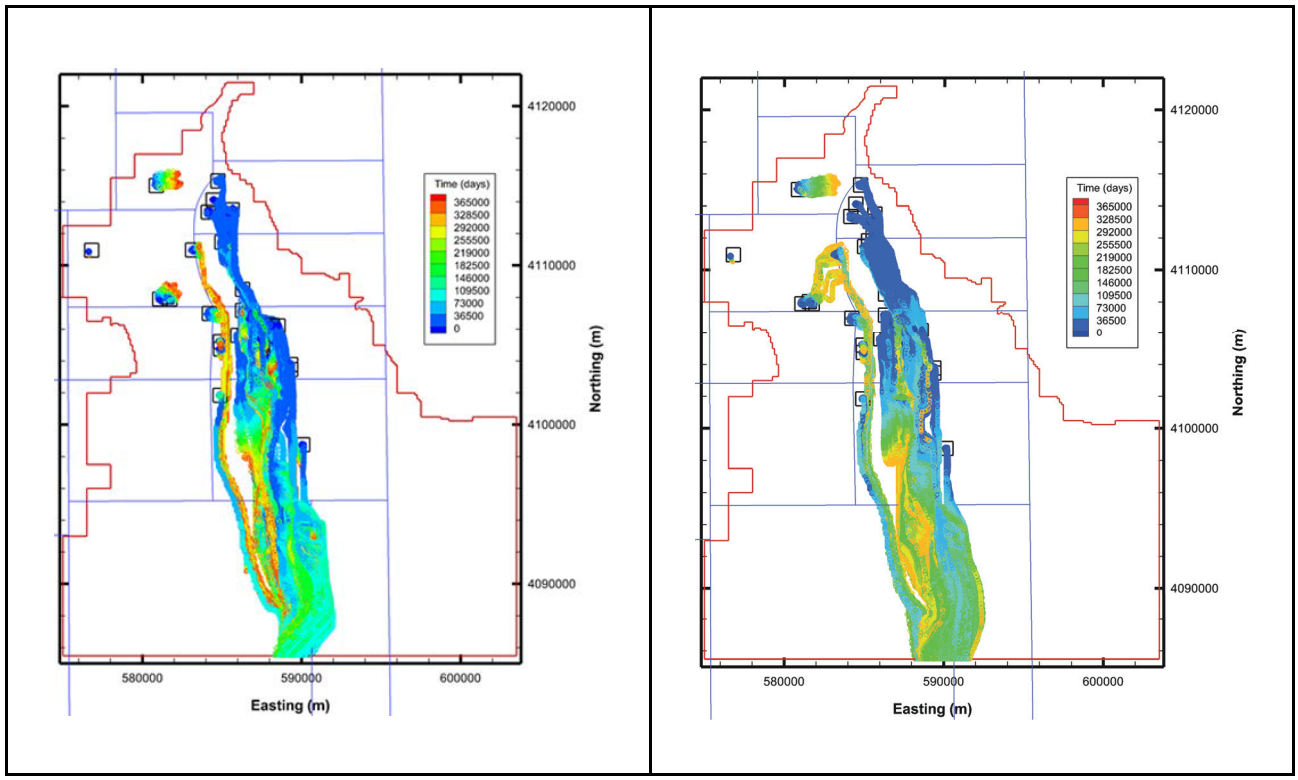

Figure 2-21
Particle Travel Paths and Times for the Base-Case (left) and Expanded Parameter Range (right) Flow Fields

detonations located in the northern area of the LCA is faster compared to the base case due to an order of magnitude higher permeability of the LCA central zone and five times higher Yucca fault permeability. Figure 2-22 illustrates the particle breakthrough for the base case and expanded parameter bound case. The 1,000-year particle breakthrough at the southern line of demarcation is less than the base case (56 percent) because the northern and eastern fluxes are a factor of 2 and 6

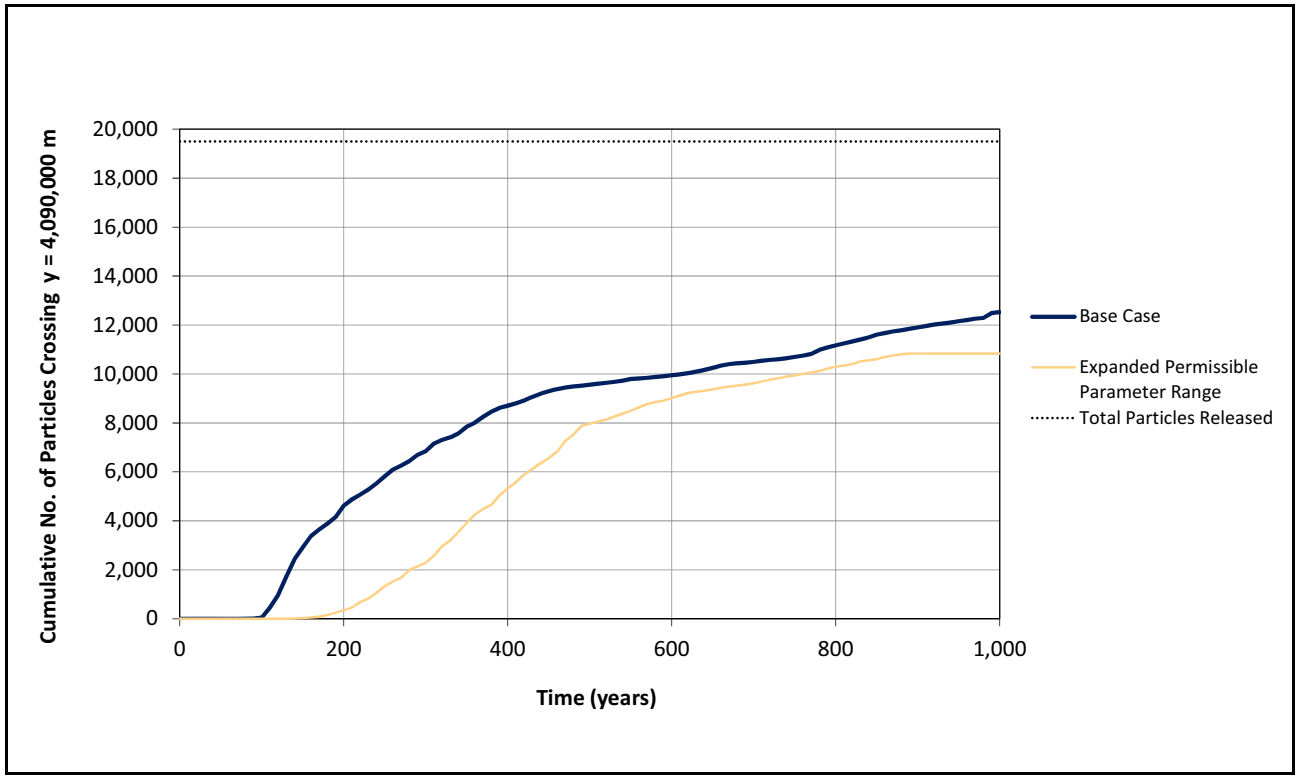

Figure 2-22
Particle Breakthroughs for the Base-Case and Calibration with Expanded Parameter Range Flow Fields

smaller, respectively, than the base case. The majority of the Yucca Flat detonations within 3 R_c of the SZ LCA are located east of Yucca fault in the model's LCA east zone.

Comparing the calibrated country rock permeability values in Table 2-4 with the pump test data and base-case calibrated permeability values in Table 2-5 (see Section 2.3.1.2) illustrate that the calibrated country rock permeabilities are generally within the range of pump test data and similar to the base-case values. Furthermore, none of the fault or country rock permeability values reached their expanded limits. These results indicate that the current conceptual model of the SZ LCA is appropriate.

2.3 Uncertainty in Hydraulic Properties and Pathways

2.3.1 Country Rock

2.3.1.1 Limited Characterization of Aquifer Properties

This uncertainty concerns large-scale hydraulic conductivity measurements.

PRC Recommendation: The MWAT at ER-6-1 (1) provided the only calibration data that somewhat reduced the non-uniqueness of the Yucca Flat model calibration yet renders only seven of the many model parameters identifiable (all in the vicinity of the MWAT) and (2) did not test the central or western portions of Yucca Flat. Consequently, the peer review team recommends additional large-scale MWATs in the central and western portion of Yucca Flat to assess hydraulic properties of the country rock and faults, and to evaluate boundary conditions. Otherwise, there is little basis to justify setting such markedly lower permeabilities in the LCA west and central zones, compared with the permeability in the LCA east and ER-6-1 MWAT results.

RESPONSE: A range of parameter values were considered during the calibration of the flow and transport model. The calibrated parameters and their uncertainty fall within the ranges of measured values. Lower permeability values for the western and central portions compared to those for the eastern portions of Yucca Flat were selected by the calibration process in order to match the observed head data in each portion of Yucca Flat.

In addition to the faults explicitly represented in the model, the LCA was divided into three regions for model parametrization: east of the Yucca fault (LCA east), west of the Carpetbag fault (LCA west), and the area between the Yucca and the Carpetbag faults (LCA central). During the model calibration, the upper ranges of rock permeabilities for the west (3.0×10^{-11} m^2) and central (4.0×10^{-11} m^2) regions were actually higher than that for the east region (1.0×10^{-11} m^2) because there are few measurements in the west and central areas, and uncertainty is greater in these areas compared to the LCA east. Model calibration led to a higher value of permeability for LCA east (1.25×10^{-12} m^2) compared to that for the LCA west and central (1.0×10^{-14} and 1.85×10^{-14} m^2, respectively).

This result is consistent with the presence of a higher-permeability eastern corridor and the conceptual model that permeability in eastern Yucca flat is higher than the permeability in the central

and western areas. Several investigators have recognized a high-permeability corridor east of Yucca fault that is made evident by a prominent north–northwest-trending trough in the potentiometric surface about 20 mi long and 2 to 8 mi wide (Winograd and Thordarson, 1975).

Low permeabilities in central and western portions of Yucca Flat were selected by the calibration process, from a range of values with upper limits greater than that specified for the eastern portion. Matching the observed hydraulic head data in the western and central portions of Yucca Flat required the model to select lower permeability values than those for the eastern portion. These portions of the Yucca Flat LCA did not respond to the ER-6-1-2 MWAT, so the calibrated permeabilities for these were constrained solely by steady-state heads that indicate west–east flow (Fenelon et al., 2012), across the structural fabric of the rock and reflect lower permeability. Further, the majority of the source locations are not in the central and western portions of the basin; if tests within 3 R_c of the top of LCA are considered, only 9 out of 39 locations lie within the central and western Yucca Flat. These 9 test locations may not contribute much to the contaminant boundary if, as indicated by potentiometric surface map of Fenelon et al. (2012, Plate 4), groundwater must first flow east of the Yucca Fault before flowing south. Hence, refining hydraulic conductivity estimates for the western and central portions of Yucca Flat may lead to relatively small gains in reducing the uncertainty in the contaminant forecasts.

Hydraulic gradients across the western and central portions of the basin appear to be west to east (Fenelon et al. 2012), indicating that in the absence of strong north–south anisotropy, these zones convey groundwater to the eastern portion of the basin rather than southward out of the basin. North–south anisotropy in these zones can be evaluated by comparing groundwater chemical and isotopic data from ER-4-1 and ER-3-3 with groundwater from upgradient areas in the northern and western parts of the basin to identify large-scale flow directions in these zones. Therefore, the fluxes through the western and central portions of the basin could be included in the north–south flux estimate of approximately 20 kg/s already estimated for the eastern corridor if the groundwater chemical data support west-to-east flow across the western and central zones.

Three new wells (ER-2-2, ER-3-3, and ER-4-1) have been drilled within the central part of Yucca Flat between the eastern strand of the Yucca fault and the western strand of the Topgallant fault. Twenty-three existing wells—with nearest-neighbor at distances about 1.13 mi (for the well pair ER-2-2 and ER-2-1), 0.3 mi (for the well pair ER-3-3 and TW-7), and 0.54 mi (for the well pair

ER-4-1 and UE-4t)—were instrumented with pressure transducers, and the water-level responses at these neighboring wells to dewatering of new wells during drilling were recorded. Preliminary results indicate that neighboring wells did not show any responses to the drilling activities. Additionally, water pumping rates out of these wells have been below 100 gallons per minute (gpm). These observations support the conceptual model of permeabilities being lower at least in the neighborhood of each well.

2.3.1.2 Model Permeabilities Inconsistent with Field Measurements

This uncertainty is focused on the apparent mismatch between the permeability values used in the model versus pumping-scale data.

PRC Recommendation: The peer review team recommends honoring the available hydraulic properties data for the country rock in assessing uncertainty in the extent of the contaminant boundary. Unless the field-measured hydraulic conductivity data are weighted more heavily in parameterizing the model, the available information suggests that the southern extent of the contaminant boundary will be underestimated. The choice of NSMC run 46 as the fast scenario in evaluating the extent of the contaminant boundary seems to be misleading. The peer review team recommends reevaluation of the choice of a fast scenario and additional simulations to account for other uncertainties described elsewhere in this report.

RESPONSE: The calibrated base-case country rock and fault hydraulic conductivity values largely honored the available hydraulic conductivity data. The NSMC flow fields from N-I (2013a) were examined using particle tracking. Additional NSMC fast flow fields were identified and run through transport. It was found that the southern extent of RN migration was not extremely different from NSMC run 46 or the base case. The LCA model was recalibrated using north–south subzones for each of the west, central, and east zones of the LCA. It was found that the current base-case model is more conservative than or similar to the alternate models with respect to particle breakthrough near the model's southern boundary.

The calibrated base-case hydraulic conductivities (N-I, 2013a, Table 5-11) span the entire range of pumping-scale *K* values measured in the LCA of Yucca Flat (roughly 10^{-03} to 10^{+02} m/day) (Figure 2-23). The relevant numbering used in the LCA model is shown in Figure 2-24. Although higher values of *K* have been estimated from borehole flow logs, these small-scale values are not at

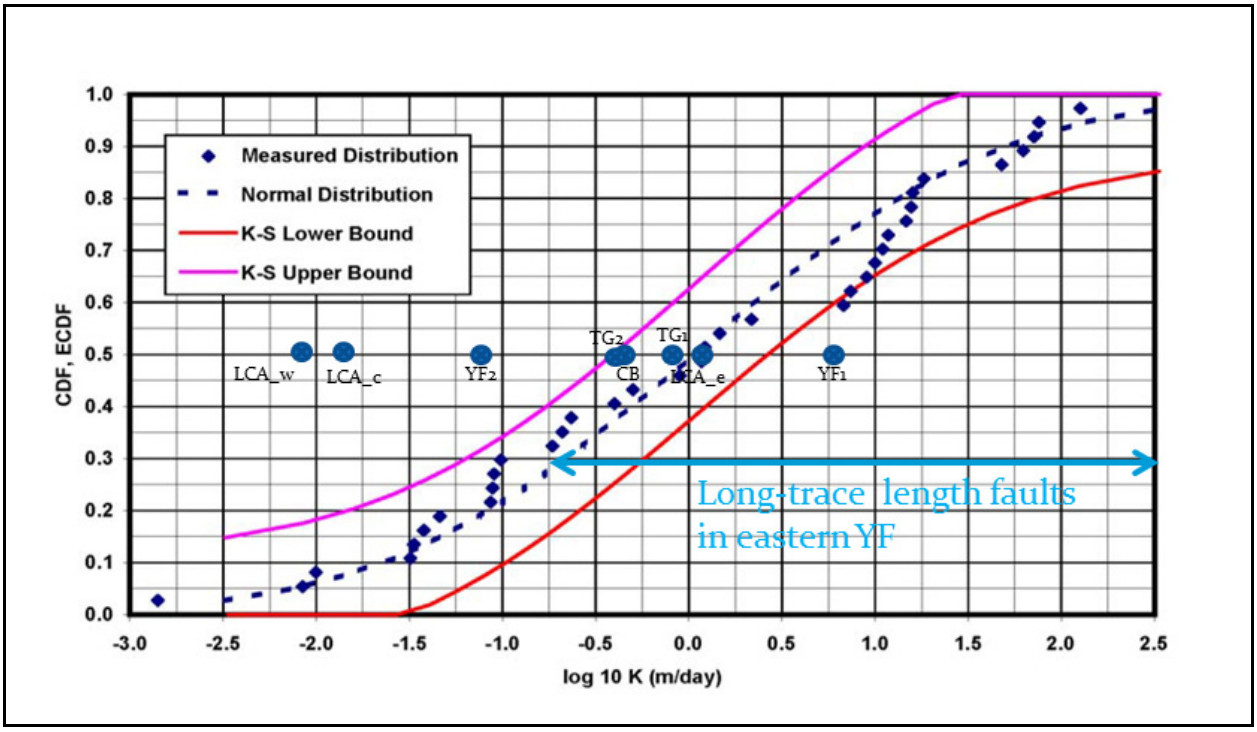

Figure 2-23
Comparison of Calibrated Base-Case Parameters for the LCA Model (N-I, 2013a, Table 5-11) with Pumping Scale Hydraulic Conductivity Measurements from Yucca Flat (SNJV, 2006b, Figure 6-19)

Note: LCA_w, LCA_c_, and LCA_e are the hydraulic conductivities for the country rock in western, central, and eastern Yucca Flat; YF2 and YF1 are the eastern and western strands of the Yucca fault; TG2 and TG1 are the western and eastern strands of the Topgallant fault; CB is the Carpetbag fault. Long-trace length faults include 171_yf_125, 149_area3n9, 150_yf_embud, 139_hp72_yf1, 156_yf_71, 147_yf_103n1, 155_yf_61a63, and 156_yf_71 of N-I (2013a, Table 5-11).

the appropriate scale to include in the model and ignore the fact that closely spaced measurements can differ widely, confirming that these are due to local heterogeneities. The large-scale cross-hole drawdown data from the ER-6-1-2 MWAT that were used to help calibrate the LCA model provide more scale-appropriate datasets.

The assignment of permeability to country rock, for example, provides for a single value, not a heterogeneous distribution as exists in nature. This does lead to cases where the calibrated value is different from a local permeability measurement.

To identify flow fields with fast and slow transport, the modeling team originally placed particles at 12 key locations where RNs originate in the LCA (N-I, 2013a). The team has expanded the set of possible contaminant sources to 39 (i.e., the detonations within 3 R_c of the SZ LCA) to identify alternate fast flow fields for transport uncertainty evaluation. Section 2.7.4 presents contaminant

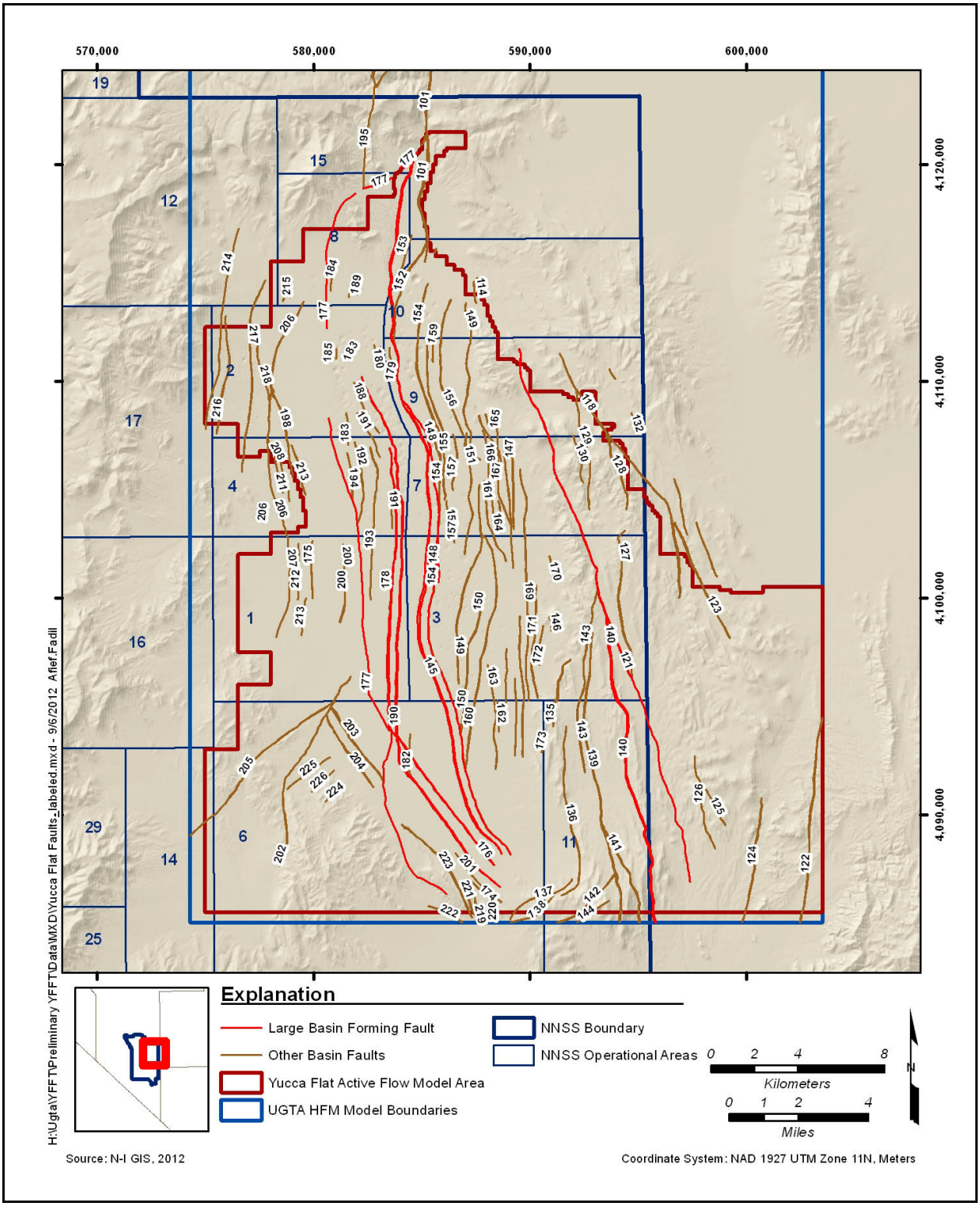

Figure 2-24
Faults Included in the Yucca Flat LCA Flow and Transport Model
Source: N-I, 2013a, Figure 5-30

boundaries using additional flow fields, including alternative *fast* cases as predicted by particle breakthrough in the NSMC simulations.

The modeling team examined the spatial distribution of Yucca Flat field scale permeability data and has created a set of simulations where country rock permeability is zoned into north/south subzones to determine whether alternative country rock conceptualizations substantially alter the flow and transport compared to the base case. The available hydraulic conductivity data from pumping tests is presented in previous reports (SNJV, 2006b). A total of 36 hydraulic conductivity measurements are available, which include 13 locations that are spatially unique within the LCA. Figure 2-25 illustrates the spatial distribution of the pumping test data. An examination of the hydraulic conductivity data using GSLIB (Deutsch and Journel, 1992) was performed to evaluate spatial correlations that would support zonation. The data exhibit a very slight spatial correlation to a distance of approximately 12 km. The sparse hydraulic conductivity data and large possible correlation distance support only a simple rezonation of the SZ LCA model. Casual inspection of the hydraulic conductivity data reveals that the three highest hydraulic conductivity measurements are located in southern Yucca Flat, and the three lowest hydraulic conductivity measurements are located in central or northern Yucca Flat.

During the LCA flow model construction, the model domain was divided into three distinct zones (east, west, and central) in order to honor the hydrogeological data while maintaining the number of parameters as low as possible. The LCA east refers to the LCA in the model area east of the Yucca fault; the LCA west refers to the LCA west of the Carpetbag fault; and the LCA central refers to the LCA in the area between the Yucca and Carpetbag faults (N-I, 2013a). The model's three north–south zones were subdivided into northern and southern components at Northing 4,100,000 (Figure 2-26).

Recognizing that permeability data are generally log-normally distributed, the geometric mean of the pumping test permeability data within each model subzone was calculated and is summarized in Table 2-5 along with the calibrated LCA model base-case and subzonation case permeabilities. The geometric mean permeability values for country rock zones are generally 1 to 2 orders of magnitude higher than the calibrated base case except for the northern subzone of the LCA east.

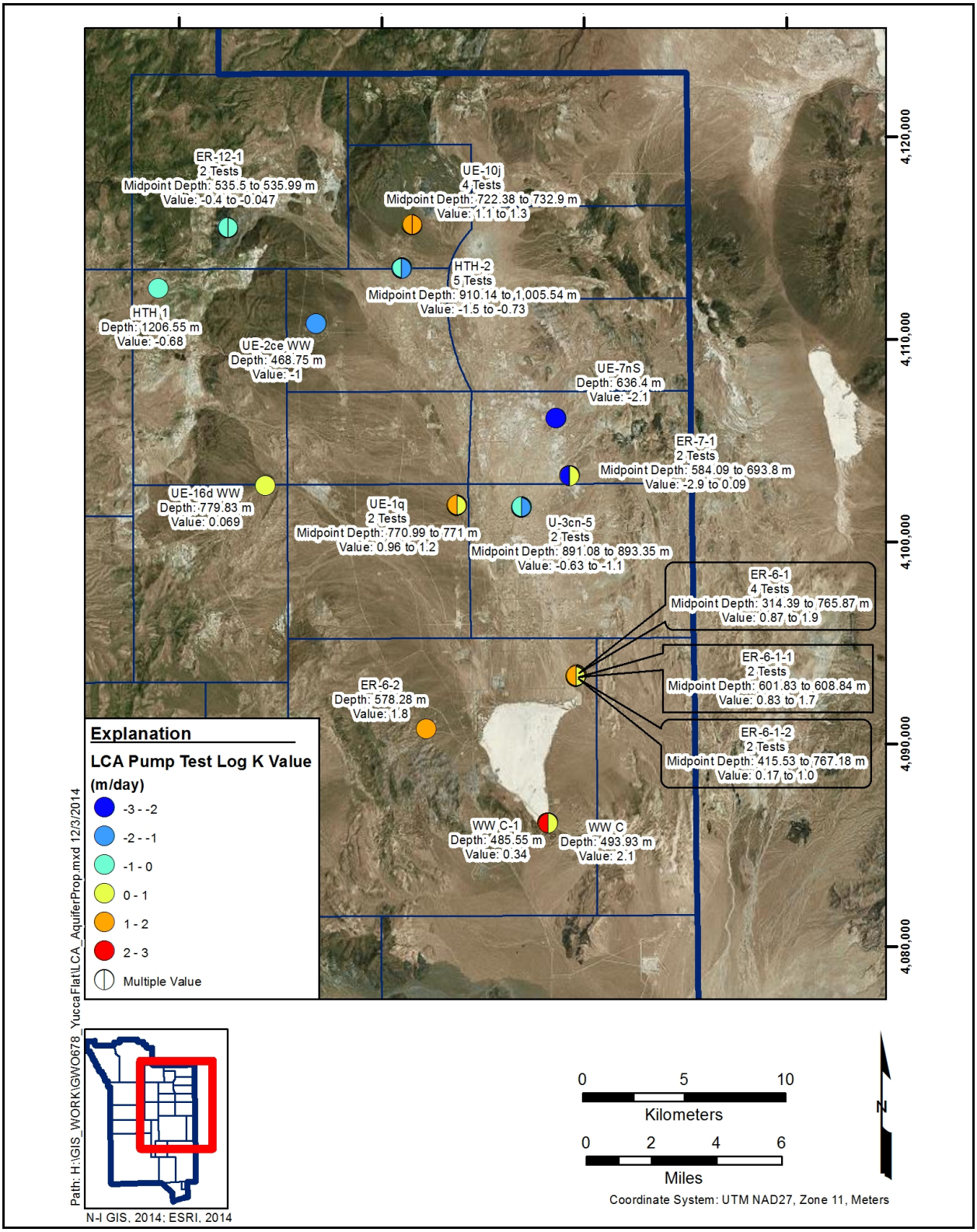

Figure 2-25
Spatial Distribution of Pumping-Scale Hydraulic Conductivity Values for the LCA
Source: N-I, 2015

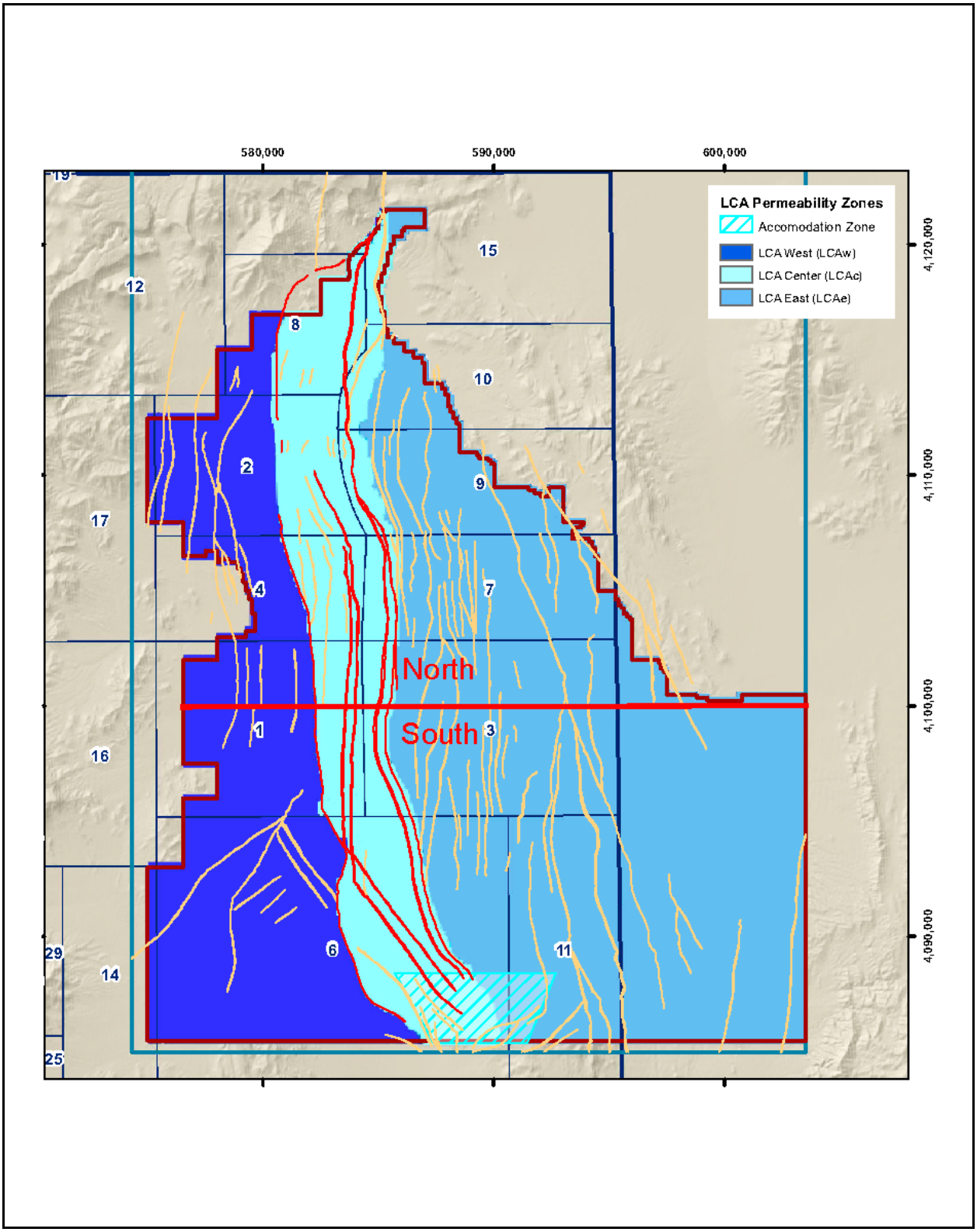

Figure 2-26
LCA Model North–South Rezonation

Table 2-5
Geometric Average Permeability of Pumping Test Data Located within LCA Model Subzones

Model Zone	Count	Average k (m^2)	Minimum k (m^2)	Maximum k (m^2)	Calibrated LCA Model Base Case (m^2)	Calibrated LCA Model with Rezonation (m^2)
North LCA east	5	5.9×10^{-14}	1.7×10^{-15}	1.4×10^{-12}	1.25×10^{-12}	1.49×10^{-12}
South LCA east	8	1.7×10^{-11}	1.7×10^{-12}	9.0×10^{-11}	1.25×10^{-12}	2.93×10^{-12}
North LCA central	11	1.4×10^{-12}	4.0×10^{-14}	2.2×10^{-11}	1.8×10^{-14}	4.25×10^{-14}
South LCA central	2	2.0×10^{-11}	2.6×10^{-12}	1.5×10^{-10}	1.8×10^{-14}	6.07×10^{-14}
North LCA west	1	1.1×10^{-13}	1.1×10^{-13}	1.1×10^{-13}	1.0×10^{-14}	1.23×10^{-13}
South LCA west	1	7.4×10^{-11}	7.4×10^{-11}	7.4×10^{-11}	1.0×10^{-14}	7.13×10^{-14}

To evaluate the LCA model's sensitivity to alternate country rock permeability parameterizations and evaluate the model's general consistency with permeability observations, the LCA model was recalibrated for three alternate country rock permeability cases:

1. Calibrated permeability within north–south subzones of the country rock zones.
2. Fixed country rock permeability calculated as geometric mean of pumping test hydraulic conductivity within each subzone.
3. Calibrated permeability using expanded bounds on country rock and fault permeability that encompass the measured values. This recalibration is presented in Section 2.2.6.

Table 2-6 summarizes the model recalibration results investigating country rock permeability and zonation uncertainty. In general, recalibration of the LCA model with north–south subzones produces higher country rock permeability compared to the base case, particularly within the LCA west zone. The higher permeability of the LCA west and LCA central zones resulted in the models underpredicting steady-state water levels in wells located in western Yucca Flat (ER-6-2, UE-1h, UE-1q, TWD, and WW-2). Figure 2-27 illustrates particle locations and times for the base case, north–south subzones, and north–south subzones with specified permeability flow fields. All simulations have a higher Yucca fault permeability, which results in faster transport from detonations located near Yucca fault. Figure 2-28 illustrates the particle breakthrough for the base case and cases with country rock subzones. The subzonation with specified country rock permeability, while increasing the particle velocities in the western part of the model, decreases them in the eastern part of

Table 2-6
Summary of Simulations Investigating Country Rock Permeability and Zonation Uncertainty

Simulation	Objective Function	Percentage of Particle Breakthrough within 1,000 Years	Calibration Summary
Base case	1.15	64	• This is a baseline metric to evaluate the influence of alternate flow simulations.
North–south subdivision of country rock zones	9.45	66	• All calibrated country rock permeability is higher than the base case. • The heads are notably lower in the model's western area due to the higher LCA west and LCA central permeability. • There is faster transport from detonations located in the LCA central zone due to higher country rock and Yucca fault permeability. • Total particle breakthrough within 1,000 years is similar to the base case.
North–south subdivision of country rock zones with specified permeability as geometric average of field data	11.1	37	• The specified permeability values for country rock are higher than the calibrated base case except for the northern subzone of LCA east zone. • The heads are notably lower in the model's western area due to the higher LCA west and LCA central permeability. • There is faster transport from detonations located in the LCA central zone due to higher country rock and Yucca fault permeability. • Flow is diverted around faults 135, 136, 137, and 138 located in southern Yucca that results in significantly less total particle breakthrough within 1,000 years.

the model where majority of the deeply buried tests are located. This increases particle travel time to the model's southern boundary from detonations located in eastern Yucca Flat and significantly decreases the total particle breakthrough within 1,000 years.

In conclusion, the alternate flow models considering a north–south subdivision of the country rock produce models that do not calibrate to the data as well as the base-case model and lead to similar or decreased particle travel over 1,000 years.

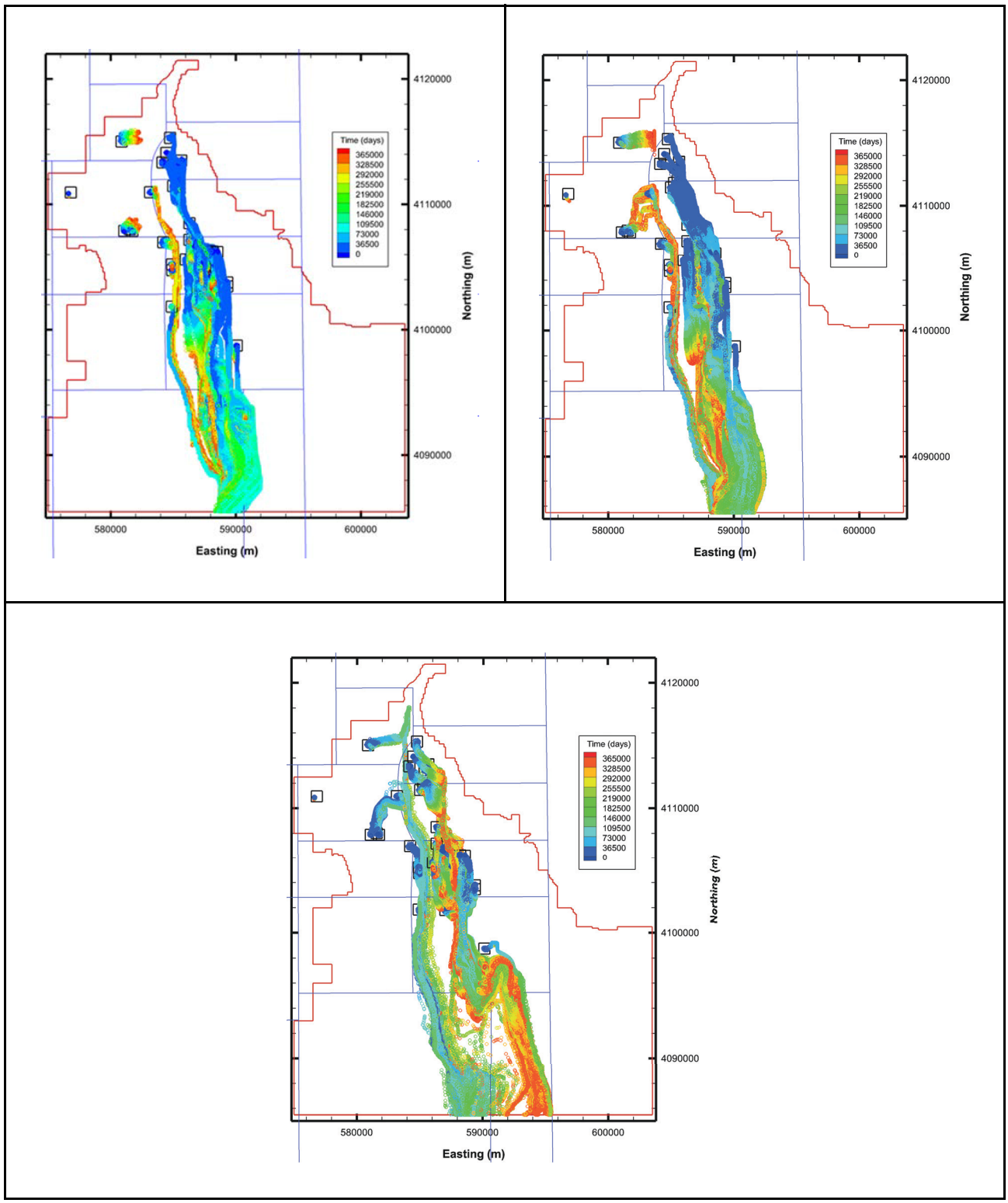

Figure 2-27
Particle Travel Paths and Times for the Base-Case (upper left), North–South Subzones (upper right), and North–South Subzones with Specified Permeability (bottom) Flow Fields

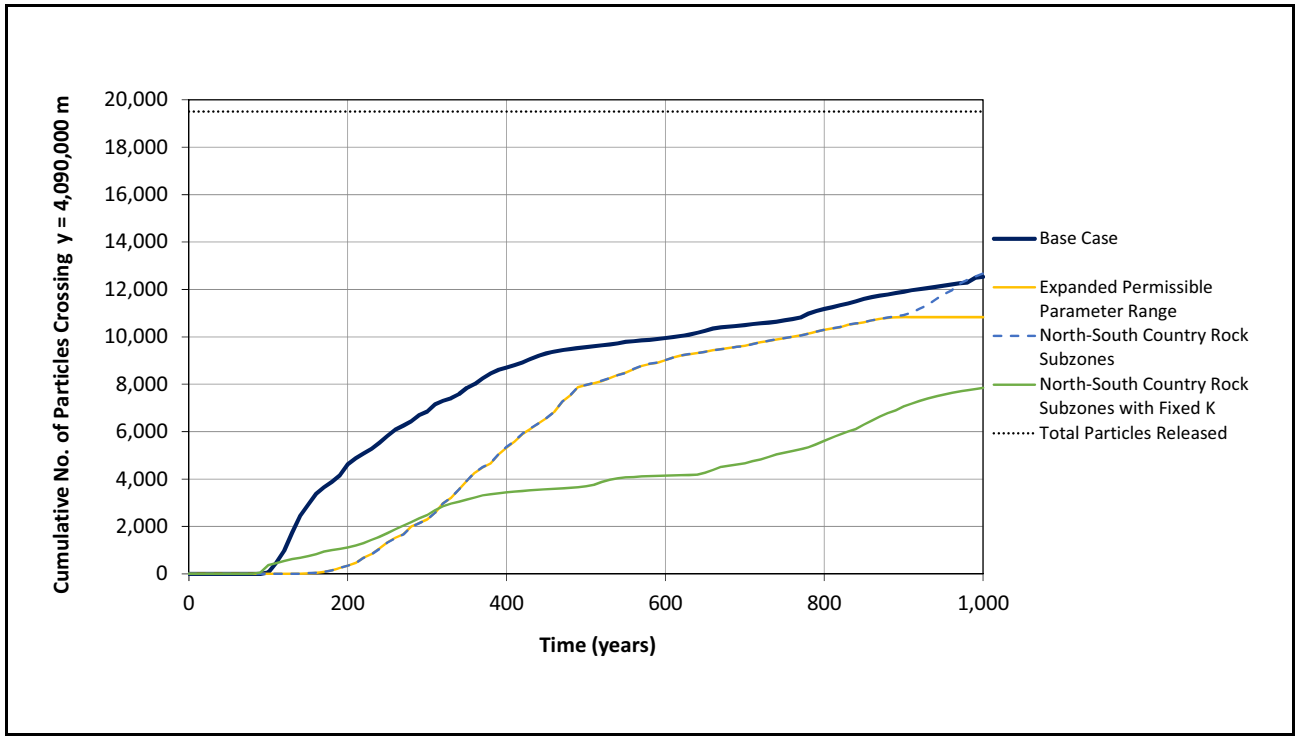

Figure 2-28
Breakthrough Plots for Base-Case and Country Rock Subzones Flow Fields

2.3.1.3 Preferential Flow

This uncertainty addresses local-scale permeable pathways in the country rock.

PRC Recommendation: The peer review team recommends a thorough examination of all the field data relevant to the question of whether karst features do exist and are continuous below the water table. This would include reviews of drill logs (e.g., lost circulation, rod drops), geologists notes, borehole flowmeter data, geophysical logs (televideo logs, caliper, others), outcrop descriptions, and stratigraphic correlations of anomalous features. New monitor wells should be analyzed specifically with karst features in mind. Determine whether the karst features do or do not exist, and if they cannot be ruled out, include alternative flow and transport simulations that do include karst features.

RESPONSE: Continuous high hydraulic conductivity pathways from northern to southern Yucca Flat through major faults were evaluated in N-I (2013a) and in ongoing alternative calibration of the LCA flow and transport model. Available subsurface and outcrop evidence, as well as hydrogeologic reasoning, indicates that extensive solution channels that could provide basin-scale transport pathways in Yucca Flat do not exist, as discussed below.

Winograd (1965) and Winograd and Thordarson (1975) argued against the existence of an integrated set of solution channels throughout the testing areas of Yucca Flat based on the following reasoning: (1) If they formed before the Yucca Flat basin was formed, they would have been dismembered by extensional block faulting tat formed the basin over the last 8 to 10 million years ago (Ma). (2) The climate at the NNSS has been relatively arid since the rise of the Sierra Nevada 10 Ma ago, and arid climates (with associated low soil P_{CO2}) are not conducive to cave formation. (3) If karst features formed near the water table during a Pleistocene pluvial period, they would now be above the water table due to water table declines and no longer relevant for groundwater transport.

In the rare instances where karst was observed, it was noted and described, such as that noted by Barnes et al. (1982) in outcrops southeast of Mercury. However, these are relatively shallow features of limited extent. The modeling team has drilled/cored 14,161 ft (40 holes) of lower carbonate aquifer thrust plate (LCA3) and 31,462 ft (in 127 holes) of LCA in the Yucca Flat model area, and observed that karst features are uncommon in the study area. There are more than 116 holes in Yucca Flat that penetrate the pre-Tertiary rocks; however, only one borehole (UE-10j) showed evidence of significant dissolution features (at UE-10j a large cavity was encountered below the level of saturation and deep in the pre-Tertiary carbonate rocks that are Cambrian in age). Well-developed and extensive karst features are not observed in exposures of pre-Tertiary carbonate rocks in the Yucca Flat area. Barnes et al. (1963) report no dissolution features (other than some “vuggy” intervals in some units) in their descriptions of the pre-Tertiary rocks in the Yucca Flat vicinity. Also, descriptions of mapped stratigraphic units on the geologic quadrangle maps of the area do not mention karst or dissolution features. This is consistent with the modeling team’s observations of the LCA exposures around the basin.

In conclusion, although karst features have been observed sporadically in boreholes (e.g., identified by a drop in the drill string while deepening Well UE-10j and later confirmed with video logs) and outcrops, karst features are relatively rare in the extensive limestone outcrops exposed in the surrounding mountain blocks, and an integrated set of saturated solution channels throughout the Yucca Flat basin is unlikely. Hence, karst is unlikely to have created extensive permeable pathways in Yucca Flat.

2.3.2 Faults

This uncertainty focuses on flow and transport through faults. The PRC recommendations on this include several sub-comments, which the modeling team will address in a serial fashion.

PRC Recommendation: It is unlikely that the only multi-well test in Yucca Flat identified the highest value of fault damage-zone permeability. The peer review team therefore recommends that the range considered for modeling extend well above the highest measured value. Given that none of the major faults have been investigated in the field, include alternative models with permeable faults and no impermeable core to determine their effect on the flow field and transport.

RESPONSE: To address this PRC concern, the LCA model was recalibrated for several alternative fault conceptualizations (Table 2-7), including fault conceptualizations without low-permeability cores. For the conceptualizations without low-permeability cores, the fault core zones within the model were assigned the same properties as the fault conduit zones. The results showed that calibration to the steady-state head and MWAT data became somewhat worse for cases without low-permeability cores compared to cases with low-permeability cores, and the east–west permeability of Yucca and Topgallant fault had to be decreased, in effect creating a lower-permeability core.

The model recalibrations without low-permeability cores demonstrate that the Yucca Flat faults do not behave solely as high-permeability conduits. The large basin-and-range fault anisotropy factors in the east–west direction are at or near the lower bounds to compensate for removing the low-permeability core. This behavior is also evident from the observation that the propagation of ER-6-1-2 MWAT drawdown was not significant across the major faults. The MWAT response seen in wells aligned with ER-6-1-2 along the longitudinal axis of the faults was prompt and substantial. However, the response at wells located transverse and across large faults was delayed and was smaller than observed responses at wells aligned with faults passing near ER-6-1-2. The wells that are separated from the production well by several major faults with substantial offsets did not show any response to pumping at ER-6-1-2.

With respect to maximizing contaminant transport to the southern boundary of Yucca Flat, there is a limit to the degree to which a long, preferential flow path such as the Yucca fault can dominate the flow system. For maximum transport, water must be optimally balanced between the flow in the

Table 2-7
Summary of Simulations Investigating Alternative Fault Conceptualizations

Simulation	Objective Function	Percentage of Particle Breakthrough within 1,000 Years	Calibration Summary
Base case	1.15	64	• This is a baseline metric to evaluate the influence of alternate flow simulations.
Faults without low-permeability cores	1.35	70	• Yucca and Topgallant fault east–west permeability is decreased to compensate for removing the low-permeability core. • Eastern Yucca Flat transport path through the faults 149 and 160 is not present in the base case. • Total particle breakthrough within 1,000 years is somewhat greater than the base case. Transport results are discussed in Section 2.7.4.
Tied calibration of tectonically similar faults	138	29	• Model calibration was unsuccessful due to large steady-state head residuals in western Yucca Flat.
Major basin-and-range forming faults as high-permeability features with low-permeability cores	65.9	78	• Model calibration was unsuccessful due to large steady-state head residuals in western Yucca Flat.
Major basin-and-range forming faults as high-permeability features without low-permeability cores	219	86	• Model calibration was unsuccessful due to large steady-state head residuals in western Yucca Flat. • There is increased MWAT drawdown residual compared to calibration with low-permeability cores.
All large faults (>3 km trace) as a high-permeability features without low-permeability cores	377	91	• Model calibration was unsuccessful due to large steady-state head residuals in western Yucca Flat.
No faults with traces <3 km	1.19	68	• The degree of calibration is similar to the base case. • East–west direction anisotropy is increased in the large basin-forming faults except for eastern strand of the Topgallant fault. • Total particle breakthrough is somewhat greater than the base case.Transport results are discussed in Section 2.7.4.
No minor faults (no faults other than the large basin-forming faults)	15.9	78	• There is higher residual than base case due to underpredicting heads in western and northern Yucca Flat. • Fault permeabilities are increased except the eastern margin faults Hp40 and Hp50. • Country rock permeability is increased.

country rock and a preferential pathway. For detonations located away from major faults, flow through the country rock must transport RNs away from the source zones to nearby faults. Country rock permeability and fault permeability together control how accessible RNs are to preferential flow paths. Transport to the southern boundary depends not only on the overall groundwater flux through the system but also on how the overall flux through the system is partitioned among various flow paths relative to the test locations. NSMC runs in which the groundwater flux is routed away from deep detonations (e.g., through major faults) tend to produce less transport to the southern boundary than NSMC runs that route flow through the country rock where most of the deep detonations are located. This reflects the decision during the testing era to locate detonations away from major faults.

The ER-6-1 well cluster is located in a faulted area of the LCA, and the hydraulic conductivity tested may be representative of highly conductive fault damage zones. The 4,200-feet-per-day (ft/day) hydraulic conductivity identified from the ER-6-1 MWAT analysis by the PRC represents a 30-ft interval out of 1,385 ft of logging (SNJV, 2005a, Table 2-4). Extrapolating this small discrete measurement over an entire fault zone spanning a potentially 36-km feature is not realistic and cannot be reconciled with the observed gradient and realistic flow rates through the LCA within Yucca Flat. The average hydraulic conductivity over the entire logged interval is 240 ft/day (8.7×10^{-11} m^2), and this value is more plausible for the upper-bound permeability of a large-scale feature such as Yucca fault. Analysis of single well and cross-hole responses from the ER-6-1 MWAT resulted in large-scale hydraulic conductivity values ranging from 4 to 249 ft/day (SNJV, 2005a, Table 3-1).

PRC Recommendation: The peer review team recommends assigning increased permeability to the material that is currently simulated as country rock near the major faults in the analysis of uncertainty.

RESPONSE: This is implicitly included in the model. The grid spacing at the explicitly simulated faults in a direction perpendicular to the fault plane in the current model is 125 m; thus, 125 m of country rock on each side of the fault gets included in the volume that is assigned damage zone properties.

PRC Recommendation: The peer review team recommends that the effect of greater fault permeability in the AA/VA model should be explored in CADD/CAP, and if model tests show that fault permeability in the AA/VA system is relevant to the LCA contaminant boundary prediction, field data should be collected to characterize AA/VA fault behavior.

RESPONSE: The SZ AA/VA model included a broad range of TCU permeability values (N-I, 2013a, Table 4-4 and Figure 4-12) that depended on the assumed background infiltration rates, and included cases with and without anisotropy in the TCU. When fault permeabilities within the TCU are included ($k_{faults} = 2.0 \times 10^{-17}$ to 10^{-12} m^2), the permeability range of the TCU (which includes the lower tuff confining unit [LTCU], Oak Spring Butte confining unit [OSBCU], and argillic tuff confining unit [ATCU]) spans most of the range of the measured values. For some faults, the need to maintain the head difference between the tuffs and the LCA resulted in estimates of fault permeability that tended to the lower end of the estimated range.

The estimated 6- to 30-m head difference between the TCU and LCA under pre-development conditions documented in Fenelon et al. (2012) places limits on the degree of hydraulic communication between the TCU and LCA through matrix, fractures, or faults before the onset of nuclear testing. Appendix F of N-I (2013a) explored the rock properties and recharge conditions that would allow these head differences to persist given plausible limits for modern and paleo-recharge, and the timing of climate change documented from pack-rat midden studies. The hypotheses that water-level differences between the TCU and LCA are due to paleodrainage is compatible with vertical permeabilities for the TCU of between 10^{-17} and 10^{-16} m^2, drainable porosities from 0.1 to 0.4, and current recharge rates less than 3 millimeters per year (mm/yr), all of which overlap with the measured range of possible values. The paleo-recharge hypothesis is also compatible with the ^{14}C ages of 10 thousand years (ka) or greater for groundwater presently in the AA/VA. Therefore, although there may be local areas and layers within the TCU with higher-permeability values (as indicated by the small-scale data), there is a basis for concluding that before the onset of testing, the large-scale permeability of the rock matrix was quite low, as was concluded by authors such as Halford et al. (2005) and Tompson (2008) based on their analysis of the dissipation of testing-induced overpressures. The SZ AA/VA model documented in N-I (2013a, Section 4.0) considered a much broader range of permeability values for the TCU to be compatible with the range of smaller-scale measurements.

The LCA transport model included bounding simulations in which the entire RN inventory for eight deep nuclear detonations in the TCU was initially in the LCA. This was intended to account for the possible, but unproven, hypothesis that fracture pathways to the top of the LCA were created by the detonations themselves. The SZ AA/VA model also included alternatives that considered the possibility that nuclear testing created fracture pathways to the top of the LCA (N-I, 2013a,

Section 4.0). Preliminary data from the new Wells ER-2-2, ER-3-3, and ER-4-1 do not indicate ^3H at concentrations above the MDL (1,500 to 1,800 pCi/L) in LCA near and below detonations, providing evidence against the occurrence of breaching. Two of the new wells were also in the vicinity of faults, indicating that in these cases faults were significant transport pathways for TCU-hosted detonations to the LCA.

Additional simulations with alternate conceptualizations of the AA/VA system are presented in Section 2.3.3. The results of these simulations show that the base-case model is more conservative with respect to transport predictions than the alternate models.

PRC Recommendation: The peer review team recommends that the uncertainty in the contaminant boundary due to all the faults serving as permeable pathways to the LCA be evaluated, and alternative models include faults without impermeable cores.

RESPONSE: Several alternate fault conceptualizations, described below, were developed to investigate the model uncertainty related to fault conceptualization and parameterization. The results are summarized in Table 2-7 showing that the alternate models specifying faults as exclusively high-permeability features did not calibrate very well; hence, they are not consistent with the hydraulic data in the Yucca Flat model area.

To develop the alternate fault conceptualizations, the LCA fault data and the base-case fault conceptualization were reviewed in context of the PRC comments. Most of the Yucca Flat faults are high-angle normal (basin-and-range) faults. These faults have apparent offsets greater than 60 m and dip to the east (BN, 2006). Located in the center of the basin, Yucca fault is the master basin-and-range forming fault. There are four other large basin-forming faults: the Carpetbag, Topgallant, Hp40, and Hp50 faults. Faults Hp40 and Hp50 are located near the eastern boundary of Yucca Flat and are the eastern range-bounding faults (N-I, 2013a).

There are a total of 107 faults in the LCA model, the traces of which at the top of the LCA vary from approximately 0.1 to 36 km. In the base-case calibration, it was decided to allow only faults with traces larger than 3 km to vary independently. The hydrogeologic properties of faults with a trace less than 3 km were tied together. These small faults were broken into two groups: faults east of the Yucca fault and faults west of the Yucca fault. The hydrogeologic properties of all faults in each of these two groups were tied and varied jointly (N-I, 2013a).

The LCA model recalibrations that considered all faults as permeable pathways are as follows:

1. Tied calibration of the tectonically similar faults. The Yucca Flat faults were assigned to five groups with tied permeability and anisotropy in each group: (1) large basin-and-range forming faults, (2) western faults with traces greater than 3 km, (3) western faults with traces less than 3 km, (4) eastern faults with traces greater than 3 km, and (5) eastern faults with traces less than 3 km.

2. Specifying the major basin-and-range forming faults as high-permeability features with a fixed permeability of 8.77×10^{-11} m^2 and low-permeability cores.

3. Specifying the major basin-forming faults as high-permeability features with a fixed permeability 8.77×10^{-11} m^2 without low-permeability cores.

4. Specifying all faults with traces greater than 3 km as high-permeability features with a fixed permeability of 8.77×10^{-11} m^2 without low-permeability cores.

As shown in Table 2-7, the above four conceptualizations did not calibrate to the data as well as the base case.

PRC Recommendation: The peer review team recommends including an alternative conceptual model that has no or many fewer minor faults in the LCA; this may require allowing flow and transport to occur between the AA/VA and LCA via the TCU (fractured) as described further below, in addition to the major faults. For example, flow in the LCA in Yucca Flat was recently modeled without faults by Halford (2012).

RESPONSE: Two alternate fault conceptualizations were developed that investigate the model uncertainty related to including fewer minor faults in the LCA. The first conceptualization removed minor faults with traces less than 3 km in length from the model. The second conceptualization removed all minor faults, thereby retaining only the large basin-forming faults (Yucca, Carpetbag, Topgallant, and the eastern range-bounding faults Hp40 and Hp50).

Most of the Yucca Flat faults are high-angle normal (basin-and-range) faults. The primary difference among faults is the trace length and offset distance. The unsuccessful calibrations using tied fault parameters or fixed high-permeability demonstrate that all faults do not have the same hydrogeologic behavior. Successful model calibration requires different behavior for some faults within similar groupings. Table 2-7 summarizes the model recalibrations using alternative fault conceptualizations.

The model recalibration excluding faults with traces less than 3 km achieved an objective function of 1.19 that is nearly equal to the base-case model calibration. A total of 64 small faults were excluded from the model. The successful calibration without the smaller faults demonstrates that the smaller faults are not needed to simulate the steady-state heads or drawdown in response to the ER-6-1-2 MWAT, and that the similar total particle breakthrough produced by the calibrated flow field indicates that the small faults do not play an important role in RN transport on a basin scale. Including the smaller faults may have overparameterized LCA model, but the overparameterization did not produce a significantly different flow field from a more parsimonious model. The simulation did partially fulfill a PRC request to explore the effect of local heterogeneities on flow and transport.

Figure 2-29 illustrates the potentiometric surface for the base case and the case including only the large basin-forming faults. The model including only the large basin-forming faults calibrated poorly, having achieved a larger objective function compared to the base case (i.e., 15.9 vs. 1.15). Though removal of the faults with traces less than 3 km in length has little effect on calibration, the calibration including only the large basin faults indicates that the faults with traces greater than 3 km improve the LCA model calibration. The larger objective function was primarily due to underpredicting the steady-state heads in western and northern Yucca Flat. The recalibration also produced higher fault and country rock permeability compared to the base case. The minor faults with traces greater than 3 km in length introduce needed permeability heterogeneity into the large country rock zones.

Figure 2-30 illustrates the particle travel paths and times for the base-case and the alternative fault models that achieved an acceptable calibration (calibration without low-permeability fault cores, without faults with traces <3 km, and without minor faults). Removing the faults with traces of less than 3 km in length did not significantly change the transport paths compared to the base case. Removing the fault cores created transport paths in eastern Yucca Flat that are not present in the base case. Removing all minor faults produces diffuse transport through the LCA east country rock. Figure 2-31 illustrates the particle breakthrough for base-case and alternative fault models that achieved an acceptable calibration. Each of these cases has increased total particle breakthrough at 1,000 years but decreased breakthrough prior to 200 years when ^{3}H contributes to the contaminant boundary. The very large objective function obtained from the LCA model calibrations with tied fault parameters and specified high fault permeability make the transport pathways predicted by these models unreliable, and the particle breakthroughs are not presented.

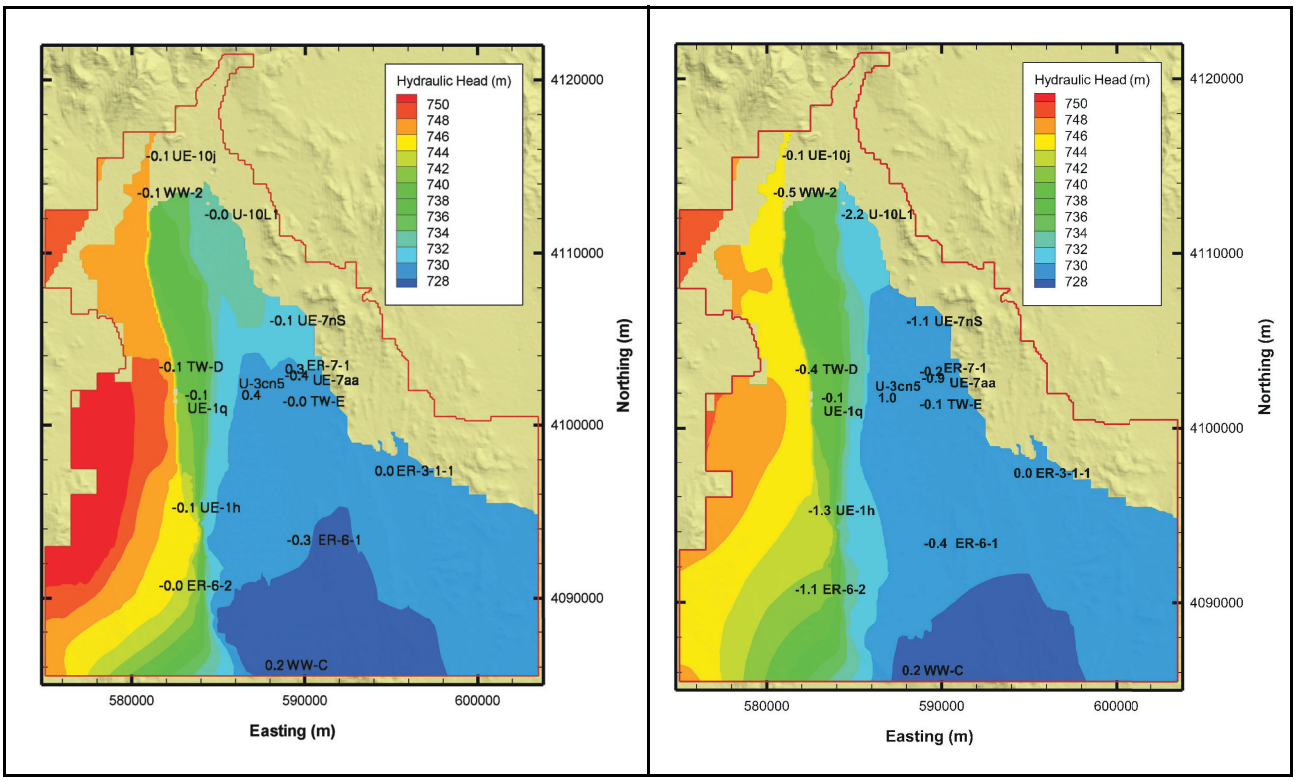

Figure 2-29
Potentiometric Surface for the Base-Case (left) and the Case Including Only the Large Basin-Forming Faults (right)

In conclusion, the alternate flow models considered either did not calibrate well to the data, or produced total particle breakthrough near the model's southern boundary that is larger at 1,000 years but smaller prior to approximately 200 years when ^{3}H largely defines the contaminant boundary.

2.3.3 Tuff Confining Unit

This uncertainty focuses on the process of flow across the TCU.

PRC Recommendation: The peer review team recommends that uncertainty in the contaminant boundary include an alternative conceptual model for analysis of the importance of flow across a TCU that is not impermeable but rather honors the available data on hydraulic properties of the TCU. Given the importance of the TCU to isolate much of the radionuclide inventory, the peer review team recommends developing new data and hydraulic field testing to determine the lateral continuity of the TCU as an effective hydraulic barrier to vertical transport.

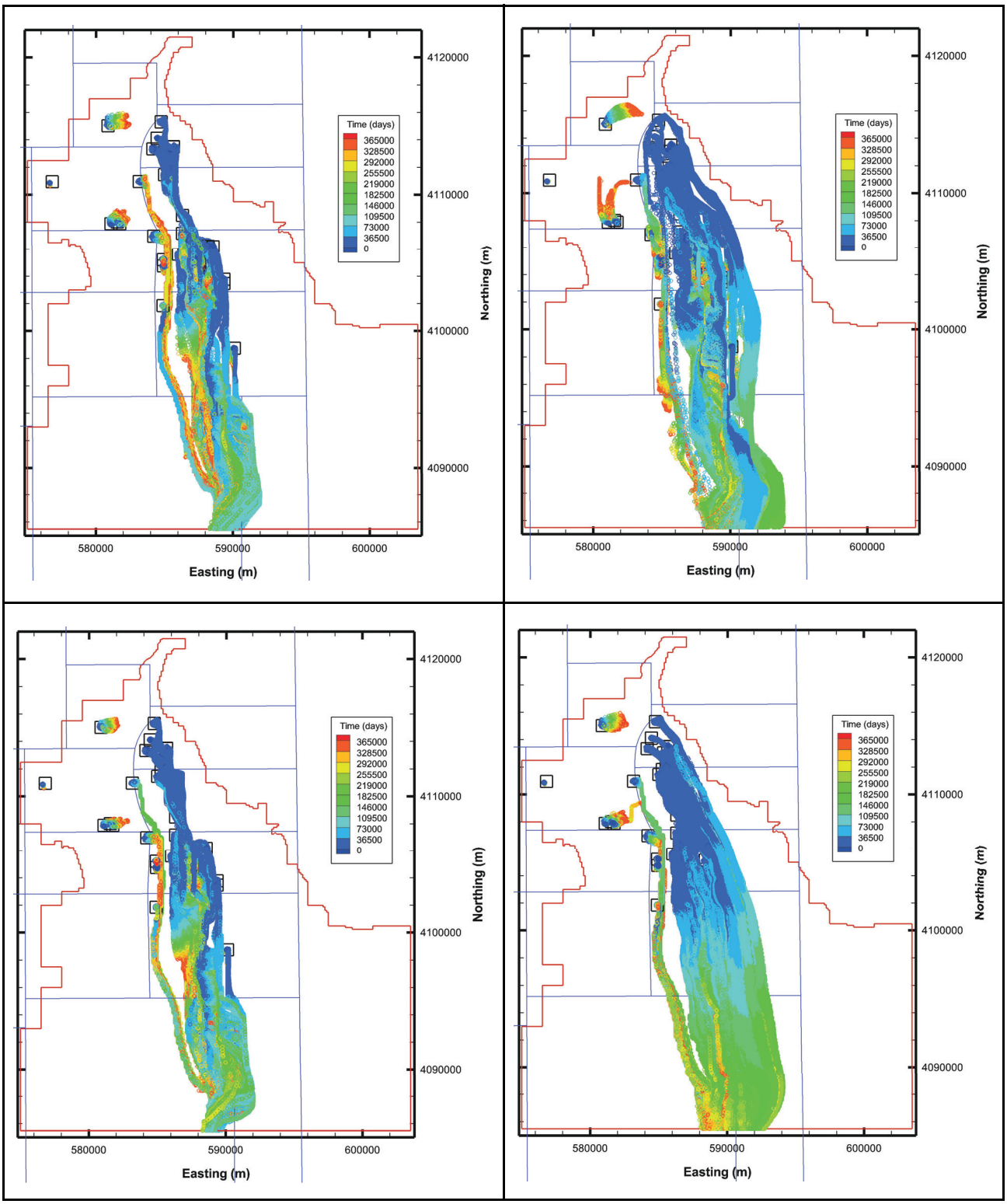

Figure 2-30
Particle Travel Paths and Times for the Base-Case (upper left), Faults without Low-Permeability Cores (upper right), No Faults with Traces <3 km (lower left), and No Minor Faults (lower right) Flow Fields

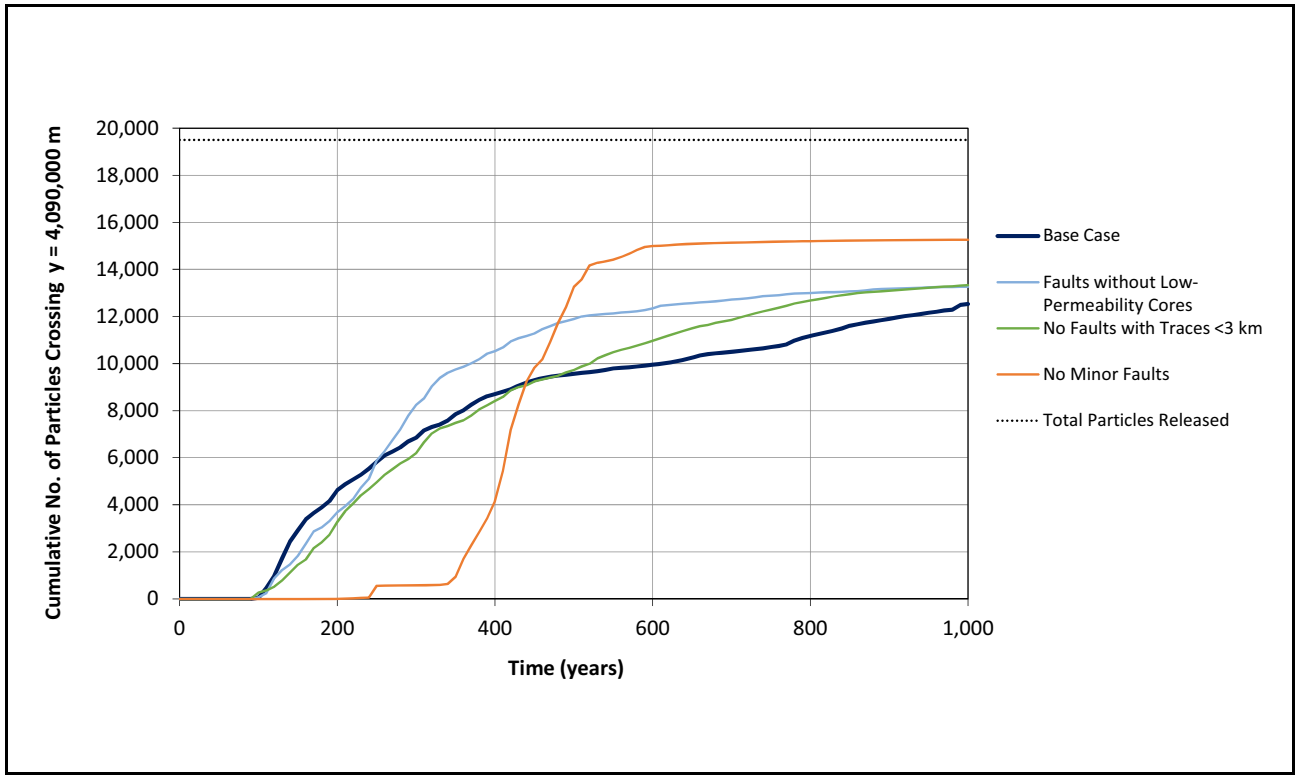

Figure 2-31
Breakthrough Plots for Base Case, Calibration without Low-Permeability Fault Cores, without Faults with Traces <3 km, and without Minor Faults

RESPONSE: The interruption of the lateral continuity of the TCU by faults—and, in certain model scenarios, by local vertical pathways to the LCA created by the force of the nuclear detonations (the "breaching scenario")—is already incorporated in the conceptual models of the SZ AA/VA documented in N-I (2013a). A wide range of lateral permeabilities (10^{-12} to approximately 1.6×10^{-17} m^2) consistent with available Yucca Flat-specific TCU hydrologic testing (N-I, 2013a, Figure 4-12) were assumed or calibrated in the above-referenced model. The upper limit of this range has been extended to 5.0×10^{-12} m^2 in recent model runs in response to the PRC comments. Regarding the lower boundary of the TCU, three breaching cases that allow transport across the lower boundary in non-faulted locations have already been run and included in N-I (2013a). In these breaching cases, hydrofracturing along the lower boundary was allowed and, if this occurred, the rock was assigned high permeability (10^{-12}) and low porosity (0.01) between the detonation and the LCA. These model runs did not significantly impact the contaminant boundary.

Other modeling cases were run such as one in which the entire RN inventory from eight key tests was initially placed directly into the LCA to simulate the effects of breaching scenarios (N-I, 2013a).

These cases did not significantly impact the contaminant boundary even though the models assumed that significant amounts of ^{3}H from deeply buried tests are initially distributed in the LCA. Further, as discussed in Section 2.3.2, the existing head data places limits on the degree of hydraulic communication between the TCU and LCA.

A number of additional model simulations of the AA/VA system were run (see Appendix A) to look at the effects of alternative parameter sets and conceptual models on RN transport to the LCA. These alternative scenarios investigated the effects of (1) more permeable faults with permeability of 10^{-11} m^2; (2) more permeable faults with permeability of 10^{-10} m^2; (3) conceptualization of the TCU as a fractured aquifer (fracture porosity $\boldsymbol{\varphi}_f = 5 \times 10^{-04}$), rather than a matrix dominated porous media (matrix porosity $\boldsymbol{\varphi}_m = 0.38$); and (4) a higher TCU permeability (5×10^{-12} m^2). All of the new scenarios resulted in smaller overall mass flux of non-sorbing, long-lived RNs to the LCA over 1,000 years compared with the base case with larger fluxes of ^{3}H to the LCA (results for ^{14}C are shown in Figure 2-32 as SUP_1 to SUP_4, respectively), although scenarios (1) and (2) resulted in greater transport to the LCA at early times compared to the base case. Three sets of transport parameters were run for each of these four scenarios, resulting in a total of 12 additional cumulative mass flux curves.

In conclusion, the interruption of the lateral continuity of the TCU by faults and breaching created by detonations are already included in the N-I (2013a) model. A wide range of the lateral and vertical permeability of the TCU is already incorporated in that model. No further work is warranted under this uncertainty.

2.3.4 Effective Porosity

This uncertainty is motivated by lack of sufficient data regarding effective porosity in the TCU.

PRC Recommendation: Evaluate the uncertainty in the extent of the contaminant boundary due to effective (fracture) porosity of the TCU.

RESPONSE: Any damage zones or chimneys in the TCU were assumed to have fracture porosity (0.01) for all testing-effects conceptual model #1. The modeling team did not, however, run any simulations where all nodes in the TCU were assumed to be fractured. Additional simulations were run with an assumed fracture porosity of 5×10^{-04} to assess potential significance of continuous

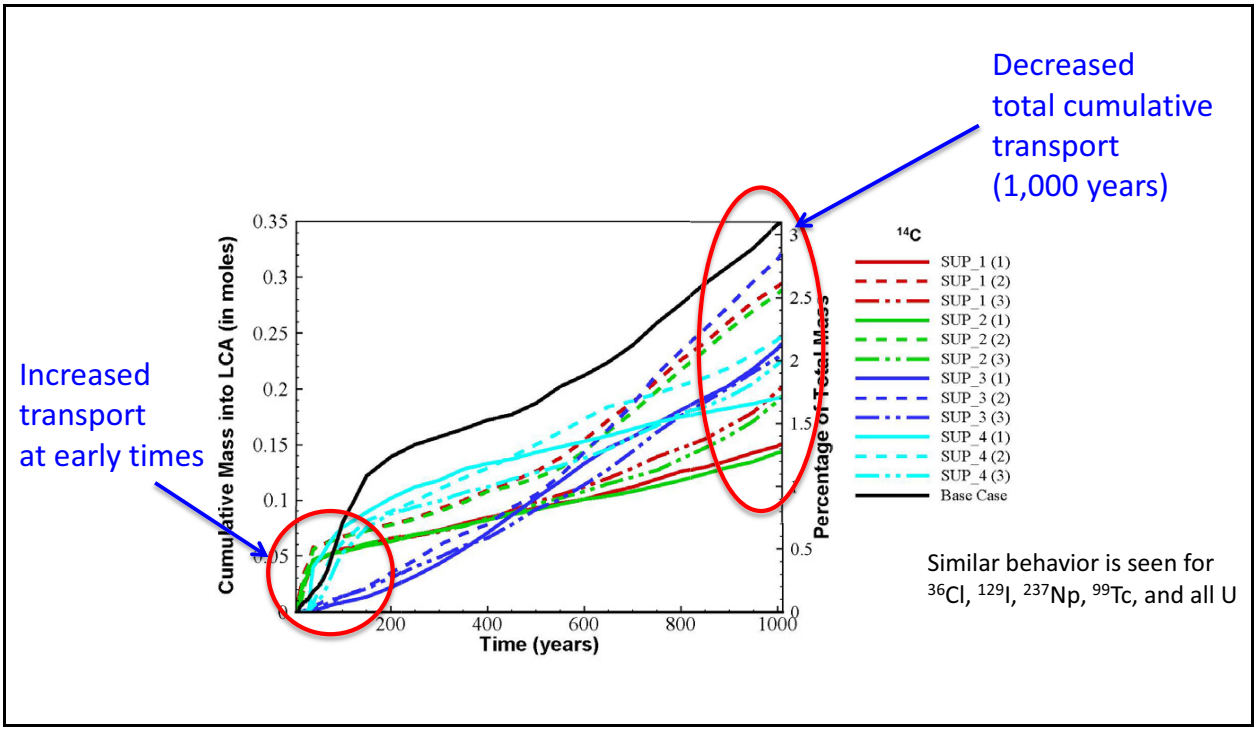

Figure 2-32
Cumulative Mass of ^{14}C Transported to the LCA for Alternative AA/VA System Models
Note: SUP_1 = alternative fault permeability ($k = 10^{-11}$ m^2), SUP_2 = alternative fault permeability ($k = 10^{-10}$ m^2), SUP_3 = Fracture flow conceptual model for TCU, and SUP_4 = high permeability for TCU ($k = 5 \times 10^{-12}$ m^2).

fracture networks on simulated RN fluxes to the LCA. These simulations, represented by the SUP_3 in Figure 2-32, indicate that ^{14}C breakthrough to the LCA is smaller when fracture flow combined with fracture-matrix diffusion is considered.

2.3.5 Potential for Flow of Surface Water into Fractures in the Alluvium

This uncertainty concerns open fractures and faults at the surface that could act as conduits for flow of surface water to water table.

PRC Recommendation: Modeling should include the reasonable and conservative approach that would permit faults to be local zones of preferential flow through the unsaturated and saturated alluvium into the underlying stratigraphic units. Field measurements are recommended to ascertain the degree to which fissures contribute to enhanced local recharge and local groundwater flow directions, including the earth fissures near Yucca Lake and the fissures associated with faults that extend to the surface in the alluvium.

RESPONSE: In the absence of the open fissures that develop every few decades, water that ponds a few inches deep on Yucca Lake appears to sit there for weeks until it evaporates, or infiltrates to a shallow depth and is later evaporated. The fine-grained nature of the playa sediments (mostly clays, silt, and limestone according to Sweetkind and Drake [2007]) and its considerable thickness (up to 244 m according to BN [2006, p.4-16]) indicate that deep infiltration rates will be small. This was confirmed by a field reconnaissance conducted on August 13, 2014, following a 100-year storm nine days earlier when water on the playa was observed to have penetrated about 4 inches after more than a week of ponded conditions (Drellack, 2014). Also, the playa is south of nuclear detonation sites, so any infiltration beneath Yucca Lake will not mobilize RNs in the UZ or in the SZ AA/VA model.

Maps of surface features associated with nuclear testing ("crack maps") produced in the days to weeks after a detonation indicate the development of both radial and concentric cracks associated with the uplift and subsequent collapse of land surface to form a subsidence crater, as well as offset across pre-existing faults due to either differential compaction or renewed fault movement (e.g., Grasso, 2000). Most of these surface cracks have since become sealed due to infilling by sediments and from weathering, but as indicated by recent photos in Appendix C of the PRC report (N-I, 2015), there are isolated areas along major faults where infilling of these cracks is incomplete. However, the photos of these open surface cracks taken before and after the August 4, 2014, storm do not suggest that these cracks have been areas of preferential water movement during runoff events (Figure 2-33); however, even if this were the case, the practice during the nuclear testing period was to avoid major fault zones, so if preferential flow into these areas were to occur, it would pass between detonations and not be available to flow into craters that formed above the detonations elsewhere. In contrast to water that infiltrates into faults located between the nuclear tests, water that infiltrates into craters (Figure 2-34) will almost certainly percolate through the exchange volume of the test. If ponding is limited, the percolation through the exchange volume likely takes over 100 years to reach the water table. However, the UZ models documented in N-I (2013a) did focus on estimating infiltration rates and water volumes at the bottoms of the nuclear subsidence craters.

Deeper in the subsurface, beneath the open cracks and elsewhere where surface cracks are not present, the hydrologic literature suggests that faults in poorly consolidated sediments are low-permeability features due to grinding of sediment grains to create deformation bands, sediment mixing adjacent to the slip plane, and smearing of fine-grained sediments into the slip plane itself (Heynekamp et al., 1999; Sigda et al., 1999; Rawling et al., 2001; Cashman and Cashman, 2000).

Figure 2-33
Carpetbag Fault Scarp on June 18, 2014 (left); and on August 14, 2014, 10 days after the August 4, 2014, 100-Year Storm Event

Open fractures typical of consolidated, low-porosity rocks appear not to form. Although much of the published literature originates from the Albuquerque basin in New Mexico, observations of fault zones in sediments at depth in the U-1a tunnel complex support this conceptual model. It should be noted, however, that in the absence of data to the contrary, all faults that cross through consolidated rocks are represented in the UZ model as high-permeability, low-porosity features through which flow and transport will be relatively rapid.

In conclusion, most of the tests are laterally offset from these features, which data from similar alluvial basins suggest will be closed at depth. Additionally, UZ tests as a group are above the SZ AA/VA, which provides additional barriers to LCA. Those UZ detonations directly above the LCA are in the north or northwest part of basin and are unlikely to influence the leading edge of contamination. Thus, as demonstrated in N-I (2013a), the UZ tests contribute in only a minor way to the definition of the contaminant boundary.

Figure 2-34
Ponded Water in the U3fd (LAGUNA) (top) and U3kp (SEAMOUNT) (bottom) Craters on August 14, 2014, 10 Days after the August 4, 2014, Storm Event

2.3.6 Anisotropy and Preferential Flow in the Unsaturated Zone

This uncertainty is motivated by concerns about preferential infiltration from crater bottoms.

PRC Recommendation: During the CADD/CAP process, data collection efforts should be undertaken at those craters determined via field testing or modeling to have high rates of enhanced recharge to determine the maximum depth of recent infiltration and possible flow through preferential pathways to detonation cavities.

RESPONSE: Several studies of infiltration occurring in Yucca Flat and Frenchman Flat subsidence craters have already been performed. These studies have included measurements or estimates of ponding depth following specific precipitation events; soil properties; soil moisture; and, in some cases, water potential beneath and adjacent to the craters (Tyler et al., 1992; Pohll et al., 1996; Hokett et al., 2000; Wilson et al., 2000). N-I (2013a) used the results of these studies to calibrate models of infiltration at subsidence craters.

The issues of anisotropy and preferential flow in the UZ have already been addressed in the Yucca Flat flow and transport report (N-I, 2013a). As demonstrated in N-I (2013a) and as acknowledged in the PRC report (N-I, 2015), anisotropy would tend to cause lateral spreading of crater infiltration, leading to a decrease in wetting front velocity with depth. Chimney sediments were modeled both with and without anisotropy, leading to less and more preferential flow down chimneys. Scenarios were run both with and without rubblized high-permeability chimneys in the consolidated tuffs. This issue can also be assigned a “low priority” status due to the fact that UZ detonations did not contribute significantly to the contaminant boundary. Roughly 90 percent of UZ detonations are above the SZ AA/VA model, and the 10 percent that are above the SZ LCA are in extreme northern end of the basin, which means that regardless of crater infiltration rates and wetting front velocity, the contaminant boundary will be defined by other, more deeply buried detonations further to the south.

Recent water table rises and low-level ^{3}H measurements at WW-3 appear to be associated with the storage of mildly tritiated water from WW-C-1 in an unlined pit between 2002 and 2010 (see Appendix B). Ponded water from this pit appears to have percolated through about 467 m of unsaturated alluvium in less than 10 years. Numerical models of this serendipitous event were used as a surrogate study for preferential flow and transport through craters. The successful modeling of this ponded infiltration event (see Section B.1.3.4), including the appearance of measured

(see Section B.1.3.1) and simulated (see Section B.1.3.5) water table rises, and low levels of ^3H at WW-3 (Section B.1.3.3) support the overall modeling approach used to simulate the effects of crater infiltration on transport (N-I, 2013a, Section 3.1.3.4 and Appendix E). One significant difference, however, is that ponded water conditions existed for more than eight years at the WW-C pond, whereas craters are only intermittently flooded every few years.

In summary, crater infiltration studies of the type proposed by the PRC have been conducted in the late 1990s and early 2000s, and were used to calibrate the rainfall/runoff/infiltration models discussed in Appendix E of N-I (2013a).

2.4 Source Term and Mass Flux to the LCA

2.4.1 No Uncertainty Associated with the RST

This uncertainty focuses on the radiologic source term (RST).

PRC Recommendation: The peer review team suggests that uncertainties in the RST values be included in the modeling. It would be possible to evaluate unclassified RST uncertainties by comparing the unclassified inventory of each detonation calculated as above with the corresponding classified inventories from Miller et al. (2002). The distribution of differences would evaluate the uncertainties in the unclassified RST values based on the average CAU inventories without revealing any information about individual classified RST values.

RESPONSE: RST uncertainty, as documented in Bowen et al. (2001), has been explicitly incorporated in the source term via screening analyses documented in Appendix C of the Yucca Flat flow and transport report (N-I, 2013a). Source term uncertainty has already been examined to varying degrees in each of the three model types (UZ, SZ AA/VA, and SZ LCA) through uncertainty analysis in melt-glass partitioning factors, exchange volume size, alternate conceptual models (constant mass or constant concentration), and inventory uncertainty based on maximum announced yields. The RST uncertainty approach used in the screening analysis, with the exception of melt glass dissolution, was also used in determining initial LCA model inventories for the detonations with partial initial inventories within the SZ LCA.

Comparison of unclassified and classified R_c, inventory, and yield for the 39 deep tests likely to impact the contaminant boundary has been completed. The results showed that R_c is generally smaller

than unclassified estimates based on maximum yield, and the number of tests intersecting the SZ LCA is reduced (cavity dimension based on maximum announced yield identified in NV-209-REV 16 [NNSA/NFO, 2015] and Equation 1 in UCRL-ID-136003 [Pawloski, 1999]). The initial source term concentrations and the total inventory deposited in the SZ LCA are not substantially impacted. These results were presented to NNSA/NFO and NDEP on June 5, 2015. The results suggest that the contaminant boundary would not be greatly impacted if classified source terms had been used.

2.4.2 Uncertainties in Partition Factors Are Not Well Defined Particularly for Cavities in Carbonate Rock

This uncertainty concerns the partition factors appropriate for modeling the concentration of RNs in cavities in silicic as well as carbonate rocks.

PRC Recommendation: Develop arguments supporting the relevance of IAEA partitioning data to tests in silicate rock at the NNSS by examining what differences would be expected between partitioning in cavities in seawater-saturated basalt and partitioning in cavities in unsaturated or fresh-water saturated rhyolite. That is, should one expect consistency between the IAEA partition factors and those from the CHANCELLOR test?

PRC Recommendation: Provide support for the partition factors used in interpreting carbonate tests. This could include theoretical considerations, laboratory examination of cavity debris, and/or—most convincing—collection and interpretation of field data from a carbonate test like those that were available to Rose et al. (2011) for the CHANCELLOR test.

RESPONSE: The International Atomic Energy Agency (IAEA) RN partitioning recommendations were developed using a combination of underground nuclear test data from the NTS, NNSS, Mururoa/Fangataufu, and other underground nuclear testing locations (IAEA, 1998a, b, and c). The following excerpt from the IAEA reports reflects the fact that RN partitioning at the French nuclear testing site was based on data from the NTS and is, thus, relevant to contaminant transport simulations in Yucca Flat:

> *The composition of the radioactive debris in the lava and on the rock surfaces is rather well known, from nuclear test sites like the Nevada Test Site in United States and the former Soviet Union test sites at Semipalatinsk and Novaya Zemlya. Open literature describing experience from these sites is the main source of information used in the*

present assessment of the volatility of individual materials and the resulting partitioning due to physical and chemical fractionation processes between the three phases (Bedford and Jackson, 1965; Borg, 1975; Borg et al., 1976; Butkovich, 1976; Thompson, 1992; Smith, 1995; Thompson, 1996; and Smith, 1997).

Support for partitioning factors for tests detonated in carbonate rock performed by the UGTA Activity, including extensive work done on NASH and KANKAKEE debris, is documented in Carle et al. (2008).

Only four carbonate-hosted tests (CORDUROY, LAMPBLACK, TORRIDO, and BOURBON) were conducted in Yucca Flat with monitoring that does not show contamination. Given these circumstances, further study is not warranted in these carbonate rock hosted tests.

2.4.3 Water Flow into Cavities

This uncertainty addresses the hydraulic properties beneath detonation cavities in the TCU and the potential for rapid transport.

PRC Recommendation: Given that liquid transport from the cavities is the dominant mechanism for downward movement, the peer review team recommends a concerted effort to measure and monitor enhanced-recharge-driven transport in and below detonation cavities, with emphasis on detonations within the TCU.

RESPONSE: As documented in N-I (2013a, Appendix E), considerable effort was made to characterized crater infiltration rates for the hundreds of craters in Yucca Flat using estimates of the watershed areas contributing to each crater, stochastic precipitation records, and simplified rainfall/runoff/infiltration models. These long-term (1,000-year) crater infiltration estimates were made for all craters but applied only to craters above UZ detonations, because crater infiltration was identified from four crater field studies as being a key component for RN migration to the water table over the next 1,000 years. Crater infiltration was not applied to the SZ AA/VA model domain because RNs associated with these tests were already in the saturated groundwater system.

Surface infiltration at the estimated crater infiltration rates would not be expected to arrive at the water table for several hundreds of years. Roughly 90 percent of the UZ detonations were located above the SZ AA/VA domain, which provides additional barriers to RN transport to the SZ LCA.

The effectiveness of the SZ AA/VA system as a barrier to RN migration from the UZ to the SZ LCA was demonstrated in N-I (2013a) by comparing RN fluxes with and without the UZ RN fluxes present. The results in both cases were the same. The 10 percent of the UZ-hosted detonations that lie directly above the SZ LCA occur in the northern parts of the LCA model (NASH, HANDCAR, KANKAKEE) or are monitored by a nearby well that shows no evidence of RN transport (BOURBON).

An opportunity was available for evaluating the overall modeling approach used for simulating transport due to enhanced crater infiltration. Fenelon (2015) reported that a water-filled sump near WW-3 used for construction held water for eight years between roughly 2002 and 2010. Recent water table rises and low-level ^{3}H measurements at WW-3 appear to be associated with the storage of mildly tritiated water from WW-C-1 in this unlined pit between 2002 and 2010 (see Appendix B). Ponded water from this pit appears to have percolated through about 467 m of unsaturated alluvium in less than 10 years. Numerical models of this serendipitous event were used as a surrogate study for preferential flow and transport through craters. The successful modeling of this ponded infiltration event (see Section B.1.3.4), and the appearance of measured (see Section B.1.3.1) and simulated (see Section B.1.3.5) water table rises and low-levels of ^{3}H at WW-3 (see Section B.1.3.3) support the overall modeling approach used to simulate the effects of crater infiltration on transport (N-I, 2013a, Section 3.1.3.4 and Appendix E). One important distinction between the WW-3 pond study and subsidence craters is that craters are only intermittently flooded every few years, unlike the WW-3 pond, which contained water continuously for at least eight years. Consequently, the WW-3 pond has much higher infiltration rates (5 m/yr) and shorter travel times (two to three years) than would be expected at the subsidence craters.

Therefore, because a considerable amount of work has already been done demonstrating that these sources do not impact the contaminant boundary, additional crater studies are not considered necessary.

2.4.4 Uncertainty in the Exchange Volume Not Fully Captured

The concern of this uncertainty is that fracturing associated with nuclear detonations could extend further than that included in the model.

PRC Recommendation: The peer review team recommends that the uncertainty analysis of the contaminant boundary include the effects of extending the exchange volume to at least 5 R_c.

RESPONSE: The concern is that fracturing associated with nuclear detonations could extend out to 5 R_c or more. If true, this could create fracture pathways directly to the LCA at many more detonations than were considered to breach the top of the SZ LCA in the flow and transport models reported in N-I (2013a). The possible 5 R_c extent of fracturing is based on Laczniak et al. (1996, Figure 7), who cited much earlier studies stating that "Intensely pulverized rock extends outward to about 1.3 R_c, and pervasively fractured rock extends outward beyond this zone to about 2 R_c on the average (Carroll, 1981), but to greater ranges laterally and above the point of explosion (Boardman, 1970)." Boardman (1970) reports that the cavity extends to 1.5 to 2 R_c beneath the point of explosion. Farther out, a surrounding zone of more widely spaced fracturing extends to about 2.5 to 5 R_c (Borg et al., 1976, p. 84).

The consensus in the more recent literature is that a high-permeability zone would not extend beyond 3 R_c. The Office of Technology Assessment (OTA) (1989), which summarized the understanding of containment successes and failures and of test phenomenology as understood by containment geologists at the time, stated that "The force of the explosion creates a cavity and fractures rock out to the distance of 2 R_c from the shot point. Out to 3 R_c, existing cracks are extended and connected, resulting in a decreasing seismic shear velocity. Outside 3 R_c, no new cracks form. At this distance, existing cracks are opened and strength reduced, but only temporarily."

Similarly, IAEA (1998a) describes the high-permeability exchange volume (Figure 2-35) as the following: "Initially a cavity is formed with a radius R_c; this is later filled with rubble when the ceiling of the cavity collapses. A thin crush zone of low permeability may form around the cavity, followed by a zone of shear failure up to 4 to 5 R_c; Inside the shear zone is a zone of about 2 to 2.5 R_c where an increase in rock permeability is apparent during post-shot drilling operations. Radial cracks are possible to an elastic limit of 10 ± 2 R_c."

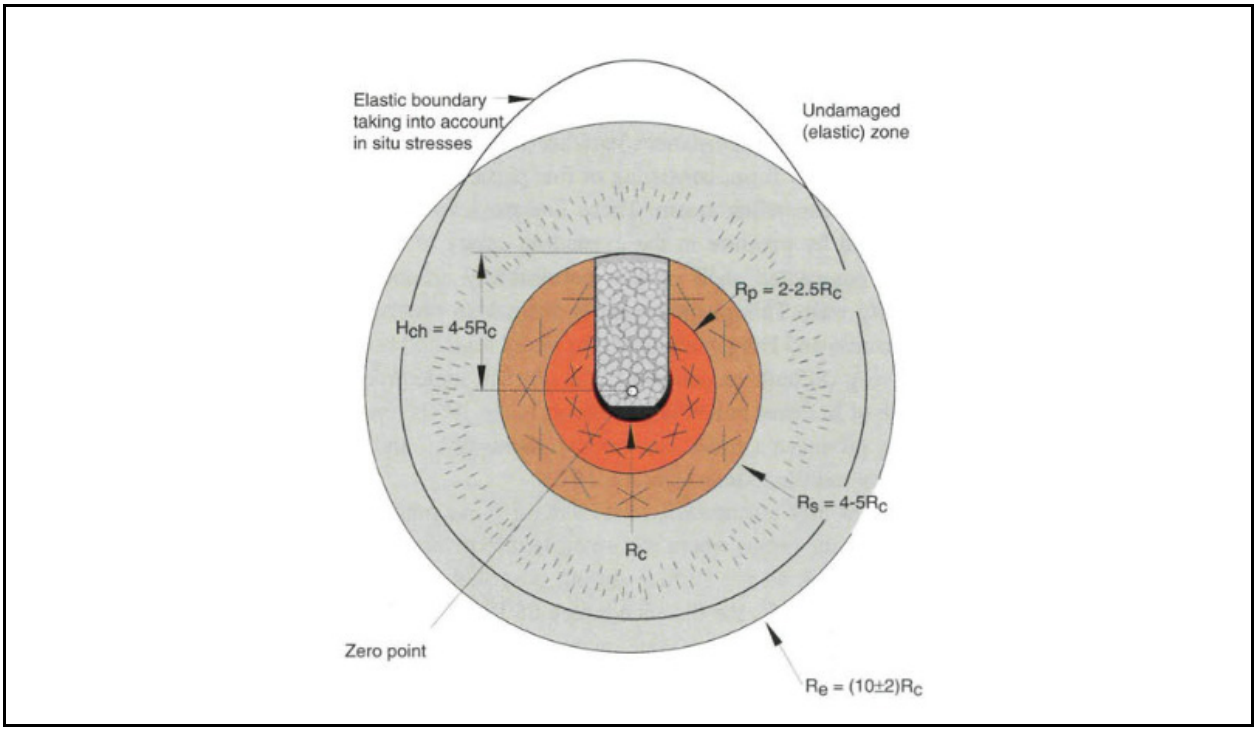

Figure 2-35
Different Zones of Damage Produced by a Nuclear Explosion in Rock

The physical phenomena associated with a nuclear explosion were described in Section 5.4 of IAEA (1998a). The explosion produces a spherical cavity and a fractured rock mass around the cavity. The following major zones have been identified (Figure 2-35):

- Cavity within a radius R_c
- High-permeability zone within a radius R_p
- Fracture zone with shear failure to radius R_s
- Crack zone between radii R_s and R_e
- Undamaged zone beyond radius R_e
- Chimney extending to a height H_{ch}

The high-permeability zone is defined in a pragmatic way by the radius where the water used to pump drilling debris back to the surface during post-shot drilling is lost. This marks the distance where the rock permeability is significantly increased because of the explosion; the drilling water is sucked into the cavity-chimney (probably via the walls of the chimney as the original cavity walls are covered with vitrified rock). This is found to occur on average at a radius of 2 to 2.5 R_c. Thus, the consensus in the literature is that a high-permeability zone would not extend beyond 3 R_c.

The general configuration of detonation-altered zones and properties described in Appendix C of N-I (2013a) is largely based on information compiled in OTA (1989). The exchange volume is related to the size of the damage zone, but is also related to volatility and molecular weight of the RNs comprising the hydrologic source and whether the exchange volume is located in a saturated or unsaturated environment. N-I (2013a) used Yucca Flat specific data and hydrologic source term (HST) modeling (Tompson, 2008) as well as cavity data from the RAINIER and CHANCELLOR detonations to estimate RN-specific exchange volumes. Only ^{14}C has a maximum exchange volume size of 5 R_c within the SZ, and the initial concentration of ^{14}C is only slightly above the MCL assuming a 1 R_c exchange volume (N-I, 2012, Figure 2-6). Using a 5 R_c for ^{14}C would lower the initial concentration below the MCL. Using the recommended 5 R_c exchange volume for all detonations and all RNs would create lower initial concentrations that are most likely unrealistic and impart an additional element of non-conservatism.

Preliminary interpretations of hydraulic and ^{3}H data obtained during drilling of Wells ER-2-2, ER-3-3, and ER-4-1 indicate that the exchange volume is less than 3 R_c laterally from the working point and possibly less than 2 R_c beneath the working point when cavity dimension is calculated based on maximum of the announced yield range (NNSA/NFO, 2015) and Equation 1 relating yield and R_c in Pawloski (1999). This conclusion is based on the fact that ^{3}H in drilling production water was below the DL of about 1,500 pCi/L, and water production was low (indicating limited fracturing) as drilling progressed past the working point depth at each of the three wells. ER-2-2 was about 3 R_c from the working point of CALABASH, and ER-3-3 and ER-4-1 passed the working point of WAGTAIL and STRAIT at a distance of 2.5 R_c.

Both the CALABASH and STRAIT detonations were expected to be within 2 R_c of the SZ LCA based on maximum announced yield. However, the TCU at ER-2-2 was thicker than anticipated, and the working point of CALABASH was actually about 4 R_c above the SZ LCA. The LCA groundwater produced during drilling at ER-2-2 and ER-4-1 did not contain ^{3}H above the DL of 1,500 pCi/L, indicating that the exchange volume did not extend into the SZ LCA at these detonations. The absence of ^{3}H in LCA groundwater at ER-4-1 near the STRAIT detonation is consistent with the absence of measurable ^{3}H in the LCA at Well U-3cn 5 near the BILBY detonation. BILBY was a 249-kt yield TCU-hosted test within 2.2 R_c of the SZ LCA (NNSA/NFO, 2015). From these observations, it appears that for SZ tests in the TCU, the exchange volume is less than 2.5 R_c from the working point in the lateral direction and about 2 R_c or less beneath the working point. The possible

asymmetry of the exchange volume was also suggested by detailed fracture studies in the vicinity of detonations in a variety of test media that included granite, dolomite, shale, and tuff (Borg, 1973). Based on measurements of actual R_c, pervasive fracturing was reported to exist out to 2.7 to 3.5 R_c laterally from the working point but only about 1.5 to 2.0 R_c beneath the working point. Chimney collapse resulted in more extensive fracturing (and presumably a larger exchange volume) above the working point. Thermally driven, buoyant flow up the chimney may have contributed to the presence of high levels of ^3H in the saturated Timber Mountain lower vitric-tuff aquifer (TM-LVTA) above the STRAIT and CALABASH tests at ER-4-1 (100,000 pCi/L) and ER-2-2 (>$20 \times 10^{+06}$ pCi/L). However, the STRAIT detonation also had nearby shallow detonations (<2.5 R_c laterally) from ER-4-1, which may have contributed contamination to the well.

The possible asymmetry of the exchange volume as suggested in the literature (e.g., Borg, 1973; Boardman, 1970) may be a critical factor in determining whether the exchange volume at deeply buried detonations extend into the SZ LCA. In the instances discussed above, the exchange volume does not appear to intersect the SZ LCA at distances greater than 2 R_c based on maximum announced yield.

2.4.5 Possible Chimney and Cavity Pathway to the LCA

This uncertainty addresses the size of the exchange volume and damage zone associated with an underground test.

PRC Recommendation: The peer review team recommends that the uncertainty analysis of the contaminant boundary include breaches from detonations not only within 5 R_c but also include a greater range in the permeability enhancement assigned to the damage zone. Where possible, consider evaluating whether post-shot holes can be used to test the field permeability of the damage zones in situ.

RESPONSE: The breaching scenarios described by the PRC in this comment were considered by the SZ AA/VA models described in N-I (2013a, Section 4.0), including cases with an enhanced permeability crushed zone (Conceptual Model 2). It is important to note that the breaching cases included the same permeability and porosity increases as all the non-breaching simulations due to "testing effects," as described in Appendix G in N-I (2013a). This allowed for the possibility of enhanced flow and transport from the tests that caused the breaching through the lower boundary and

into the LCA. An example of the permeability changes associated with a breaching scenario is shown for the BILBY detonation in Figure 2-36, which shows the permeability fields near the detonation before (left) and after (right) detonation. The testing-effects model predicts permeability increases of several orders of magnitude at BILBY. In addition to the permeability increases, transport porosity was set to 0.01 because the permeability increases were assumed to be due to the creation of fracture pathways. However, the water-level recovery data for the BILBY post-shot hole U-3cn PS 2 discussed later in this section, and the absence of measurable ^{3}H in the underlying LCA at U-3cn 5 indicate that the breaching scenario is overly conservative, at least at BILBY (as described below).

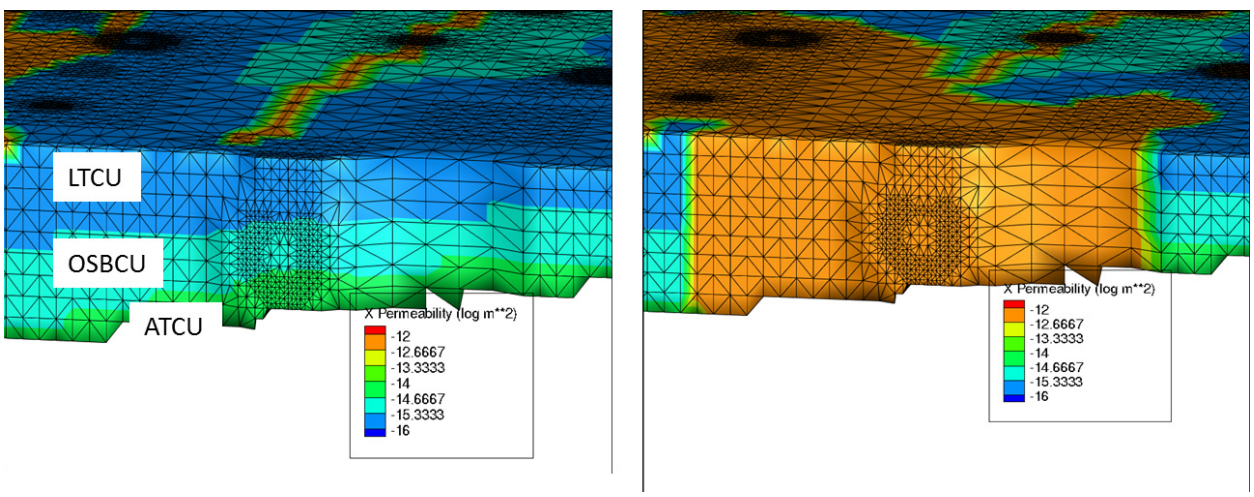

Figure 2-36
Simulated Changes to the Permeability Field near the BILBY Detonation for the Breaching Scenario: (left) before the BILBY Detonation and (right) after the BILBY Detonation

Figure 2-37 shows that at many locations, permeability increase penetrated through the entire thickness of the TCU. This is demonstrated by comparing the locations of high-permeability zones ($k = 10^{-12}$ m^2) along the lower boundary of the SZ AA/VA model (left) with the locations of high-permeability zones of the TCU (right).

Figure 2-38 shows the location of boundary "breach" (circles), and the volumes around tests where testing effects increased the permeability significantly. The left panel of Figure 2-38 indicates the faults and breaches along the lower boundary of AA/VA model whereas the right panel shows the

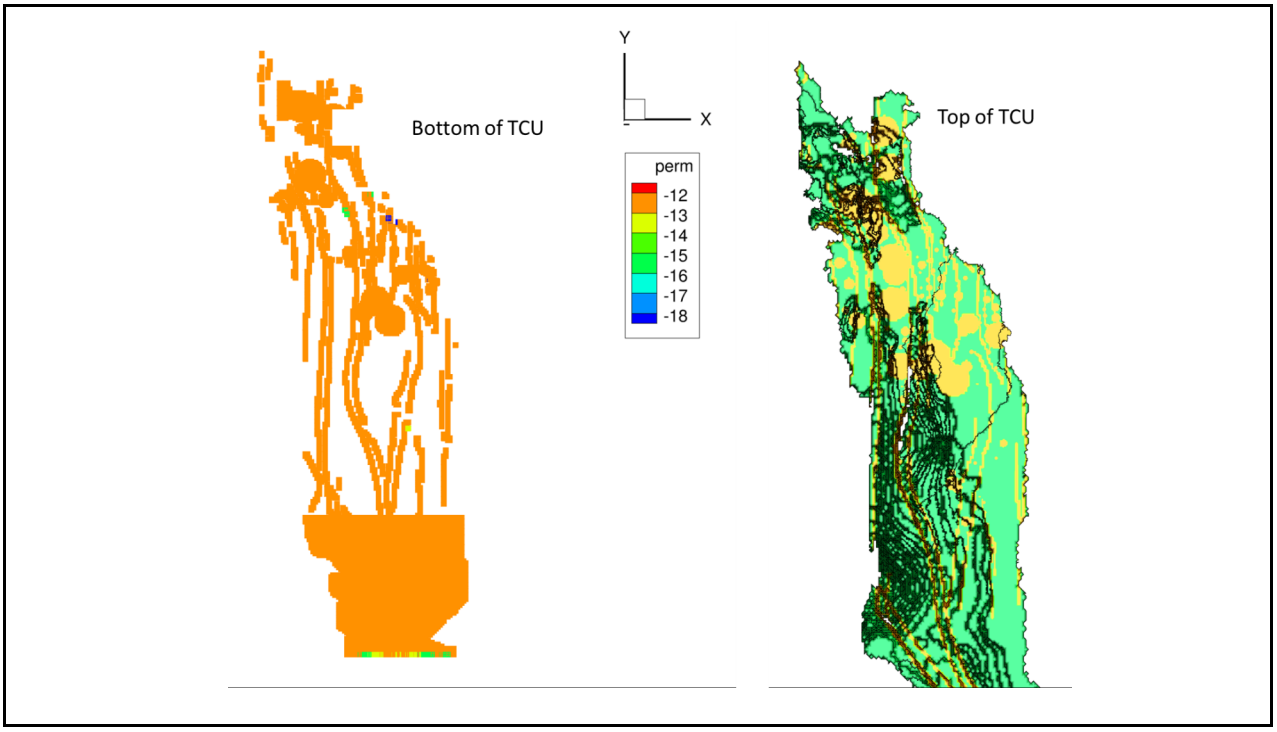

Figure 2-37
Permeability Fields at the Bottom (left) and Top (right) of the TCU after the End of Testing (1992)

Note: Only constant head nodes are shown for the bottom of the TCU in the panel on the left (no-flow nodes are not shown), and these constant head nodes all have permeabilities of $k = 10^{-12}$ m^2.

location and magnitude of permeability enhancement due to testing effects. Figure 2-39 shows a close-up of the same phenomena in a region of deeply buried tests in the north–central part of the model.

The available data, however, indicate that the type of breaching proposed by the PRC does not occur. For example, BILBY was detonated in the TCU at a depth of 714 m on September 13, 1963, with an announced yield of 249 kt (NNSA/NFO, 2015). The working point was located roughly 205 m below the water table and, with an R_c of 70 m, the working point was 2.2 R_c above the SZ LCA (N-I, 2013a, Table B-1). Hydrographs from a well drilled into the cavity/lower chimney region (U-3cn PS 2) and a satellite well (Figure 2-40) drilled and screened (U-3cn 5) in the LCA indicate that hydraulic communication between the TCU and LCA is limited (Figure 2-41). The hydrograph from the TCU (U-3cn PS 2) indicates that water levels in the TCU took more than five years to recover following the detonation, indicating very small flow either laterally inward through the TCU toward the cavity, or upward from the LCA through the hypothesized breached zone (head gradients between the TCU and LCA appear to have been upward prior to 1967). Preliminary data from the new Wells ER-2-2,

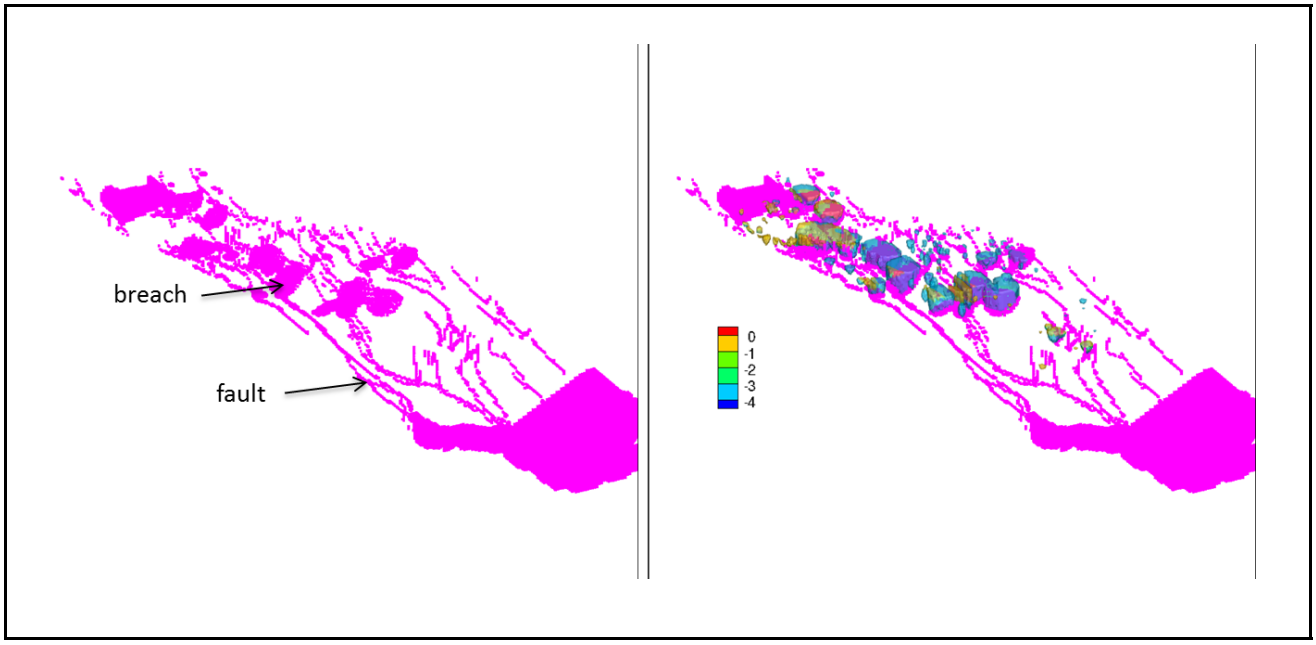

Figure 2-38
Location of Boundary "Breaches" (circles) (left) and the Volumes (right) around Tests Where Testing Effects Significantly Increased the Permeability

Note: The color legend indicates the order of magnitude of permeability enhancement in the right panel.

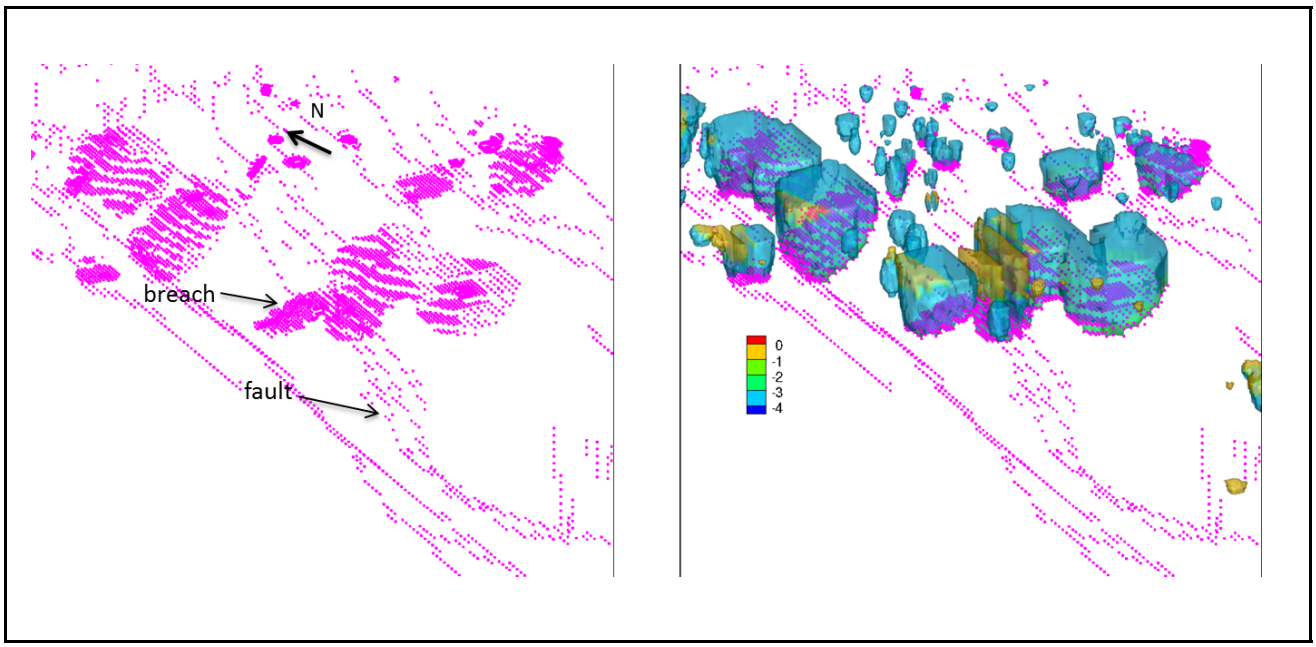

Figure 2-39
Close-up of Faults and Breaches (left) and Zones of Permeability Enhancement (right) in the North–Central Part of the SZ AA/VA Model

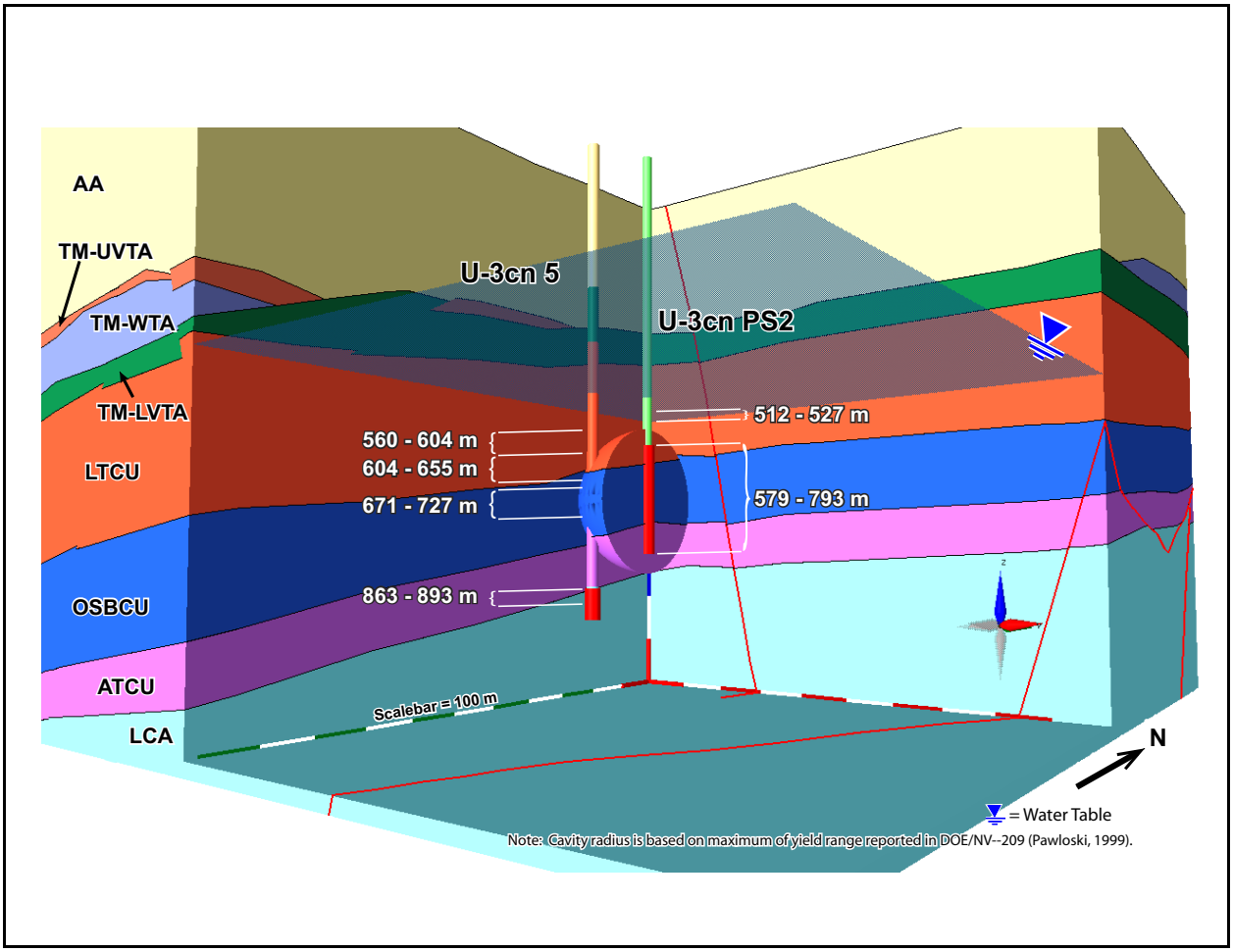

Figure 2-40
Location of the LCA Satellite Well (U-3cn 5) and the Post-Shot Well (U-3cn PS 2) Relative to the 2 R_c Exchange Volume of BILBY
Source: N-I, 2013a, Figure D-8

ER-3-3, and ER-4-1 do not indicate ^{3}H at concentrations above the MDL (1,500 to 1,800 pCi/L) in LCA near and below detonations, showing that the results from BILBY are representative these tests detonated near the boundary between the TCU and LCA.

The ^{3}H data from U-3cn PS 2 show little or no ^{3}H mobility away from BILBY—decay-corrected ^{3}H concentrations in U-3cn PS 2 had not changed significantly between 14 and 41 years after detonation (Figure 2-42, lower right), indicating little or no ^{3}H mobility over 27 years. If ^{3}H were mobile, some decrease in decay-corrected ^{3}H concentration would be evident. (Note that data collected at 0.85 years were closer to working point [579 to 793 m depth] and not directly comparable to later samples [512 to 527 m depth]). This was corroborated by the fact that the LCA satellite well U-3cn 5 has been ^{3}H-free.

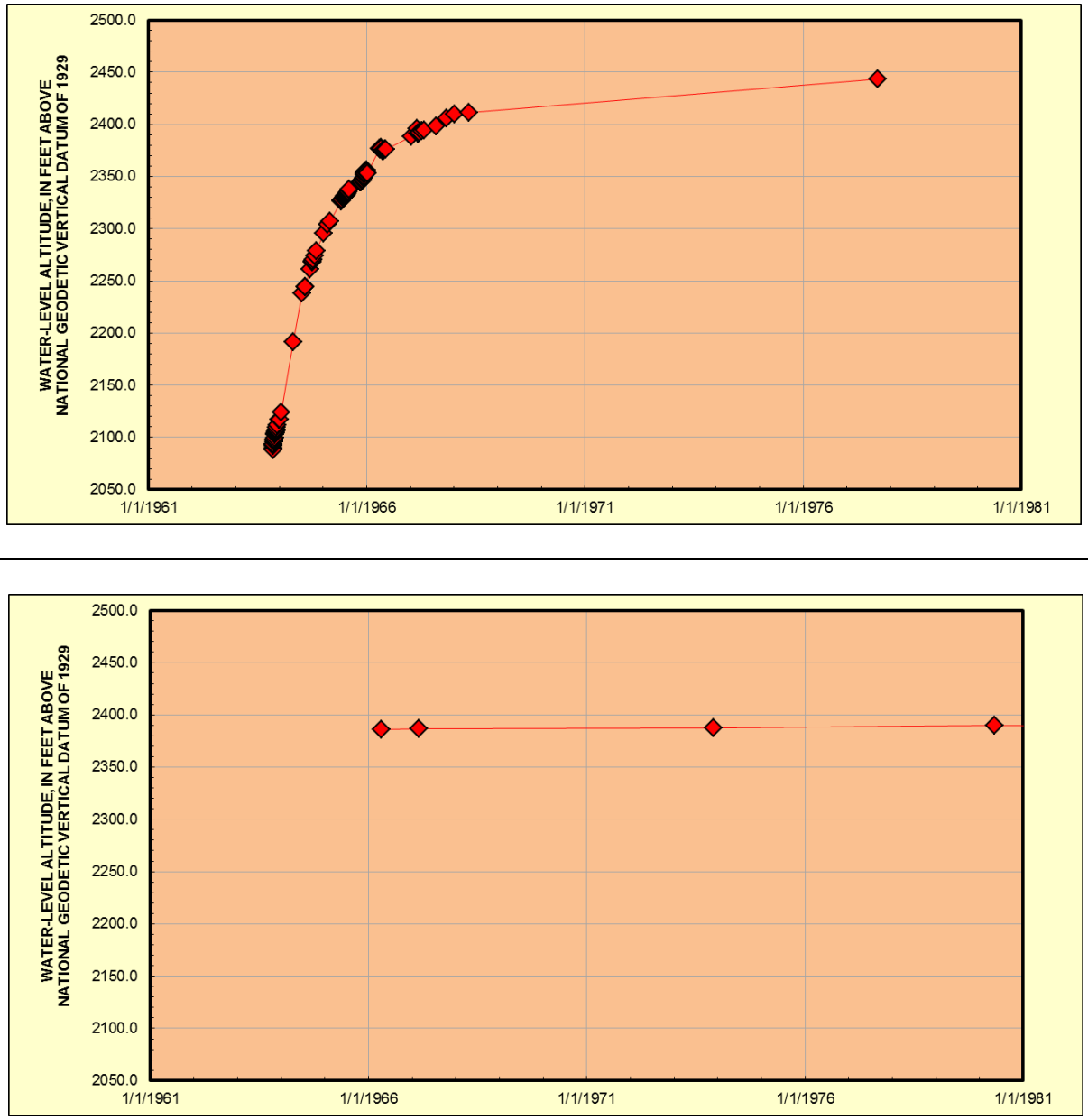

Figure 2-41
Hydrographs of Hydraulic Head in the TCU at U-3cn PS 2 (top) and in the LCA at U-3cn 5 (bottom)
Source: Elliott and Fenelon, 2013

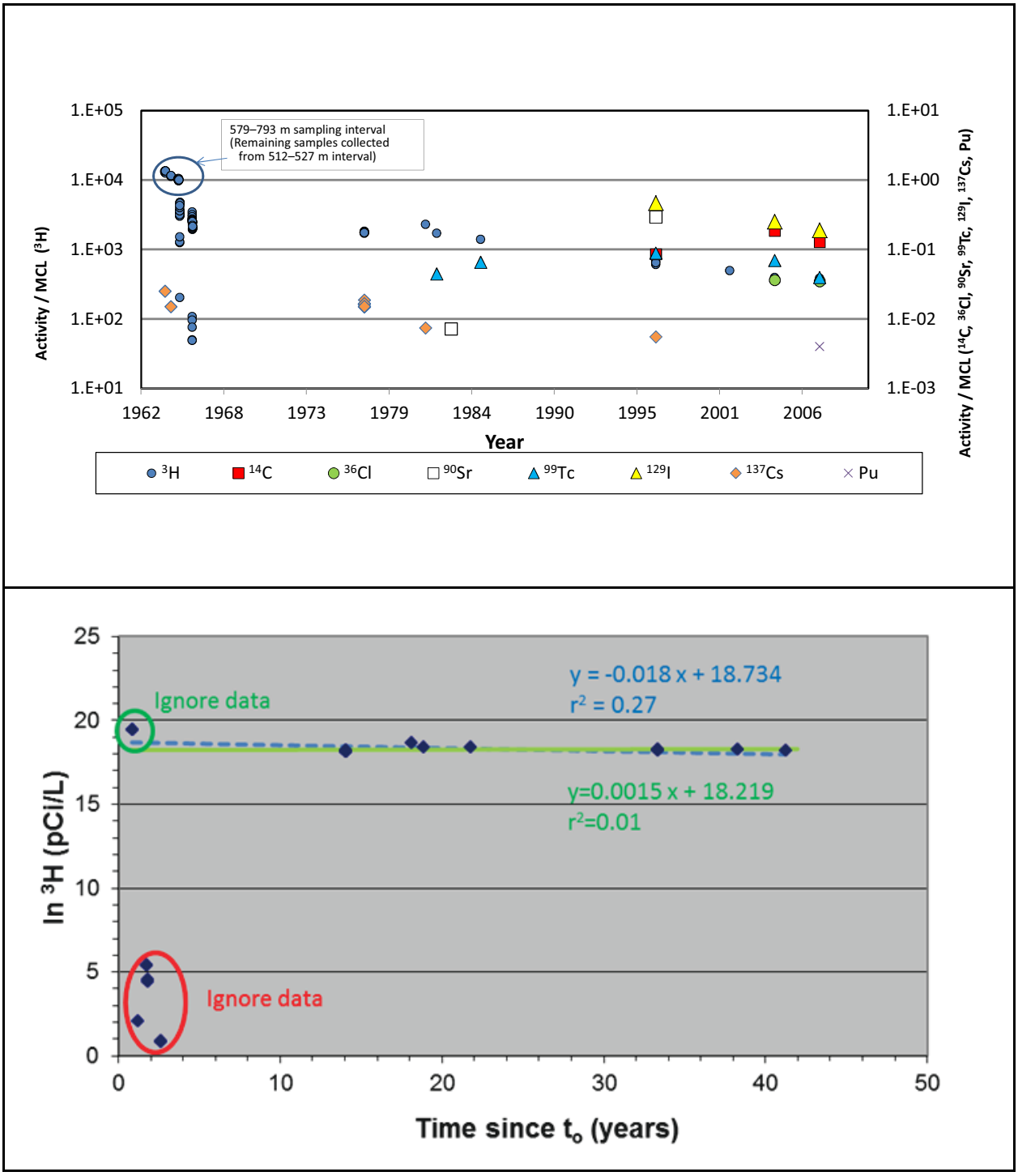

Figure 2-42
Well U-3cn PS 2 Raw RN Data (top) and ^{3}H Data Adjusted to the Time of Detonation (bottom)

Note: The fitted regression line in the lower right panel as a slope of nearly zero, indicating there has been little or no change in ^{3}H concentrations over more than 40 years.

The potential use of post-shot holes to characterize the permeability near cavities and chimneys is insightful and, in fact, has been done in the past at the NNSS. Historical studies using air injection and gas tracers have been used to characterize cavities and chimneys in the TCU at Rainier Mesa (Peterson et al., 1977a and b, and 1978). The studies involved injecting air and gas tracers into one post-shot hole in the cavity/chimney system, monitoring for pressure and tracer responses at post-shot holes penetrating other parts of the cavity/chimney system, and interpreting the cross-hole responses with numerical models to estimate effective permeability to air and air-filled porosity. Because the rocks are partially water-filled, estimated air-permeabilities and porosities are minimum estimates of the absolute (single-phase) permeabilities and porosities. The resulting analyses indicated the air-permeabilities were variable within the chimney. Air-permeabilities were on the order of 8 to 150 Darcies (roughly 8×10^{-12} to 1.5×10^{-10} m^2) in the upper parts of the chimney above the injection hole, and sometimes much less (0.001 to 12 Darcy; roughly 10^{-15} to 1.2×10^{-11} m^2) in the lower part of the chimney that includes the cavity region. Air-filled porosity (accessible void volume) was on the order of 0.09 to 0.17 (Peterson et al., 1978, Table 1). For comparison, the average air permeability of the surrounding media was estimated to be about 1 Darcy (roughly 10^{-12} m^2) in the vitric tuff and 0.001 to 0.36 Darcies (10^{-15} to 3.6×10^{-13} m^2) in the adjacent undamaged zeolitic rocks. The chimney/cavity systems therefore had enhanced permeability relative to the surrounding rock.

The three new wells drilled in Yucca Flat were within 2.3 R_c from CALABASH (ER-2-2), STRAIT (ER-4-1), and WAGTAIL (ER-3-3) detonations. Preliminary data from these wells do not indicate ^3H at concentrations above the MDL (1,500 to 1,800 pCi/L) in the LCA, indicating that the extent of permeability enhancement and initial contamination does not extend beyond 3 R_c.

The modeling team also note that the range of permeability enhancement considered in the SZ AA/VA model was very large–the team considered slight permeability reduction and order-of-magnitude permeability increase. Chimney and cavities were always assumed to be instantaneously high permeability (10^{-12}) and low porosity (0.01). Higher chimney permeabilities are possible based on the air-pressurization studies cited above, but this would tend to promote flow up the chimney to an overlying strata. Although there is evidence on Pahute Mesa of RNs migrating up chimneys to overlying aquifers, the modeling team has yet to find widespread evidence of RN transport along chimneys to the underlying LCA. Migration of RNs to the LCA via chimneys would require that RNs first move upward through the chimney to an overlying aquifer, laterally toward a fault, and then down the fault to the LCA. This scenario was considered in the AA/VA system model

by starting particles in the overlying aquifer rather than in the exchange volume for selected detonations where an overlying saturated aquifer was present. As in the response to Section 2.4.4, there is little evidence in the literature for substantial permeability enhancement beyond 3 R_c.

In conclusion, the SZ AA/VA model simulations documented in N-I (2013a) included numerous scenarios in which widespread breaching and direct communication between TCU and LCA was permitted. The "breached" zones had orders of magnitude higher permeability than the pre-testing rock and often extended the entire thickness of the TCU. It should be noted, however, that these scenarios did not produce well calibrated models. Additionally, these breaching models are not consistent with observations at BILBY that indicate heads at BILBY post-shot well U-3cn PS 2 took years to recover following the detonation (Section 2.3.3), or that the underlying LCA monitored by U-3cn 5 did not show significant ^3H in over 50 years of sampling.

2.5 Transport

2.5.1 Values Used for Pu Retardation Are Not Well Supported and May Be Too High

This uncertainty is associated with the concern that the sorption coefficient distributions used in the transport model for Pu may not be sufficiently conservative.

PRC Recommendation: The Pu K_d values used for modeling should be decreased to reflect the lower end of the measured range, and values lower than those measured should be used to evaluate the uncertainty associated with the lowest measurement. This would be a more conservative approach than emphasizing the high end of the range as is now done. Sensitivity analyses would also be useful to determine at what a range of retardation values Pu transport would be a concern.

PRC Recommendation: With respect to additional data, site-specific data should be collected to develop a better mechanistic understanding of Pu retardation processes and improve the representation of the in situ chemical conditions in which the retardation takes place in Yucca Flat. In addition, evaluation of existing data should continue to determine whether it is possible that retardation values can reach levels that the modeling indicates may cause concerns.

RESPONSE: As discussed below, field measurements of Pu concentrations are significantly lower than even the current model predictions. Lowering the bounds of Pu distribution coefficient (K_d) distributions would lead to even higher model predictions. However, there are several conservative

assumptions not associated with sorption that contribute to high predicted RN concentrations—most notably, the very conservative estimates of total flow through the model, which overestimates groundwater velocity. In spite of team reservations, an additional transport simulation with decreased Pu retardation was performed demonstrating that uncertainty in Pu retardation does not significantly affect the contaminant boundary.

The modeling team reviewed the available Pu concentration observations in wells that have been completed within or near the SZ LCA, and compared the observations to initial Pu concentrations implemented in the SZ LCA flow and transport model. In addition, a review of available carbonate rock sorption literature was performed, and a probabilistic transport simulation has been run where the LCA matrix K_d and fracture retardation factor (R_d) for Pu is decreased to show the impact on contaminant boundary.

Observation wells are located in the SZ LCA near the BILBY, BOURBON, NASH, and TORRIDO/MICKEY underground nuclear detonations. While the working point for the BILBY detonation is in the saturated TCU and the working points for the TORRIDO and MICKEY detonations are in the unsaturated TCU above the LCA, these working points are close to the SZ LCA and Pu concentration data from nearby observation wells are included in this review. Table 2-8 summarizes the available Pu data near or within the SZ LCA. Pu has been positively detected only in the SZ LCA near the BILBY detonation in Well U-3cn 5 (Table 2-8). The MDL associated with this sample was not reported by Lawrence Livermore National Laboratory (LLNL) (Smith et al., 1998), but the lowest MDL for LLNL Pu analyses reported in the UGTA Geochemistry Database is 3.0×10^{-04} pCi/L (Navarro, 2016b). This suggests that the 2.3×10^{-04} pCi/L reported in Smith et al. (1998) was also below the MDL and therefore likely not present in U-3cn 5. Nevertheless, the reported concentrations is far below the MCL of 15 pCi/L.

Calculating the initial Pu concentrations used for LCA modeling requires estimating the volume of water within the cavity and the attenuation resulting from sorption and partitioning into the melt glass or carbonate rock decomposition debris. The fraction of RNs partitioned into the melt glass or carbonate rock decomposition products that accumulates in the bottom half of the cavity will be largely unavailable to groundwater due to the very low solubility of the glass or carbonate rock

Table 2-8
Pu Concentration Observations at Locations within or near the SZ LCA

Detonation	Working Point HSU	Working Point Distance to SZ LCA [m/(number of R_c)]	Observation Well	Open Interval HSU	Location Relative to Detonation (km)	Pu Concentration (pCi/L)
BILBY	OSBCU	865/2.2	U-3cn PS 2	OSBCU	Chimney	2.0×10^{-03} pCi/L (1983) to 6.0×10^{-02} pCi/L (2007) Below the MDL <0.01 to <0.08 pCi/L (1997 through 2004)
			U-3cn 5	LCA	0.12 southwest	2.3×10^{-04} and 2.1×10^{-04} pCi/L (1980) Below the MDL <0.01 to < 0.08 pCi/L (1997 through 2000)
BOURBON	LCA	601/0.8	UE-7ns	LCA	0.17 southeast	Below MDL <0.01 to <0.07 pCi/L (1993 through 2012)
NASH	LCA3	441/2.6	UE-2ce WW	LCA3	0.18 southwest	Below the MDL <0.01 to <0.09 pCi/L (1993 through 2008)
TORRIDO	OSBCU	566/0.7	ER-7-1	LCA	0.20 southeast	Below the MDL <0.02 to <0.05 pCi/L (2003 through 2014)

decomposition products. The R_c in meters for a silicic-rock representative detonation can be calculated with the following equation (Pawloski, 1999):

$$R_c = \frac{70.2\,Y^{\frac{1}{3}}}{(\rho_b DOB)^{\frac{1}{4}}} \qquad (2\text{-}1)$$

where

Y = maximum yield (kt)

ρb = overburden density (g/cm^3)

70.2 = constant developed for variably saturated silicic rocks at the NNSS

DOB = depth of burial (m)

The carbonate working point detonations have significantly smaller measured R_c (in meters) values than predicted with the empirical relationship for silic-rock detonations, and the cube-root energy-scaling equation developed by Boardman (1970) can be used to calculate the R_c:

$$R_c = CY^{\frac{1}{3}} \tag{2-2}$$

where

C = the constant developed for NNSS-dense dolomite and limestone rock (9.05).

Table 2-9 summarizes example initial cavity concentrations for the Pu isotopes carried forward into the LCA contaminant boundary calculations after the screening analysis using transport parameter mean values. The Yucca Flat SZ LCA transport simulations were probabilistic; distributions of exchange volume size, sorption distribution coefficient (K_d), porosity, and melt glass/carbonate debris partition factor were sampled; and the model initial concentrations are a distribution of values. The UZ and SZ AA/VA modeling neglected Pu transport because the Pahute Mesa (SNJV, 2009) and Frenchman Flat (NNES, 2010) contaminant boundaries in alluvium and volcanic rocks were defined by relatively few RN species that are non-sorbing or weakly sorbing. The example silic rock concentrations are average values for the tuff confining units provided in SNJV (2007) and do not represent model values. The initial cavity concentrations for Pu excluding the fraction within melt glass or carbonate decomposition products and including sorption are approximately 1,000 pCi/L for a silic-rock detonation and 50 pCi/L for a carbonate rock detonation. The near-field observations are much lower than the initial model concentrations, which demonstrates that the modeling is conservative in nature. The conservatisms are likely multifarious and may include the following: overestimating recharge and flow through the LCA model, overestimating the initial extent of the exchange volume, underestimating matrix and fracture sorption, and underestimating the fraction made unavailable to groundwater due to partitioning within melt-glass or carbonate decomposition product debris.

Sutton (2009) reviewed distribution coefficients for RNs in carbonate minerals and a range of log10 K_d value from -0.119 to 3.04 mL/g for Pu (IV) and Pu (V); both valence states may be present in Yucca Flat LCA water (Hu et al., 2008; and Powell et al., 2011). Hu et al. (2008) measured sorption on LCA core in water with controlled redox conditions and salinities thought to represent those within the Yucca Flat LCA. Their results range from 116 to 162 mL/g. Fracture retardation values reported by SNJV (2007) range from 0 to 50. Table 2-10 summarizes the LCA matrix K_d and fracture

Table 2-9
Example Initial Cavity Concentration for Pu

Working Point Rock Type	^{238}Pu (pCi/L) [a]	^{239}Pu (pCi/L) [a]	^{240}Pu (pCi/L) [a]
Silicic	684	3,013	766
Carbonate	19	83	21

[a] Initial concentrations assume the following conditions: burial depth = 400 m, cavity porosity = 0.4, overburden bulk density = 2.0 g/cm^3, silicic rock K_d = 93.3 mL/g, carbonate rock K_d = 1,050 (mL/g), glass fraction = 0.975, and carbonate debris fraction = 0.95.

g/cm^3 = Grams per cubic centimeter
mL/g = Milliliters per gram

Table 2-10
Carbonate Rock Matrix K_d and Fracture R_d Distributions for Pu

Parameter	Minimum	Maximum	Mode
Phase I Transport			
Matrix K_d (mL/g)	900	20,000	10,450
Fracture Retardation	2.4	50	26.2
Reduced K_d and R_d Sensitivity			
Matrix K_d (mL/g)	0.76	1,096	548
Fracture Retardation	0	50	25

retardation distributions sampled in the Phase I flow and transport modeling and the alternative distributions sampled for the reduced sorption sensitivity simulations.

Figure 2-43 illustrates the time-cumulative and 800-year probability of MCL exceedance for base-case and alternative Pu K_d case considering all RNs. ^{3}H, ^{90}Sr, and ^{137}Cs are the dominant RNs contributing to the contaminant boundary. The extent of contamination migration and the time-cumulative contaminant boundary is identical for base-case and reduced Pu sorption simulations. The maximum extent of contamination decreases significantly after a few hundred years because the dominant RNs are naturally attenuated by decay. ^{239}Pu and ^{240}Pu have the largest percent of total activity after 800 years and largely define the contaminant boundary at this late time. Reducing the Pu matrix K_d and fracture R_d increases the contaminant boundary area after 800 years, but the area of contamination is very small compared to the time-cumulative contaminant boundary. The fractional exceedance volume is the volume of aquifer exceeding the drinking water standards for a single contaminant species. Figure 2-44 illustrates the $^{238/239/240}$Pu fractional exceedance volumes

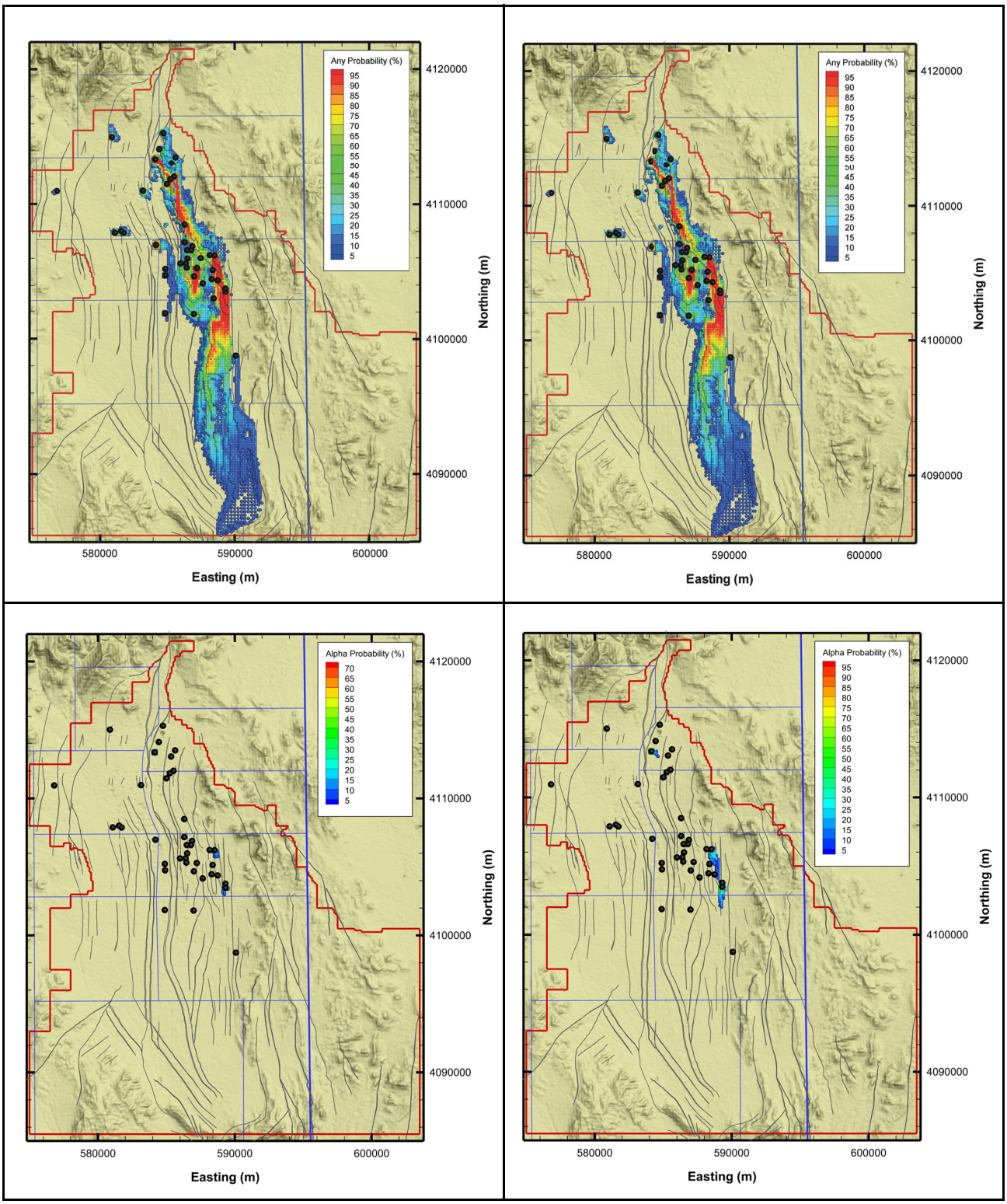

Figure 2-43
Time-Cumulative (top) and 800-Year (bottom) Probability of MCL Exceedance for Base-Case (left) and Alternative Pu Sorption Case (right)

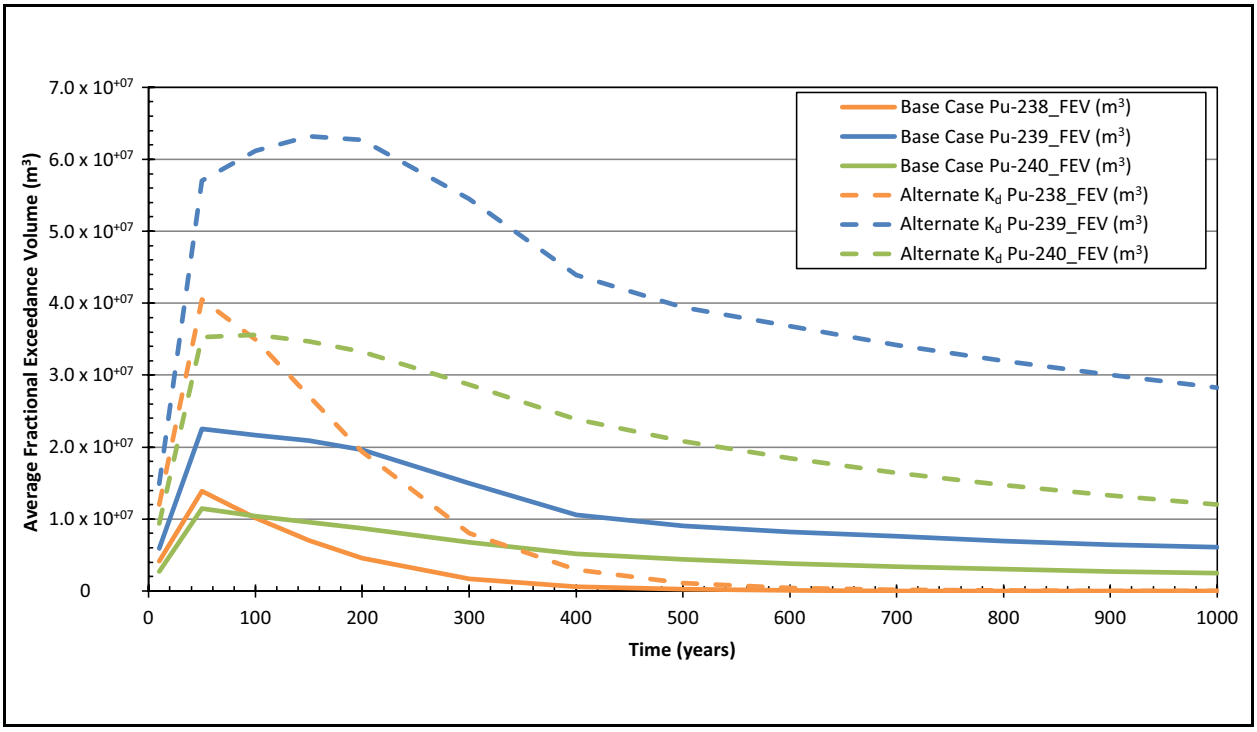

Figure 2-44
Pu Fractional Exceedance Volume for Base-Case and Alternate K_d Case

through time for the base case and alternative Pu K_d case. The fractional exceedance volume increases by a factor of 3 or 4 for the decreased sorption as expected, but the Pu fractional exceedance volume is 3 orders of magnitude smaller than the ^{3}H or ^{90}Sr fractional exceedance volume.

Hence, further work under this uncertainty is not warranted.

2.5.2 Melt-Glass Dissolution Is Largely Neglected

This uncertainty concerns the initial inventory assigned to each detonation and melt-glass dissolution.

PRC Recommendation: Include melt-glass dissolution in UZ models that allow for enhanced flow. Consider additional processes affecting cavity-debris behavior in the LCA model. Include an instant-release case among the sensitivity analyses, similar to that in the AA/VA model.

RESPONSE: Melt-glass dissolution in the UZ is not important because of dry conditions following the detonation and the fact that the wetting front from crater infiltration will not arrive until long after melt glass has cooled (in some cases, hundreds of years). Additionally, UZ detonations were demonstrated in N-I (2013a) to be secondary to other detonations for defining the contaminant

boundary, so late-time melt-glass dissolution would have only a minor impact. In view of these considerations, this is considered a low-priority issue that does not require further analysis. Significant glass dissolution occurs only at elevated temperatures, and transport of liberated Pu due to glass dissolution will be limited by sorption and filtration of colloids (Zavarin et al., 2015).

The initial glass mass, temperature, and associated cooling history will control the extent of glass dissolution. The HST screening analysis presented in Appendix C of N-I (2013a) categorized Yucca Flat detonations by yield, which correlates with glass volume and initial temperature, and calculated that glass dissolution in presence of water ranges of 0.001 to 2.6 percent for the first 100 years of glass dissolution. Tompson et al. (2011) calculated melt-glass dissolution using a range of working-point depths and glass-dissolution parameters for the Rainier Mesa/Shoshone Mountain HST. Only the very deep detonations (average depth of 534 m) were expected to have a maximum melt-glass dissolution of more than 1 percent over 1,000 years. The Frenchman Flat unclassified source term analysis (SNJV, 2005b) calculated melt-glass dissolution for the CAMBRIC test to be approximately 0.5 percent quickly dissolving during the first year and approximately 5 percent dissolving after 1,000 years. The parametric uncertainties associated with calculating the HST for the SZ LCA included inventory uncertainty and melt-glass partition fractions. The inventory uncertainty varied from a factor of 0.1 to 10 depending on the RN group (i.e., residual ^{3}H, activation products, fission products or unspent fuel) and melt-glass fractions varied from zero to 100 percent depending on the RN. The uncertainty associated with initial inventory and melt-glass partition factors is much larger than the total expected melt-glass dissolution and immediately releasing a small percentage of the RNs incorporated in melt-glass to the LCA will not significantly change the contaminant boundary.

Hence, further work under this uncertainty is not warranted.

2.6 Simulating Critical Observations

2.6.1 Field Measured ^{3}H Concentrations Are Not Simulated by the N-I (2013a) Model

This uncertainty focuses on the non-zero levels of ^{3}H concentrations detected in the Wells ER-2-1, UE-6e, UE-6d, TW-B, and WW-A.

PRC Recommendation: The peer review team recommends the following actions to address ^3H observations:

- *Simulate a sub-region of the model encompassing an unexpectedly high measured concentration using many more particles to determine whether the reason for the mismatch is the low number of particles used to represent ^3H transport.*
- *Simulate a sub-region of the model encompassing an unexpectedly high measured concentration using smaller block sizes.*
- *Determine what processes could lead to the observed apparent lateral transport of ^3H in the AA/VA and incorporate them into the model.*
- *Evaluate whether the timing of the sampling or the nature of the completion of the non-detect wells may be such that ^3H occurrences were missed.*
- *Given that there are so few contaminant data in the LCA, results of comparisons are mixed, and contaminant movement in the LCA is expected to follow discrete pathways, the next step is to gather field data that will define the current extent of contamination to better evaluate the simulations and adjust the model to better represent the field system.*

RESPONSE: The focus of the SZ AA/VA model was to estimate contaminant fluxes to the SZ LCA, which provides the only groundwater pathway out of Yucca Flat. The grid, boundary conditions, and other aspects of the model design were set up to achieve this objective and not to focus on interpreting sporadic measurements of low-level ^3H concentrations in the shallow system, which are peripheral to the more central issue of deep transport. However, the modeling team recognizes that overall confidence in the combined AA/VA and LCA transport models will benefit from successful comparisons of models and field data. Therefore, in the interest of confidence building, UGTA is committed to verifying low-level ^3H concentrations in the shallow system where well access permits resampling, and modeling the confirmed observations to better constrain model parameters and build confidence.

Since the completion of the Phase I flow and transport model document (N-I, 2013a), UGTA has resampled ER-6-2, UE-7nS, WW-3, WW-2, ER-2-1, UE-6d, UE-6e, TW-7, and TW-B. Five of these wells (ER-2-1, ER-6-2, TW-B, UE-6d, and UE-6e) were identified by the PRC as of special concern (N-I, 2015, Table 6-4) based on previous ^3H measurements.

A complete discussion of the likely sources of low ^3H concentrations outside of the immediate cavity/chimney environment, including some interpretive models of selected ^3H occurrences, is provided in Appendix B.

Near-field contamination in the LCA would be expected to evolve more quickly and require a high frequency of sampling to detect than far-field wells, where a contaminant plume is more spatially extensive and concentration changes would be expected to change more slowly with time. Near-field LCA wells near BOURBON (Well UE-7nS) and BILBY (Well U-3cn 5) have hundreds of samples each spanning multiple decades but show at most low-level (<<MCL) ^3H contamination. However, both of these wells showed very high initial ^3H values that probably reflect contamination that was brought down from shallower depths during drilling but was not evident in later sampling events. Well ER-7-1 near the MICKEY/TORRIDO detonation has 20 samples taken since 2003 and has never shown ^3H in the LCA over that time, including low-level measurements (DL = 1.1 pCi/L). Each of these wells is completed near the top of the LCA where contamination would be expected to highest: ER-7-1 is open to the upper 725 ft of the LCA: U-3cn 5 is open to the upper 198 ft of LCA; and UE-7nS is open to the upper 235 ft of SZ LCA.

Far-field LCA Well ER-6-1-2 was sampled on five separate dates between 1999 and 2004, but all samples were ^3H free (minimum DL of 9 pCi/L). ER-6-1-2 is open to 1,425 ft at the top of the LCA. Nearby Well ER-6-1-1 was open over 217 ft near the top of the LCA but was also ^3H-free on eight separate sampling dates between 1992 and 2004. As water-supply wells, WW-C and WW-C-1 were sampled almost every year since 1973. Early samples taken before 1983 showed some low-level ^3H, which Lyles (1990) attributed to an early tracer test that involved ^3H. Since the 1980s, however, ^3H concentrations have been below the DL, which has varied over time from 10 to 900 pCi/L. ^3H has been measured more than 30 times since 1976 at TW-D, which is open to the upper 227 ft of SZ LCA. Early samples indicated low-level concentrations of ^3H (<100 pCi/L). Samples since 1987 have been below the DL (as low as 10 pCi/L). Yearly samples from UE-1q taken since 1999 have shown the LCA at the well to be free of ^3H. UE-1q is open over 141 ft near the top of the LCA. In conclusion, the frequency of sampling at many locations in the LCA indicates that sample frequency and shallow open intervals have been adequate to detect ^3H if it were present. Except for near-field Well UE-2ce (this is not one of the wells identified by the PRC as being of special concern) near the NASH detonation in the northwest corner of Yucca basin, no LCA wells have measured ^3H above its MCL (20,000 pCi/L), and most LCA wells are ^3H-free altogether.

Low-level ^3H measurements indicate that groundwater at TW-B, ER-6-2, UE-6d, WW-2, and TW-7 is currently free of measurable ^3H. Low-level ^3H measurement results are not possible for UE-6e because of matrix problems with the sample, but this well also is free of ^3H but at a higher DL (Table 2-11). Therefore, although historical measurements of uncertain quality have indicated that low levels of ^3H may have been present at UE-6d, ER-6-2, and UE-6e, the new data indicate that even if the historical measurements were accurate and not the result of cross-contamination during sampling or analysis, the low levels of ^3H were not harbingers of a contaminant plume migrating at unexpected rates or directions.

Well TW-B has historically had much higher ^3H concentrations. As explained in Appendix B, Lyles (1990) attributed these historical ^3H concentrations to infiltration into cracks that periodically develop in the playa, including periods in the 1960s when atmospheric ^3H levels were at their highest (thousands of pCi/L). However, considerable doubt exists around this interpretation due to the fact that the well has low transmissivity (50 square feet per day [ft^2/day]) and the cracks are not oriented in a way that would facilitate transport from the playa to TW-B. Flow from the playa 0.75 km north to TW-B would require velocities of about 150 meters per year (m/yr), which is not supported by the low transmissivity of the well. Lyles (1993) discussed well conditions (well annulus cemented to the bottom of the casing at 510 m depth, mud diesel fuel and drill bits at the bottom of the well) that make it clear that the well was never cleaned out and that the ^3H was probably introduced during drilling.

The low levels of groundwater ^3H measured at WW-2 and ER-7-1 continue to indicate that groundwater is free of measurable ^3H, despite being downgradient of about 10 UZ nuclear tests at Climax Stock in the case of WW-2 and the nearby deep UZ MICKEY/TORRIDO tests in the case of ER-7-1.

Recent measurements from the TCU at TW-7 near the AARDVARK detonation also confirmed an earlier non-detect of ^3H on January 1, 1994 (N-I, 2016a).

Appendix B presents a UZ model that indicates that low-levels of ^3H at WW-3 are plausibly attributed to infiltration from an adjacent pond that existed between about 2002 and 2010 and which held water trucked from WW-C-1, a well that was contaminated in the early 1960s during an aborted tracer test involving ^3H (Lyles, 1990).

Table 2-11
Groundwater ^{3}H Data Measured since the PRC Initiation
(Page 1 of 2)

Location	Sample Date	Sample Method	EOI Top or Bailer Depth	EOI Bottom or Bailer Depth	Result [a]	DL	Error	Laboratory [b]
			(ft)		(pCi/L)			
TW-B	05/20/2015	DIS BAIL [c]	1,625	1,625	U 2.84	2.32	1.67	Commercial
UE-6e [d]	05/19/2015	DIS BAIL [c]	2,142	2,142	<102	102	--	
UE-6d	05/18/2015	DIS BAIL [c]	2,950	2,950	<2.44	2.44	--	
	05/19/2015	DIS BAIL [c]	2,950	2,950	<2.22	2.22	--	
WW-3	06/03/2014	DIS BAIL [c]	1,650	1,650	7.28	1.97	2.56	
	06/09/2015	WH	WL	2,349	5.63	2.03	2.16	
	06/09/2015	WH	WL	2,349	6.27	2.25	2.4	
ER-2-1 Main	03/26/2015	WH	WL	2,177	840	370	280	
	03/26/2015	WH	WL	2,177	1,013	288	220	
	03/26/2015	WH	WL	2,177	920	370	280	
	03/26/2015	WH	WL	2,177	909	287	212	
	03/26/2015	WH	WL	2,177	682	298	134	LLNL
	03/26/2015	WH	WL	2,177	795	297	239	
ER-7-1	06/19/2014	WH	WL	2,500	U 2.67	2.25	1.60	
	06/19/2014	WH	WL	2,500	<2.26	2.26	--	
	06/20/2014	WH	WL	2,500	<1.1	1.1	--	
	06/20/2014	WH	WL	2,500	<340	340	--	Commercial
	06/20/2014	WH	WL	2,500	<2.26	2.26	--	
	06/20/2014	WH	WL	2,500	<2.17	2.17	--	
	06/20/2014	WH	WL	2,500	<340	340	--	
ER-6-2	06/18/2014	WH	1,746	3,430	<2.24	2.24	--	
	06/18/2014	WH	1,746	3,430	<2.28	2.28	--	
	06/19/2014	WH	1,746	3,430	<1.1	1.1	--	LLNL
	06/19/2014	WH	1,746	3,430	<1.76	1.76	--	Commercial
	06/19/2014	WH	1,746	3,430	<2.22	2.22	--	
UE-7nS	06/10/2015	DIS BAIL [c]	2,018	2,018	J 45.16	2.28	13.53	
	06/10/2015	DIS BAIL [c]	2,018	2,018	<370	370	--	
	06/10/2015	DIS BAIL [c]	2,018	2,018	<280	280	--	

Table 2-11
Groundwater ^3H Data Measured since the PRC Initiation
(Page 2 of 2)

Location	Sample Date	Sample Method	EOI Top or Bailer Depth	EOI Bottom or Bailer Depth	Result [a]	DL	Error	Laboratory [b]
			(ft)		(pCi/L)			
WW-2	04/22/2015	WH	2,563	3,422	<2.17	2.17	--	Commercial
	04/22/2015	WH	2,563	3,422	<2.18	2.18	--	
TW-7	05/21/2015	DIS BAIL [c]	1,950	1,950	<2.47	2.47	--	

[a] Measured values that are less than the MDL are reported as "<MDL."
[b] Samples were analyzed by a commercial laboratory certified by NDEP Bureau of Safe Drinking Water and in some cases by LLNL for confirmatory purposes.
[c] The depth bailed is reported as EOI top and EOI bottom.
[d] Low-level ^3H analysis was not possible because of a matrix issue with the sample; the sample was very muddy. A 102-pCi/L detection was the lowest that the commercial laboratory could achieve.

EOI = Effective open interval
WL = Water level

DIS BAIL = Depth-discrete bailed sample
WH = Pumped sample collected from the wellhead

J = Estimated value.
U = Compound was analyzed for, but not detected.

-- = Not applicable

Although not sampled in 2014 or 2015, groundwater from WW-A sampled on February 8, 2012, had a ^3H concentration of 355 pCi/L. Numerical models presented in Appendix B support the Lyles (1990) hypothesis that water supply pumping from WW-A between 1961 and 1987 drew contamination from the 1961 HAYMAKER detonation toward WW-A by the late 1980s.

The low levels of groundwater ^3H in recent samples from Well ER-2-1 continue to be surprising in that they would reasonably be expected to be much higher, especially if the speculation of the PRC regarding larger exchange volumes is valid. Well ER-2-1 had two SZ detonations within a lateral distance of 4.1 R_c. Measured ^3H at ER-2-1 was 228 pCi/L based on the September 3, 2003, sample and is now in the range of 682 to 1,013 pCi/L. The trend with time at ER-2-1 is consistent with contaminated water moving outward from an initial exchange volume of 4 R_c or less.

Well UE-7nS was open in the SZ LCA within 2 R_c of the BOURBON working point based on its maximum announced yield. Measurements from BOURBON date back to the mid-1970s (Lyles, 1990). The low levels of groundwater ^3H in recent samples from UE-7nS (<280 pCi/L)

continue to be surprising in that they would reasonably be expected to be much higher, especially if the speculation of the PRC regarding larger exchange volumes is valid.

Preliminary data from the new Wells ER-2-2, ER-3-3, and ER-4-1 do not indicate ^{3}H at concentrations above the MDL (1,500 to 1,800 pCi/L) in LCA. Two of these wells, ER-3-3 and ER-4-1, will be developed, and additional samples will be collected in future.

The UGTA Activity will continue to confirm/update existing dataset of low-level ^{3}H detects, and will evaluate the data with respect to the flow and transport model forecasts as well as with the current conceptual model as described in the NNSS Integrated Sampling Plan (NNSA/NFO, 2014).

2.6.2 Crater-Infiltration Data Are Not Well Matched in the Model

This uncertainty addresses the rate of surface flux into the UZ by enhanced recharge through craters.

PRC Recommendation: Determine why the modeled crater-recharge estimates do not match well the limited observations, and ensure that the crater-recharge model is conservative in its estimates of enhanced recharge.

RESPONSE: The three craters used to calibrate the crater infiltration model are the craters formed by the HYRAX, LAGUNA, and BYE detonations. At HYRAX (U3bh), the difference between the noisy moisture content data of holes drilled beneath versus adjacent to the HYRAX crater (as fit by the smoother model results in N-I [2013a, Figure E-21a]) suggests a somewhat smaller average moisture content difference (0.05) over the 55-m depth than the 0.1 moisture content difference used by the PRC. This accounts for the smaller estimate of 79 mm/yr (N-I, 2013a, Table E-5) over 33.4 years between September 1962 and February 1996.

At LAGUNA (U3fd), the estimated flux over the 13-year calibration period between the time the crater formed (1971) and the time sampled (1986) was about 600 mm/yr based on meteoric ^{3}H peaks and moisture content differences (Tyler et al., 1992; Pohll et al., 1996), whereas the simulated flux over the calibration period was about 500 mm/yr (N-I, 2013a, p. E-34); therefore, over the calibration period, the published infiltration estimates for LAGUNA and those estimated by the N-I modeling teams are in good agreement. However, because the period 1972 through 1985 was an anomalously wet period compared to the 45 years of record (1960 through 2005) that were used for generating the 1,000-year synthetic precipitation record (Figure 2-45), the 1,000-year infiltration estimate for U3fd

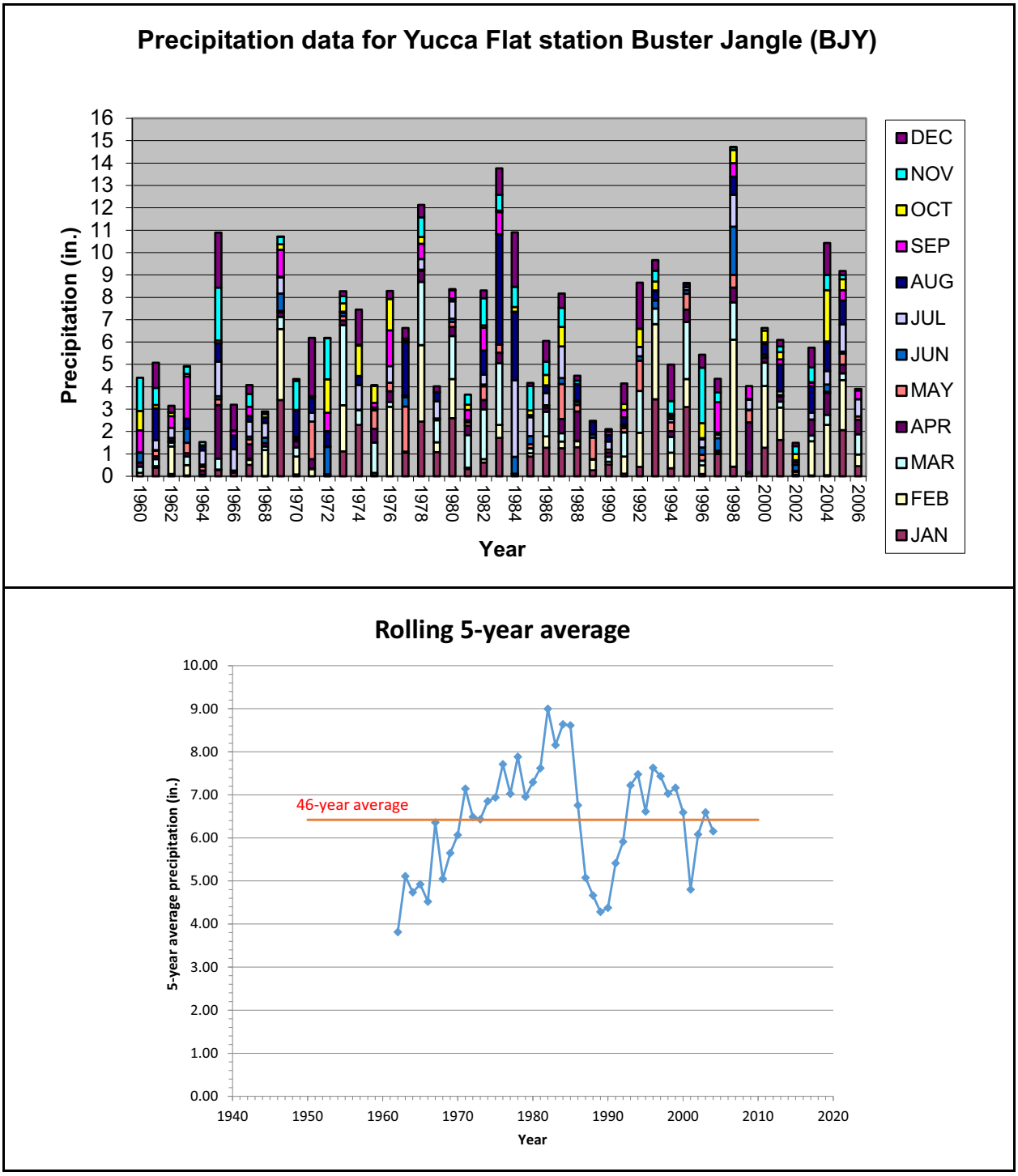

Figure 2-45
Monthly and Yearly Precipitation Record from the BJY Precipitation Station in Yucca Flat (top) and the Rolling 5-Year Average Annual Precipitation (bottom)

listed in Table E-5 (72 mm/yr for LAGUNA; N-I 2013a, Appendix E, p. E-54) is an order of magnitude lower. The anomalous wetness of the period 1971 to 1986 is not evident in the raw precipitation record (Figure 2-45, top) but becomes obvious when one compares the rolling 5-year average with the 45-year mean (Figure 2-45, bottom).

This interpretation of the order-of-magnitude difference is supported by comparing the percentage of days in the model that had ponding events exceeding 0.1 m in the 13-year calibration period (0.4 percent) with the percentage of days with similar ponding events over the 1,000 years (0.06 percent).

For the BYE crater (U10i), moisture content measurements in boreholes within and adjacent to the crater were not deep enough to capture the depth of the wetting front, based on the fact there was sedimentological evidence for an estimated six ponding events between the time of crater formation (July 1964) and the time the boreholes were drilled (1997). Neutron-probe moisture logging tracked the infiltration and drainage of the February 23 and 24, 1998, ponding event below the depth of the crater borehole (32 m) in a matter of weeks, so the other earlier ponding events were lost from the subsurface moisture record. The modeling team could not locate infiltration estimates in the Hokett et al. (2000) report that documents the BYE crater study; however, the team notes that the BYE watershed area of 18.6 square kilometers (km^2) is among the largest estimated for Yucca Flat, which is consistent with the high infiltration estimate at this crater. There is also evidence that over time, craters will become sealed with fine-grained sediments and infiltration rates will decrease over time due to this self-sealing mechanism. This self-sealing process was not invoked to decrease infiltration rates over time due to the uncertainty in the rates of these processes; however, the likelihood is that craters will fill with fine-grained sediment over time and effectively stop behaving as sources of recharge.

No further work is warranted under this uncertainty.

2.6.3 Geochemical and Environmental Isotopes Not Fully Evaluated

This uncertainty addresses the interpretation of ^{36}Cl and ^{14}C data.

PRC Recommendation: The choice of initial Cl concentrations used to adjust the measured $^{36}Cl/Cl$ ratios should be examined carefully, and strong justification should be provided for the value finally chosen.

RESPONSE: The groundwater velocities estimated by ^{14}C ages in Appendix L of N-I (2013a) and Kwicklis and Farnham (2014) were not used to constrain the LCA groundwater flow and transport models, and therefore no action is required to address this uncertainty. The modeling team recognizes that there is uncertainty in the assumed Cl concentrations of recharge used to reconstruct the original meteoric $^{36}Cl/Cl$ ratios in groundwater from the LCA. The use of a Cl value of 7 milligrams per liter (mg/L) is based on the mean Cl concentration of dozens of tunnel seeps in tuffs at Rainier Mesa (Cooper et al., 2013, Appendix C). The use of this value in recharge to the LCA in Yucca Flat is reasonable in that water in the tuffs at Rainier Mesa (a regional recharge area) has undergone no or minimal Cl leaching (as in the LCA) or evaporative enrichment after discharge (as do perched spring data). Furthermore, the use of 7 mg/L to correct the LCA samples that appear to have been affected by halite dissolution allows for a range in $^{36}Cl/Cl$ ratios similar to those measured in packrat middens between 10,000 and 40,000 years ago (a range that is neither too high or too low) and which matches the temporal variations in the packrat midden data. While this does not prove the use of 7 mg/L is correct, it is at least internally consistent with the ranges and timing of $^{36}Cl/Cl$ variations estimated from the packrat midden data.

PRC Recommendation: The behavior and interpretation of ^{14}C in the Yucca Flat and Ash Meadows flow systems should be compared and contrasted. If results of such a study indicate retardation in Ash Meadows but not in Yucca Flat, an explanation should be sought for such a profound difference in the behavior of two otherwise similar flow systems.

RESPONSE: Appendix L of N-I (2013a) and Kwicklis and Farnham (2014) argue that simple correction methods to adjust the ^{14}C activities of dissolved $H^{14}CO_3^-$ could be applied in Yucca Flat based on agreement between the temporal record of adjusted $^{36}Cl/Cl$ ratios of LCA groundwater with terrestrial records from packrat middens, but that these same correction methods did not appear to be applicable to groundwater at Devils Hole. At Devils Hole, other independent age estimates indicated

that the groundwater was much younger (2,000 to 7,000 years) (Winograd et al., 2006) compared with the age estimated from adjusted $H^{14}CO_3^-$ (roughly 25,000 years) based on the same corrections. This response provides an answer for the different behavior.

Differences in the mineralogy of the LCA in Yucca Flat and near and upgradient of Devils Hole were examined. Figure 3-1 of BN (2006) shows that the high transmissivity eastern corridor of Yucca Flat where most of the groundwater ^{14}C data were taken is composed of Cambrian, Ordivician, Silurian, and Devonian rocks that are part of the Yucca Flat syncline. Table 4-2 of BN (2006) indicates that rocks from these geologic eras are mostly a mixture of limestones and dolomites, with some quartzite and shale. The Cambrian rocks in Yucca Flat include the limestones and dolomites of the Bonanza King formation, which constitutes the formation in the vicinity of Devils Hole (Carr, 1988). The distinction between dolomite and limestone is of interest because crushed samples used in batch tests suggest that limestone has a much greater tendency than dolomite to recrystallize, and therefore has a larger tendency to incorporate and sequester ^{13}C and ^{14}C in its mineral structure than dolomite (Reimus et al., 2008). However, there is limestone and dolomite present in both Yucca Flat and at Devils Hole, suggesting that mineralogic differences between the sites would not explain any differences in behavior.

The correction methods used to adjust ^{14}C ages in Yucca Flat account for the dissolution of calcite and dolomite by calculating increases in dissolved inorganic carbon (DIC) and delta carbon-13 ($\delta^{13}C$) in the groundwater relative to recharge. Local springs on the northern periphery of Yucca Flat such as White Rock Spring and Oak Spring are undersaturated with respect to both dolomite and calcite (SNJV, 2006a, Table 5-1), indicating the potential for recharge water to react with these minerals once it reaches the LCA (Figure 2-46). The shallow interval of UE-10j (UE-10j-3) was estimated to be derived primarily from local paleo-recharge (SNJV, 2006a, Section 6.0) and is saturated with respect to dolomite and calcite, suggesting that these dissolution reactions have in fact occurred (though the two deeper intervals—UE-10j-2 and UE-10j-1—are curiously undersaturated with respect to both minerals (SNJV, 2006a, Table 5-1). Further south in Yucca Flat, most LCA wells are saturated or even oversaturated with these minerals, including groundwater at WW-C and WW-C-1. Like the groundwater from southern Yucca Flat at WW-C, the groundwater from Devils Hole is supersaturated with respect to both dolomite and calcite.

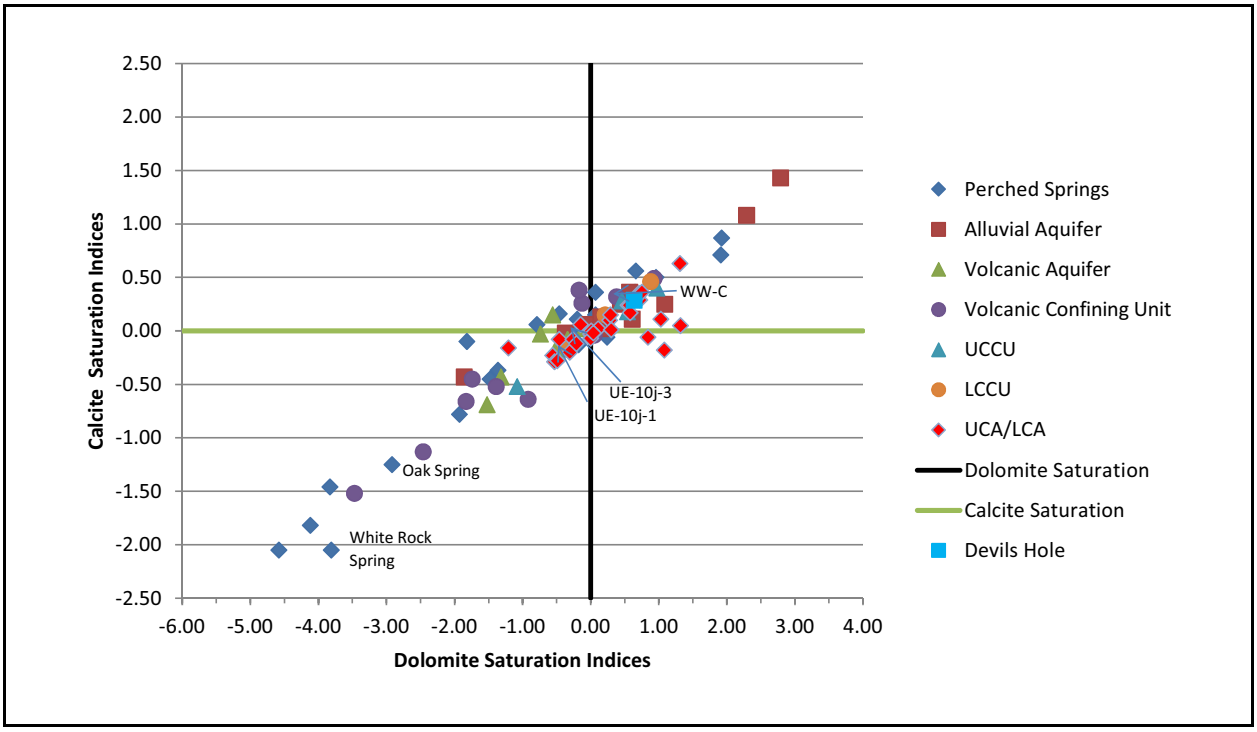

Figure 2-46
Dolomite and Calcite Saturation Indices for Yucca Flat Area Groundwater (from SNJV, 2006a, Table 5-1) and Devils Hole

The correction methods account for dolomite and calcite dissolution, but would not account for ^{14}C loss through isotope exchange (Wigley et al., 1978; Glynn and Plummer, 2005) if this were to occur after these dissolution reactions were complete. Isotope exchange would basically take place during recrystallization of calcite, as evidenced by ^{14}C uptake during batch experiments when crushed calcite or dolomite is used. These same experiments (Reimus et al., 2008) show that uptake is much less when the calcite or dolomite is aged before the addition of the ^{14}C spike, presumably because some or most of the recrystallization has already taken place and the calcite and dolomite has reached a more stable crystal form. One possible difference between Yucca Flat and Devils Hole is that calcite is thought to be actively precipitated at Devils Hole due to degassing of carbon dioxide (CO_2) near the water table (Landwehr and Winograd, 2012). Degassing of CO_2 results in the precipitation of calcite deposits referred to as folia at the water table, and these have been dated and used to establish paleo-water table changes over the last 120,000 years up to the present day (Szabo et al., 1994). Szabo et al. (1994) describe the mammillary and vein calcite precipitated below the water table as very dense with porosity <<1 percent and with large elongate crystals 1 to 4 millimeters (mm). Mammillary calcite coats the walls from Devils Hole to depths of 130 m below the present water table and has estimated deposition rates of 0.7 mm per 1,000 years (Plummer et al., 2000). Calcite

precipitated at or above the present water table (including the folia from a previously higher water table) often has porosities of 15 to 20 percent and crystals that are small and equant, factors that would increase the surface-to-volume ratio and the potential for isotope exchange. Folia are absent deeper than 1 m below the present water table. The calcite in the LCA at Yucca Flat more probably resembles the mammillary and vein calcite at Devils Hole. Recrystallization of the relatively young porous folia deposits through continued interaction with groundwater flowing through Devils Hole would tend to sequester any dissolved ^{14}C into the calcite structure, as observed in the aforementioned batch experiments of Reimus et al. (2008). This isotope exchange process would not result in an increase in DIC or shift in $\delta^{13}C$ (the $\delta^{13}C$ of the calcite presumably resembles the $\delta^{13}C$ of the precipitating groundwater), and hence would be invisible to the correction methods that were used. The older, more stable calcite crystal structure in Yucca Flat is less susceptible to recrystallization, and isotope exchange is not an issue in Yucca Flat as it is in Devils Hole.

The Devils Hole groundwater sample used in this analysis is taken from Winograd and Pearson (1976), who reported that it was pumped from a point about 3 to 4 m below the water table. The calculated P_{CO2} of LCA groundwater at Devils Hole is 10^{-02} atmospheres (atm). Yucca Flat groundwater from the LCA spans the range of P_{CO2} values 10^{-03} to $10^{-0.5}$ atm, or roughly 3.2 to 1,000 times higher than atmospheric concentration of $10^{-03.5}$ atm). However, both the P_{CO2} and DIC of the groundwater at Devils Hole are much lower than groundwater at the southern end of Yucca Flat at WW-C or WW-C-1, or in northern Yucca Flat at UE-10j (Figure 2-47), indicating that some degassing of the Devils Hole groundwater may have occurred as hypothesized.

Another factor that would increase the likelihood of isotope exchange due to precipitation/dissolution reactions in the Devils Hole flow system is that, according to Winograd and Pearson (1976, p. 1137),

> *The spring waters at Ash Meadows are saturated to slightly supersaturated with respect to both calcite and dolomite, and dolomite, and such [isotope] exchange might therefore be enhanced during alternate dissolution and precipitation of these minerals as the water moves through regions of differing temperature and pressure en route to the discharge areas. For example, owing to the varying depths of burial of the aquifer, water temperature varies at least 15 °C (from 25° to 40°C) in the central and distal ends of the groundwater basin, and pressure differences of up to 1700 psi (about 120 atm) are not unlikely.*

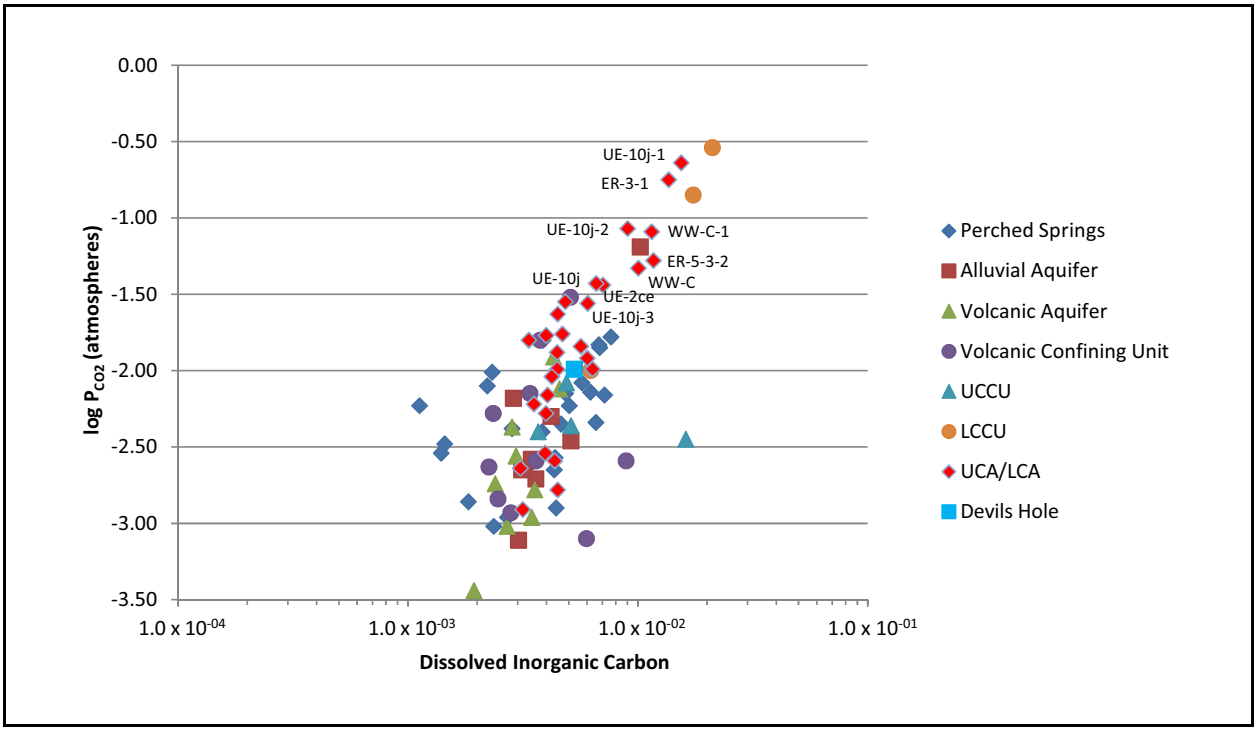

Figure 2-47
Relation between P_{CO2} and DIC for LCA Groundwater in and near Yucca Flat and at Devils Hole

In contrast, in the absence of significant recharge through the thick alluvium, ground-water flow through the LCA in Yucca Flat is predominantly horizontal, so that the large changes in temperature and pressure associated with strong vertical flow components in the Spring Mountains/Devils Hole flow system are absent.

Another means by which isotope exchange could effectively take place is through the dissolution of dolomite and the precipitation of calcite as fracture coatings. Dolomite dissolution takes place through the following reaction:

$$CaMg(CO_3)_2 + H_2O + H^+ = Ca^{2+} + Mg^{2+} + 2HCO_3^- + OH^-$$

Calcite precipitation can be expressed as:

$$Ca^{2+} + {}^2HCO_3^- + OH^- = CaCO_3 + HCO_3^- + H_2O$$

Adding these equations together gives the combined dolomite dissolution and calcite precipitation reaction:

$$CaMg(CO_3)_2 + H_2O + H^+ = CaCO_3 + Mg^{2+} + HCO_3^- + H_2O$$

Dolomite dissolution combined with calcite precipitation would thus lead to an increase in dissolved Mg^{2+} and alkalinity (HCO_3^-), and would likely shift the $\delta^{13}C$ of the alkalinity toward that of marine dolomite ($\delta^{13}C$ = 0 ‰) while the $\delta^{13}C$ of the calcite would resemble the $\delta^{13}C$ of the groundwater plus a fractionation factor of about 0.9 ‰ at 25°C. The increase in Mg^{2+} from this reaction is accompanied by the consumption of H^+, leading to a rise in the pH. However, an order of magnitude reduction in H^+ leads to an increase in 1 pH unit (pH = -log[H^+], so as H^+ goes from 10^{-07} to 10^{-08} (pH goes from 7 to 8), a total of 9.0×10^{-08} moles of H+ is consumed. From the stoichiometry of the dolomite dissolution/calcite precipitation reaction, there are 9.0×10^{-08} moles of Mg^{2+} produced for the same unit pH change. This is equivalent to 0.0022 mg/L Mg^{2+}, which is essentially a non-measurable increase in Mg^{2+}.

An examination of the data from the LCA in Yucca Flat and nearby areas shows that dissolved Mg^{2+} does increase with an increase in alkalinity (Figure 2-48), but that Mg^{2+} actually decreases with increasing pH (Figure 2-49) rather than increasing or staying constant, indicating that the hypothesized dissolution/precipitation reaction does not explain the trends in LCA groundwater from Yucca Flat. These apparent trends more likely reflect the fact that groundwater has different origins, rather than originating from a single groundwater source that evolves along predictable water/rock interaction pathways. The groundwater at both the northern and southern ends of Yucca Flat appears to be more evolved than groundwater elsewhere in the basin. The fact that groundwater at the southern end of Yucca Flat at WW-C and WW-C1 has similarly high Mg^{2+} and alkalinity as deep groundwater in the northern end of Yucca Flat at UE-10j-1 or groundwater east of Yucca Flat at ER-3-1 suggests that other, more dilute groundwater in Yucca Flat does not constitute a significant volume of the groundwater reaching the southern end of the basin, either because (1) UE-10j-1 groundwater flows relatively unchanged directly south along the Yucca fault to WW-C and WW-C-1, and the flow of other, more dilute groundwater in Yucca Flat to WW-C and WW-C-1 is volumetrically insignificant; or (2) ER-3-1 groundwater flows toward WW-C and WW-C-1, and all other flow from Yucca Flat is volumetrically insignificant in comparison. In the first case, isotope

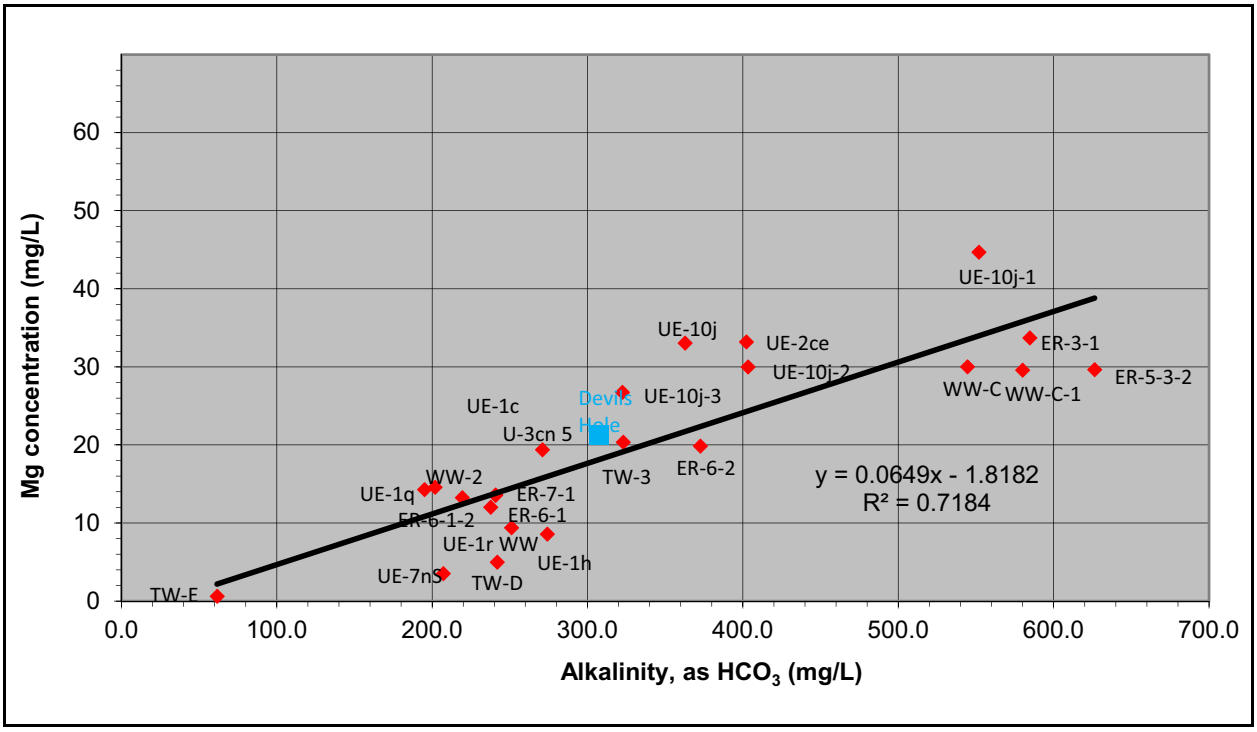

Figure 2-48
Relationship between Mg^{2+} Concentration and Alkalinity (as HCO_3^-) in LCA Groundwater in and near Yucca Flat and at Devils Hole

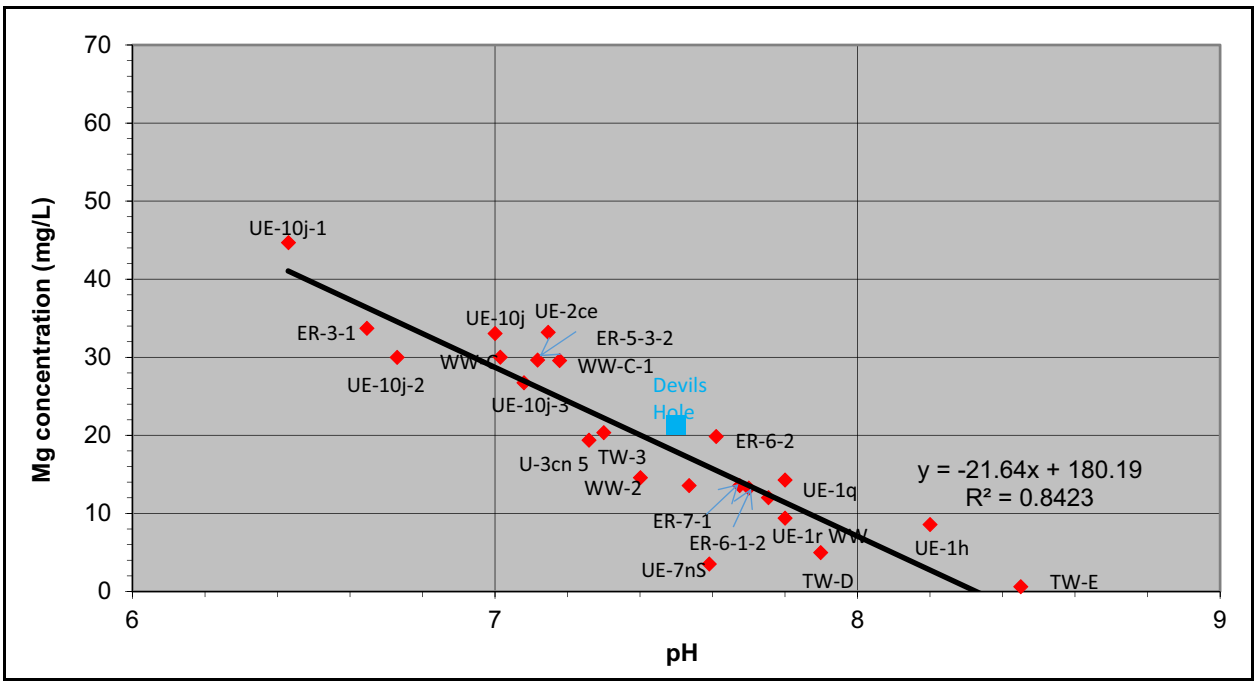

Figure 2-49
Relation between Mg^{2+} Concentration and pH for LCA Groundwater in and near Yucca Flat and at Devils Hole

exchange through dolomite dissolution and calcite precipitation does not occur, and in the second case, it does not matter because the flux in Yucca Flat is volumetrically insignificant.

PRC Recommendation: Finally, it should be made clear whether the rates of groundwater flow supporting the modeled transport of detonation-derived radionuclides are more similar to those based on retarded or on unretarded ^{14}C flow rates.

RESPONSE: Groundwater velocity vectors are probably not a good basis for comparison with ^{14}C because ^{14}C undergoes matrix diffusion that further slows its movement relative to groundwater moving in the fractures. A more meaningful comparison would be to examine the migration velocities necessary to produce the contaminant boundaries shown in Figures ES-3 and ES-4 of N-I (2013a) because the contaminant boundary includes the effects of matrix diffusion. The tests that define the maximum southern extent of the contaminant boundary appears to originate from Area 7 with a mean Universal Transverse Mercator (UTM) Northing of about 4,105,000 m. Well WW-C at the southern end of Yucca Flat is located at a UTM Northing of about 4,085,000 m, a distance of about 20 km south of the middle of Area 7. For these unlikely outlier cases where the contaminant boundary reaches WW-C, it does so only after 50 years and just within 100 years (e.g., N-I, 2013a, Figure 6-62), after which radioactive decay causes the contaminant boundary to shrink. The migration velocity required to reach WW-C in 100 years from Area 7 is about 200 m/yr, or roughly 100 times faster than the migration velocity implied by unretarded ^{14}C (20 m/yr) and about 10 times faster than estimated (20 m/yr) if ^{14}C is assumed to be retarded by a factor of 10. In either case, simulated migration velocities are very fast relative to ^{14}C-derived groundwater velocity estimates. For cases like the low northern flux alternative of 1 kg/s, the contaminant boundary extending from tests in Area 7 moves about 5 to 8 km in 100 years, yielding migration velocities of 50 to 80 m/yr, which are also high relative to the migration velocities of 2 to 20 m/yr estimated from ^{14}C. For comparison, the transport velocities of $\delta^{18}O$ to Devils Hole from the Spring Mountains (80 km over 2,000 to 7,000 years) in what is believed to be a much more active flow system are only 11 to 40 m/yr (including the effects of matrix diffusion). Once again, the evidence suggests that contaminant boundaries estimated thus far have been extremely conservative.

PRC Recommendation: The existence of DO^{14}C data needs to be mentioned, but no age interpretations should be reported unless it can be demonstrated that the data are sound and that the interpretive methods are appropriate.

RESPONSE: The organic ^{14}C data will not be used to make any interpretations regarding groundwater velocities in Yucca Flat.

2.6.4 Interpretation of Temperature Data

This uncertainty concerns the interpretation of temperature data in the Yucca Flat area.

PRC Recommendation: Investigate and explain temperatures at the water table; use the temperature data to inform the calibration of the coupled flow model that integrates flow in the AA/VA and LCA (recommended in Section 6.2.1 of N-I, 2015); and incorporate water fluxes that may be indicated by the temperature data into the determination of the contaminant boundary.

RESPONSE: A considerable effort has already been expended to explain groundwater temperature patterns and to collect new temperature data near the water table. This effort is described in detail in Appendix H of N-I (2013a). From the data and associated models, it was interpreted that drainage from the AA/VA might be occurring near the major basin-bounding faults, consistent with groundwater ^{14}C age distribution in the LCA. It was also possible to limit the possible range of groundwater inflow from the north to between 0 and 50 kg/s, based on temperature profiles from Wells UE-10j and ER-8-1. Although many aspects of the temperature dataset have been useful, other aspects of the dataset, such as high groundwater temperatures in the eastern part of the basin, remain unexplained.

The PRC hypothesized that the shallow detonations have displaced cooler and younger, antecedent soil moisture and perched groundwater to the water table, and the low-temperature anomalies seen near the major basin-bounding faults are due to drainage from detonation induced breaches in the hydrostratigraphy. This is unlikely because the low temperature anomalies often are present in areas with no nearby detonations. For example, Wells UE-1h, UE-6d, UE-6d, TW-B, WW-3, and WW-4 in southern Yucca Flat have low temperatures at the water table, but there are no nearby detonations. Furthermore, the thermal modeling described in Appendix H of N-I (2013a) determined that the time period for the low temperatures to evolve from drainage near the major basin-bounding faults is extremely large compared to the time period that has elapsed since nuclear testing began at Yucca Flat in the 1950s.

The PRC expressed a concern that temperature lows in the LCA might be indicative of downward flow through breaches in the TCU. As discussed in Section 2.3.3 of this report, the interruption of the lateral continuity of the TCU by faults and breaching created by detonations are already included in the N-I (2013a) model. A wide range of the lateral and vertical permeability of the TCU is already incorporated in that model. Several additional breaching scenarios have been considered (see Appendix A) as alternate flow models but found to calibrate poorly to existing head data. Further, preliminary data from the new Wells ER-2-2, ER-3-3, and ER-4-1 do not indicate ^{3}H at concentrations above the MDL (1,500 to 1,800 pCi/L) in LCA near and below detonations, providing evidence against the occurrence of breaching.

Although the temperature data are interesting as an independent dataset, there are still questions regarding applicability and utility. The temperature data do not reduce the uncertainty in the flow and transport model. Hence, further work under this uncertainty is not warranted.

2.6.5 Realistic Geologic Features

This uncertainty addresses geological simplifications incorporated in the hydrostratigraphic model.

PRC Recommendation: Realistic geologic features (normal faults cutting the Paleozoic strata; variable dips on normal faults; fault intersections and active faults as higher permeability zones; alternative interpretations of faults based on geophysical data; narrow fault cores; gaps in the fault cores; lack of fault cores for some faults; and attitude of LCA strata, including high-permeability layers) should be incorporated in the model as computational capabilities, software, and data improve.

RESPONSE: The current model and the alternate conceptualizations presented here already encompass these uncertainties.The discussion in the PRC report (N-I, 2015) noted several issues that merit clarification:

- The fault dip of 75 degree used in the Yucca Flat HFM is the average of outcrop and borehole data. The modeling team does recognize that the range is broader, 55 to 85 degrees. The shallower dipping faults tend to be rare. A decision was made not to present fault planes as listric but rather as simple planar surfaces. Most of the curving lower-angle portions are thought to be at significant depths below the top of LCA where most of the transport is expected to occur.

- The intersections of west-dipping and east-dipping faults would be linear features that are on a scale smaller than the planer fault features explicitly incorporated in the flow model. Their influence on fluid flow is implicitly incorporated in an average sense in the calibrated flow model.

- PRC comments have correctly noted that the thickness of the fault core represented in the numerical model is considerably greater than that actually expected to occur in the field. The base-case flow model represents the fault cores as impermeable while being surrounded by high-permeability damage zones. The permeabilities of the damage zones are calibrated to observed head data through the parameter estimation process described in N-I (2013a), implicitly compensating for the influence of the fault core thickness. This is confirmed by calibrating an alternate model without low-permeability fault cores to the head data, as discussed in Section 2.3.2, which was found to lead to 1,000-year particle transport not significantly faster (70 percent) compared to the base case (64 percent). The model calibration without fault cores compensated for not having a low-permeability fault core by increasing the east–west anisotropy in the fault damage zones.

- The east-striking faults are older pre-Tertiary structures as noted on the Paiute Ridge Geologic Quadrangle (Byers and Barnes, 1967). Those shown in Figure 1 of Phelps and McKee (1999) are quite short. Based on observations, the older pre-Tertiary structures tend to be calcified/healed and appear to be less conductive (Prothro et al., 2009). For this reason, most structures in the HFM are the basin-and-range normal faults. The only pre-Tertiary structures in the model are the thrust faults.

- As discussed in detail in Section 2.3.1.3, while local high-permeability features may exist, available subsurface and outcrop evidence, as well as hydrogeologic reasoning, indicates that extensive solution channels that could provide basin-scale transport pathways in Yucca Flat do not exist.

- The EarthVision software used for constructing the HFM was not able to maintain offset at the base of the LCA. This problem is at the bottom of the 10,000- to 12,000-ft-thick LCA section and below the region of active flow and transport in Yucca Flat. It was decided to accept this to focus on the shallower portions of the model where flow and transport would likely be most important.

2.6.6 Other Sources of Data Are Available but Unused

This uncertainty addresses sources of data from outside the CAU area that could potentially be used in the conceptual model.

PRC Recommendation: Data from the surrounding DOE and DoD facilities need to be reviewed and used to further constrain water levels, boundary fluxes, and estimates of hydraulic properties of the LCA.

RESPONSE: Regional hydrologic data and transport data from the NNSS and surrounding areas, including extensive datasets from Yucca Mountain, were included in data compilations for Yucca Flat (SNJV, 2006b and 2007). Additionally, all available data that may be used to constrain water levels within Yucca Flat, including data from surrounding DOE and U.S. Department of Defense (DoD) facilities, have been included and incorporated into the modeling team's knowledge of Yucca Flat hydraulic data. Fenelon et al. (2010) and Fenelon et al. (2012) provide coverage of the Yucca Flat hydrographic basin and the region surrounding Yucca Flat. Several wells to the north and northeast of Yucca Flat (Fenelon et al., 2012, Plate 3) consistently demonstrate significantly higher heads than in Yucca Flat and likely indicate a relatively effective barrier, and thus no or little influence on Yucca Flat from the north and northeast. No additional data from the east are available. Influences of the regions from the west, Rainier Mesa, Shoshone Mountain, and Pahute Mesa areas are included via boundary conditions as discussed in Section 2.1.

PRC Recommendation: Among other approaches discussed in previous sections of this report, the peer review team recommends building confidence in the Yucca Flat model by using the Yucca Flat modeling approach to simulate single-test detonations outside Yucca Flat in similar geological units where there has been groundwater monitoring (e.g., the 40-kt RULISON test in 1969 in Colorado, the 200- to 1,000-kt FAULTLESS test in 1968 in central Nevada, or the 12-kt SHOAL test in 1963 in northern Nevada).

RESPONSE: Due to the uniqueness of the different testing environments, direct extrapolation of the results of offsite nuclear testing is unlikely to add new insights to the processes already included in the Yucca Flat flow and transport model.

2.7 Uncertainty Assessment

2.7.1 Current Evaluation Does Not Capture the 95th Percentile

This uncertainty addresses the perception that some of the extreme parameter values may not be sampled in the uncertainty analysis.

PRC Recommendation: The peer review team recommends an approach where models that represent combinations of values from the upper end of their parameter distributions (those that would enhance transport) are generated manually and explored. Such exploration would start with the alternative

flow model scenarios (including those listed in Section 6.7.2 of N-I, 2015) using the most extreme parameters. For example, very high values for continuous, high hydraulic conductivity zones from the northern to the southern boundary and passing through sources would be held constant while other values are adjusted to determine whether an acceptable calibration can be obtained. If it cannot, the process would be repeated with a substantially lower value of continuous high hydraulic conductivity, and if that calibration is successful, then the difference (in log space) between the values of hydraulic conductivity would be halved until the maximum acceptable continuous high hydraulic conductivity value for the pathway is identified. A sampling scheme that captures combinations of parameter values from the portion of the transport parameter distributions that would enhance transport should be coupled with the faster flow fields.

RESPONSE: The modeling team has identified several examples where the team has manually changed parameters to investigate the impact to the model (Section 2.3.2). The team does not, however, believe that it is reasonable to manually pick the upper end of multiple distribution simply to enhance the transport prediction. Using biased sampling of transport parameters will result in improbable and unrealistic predictions, and misallocation of monitoring or remediation resources.

What is required based on the FFACO (1996, as amended) is the modeling team's ability to define a boundary representing the maximum extent of transport for 95 percent of simulations, based on uncertainty. Choosing end points of distributions may generate a statistically possible result but not one that falls within the 95 percent boundary. Therefore, it is not necessary to create an extreme transport case simulation to meet the requirements of the FFACO. Additionally, the position of the base case in Figure 6-6 of N-I (2013a) as perceived in N-I (2015) is not accurate. Figure 2-50 presents a bar chart depicting the number of particles reaching the southern line of demarcation for each of the NSMC flow fields. The position of the base case in Figure 2-50 illustrates that the base case is not more conservative than the range of uncertainty considered in the NSMC analysis. The PRC believed the base case to be at the top end of the simulation results, but the NSMC shows that the base case is not at the top. In fact, 30 percent of the NSMC cases have advective velocities above the base case, using the breakthrough of particles near the model's southern boundary within 1,000 years as the metric.

The PRC identified that lower K_d value assigned for the Pu isotopes in the LCA matrix and that greater initial mass of ^{90}Sr should be considered in the uncertainty analysis as specific examples. In

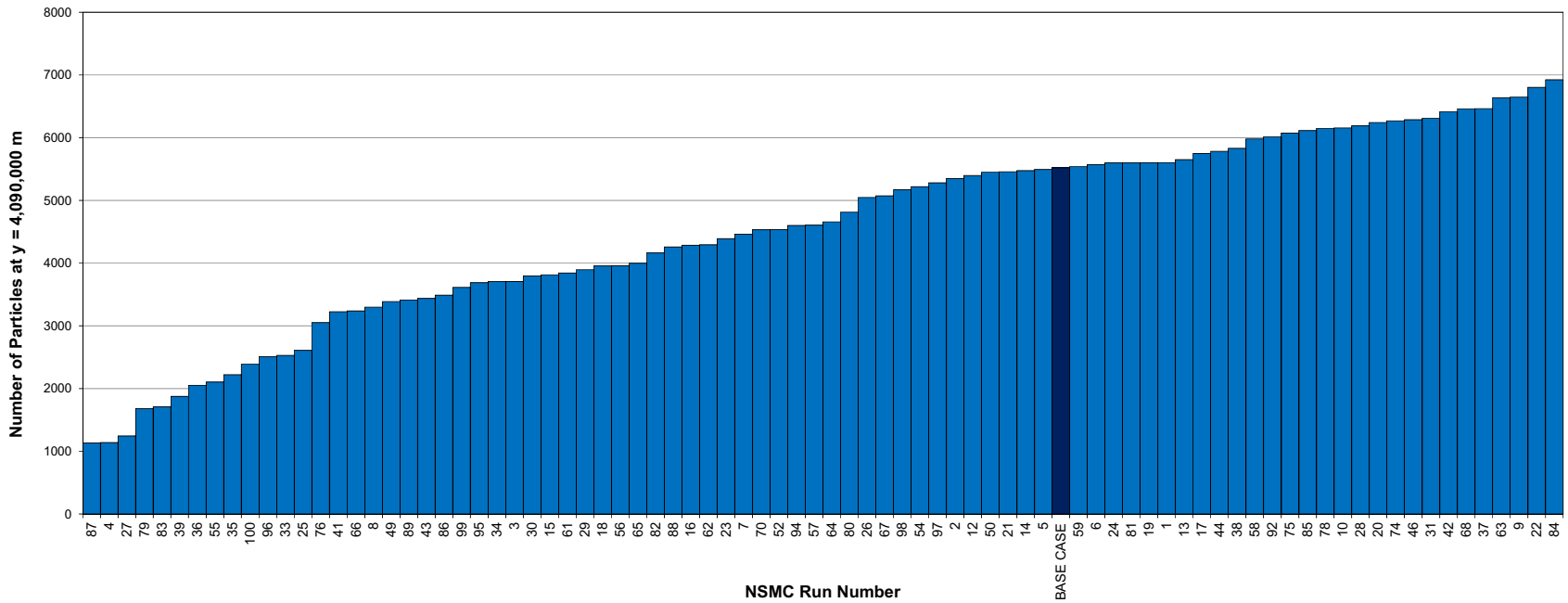

Figure 2-50
Particle Tracking Results Showing the Number of Particles Reaching the Southern Line of Demarcation for Simulations Based Upon the NSMC Flow Fields

regards to these two examples, Section 2.5.1 presents a probabilistic transport simulation where the LCA matrix K_d and fracture R_d for Pu was decreased. Although the Pu fractional exceedance volume increased by several orders of magnitude, the contaminant boundary was unchanged because Pu contributes little to the all species time-cumulative contaminant boundary. The ^{90}Sr transport described in N-I (2013a) is probably overestimated because ^{90}Sr was assumed to be non-sorbed (i.e., $K_d = 0$) due a limited availability of information with which to develop K_d distributions. However, the available literature does indicate that the sorption of Sr in carbonate rock does occur to varying degrees. Sutton (2009) presented a range of log10 K_d value from -1.99 to 1.86 mL/g for limestone, dolomite, and unidentified carbonate rocks. Further amplifying the transport of ^{90}Sr by using greater initial mass is unrealistic.

In conclusion, the uncertainty analysis in N-I (2013a) and the alternate models presented in this document together provide reasonable statistical bounds for realistically plausible transport scenarios that are consistent with the regulatory requirements of the FFACO (1996).

2.7.2 Expected Alternative Flow Models Were Not Included

This uncertainty addresses the concern that some of the alternate conceptual models were not included in the uncertainty analysis.

PRC Recommendation: The peer review team recommends the models listed in this section be evaluated as described in Section 6.7.1 of N-I (2015) and the fast flow fields from many strong source locations be used in combination with source and transport parameters that result in the most distant locations of MCL exceedance.

RESPONSE: The modeling team believes that the LCA model has already appropriately included fast path cases. As demonstrated by the NSMC analysis (N-I, 2013a), and also discussed in Sections 2.1.3 and 2.2.3 of this document, a wide range of parameters combinations were simulated, each matching observed steady-state water levels and ER-6-1 MWAT drawdown. Some of these parameters sets include very fast path cases with parameter values for increased fault permeability. For example, the maximum permeability for the western and eastern strands of the Yucca fault is 1.0×10^{-09} m^2, which is large enough for a velocity that results in 30 km of RN migration in under three years assuming advection alone.

The modeling team performed an analysis of the NSMC model parameters and several alternative simulations to investigate the effects of the PRC-recommended changes on RN transport. Some of these simulations involved the LCA model and others the shallow aquifer and UZ models. Among the simulations performed, no changes to the models produced dramatically increased transport compared to the base case. In general, the near-field observations of RNs within the SZ LCA are much lower than the model concentrations (see Section 2.5.1 and N-I, 2013a). These simulations and near-field RN observations demonstrate that predictions of RN transport described in N-I (2013a) conservatively bound the extent of transport. Additional models to explain and quantitatively interpret the data will be created as appropriate following drilling, RN sampling, and hydraulic testing at the new wells.

The PRC identified 10 alternative cases they felt should be simulated. For each of these, the corresponding location where the case was addressed is indicated within each of the bullets below:

- ***Fully integrated model that includes shallow aquifers and the LCA, and extends to Rainier Mesa.*** The modeling team has already noted that such a model is unnecessary because while it adds new calibration targets, it also adds new parameters to investigate. Uncertainty in the influx from Rainier Mesa has been discussed in Section 2.1.1 The hydraulic connection between shallow aquifers and the LCA has been addressed in Sections 2.1.5 and 2.3.3.

- ***Boundary flux from the northwest to represent possible recharge from Rainier Mesa.*** The modeling team investigated different simulations with flux from the northwest. Section 2.1.1 presents LCA model calibrations using a fixed and calibrated recharge on the model's northwest boundary. A fixed 47 kg/s northwest boundary recharge increased transport from detonations located in western Yucca Flat compared to the base case. Total particle breakthrough near the model's southern boundary was increased; however, southern extent of the contaminant boundary was not significantly different from that for the base case. Treating the northwest recharge as a calibration parameter produced a low recharge value (0.7 kg/s), and transport was nearly identical to the base case. The objective functions for the calibrated (0.7 kg/s) case and the 47 kg/s cases were nearly identical, indicating that neither scenario can be discounted on the basis of the objective function alone.

- ***Model that views faults as the major conduits for flow.*** The NSMC already includes cases with very large permeability for faults. The modeling team also recalibrated the LCA model for several alternative fault conceptualizations. Section 2.3.2 presents LCA model recalibrations specifying all large faults as a high-permeability features with a fixed permeability and specifying fewer minor faults. The high-permeability fault calibrations were largely unsuccessful due to very large steady-state head residuals in western Yucca Flat. One way to increase the importance of the major faults in the LCA model is to calibrate the model removing minor faults. A calibrated alternate model was constructed by removing faults with a trace length of less than 3 km. Transport calculations for this alternate model led to a

95 percentile contaminant boundary very similar to the base case. Another model calibration removing all minor faults was poor, resulting in a calibration function value of approximately 15.9 compared to the base-case value of 1.15. This alternate model led to a 95 percentile contaminant boundary that did not extend beyond the southern boundary of the model.

- ***A model with increased hydraulic conductivity of the material that is currently simulated as country rock.*** The modeling team recalibrated the LCA model for several alternative country rock parameterizations for a model with the three country rock zones divided in north and south subzones (Section 2.3.1.2). The recalibrations include specifying the country rock permeability as the geometric mean of the pumping test data within each model subzone. The specified permeability values for the country rock are generally 1 to 2 orders of magnitude higher than the calibrated base case. The model recalibration produced faster transport from detonations located in central Yucca Flat due to the higher specified country rock and calibrated Yucca fault permeability but, the total particle breakthrough near the model's southern boundary was significantly less than the base case. Calibrating a model with higher fixed country rock permeability generally requires a lower average fault permeability. The geometric mean permeability of all faults with traces greater than 3 km was approximately half that of the base case.

- ***Model that simulates small but continuous heterogeneity in the LCA such as karstic features.*** The issue of karst features in the LCA was discussed in details in Section 2.3.1.3. Extensive karst features have not been observed in outcrops near Yucca Flat in the LCA. The modeling team will not consider this scenario. The team believes that potential preferential flow scenarios are already adequately covered by the fault flow and country rock flow cases.

- ***Another fault case to mimic the high permeability in ER-6-1-2.*** It is not reasonable to try to match a specific interval in a specific well with a CAU scale model. Upscaled permeability as applied in the CAU model will by definition not necessarily represent a specific value within a specific interval of a borehole. The modeling team recalibrated the LCA model for several alternative fault conceptual models including specifying the large basin-and-range forming faults as high-permeability features using the average permeability over the entire logged interval in Well ER-6-1-2 (8.7×10^{-11} m^2) (Section 2.3.2). The model recalibration was largely unsuccessful due large steady-state head residuals in western Yucca Flat.

- ***A model that has no or many fewer minor faults.*** This is a significant departure from known conditions and non-conservative in that it ignores potential preferential flow and RN transport associated with these features. A more fruitful approach is to consider additional fracture zones associated with testing that create direct pathways to the LCA, as has already been done and documented in the SZ AA/VA flow and transport model (N-I, 2013a, Section 4.0). An additional consideration is that significant increases in TCU permeability associated with widespread fracturing are not compatible with known head differences between the TCU and LCA and present-day limited recharge. Further, several models constructed by removing minor faults, as discussed above, were calibrated and found not to lead to calibrations as good as the base case and forecasted transport no further than the base case.

- ***A model including higher-permeability zones in the TCU matrix (to complement, or in lieu of faults) coupled with enhanced recharge through craters.*** The interruption of the lateral continuity of the TCU by faults and, in certain model scenarios, by local vertical pathways to the LCA created by the force of the nuclear detonations (the "breaching scenario") is already incorporated in the conceptual models of the SZ AA/VA documented in N-I (2013a). These model runs did not significantly impact the overall RN flux to the LCA (Section 2.3.3). A number of additional model simulations of the AA/VA system were run to look at the effects of alternative parameter sets and conceptual models on RN transport to the LCA. These alternative scenarios investigated the effects of (1) more permeable faults, (2) a more permeable TCU matrix, and (3) conceptualization of the TCU as a fractured aquifer, rather than a matrix dominated porous media. All of the new scenarios resulted in smaller overall mass flux of conservative, long-lived RNs to the LCA over 1,000 years compared with the base case (Section 2.3.3).

- ***A model including enhanced-recharge-driven transport in and below detonation craters.*** Currently, further characterization of recharge and contaminant transport beneath UZ-hosted detonations is considered a low priority, due to the fact the approximately 90 percent of UZ-hosted tests are above the SZ AA/VA and must pass through that additional barrier before reaching the LCA; and the remainder of the UZ-hosted detonations are located in the northern part of the basin, and hence are unlikely to define the leading edge of the contaminant boundary. Therefore, drilling a new well to specifically characterize this process is a low priority. However, an opportunity to test UZ flow and transport models is available by modeling infiltration and recharge from a sump near WW-3 that had water in it for eight years (approximately 2002 to 2010) and resulted in water-level increases at UE-6d. This dataset was modeled, and the results are summarized in Appendix B.

- ***A model with a greater range of enhanced permeability assigned to the detonation damage zone.*** The hydraulic head and RN data from the BILBY detonation discussed in Section 2.4.5 demonstrate that breaching of the type hypothesized by the PRC and considered by some of the models in Section 4.0 of N-I (2013a) does not occur. The absence of ^{3}H at concentrations above the MDL (1,500 to 1,800 pCi/L) in the LCA at new Well ER-4-1 near the STRAIT detonation (200 to 500 kt yield range) as well as the absence of ^{3}H at concentrations above the MDL (1,500 to 1,800 pCi/L) in the LCA at Well ER-3-3 downgradient of scores of deeply buried detonations confirm the generality of the BILBY dataset that indicates that the TCU is an effective barrier to downward migration of RNs from the TCU even in a post-detonation environment.

2.7.3 Limited Number (100) of NSMC Realizations of the Flow Model Produced Parameter Value Combinations That Do Not Capture the 95th Percentile of Parameter Combinations That Lead to Rapid Transport

This uncertainty addresses the possibility that the effect of most permeable pathways was not captured by the range of uncertainty used in the model.

PRC Recommendation: Use the manual modification of a bias sampling approach as described in Section 6.7.1 of N-I (2015) to capture fast flow fields without excessive numbers of simulations. Confirm that the calibrated hydraulic conductivities are consistent with maximum field measurements. This requires increasing the range of considered permeabilities to include values beyond that measured in the spinner logs in Wells ER-6-1 and ER-6-1 #2.

RESPONSE: Alternative fault and country rock conceptualizations (Sections 2.3.2 and 2.3.1.2) have been run to evaluate possible fast flow fields. Fast flow path cases that do not match observed water levels in the basin are not acceptable alternatives. For example, the LCA model recalibrations specifying large faults as a high-permeability features produced faster transport than the base case but were largely unsuccessful in matching steady-state heads in western Yucca Flat. Each of the NSMC runs that achieved an acceptable calibration do match observations and represent an acceptable flow field for transport simulations. The transport results from the NSMC runs are based on very different sets of calibrated parameters that for any individual parameter can span several orders of magnitude. These NSMC simulations likely capture the acceptable range of uncertainty in the model parameters. The PRC's perception of where the base case resides, with the respect to contaminant transport based on the NSMC flow fields (as depicted in Figure 6-6 of N-I, 2015), is not consistent with results of particle tracking simulations for the 83 calibrated NSMC flow fields. As a surrogate for advective transport based on the NSMC flow fields, the number of particles reaching the southern line of demarcation for each flow field demonstrates that many of the NSMC cases have faster flow fields than the base case. Figure 2-50 presents a bar chart depicting the number of particles reaching the model's southern boundary within 1,000 years, and 30 percent of the NSMC simulations manifest faster transport than the base case.

2.7.4 Limited Calibrated Flow Models Used to Evaluate Transport Uncertainty

This uncertainty addresses the concern that the model did not include continuous high-conductivity pathways.

PRC Recommendation: More flow fields (relative to the previous stage, which included only three) should be considered for the transport uncertainty evaluation, and biased sampling of transport parameters (in the direction that enhances transport) should be used to limit the number of transport simulations required to capture the 95th percentile. Additional flow fields should be generated by

considering alternative conceptual models as described in Section 6.7.2 of N-I (2015) and associated parameters that lead to fast transport from source locations to the south end of Yucca Flat.

RESPONSE: Considering additional flow fields for transport uncertainty is a reasonable recommendation. However, biased sampling toward conservative parameters creates an unreasonable transport case with very low probability (less than 5 percent) of occurrence. Using such unlikely predictions to guide regulatory decisions may result in misallocation of monitoring resources or overly restrictive constraints on access to groundwater.

To identify flow fields with *fast* and *slow* transport to the southern boundary of Yucca Flat, the modeling team originally placed particles at 12 key locations where RNs either enter the LCA from the overlying UZ and SZ AA/VA, or originate from detonations with initial contamination within the LCA (N-I, 2013a). In response to the PRC's concerns, the team selected a larger alternate set of 39 detonations within 3 R_c of the SZ LCA as possible contaminant sources to identify alternate fast flow fields for transport uncertainty evaluation. In addition, the LCA flow model recalibrations that achieved an acceptable calibration and had faster advective particle transport than the base case were selected for the transport uncertainty evaluation. The model calibrations that achieved an objective function of 20 or less were considered acceptable, which approximately translates to an RMS error that is 5 percent of the range in steady-state heads and ER-6-1-2 MWAT drawdowns.

The particle breakthrough from the 39 detonations with initial contamination within 3 R_c of the SZ LCA identifies NSMC case 1 as the fastest flow field at 100 years with 9 percent of the particles arriving near the model's southern boundary within 100 years, and NSMC case 84 as the fastest flow field at 1,000 years with 82 percent of the particles arriving near the model's southern boundary within 1,000 years. The LCA flow fields selected for transport include the following:

1. NSMC case 1 alternative *fast* flow field at 100 years
2. NSMC case 84 alternative *fast* flow field at 1,000 years
3. Additional steady-state target wells that are screened across the TCU and LCA; the additional wells are U-7a, UE-10bf, UE-10 ITS 3, and UE-10 ITS 5
4. Northwest recharge specified as the total net infiltration (47 kg/s) occurring in the area east of the Eleana range high points and west of the LCA model's western boundary

5. Northwest recharge estimated (0.7 kg/s) during the calibration process
6. Calibration considering data quality in the steady-state target weights
7. Faults without low-permeability cores
8. No faults with trace lengths less than 3 km
9. No minor faults
10. North–south subzones for the country rock

Figure 2-51 illustrates the time-cumulative probability of MCL exceedance at 1,000 years for base-case, NSMC 1 alternative *fast*, NSMC 84 alternative *fast,* and additional steady-state calibration wells flow fields. The alternative NSMC 1 alternative *fast* contaminant boundary is much more disperse than the base case and does not exhibit northerly flow in the northwest area of Yucca Flat. The contaminant boundary from the NSMC 84 *fast* case is bifurcated in south–central Yucca Flat due to lower LCA central and LCA east country rock permeability compared to the base case. The transport in southern Yucca Flat for the NSMC 84 *fast* case is largely restricted to Yucca fault in the west and several smaller faults in the east. The contamination boundary from the additional calibration wells flow field case is more disperse in central Yucca Flat compared to the base case and does not extend to the model's southern boundary.

Figure 2-52 illustrates the time-cumulative probability of MCL exceedance at 1,000 years for north–south country rock subzones, 47 kg/s northwest recharge, calibrated northwest recharge, and calibration considering data quality in steady-state head weights flow fields. Adding north–south subzones produces faster transport from detonations located in the LCA Central and Yucca fault due to higher permeability of these features, but the southerly extent of the contaminant boundary is reduced. Including a 47 kg/s northwest recharge facilitates more transport from the detonations located in the northwest area of the LCA model compared to the base case. The contaminant boundary for the calibrated northwest recharge flow field is very similar to the base case. The contaminant boundary for the calibration considering data quality in the steady-state head weights has reduced southerly extent of the contaminant boundary compared to the base case.

Figure 2-53 illustrates the time-cumulative probability of MCL exceedance at 1,000 years for faults without low-permeability cores, no faults with trace lengths less than 3 km, and no minor faults (i.e., the model includes only the large basin-forming faults). The flow field without low-permeability

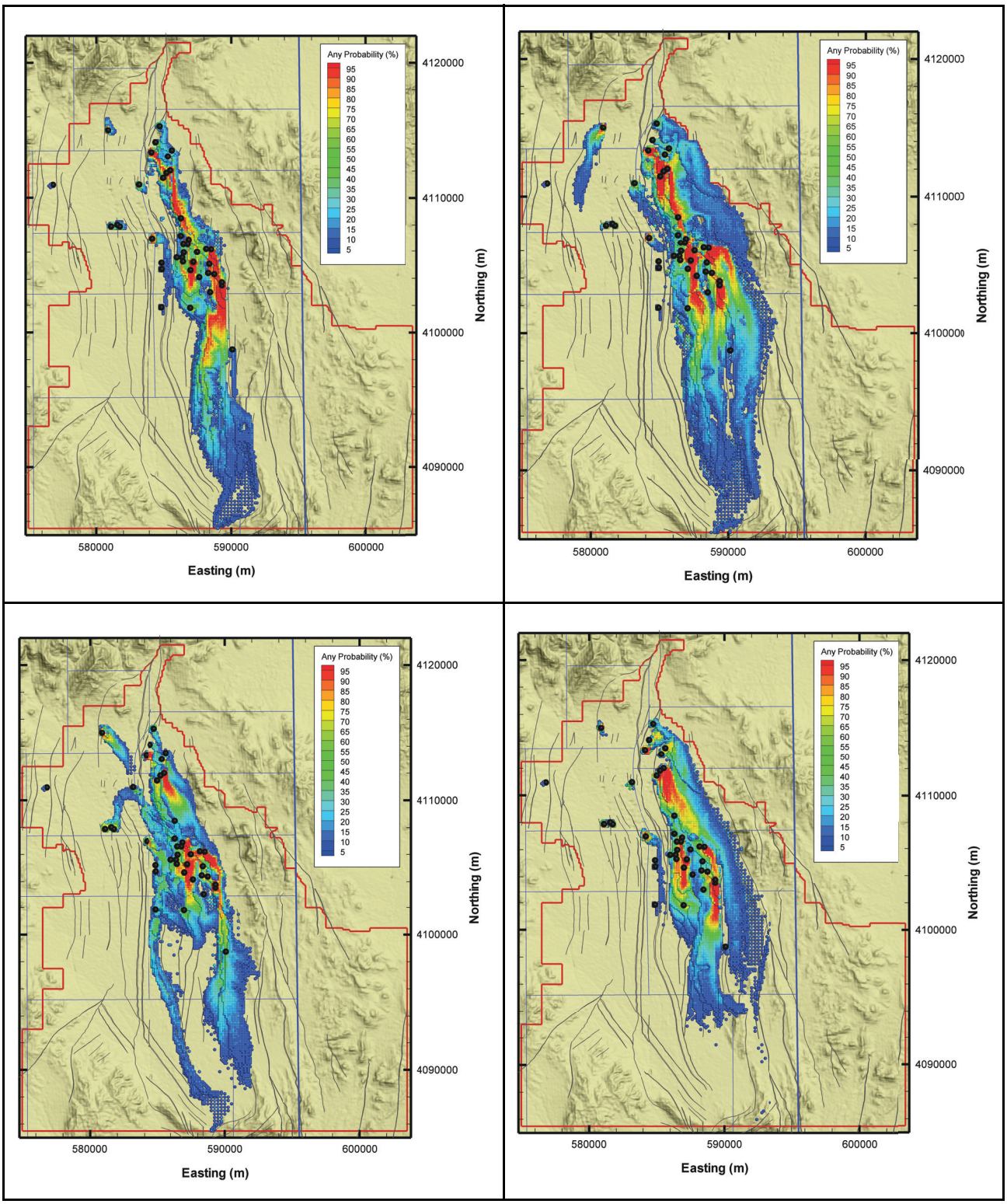

Figure 2-51
Time-Cumulative Probability of MCL Exceedance for Base-Case (upper left), NSMC 1 Fast (upper right), NSMC 84 Fast (lower left), and Additional Steady-State Target Wells (lower right) Flow Fields

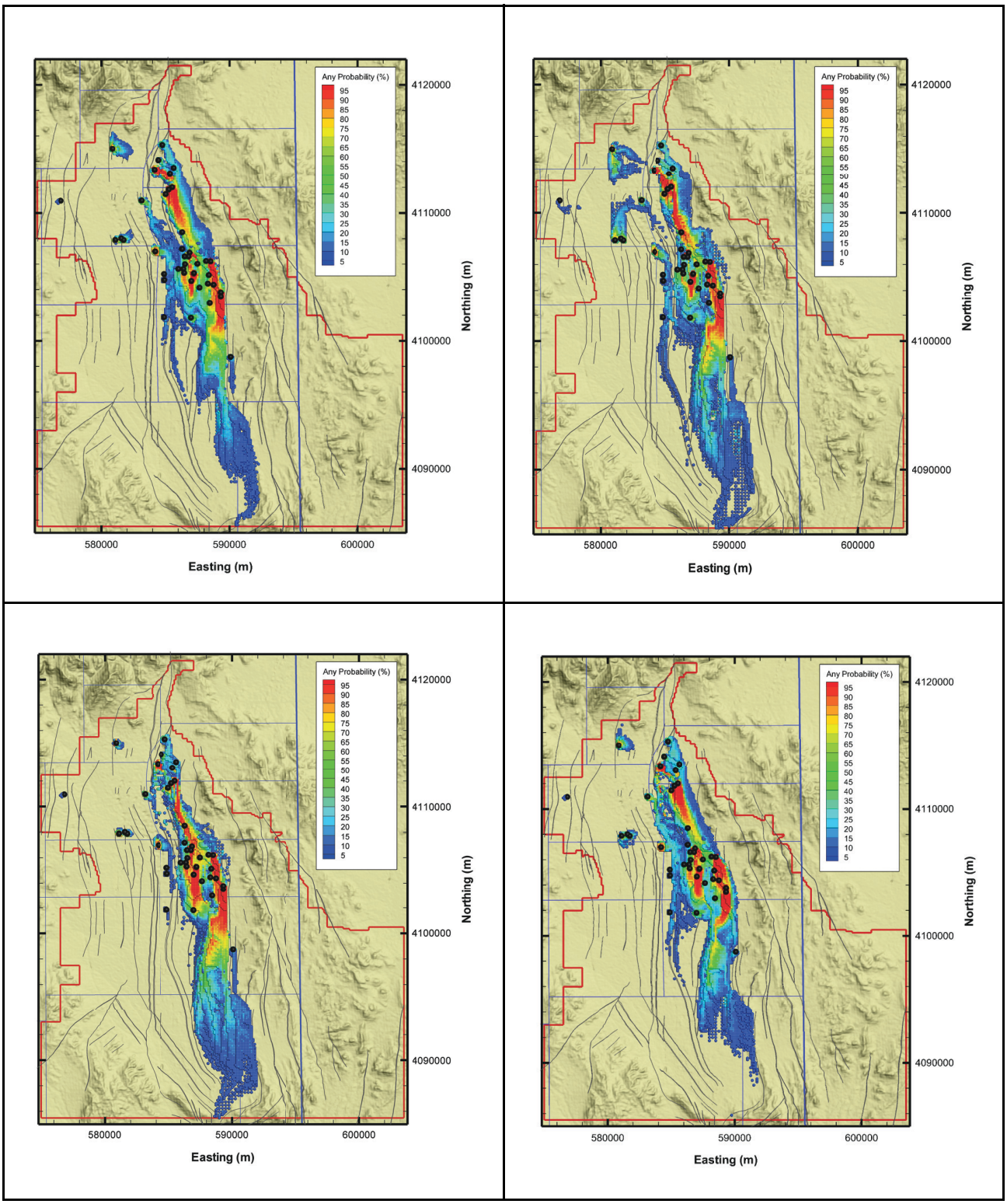

Figure 2-52
Time-Cumulative Probability of MCL Exceedance for North–South Subzones (upper left), 47 kg/s Northwest Recharge (upper right), Calibrated Northwest (lower left), and Quality Weighted Steady-State Targets (lower right) Flow Fields

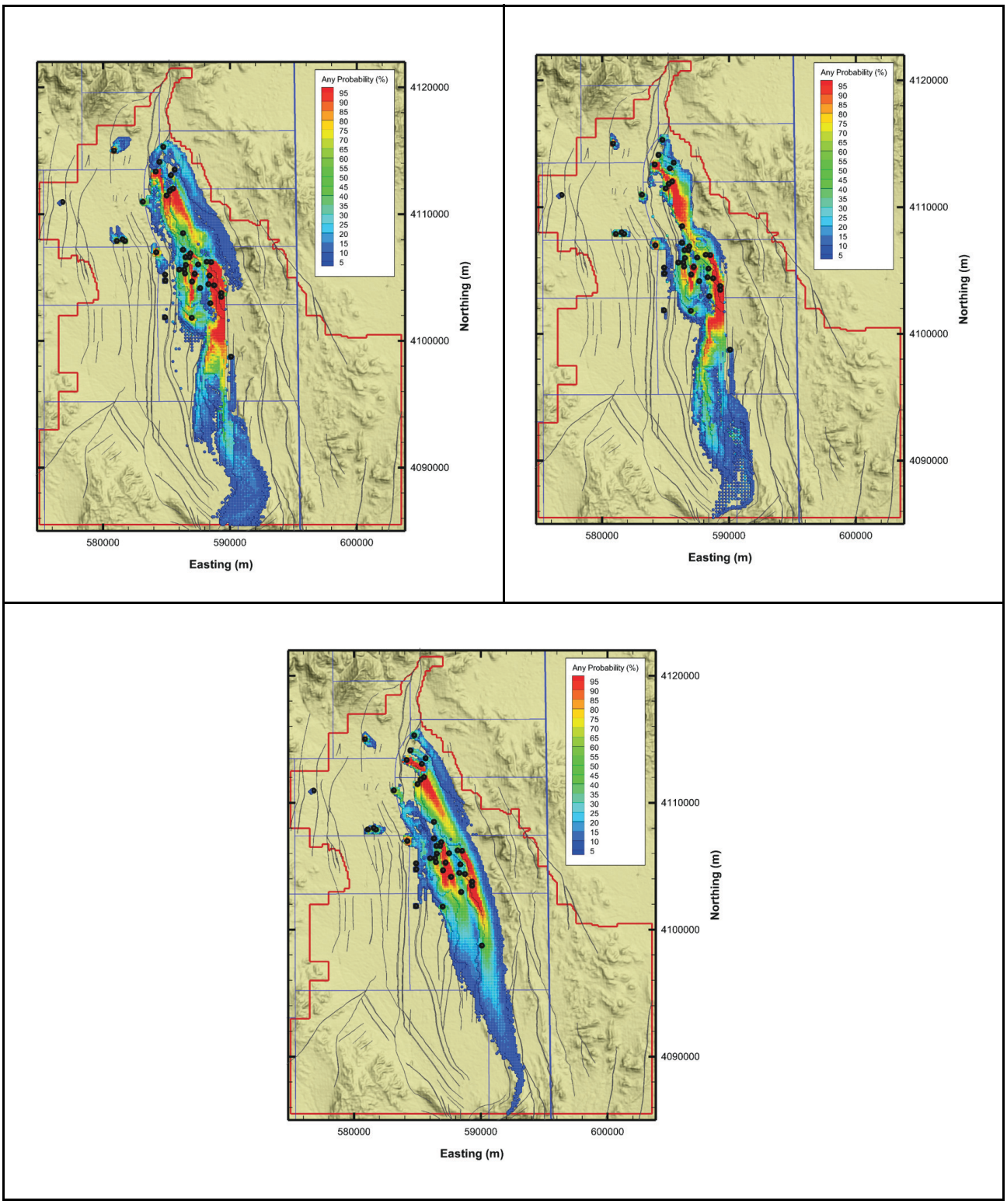

Figure 2-53
Time-Cumulative Probability of MCL Exceedance for Faults without Low-Permeability Cores (upper left), No Faults with Trace Lengths <3 km (upper right), and No Minor Faults (lower center) Flow Fields

cores has faster transport than the base case because of increased LCA vertical anisotropy and higher LCA east permeability compared to other cases. The additional vertical anisotropy keeps much of the flow within the upper section of the model, thereby producing faster transport. The flow field excluding faults with traces less than 3 km in length has a contaminant boundary that is very similar to the base case. A flow field that includes only the large basin-forming faults produces a more diffuse contaminant boundary in central Yucca Flat and predicts that only the leading edge of the contaminant boundary reaches the southern boundary within 1,000 years.

The flow and transport behavior seen in the contaminant boundary uncertainty evaluation is consistent with the behavior seen the NSMC parameter analysis presented in Section 2.3.2 in that moderately high permeability permitting flow to occur in both the country rock and the faults is needed. Country rock permeability and fault permeability together provide a control on how RNs are transported. Although the NSMC 1 alternative *fast* case has a much wider contaminant boundary within Yucca Flat, none of the additional calibrated flow models used to evaluate transport uncertainty suggest that the base case significantly underpredicts the southerly extent of the contaminant boundary except the flow field excluding low-permeability cores. Increased vertical anisotropy and LCA east permeability for this flow field produced faster groundwater velocity in the shallow LCA and faster overall transport. However, an LCA model calibration constraining the total inflow of water to the model to approximately 40 kg/s (Section 2.1.2) had similar anisotropy and LCA east permeability values, and the contaminant boundary did not extend to the southern boundary. Fenelon et al. (2016) report Yucca Flat sub-basin discharge of about 1,000 acre-ft/yr (40 kg/s).

2.7.5 Limited Alternative Models Used to Evaluate Relevant Detonations

This uncertainty focuses on the concern that some potentially important contaminant sources were excluded from the model.

PRC Recommendation: Alternative source terms need to be considered with associated flow conditions that move radionuclides rapidly to the LCA (e.g., breaches, high infiltration) and rapidly through the LCA (continuous high-permeability zones connected to source locations) in order to capture the upper end of the cases that will provide the 5 percent exceedance of MCLs.

RESPONSE: To determine the parameters controlling flow and transport and better understand how change in parameters values affect transport, the modeling team queried the existing CAU model, in particular the NSMC analysis. This process provides insights into the controlling factors of the hydrologic system. Section 5.6.2 of N-I (2013a) presented the results of NSMC analysis of alternative calibrations of the LCA flow model. A wide range of parameter values for the LCA country rock and fault damage zone permeability were developed that are consistent with the wide range of boundary condition fluxes by the calibration of each NSMC model. Both of these ranges reflect the large uncertainty in the individual feature properties, subject to the constraints of the boundary flux ranges and the calibration to the MWAT hydraulic test response and steady-state water levels. Particle tracking runs were conducted using the 83 NSMC flow fields that achieved an acceptable calibration. The sources for particle release included all 39 detonations within 3 R_c of the SZ LCA and the particle breakthrough near the model's southern boundary were used to determine whether any significant pathways defined by acceptable NSMC parameter combinations were missed.

The calibrated parameters from the 83 NSMC cases were analyzed by calculating the correlation matrix between model parameters and particle breakthrough at the line of demarcation near the model's southern boundary. The particle breakthrough is from 39 key sources that represent detonation working points located within 3 R_c of the SZ LCA that reaches the line of demarcation near the model's southern boundary. Through inspection of the correlation matrix, a bivariate analysis of the model parameters possibly controlling transport was performed. The 10 model parameters most strongly correlated with particle breakthrough at times of 200, 400, 600, 800, and 1,000 years are presented in Table 2-12. During early times, the eastern strand of Yucca fault (parameter f148_yf2) is not strongly correlated to particle breakthrough but becomes inversely correlated at late times. None of the detonations located within 3 R_c of the SZ LCA are located very near Yucca fault, and by focusing flow through Yucca fault, less flow is available to move through the exchange volume beneath detonations overlying country rock or smaller faults located nearer to the deeper detonations. The transport path provided by Faults 156 (f156_yf_71) and 160 (f160_area3eas), located approximately 2 km east of Yucca fault, is correlated to breakthrough at both early and late times. Eastern lateral recharge (Eastsoflux) is positively correlated to particle breakthrough. In general, it is the parameters for features located east of Yucca fault that are most positively correlated with particle breakthrough near the model's southern boundary. The analysis of

Table 2-12
Model Parameters Most Strongly Correlated with Particle Breakthrough

200-Year Particle Breakthrough		400-Year Particle Breakthrough		600-Year Particle Breakthrough		800-Year Particle Breakthrough		1,000-Year Particle Breakthrough	
Parameter and Correlation Coefficient									
Hevesi_east	-0.39	f156_yf_71	0.39	f160_area3eas	0.41	f148_yf2	-0.41	f148_yf2	-0.39
f140_hp50_yf1	-0.31	f160_area3eas	0.35	f148_yf2	-0.39	f160_area3eas	0.40	f160_area3eas	0.37
f163_yf_97a	0.29	f148_yf2	-0.32	f156_yf_71	0.33	f156_yf_71	0.36	f114_yf_91bn1	0.35
f154_piranha	0.23	f140_hp50_yf1	-0.29	f167_yf_75	0.31	f167_yf_75	0.34	f156_yf_71	0.34
f139_hp72_yf1_m2	-0.22	Hevesi_east	-0.29	f114_yf_91bn1	0.31	f114_yf_91bn1	0.33	f167_yf_75	0.32
Aniso178x	0.21	f114_yf_91bn1	0.26	Aniso148x	-0.29	f124_hp10	0.32	f124_hp10	0.32
f114_itfc	0.21	Hpflux	-0.26	cr11_lcae_m2	0.28	Aniso148x	-0.31	Aniso148x	-0.30
f156_yf_71	0.20	f101_itfc	-0.25	f124_hp10	0.27	f149_area3n9	0.28	Aniso178z	-0.28
f124_hp10	0.19	f167_yf_75	0.24	Aniso178x	0.27	Eastsoflux	0.27	f149_area3n9	0.27
f161_yf_7y	-0.19	Aniso148z	-0.24	Eastsoflux	0.26	Aniso178x	0.26	Eastsoflux	0.26
f160_area3eas	0.19	Aniso190z	-0.24	Aniso148z	-0.25	cr11_lcae	0.26	cr11_lcae	0.24

the NSMC models indicate that moderately high permeability permitting flow to occur in both the country rock and the faults is needed.

The percentage of particles arriving near the model's southern boundary within 1,000 years varied from 13 to 82 percent. The 95 percentile contaminant boundary (Figure 2-51) for the NSMC simulation with the largest total particle breakthrough was similar to that for the base case.

In conclusion, the particle tracking results indicate that among parameter combinations which produce a calibrated model, models with more extensive transport are unlikely.

2.7.6 Limited Range of Transport Parameters Values Used to Evaluate Transport Uncertainty

This uncertainty addresses the concern that the ranges considered in the model for some of the transport parameters were not sufficiently wide.

PRC Recommendation: Pu isotopes need to be included in the transport model with combinations of lower K_d values and higher mass in the source term than presently specified in the uncertainty analysis.

PRC Recommendation: Improve the estimates of matrix diffusion or expand the evaluated uncertainty range such that the simulations will have little doubt of capturing the upper 5 percent tail of the contaminant boundary. Include higher values of dispersivity in the uncertainty evaluation.

PRC Recommendation: The range of dispersivity included in the uncertainty analysis needs to be commensurate with the degree of heterogeneity in the hydraulic conductivity field incorporated in future models.

RESPONSE: Several alternative transport simulations have been performed with reduced Pu K_d values for the LCA matrix, reduced retardation (R_d) values for the LCA fractures and increased dispersivity values. Section 2.5.1 summarizes K_d and R_d values for Pu in carbonate minerals and defines alternative distributions for a reduced sorption sensitivity case. The matrix K_d distribution is reduced by approximately an order of magnitude, and fracture R_d has a lower bound reduced to zero.

The impact of using lower value of K_d for plutonium (Pu) was demonstrated to have negligible impact on the contaminant boundary, which is dominated by short-lived RNs (^{3}H, ^{90}Sr, and ^{137}Cs) during the first few hundred years.The modeling team agrees that the dispersivity values used in the LCA model may not represent the upper range of possible values given the transport distances in the LCA model. The influence of dispersivity on RN transport is twofold. An increase in dispersivity (both longitudinal and transverse) will tend to enhance the process of dilution lowering the concentration of transported RNs. When considering RNs with short half-lives, the accelerated movement (spreading) ahead of the center of mass will contribute to a diminishing influence of decay resulting in increased transport distances. The dispersivity values used in the LCA transport modeling (N-I, 2013a) were fixed values of 20 m longitudinal, 2 m transverse, and 0.2 m vertical. The sensitivity of the contaminant boundary to increased dispersivity is investigated for two cases, one in which only longitudinal dispersivity is increased 1 order of magnitude and a second case where all three components of dispersivity are increased 1 order of magnitude. Figure 2-54 illustrates the time-cumulative probability of exceeding the MCL for the base case and increased dispersivity cases. As expected, the increased dispersivity values result in more diffuse transport and a wider contaminant boundary for both cases of increased dispersivity. The width of the contaminant boundary is approximately doubled in north–central Yucca Flat. The case with increased dispersivity for all components results in less MCL exceedances near the model's southern boundary compared to the base case. This shows that the cases with increased dispersivities lead to less extensive transport than the base case. This will be confirmed by performing this comparison with the inflow-constrained models.

2.7.7 Mesh Refinement Not Necessarily Conservative

This uncertainty focuses on the effects of the mesh size on model predictions.

PRC Recommendation: Evaluate higher level meshes to determine definitively the mesh-refinement level for which there is no change in the contaminant boundary.

RESPONSE: Comparison of particle tracking using calibrated flow model results for level 2 and level 3 demonstrates that the overall particle paths and travel times do not change significantly with mesh refinement. Convergence of mesh refinement was considered in N-I (2013a) by running the level 3 mesh (minimum 62.5-m spacing) with calibrated parameters produced by the level 2 mesh (minimum 125-m spacing). To further demonstrate the convergence of mesh refinement on flow and

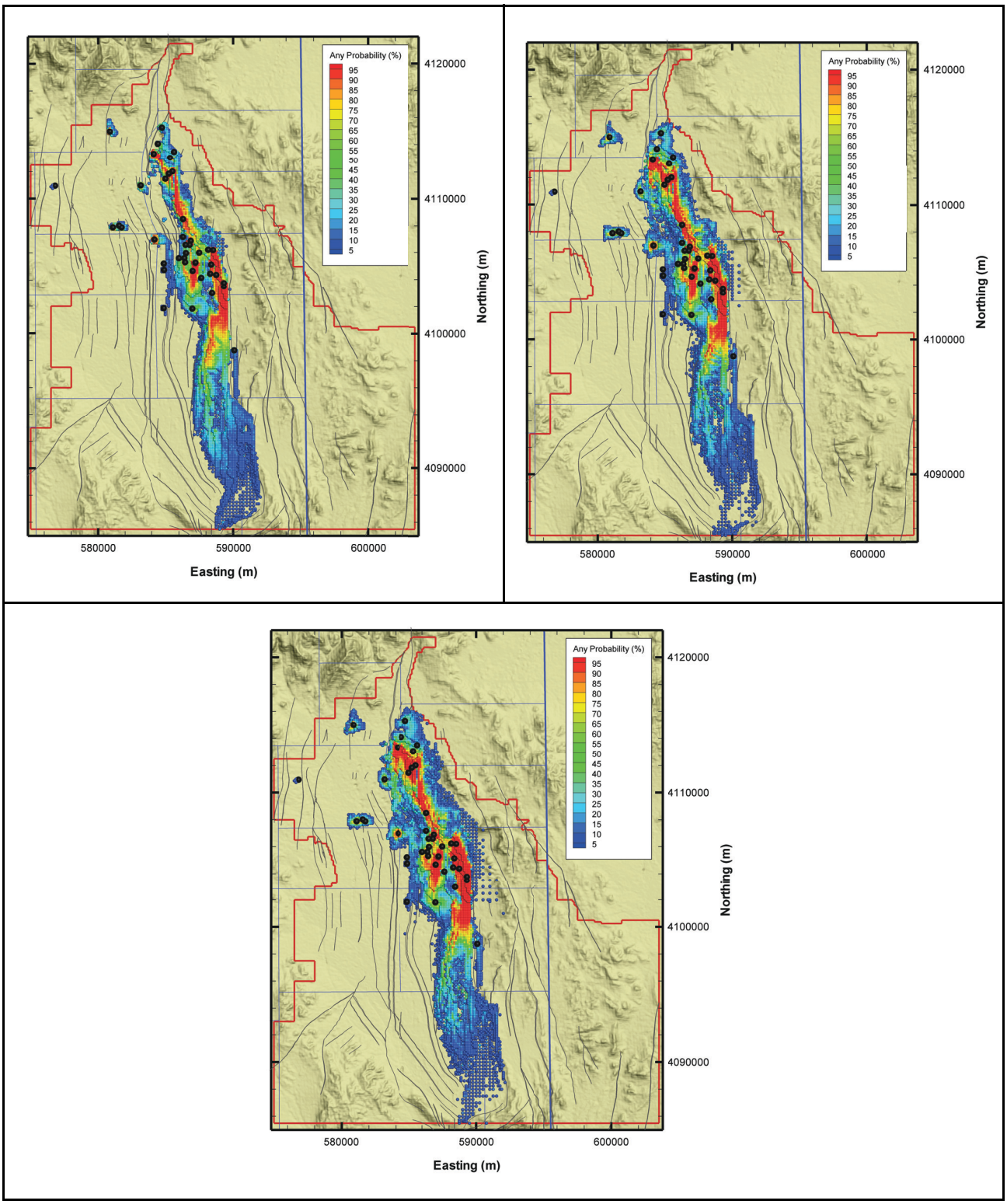

Figure 2-54
Time-Cumulative Probability of MCL Exceedance for Base-Case (upper left), Increased Longitudinal Dispersivity (upper right), and Increased Dispersivity for All Components (lower center) Flow Fields

transport, the level 3 mesh was calibrated for the base case and particle tracking from the 39 detonations within 3 R_c of the SZ LCA, and was used to evaluate the influence of mesh refinement on transport.

Figure 2-55 illustrates the base-case-calibrated parameters for level 2 and level 3 meshes. Figure 2-56 illustrates the potentiometric surfaces for the two meshes. The calibrated model parameters from the two meshes are very similar, as is the potentiometric surface. These results demonstrate that mesh convergence was achieved for flow.

Figure 2-57 illustrates the particle travel paths and times for the base-case level 2 and base-case level 3 meshes. The particle tracks from the level 2 and 3 base case have a very similar pattern of paths and times, but the fault conduits are narrower using the level 3 mesh. Figure 2-58 compares the percentage of particle breakthrough near the model's southern boundary within 1,000 years for each detonation within 3 R_c of the SZ LCA for level 2 and 3 meshes. Figure 2-59 illustrates the total particle breakthrough for the level 2 and 3 meshes. The total particle breakthrough for the level 3 mesh (60 percent) was slightly smaller but generally equivalent to the level 2 mesh (64 percent). A few detonations had increased or decreased transport in the level 3 mesh compared to the level 2 mesh. The detonation with the largest increase in breakthrough for the level 3 mesh was the MIERA detonation, which had total particle breakthrough increased by a factor of 7 for the base-case flow field. The GRAPE-B, LAREDO, and HERMOSA detonations have total particle breakthroughs from the level 3 mesh that are a factor of 1.3 to 1.9 higher than the level 2 mesh. It is noteworthy that where data are available—such as at MICKEY/TORRIDO (Well ER-7-1), BOURBON (Well UE-7nS), and BILBY (Well U-3cn 5)—the LCA currently has ^3H concentration that is non-detectable, whereas the models using either mesh predict 100 percent of the particles placed in the SZ LCA model beneath these detonations exit the southern boundary after 1,000 years. This highlights the fact that RNs must first reach the LCA before they can leave the basin, an aspect that is not reflected in the particle breakthrough results using either mesh, which conservatively assume initial concentrations within the LCA that are not seen in the observation wells near the source detonations.

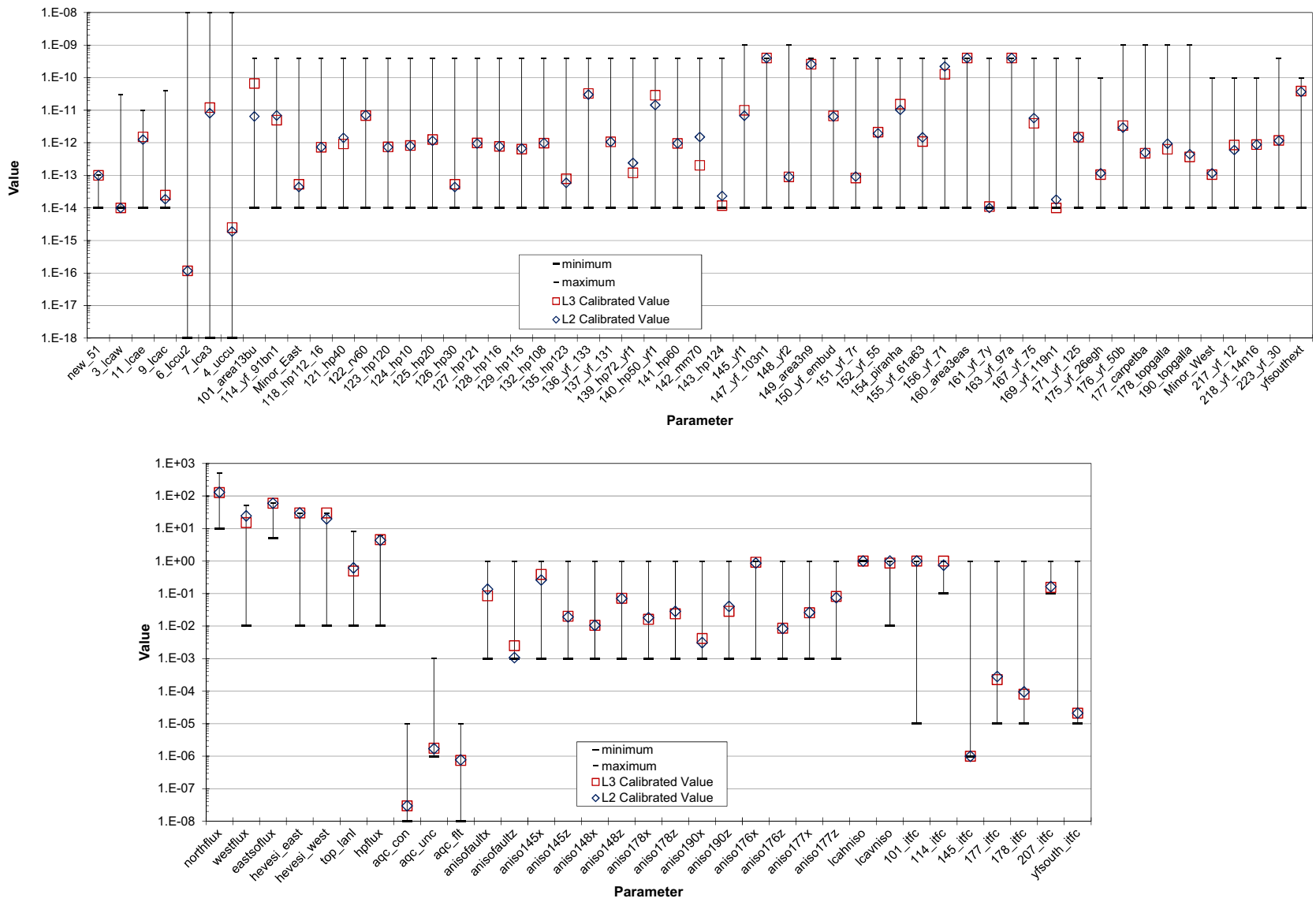

Figure 2-55
Calibrated Parameters for the Base-Case Level 2 and Level 3 Meshes

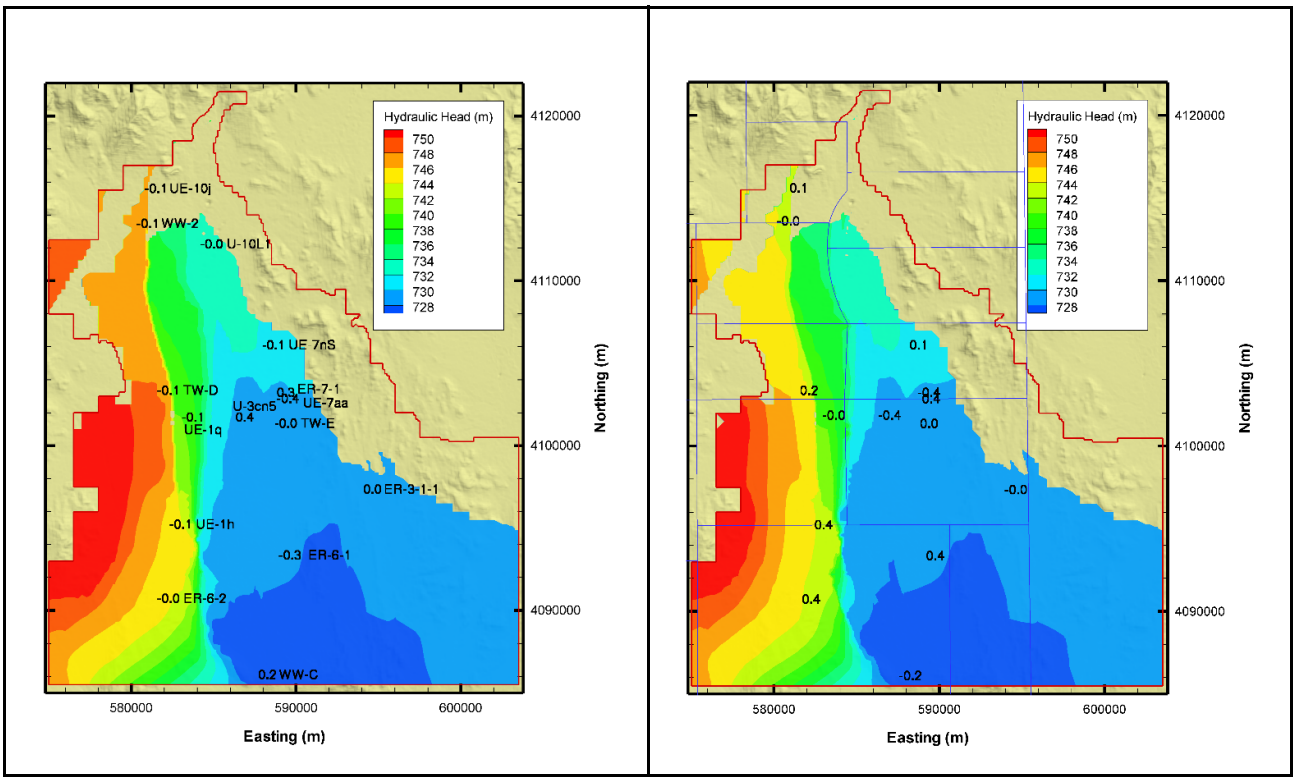

Figure 2-56
Calibrated Head Field in the LCA for the Base-Case Level 2 (left) and Level 3 (right) Meshes

The different transport generally occurs from detonations located on or very near faults due to several reasons:

- Narrower faults may have a higher velocity due to faults transmitting similar amounts of water in the narrower channels.
- On average, the level 3 fault permeability is a factor of 1.3 higher than the base case on average, but it can be different by approximately a factor of 10.
- Narrower fault zones in the level 3 mesh can place less initial contamination in the fault core or conduit zones compared to the level 2 mesh.
- Narrower fault zones in the level 3 mesh can produce less fault connectivity in areas of closely spaced faults compared to the level 2 mesh.

In conclusion, although some test-specific differences in particle breakthrough occur, the overall particle paths and travel times do not change significantly with mesh refinement, indicating that adequate convergence of mesh refinement was achieved. No further work is warranted under this uncertainty.

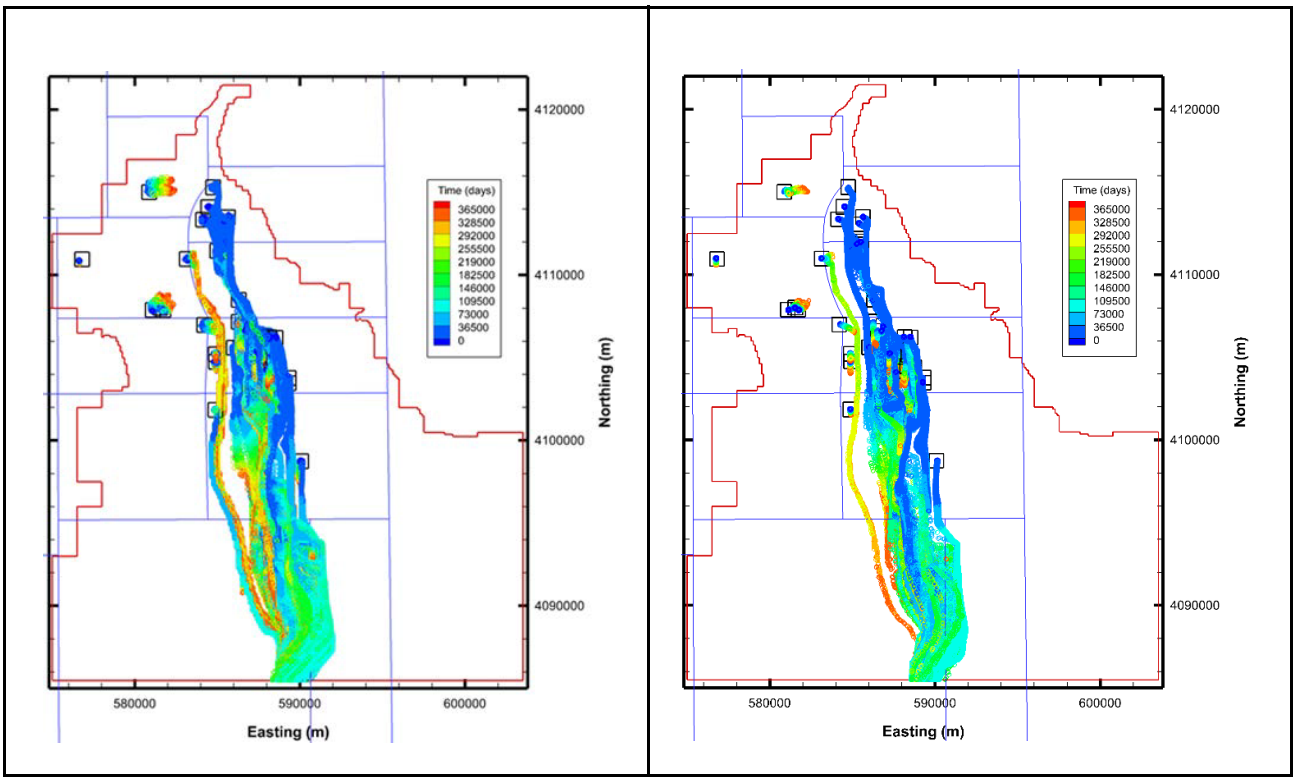

Figure 2-57
Particle Travel Paths and Times for the Base-Case Level 2 (left) and Level 3 (right) Meshes

2.8 Unforeseen Uncertainties and the Need for Extended Peer Review

2.8.1 New Concerns and Approaches Will Likely Arise

This uncertainty is motivated by a desire for UGTA to employ external reviewers more frequently throughout the life of the project.

PRC Recommendation: The peer review team recommends that DOE initiate a wider "vetting" of the models and monitoring, and continued review of assumptions and rationale for choices made in data gathering, inclusion, and exclusion.

PRC Recommendation: The peer review team recommends that DOE should consider annual or biennial independent and external review of the hydrologic modeling, testing, and characterization efforts at Yucca Flat. This would foster development of new conceptual models; would lead to efficiencies in developing characterization plans, as it would provide an independent and unbiased assessment of the efficacy of new characterization efforts; and would help focus DOE efforts on

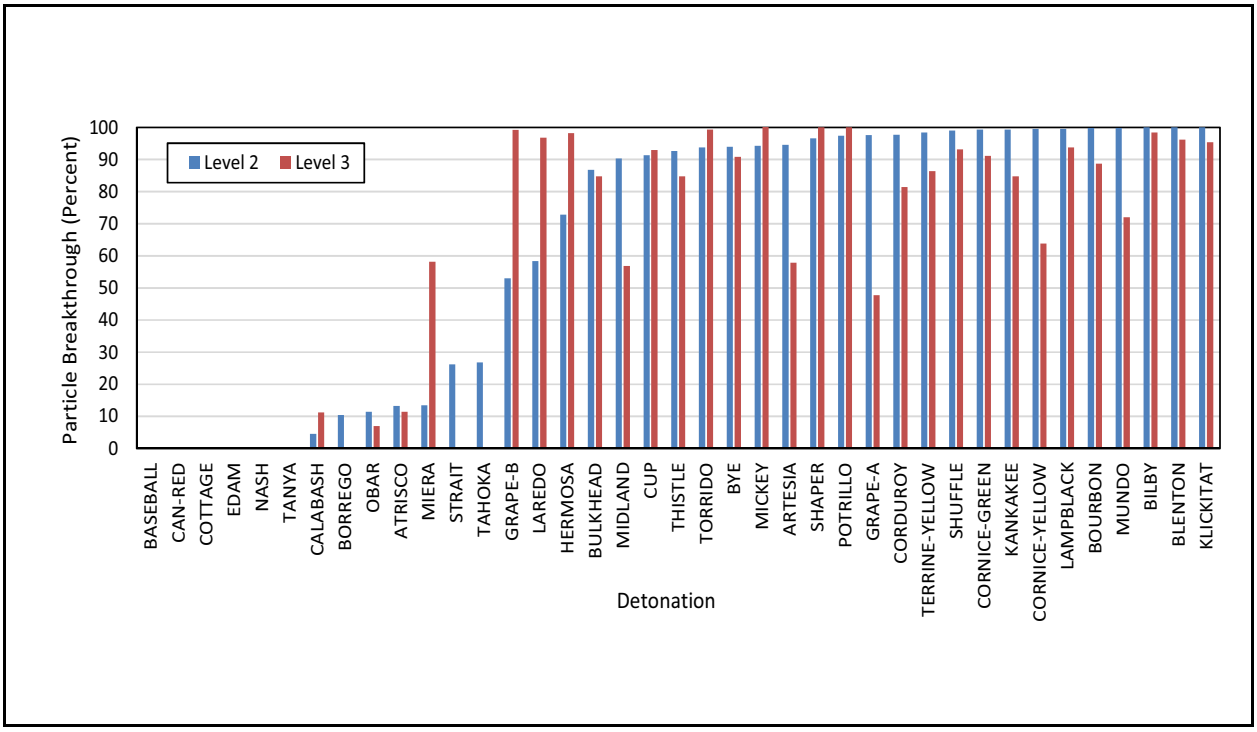

Figure 2-58
Percentage of Particle Breakthrough in 1,000 Years near the Model's Southern Boundary for the 30 Detonations within 3 R_c of the SZ LCA

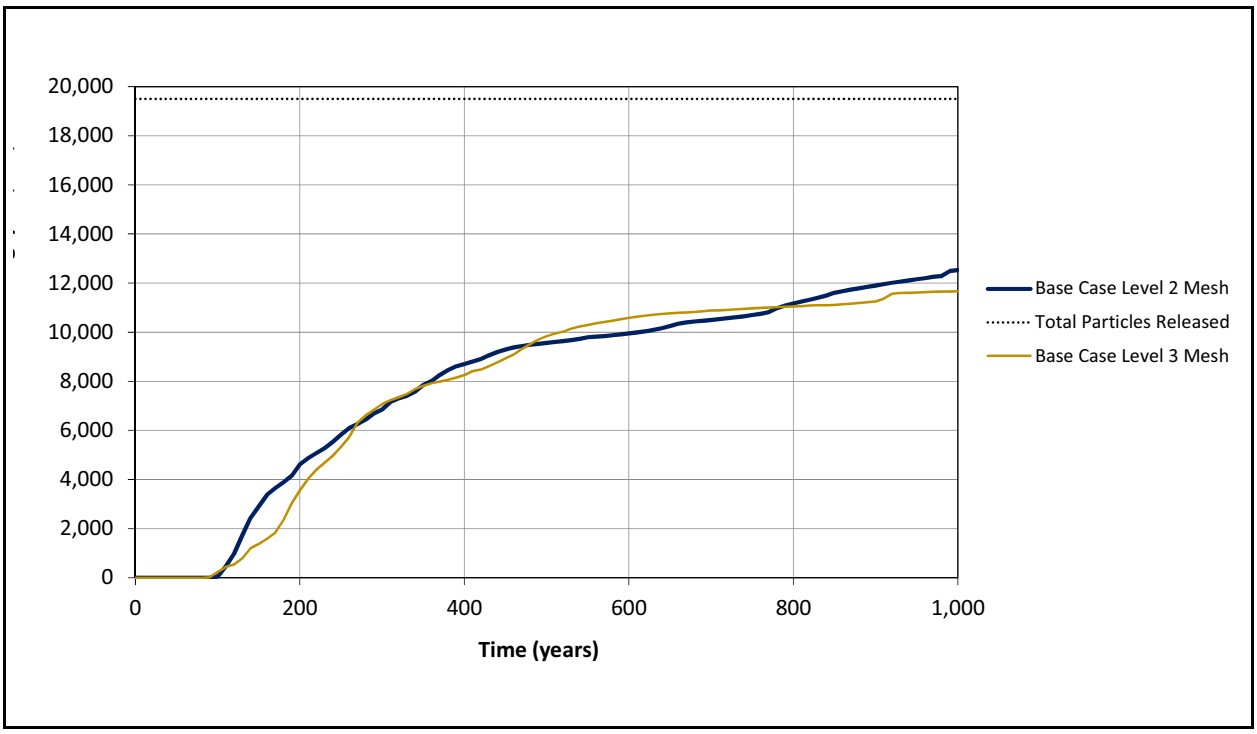

Figure 2-59
Base-Case Breakthrough for the Level 2 and 3 Meshes

critical characterization gaps. An outside evaluation could take, as this peer review team has been able to do, a "30,000-foot" view of the conceptual flow model and characterization efforts in a continuous manner to help guide efforts to close the most important knowledge gaps and build model confidence.

RESPONSE: All UGTA products are reviewed by a pre-emptive review committee and are frequently presented in technical meetings, as well as to a public advisory board, where open discussion of objectives, methods, opinions, and suggestions are provided by the broader scientific community, as well as the general public. The pre-emptive review committee includes experts in a variety of fields (e.g., geology, radiochemistry, and hydrology) and an ex officio NDEP member. Additional reviewers are added as necessary. This committee is highly knowledgeable regarding the CAU and different aspects of the flow and transport model. New contractors are introduced throughout the life of each CAU and therefore bring new perspectives to the work.

2.8.2 Climate Change

This uncertainty addresses the concern that the climate may change radically over the 1,000-year time frame of concern.

PRC Recommendation: As climate models are refined in the future, modeling should evaluate whether long-term climate change and associated extreme weather events would have a significant impact on the transport of radionuclides from Yucca Flat.

RESPONSE: Climate change is likely to impact nearly all of society over the next 100 years or so. However, the modeling team cannot predict at this time what the impact will be. A preliminary assessment is that the U.S. Southwest will experience warmer and drier conditions (e.g., Seager, 2007). If true, then current models are already conservative. By continued execution of the UGTA strategy (FFACO, 1996 as amended), any such assessment of regional scale climate change will occur when monitoring indicates a need for this action.

2.9 Location of Radionuclide Plumes—Recommendations for Monitor Wells and Testing/Sampling Programs during the CADD/CAP Stage

2.9.1 The Extent of Contamination Is Poorly Defined at Present

This uncertainty focuses on the need to define the bounds of contaminant migration.

PRC Recommendation: The peer review team recommends determining the bounds of contaminant migration in both the AA/VA and LCA aquifer systems. The emphasis should be on delineating the downgradient edge of the plume, targeting preferential geologic pathways (including faults) and placing monitor wells in the path predicted by the model for the year 2020, for example.

RESPONSE: A summary of RN detections in the SZ AA/VA and LCA domains spanning five decades in some cases was included in Tables 4-45 and 4-46 and as Appendix D in N-I, (2013a). The NNSS Integrated Sampling Plan (NNSA/NFO, 2014) ensures that samples are collected routinely, and ^{3}H concentration maps are presented in the Annual Site Environmental reports and will also be presented in UGTA Annual Sampling reports. Selection and placement of monitoring wells is the focus of the closure report (CR) stage, not the CAI or CADD/CAP stages. Continued execution of the UGTA strategy (FFACO, 1996 as amended) and implementation of the NNSS Integrated Sampling Plan (NNSA/NFO, 2014) will continue to address this comment.

It should also be noted that three new wells in Yucca Flat have been drilled to better define the extent of contamination in both the AA/VA and LCA systems. In addition, 10 wells with reported ^{3}H detections that had not been sampled in some cases for decades were resampled since the Peer Review was conducted in 2014. Results of ^{3}H for these resampled wells are given in Table 2-11. Preliminary data from the new wells (ER-2-2, ER-3-3, and ER-4-1) do not indicate ^{3}H at concentrations above the MDL (1,500 to 1,800 pCi/L) in the LCA, despite the fact that the wells sample the shallow part of the LCA along major structural features that are likely to form the dominant transport pathways.

At present, no further work is warranted under this uncertainty.

2.9.2 The Existing Observation Well Network Is Inadequate

This uncertainty addresses the well network necessary to determine the extent of contamination.

PRC Recommendation: The peer review team recommends a comprehensive formal review of existing data quality, including chemical sampling and laboratory testing methods. Going forward, a groundwater monitoring program should be maintained to collect samples for purposes such as evaluating model uncertainties and delineating contaminant boundaries. Existing observation wells included in the monitoring program should be flagged with appropriate data-quality designations. New monitor wells are recommended in the near field and far field downgradient of key detonations, especially west of Yucca fault; in one or more permeable fault zones; and at the southern end of Yucca Flat where contamination is anticipated based on modeling.

Initial CADD/CAP monitor wells should be sited with the goal of finding contaminant plumes and simultaneously collecting valuable hydraulic property data from the fault zones and country rock of the AA/VA, TCU, and LCA. The peer review team recommends at a minimum additional monitor wells for two purposes:

1. *To further evaluate the nexus between large detonations and the LCA via major faults, such as in the vicinity of STRAIT and the Topgallant fault, or near the impacted AA/VA holes U-4uPS 2A/U-7ba PS 1AS and Yucca fault, and*

2. *To find the extent of contamination along expected pathways bordering the detonations on the south, between ER 6-1 and ER 6-2.*

   - *One well near the Topgallant fault and*

   - *One well near the junction of Yucca fault and other minor faults such as those extending south from BILBY.*

   - *If either of the above two monitor wells show impacts, add two additional monitor wells to the south of Yucca Lake (e.g., near the outlet to CP Basin and Frenchman Flat).*

Regarding construction of the wells, the peer review team recommends using angled drilling and doglegs when possible to cross the faults at multiple positions and investigate multiple issues with one hole.

In addition, the peer review team recommends resampling some of the drill-back holes and, as needed, sampling from new drill holes to understand whether radionuclides are migrating out of cavities. Drill holes near detonations with working points in and near the LCA may be most useful.

Furthermore, the peer review team recommends aquifer testing and sampling, and new drilling if necessary, to determine inflow to Yucca Flat from the north.

PRC Recommendation: In addition to new monitor wells, existing wells may be used to better understand processes and decrease uncertainty in hydraulic and geochemical properties. The testing and sampling programs listed in Table 14 should be undertaken in the CADD/CAP stage of the project to build confidence in the conservative nature of the predicted contaminant boundary. This list is neither exhaustive nor prioritized, and NNSA/NFO or NDEP may identify other key processes and pathways that require additional characterization during the next stage of work. The models should be used to identify additional data that would lead to the greatest reduction of uncertainty in the extent of the contaminant boundaries.

RESPONSE: Three new wells were sited and drilled in 2016 that address many of these concerns and those listed in Table 2-13 (Kwicklis, 2015). The three new wells are located, respectively, (1) in the central part of the basin near the Yucca fault (ER-3-3), downgradient of scores of deeply buried, large-yield tests; (2) near a deeply buried, large-yield detonation that had a nearby fault (ER-2-2); and (3) near a deeply buried, large-yield detonation approximately 2 R_c distant from the LCA (ER-4-1). Each well had shallow completions in the LCA. Preliminary data from Wells ER-2-2, ER-3-3, and ER-4-1 do not indicate ^3H at concentrations above the MDL (1,500 to 1,800 pCi/L) in the LCA. In addition, 10 wells with reported ^3H detections that had not been sampled in some cases for decades were resampled since the Peer Review was conducted in 2014. Results of ^3H for these resampled wells are given in Table 2-11. The LCA in these wells has no measurable ^3H. The resampled wells included some wells in the western part of the basin near the Topgallant and Carpetbag faults, as well as those in the high-transmissivity eastern corridor downgradient of many deeply buried detonations. Therefore, the wells are in an excellent configuration to detect RNs if they were presently flowing south in the LCA at these locations. The LCA in the southern half of Yucca Flat has no measurable ^3H.

A groundwater sampling plan for Yucca Flat and other areas of the NNSS is now in place that will ensure annual evaluations of the sampling results for quality and consistency with the conceptual

Table 2-13
Recommended Non-exhaustive List of Testing and Sampling Programs To Better Characterize Key Pathways That Control the Contaminant Boundary

Multi-well hydraulic testing on the central and western portions of the LCA to investigate both the fracture/fault hydraulic properties of the LCA and the vertical hydraulic continuity of the TCU. Water samples should be collected from known intervals and with time during testing in order to define the vertical as well as the horizontal distribution of water types and to define chemical changes (e.g., changing RN concentrations) with the increasing aquifer volume sampled as pumping continues. Where appropriate, intervals should be packed off during sampling to prevent sample mixing due to vertical gradients.

Multi-well hydraulic testing and water sampling at the northern boundary of Yucca Flat to investigate inflow from the north, including the fracture/fault hydraulic properties of rocks that occur along the northern extension of the Boundary/Yucca fault across the topographic divide to the north (Climax Stock, LCA, contact-metamorphosed LCA, and overlying Tertiary volcanic rocks).

Sampling and testing designed to maximize the ability to interpret data from hydraulic testing:
- Temperature profiling through the TCU to estimate vertical leakage
- Lithologic logging (preferably of drill core) and geophysical logging of the TCU and LCA, with an emphasis on characterization of flow in fractures and faults in both units, and, in the case of the LCA, subsurface mapping of individual stratigraphic units that may contain karst or fracturing that would provide fast pathways
- Packer testing to investigate hydraulic and chemical character of discrete preferred flow zones as well as the TCU
- Spinner logs (as undertaken in ER-6-1) to investigate preferred flow zones
- Head measurements at discrete depth intervals across the TCU and in the LCA to quantify the gradient

Chemical data collected from discrete depth intervals and during pumping to define changes as boreholes are cleaned out and with increasing volume pumped:
- Key RNs (^{3}H, ^{14}C, ^{90}Sr, ^{99}Tc, ^{36}Cl)
- Major constituents (including field determinations) for charge balance (pH, major ions) as well as constituents required to assess equilibrium with formation minerals and aqueous speciation of RNs affecting their solubilities and sorption behavior

models of flow and transport (NNSA/NFO, 2014). In addition, numerous historical reports have been identified to help constrain permeability variations in the vicinity of underground nuclear tests, including those that involve post-shot holes. Continued execution of the UGTA strategy (FFACO, 1996 as amended) and implementation of the NNSS Integrated Sampling Plan (NNSA/NFO, 2014) will continue to address this comment.

Existing wells rendered unusable for various reasons will be evaluated for potential rehabilitation. This includes Wells U-2gg PSE 3a, U-10L-1, and UE-1r WW. Evaluation of slanted post-shot hole U-2gg PSE 3a in December 2015 indicated a depth to water of 1,915.38 ft (corresponding to a vertical depth of 1,821.6 ft) and revealed an obstruction within the casing at a borehole depth of 1,966 ft, approximately 94 ft above the open borehole interval. The fluid was nearly opaque and appeared to have a significant content of drilling fluid, which essentially precluded the usefulness of a video log. However, a chemistry log was run, and fluid samples were collected within the casing above the obstruction. ^{3}H results of 3,500 and 3,650 pCi/L were obtained. Further evaluation of the obstruction,

and whether it can be removed, is necessary to determine whether U-2gg PSE 3a can be used to monitor conditions below the INGOT detonation.

U-10L-1 was also evaluated in December 2015. A total depth (TD) of 1,854.75 ft was measured, and no water was detected in the open borehole. This TD is approximately 2.5 ft above the last measured water level of 1,857.3 ft in 1980 indicating that this well no longer reaches the SZ. The video log revealed numerous breakouts and rock ledges along the open borehole wall and rock debris at the bottom. It appears that this well would need to be re-drilled in order to regain the original TD of 2,208 ft.

3.0 COMMENT RESPONSE SUMMARY

This report carefully addresses the concerns and recommendations of the PRC as documented in N-I (2015). The PRC identified uncertainties in nine main areas related to the YF/CM flow and transport model documented in N-I (2013a): (1) model domain/boundary conditions, (2) model calibration, (3) hydraulic properties and pathways, (4) source term and mass flux, (5) transport, (6) simulating critical observations, (7) uncertainty evaluation, (8) unforeseen uncertainties, and (9) location of RN plumes. There were several comments under each of these areas, and some of the comments contained sub-comments, thus leading to 52 rows in the summary table (Table ES-1). Each of the comments is discussed in detail in Section 2.0

In the process of responding to the comments and recommendations, the YF/CM modeling team reanalyzed existing data and models, ran new models recommended by the PRC, and collected data from existing and new wells. The overall conclusion from this effort is that the original YF/CM flow and transport models documented in N-I (2013a) conservatively bounded the contaminant migration in YF/CM, and that the new models recommended by the PRC did not lead to the development of credible transport scenarios with different transport pathways or contamination over a larger spatial extent.

This report notes that the philosophy adopted for the Phase I LCA groundwater flow model (N-I, 2013a) was to be conservative in the modeling assumptions when they were likely to affect the forecast extent and magnitude of RN transport, especially when data were sparse or subject to alternative interpretations. The goal of the LCA modeling was to develop a range of plausible groundwater flow fields that reproduce the steady-state and transient water-level observations and to not underrepresent the possible extent of contaminant migration. Given this goal, overestimating the transport was considered acceptable by the YF/CM modeling team.

Uncertainties in model domain/boundary conditions (Section 2.1) were addressed by calibrating flow models designed to explore alternate conceptual models and bounding scenarios. Particle tracking calculations were performed, and transport modeling was done on a subset of cases to assess the 95th percentile contaminant boundary. It was found that these simulations led to less extensive transport

results compared to the base case. However, it was noted that a small fraction of realizations (low probability, less than 10 percent) led to the 95 percentile contaminant boundary crossing the southern extent of the model domain, for the existing base case model that has high values of flux through the model domain. Flux estimates resulting from the reanalysis of the data from the ER-6-1-2 MWAT led to boundary flux values (19 kg/s) that are nearly an order of magnitude smaller than those from the base case (189.6 kg/s). Preliminary simulations using these flux values based on the reanalysis of the ER-6-1-2 MWAT led to 95 percentile contaminant boundary forecasts (Section 2.1.2) that were well north of the southern boundary of the model. This supports the present model boundaries as sufficiently large to include all expected contaminant boundary locations. These models will be explored more fully during the model evaluation phase of the CADD/CAP stage.

Following the recommendations regarding model calibration (Section 2.2), alternate conceptual models were explored. The models that could achieve acceptable calibrations led to particle breakthroughs and transport forecasts that were equivalent to or less extensive than the base case. Hence, it was concluded that it was not necessary to further address these recommendations.

Uncertainties in hydraulic properties and pathways (Section 2.3) were addressed by reviewing the previously existing data and calibrating flow models with the alternate conceptualizations recommended by the PRC. Drilling data from the new wells (ER-2-2, ER-3-3, and ER-4-1) corroborate the existing simulations and do not lead to scenarios of increased permeability in the vicinity of the Yucca Fault. It was also noted that in some cases, the models recommended by the PRC were already encompassed in the discussions presented in N-I (2013a). The alternate flow models considered did not calibrate to the data as well as the base-case model, and showed similar or decreased particle travel over 1,000 years; or produced total particle breakthrough near the model's southern boundary that was larger at 1,000 years but smaller prior to approximately 200 years, when ^{3}H largely defines the contaminant boundary. Three alternate models with alternative fault conceptualizations led to percent particle breakthrough at 1,000 years greater than that for the base case: (1) faults without low permeability cores, (2) no faults with traces <3km, and (3) only considering the large basin-forming faults. These alternate models will be explored using more realistic flux constraints during the CADD/CAP stage.

Source term and mass flux uncertainties were discussed (Section 2.4) to show that these were already encompassed by the N-I (2013a) model, and the approach taken in that model was consistent with observations. Hence, further work recommended under these uncertainties was not necessary.

Discussion of the uncertainties related to transport parameters (Section 2.5) showed that the approach taken in N-I (2013a) was consistent with field and laboratory data. Alternate model calibrations were conducted to demonstrate that the contaminant boundary was not significantly impacted by the alternate parameter ranges suggested by the PRC.

Recommendations regarding simulation of critical observations (Section 2.6) were addressed with a combination of modeling and groundwater sampling. Many aspects of these recommendations were addressed by alternate models considered under model calibration, hydraulic properties and pathways, and uncertainty assessment. Additionally, three new wells (ER-2-2, ER-3-3, and ER-4-1) were drilled near deeply buried, large-yield detonations (ER-2-2 and ER-4-1) or near faults (ER-2-2 and ER-3-3) to investigate the extent of contamination associated with tests near the LCA or faults. No new detections of elevated ^{3}H concentrations above the field screening level of about 1,500 pCi/L in the LCA were observed in the resampled wells or in the LCA during drilling of the three new wells. These field analyses support a hypothesis of limited direct interaction of test cavities with the LCA. Some wells with a history of sporadic, low-level ^{3}H detections were demonstrated to be ^{3}H-free in 2015, indicating that many earlier, low-level ^{3}H detections were probably sampling artifacts (ER-6-2) or cross-contamination transferred between wells by sampling equipment (UE-6e, UE-6d), and not the leading edge of an unanticipated contaminant plume. In other instances where low-level ^{3}H detections were repeated over several years or decades (TW-B), or were confirmed by recent low-level ^{3}H measurements (WW-3), explanations unrelated to RN transport from nuclear tests were provided. In one instance, new models demonstrated that ^{3}H transport from the HAYMAKER detonation to a water-supply well (WW-A) resulted from pumping over a long period of time combined with hydrodynamic dispersion.

Recommendations regarding uncertainty assessment (Section 2.7) were addressed by exploring alternate flow and transport models. It was noted that the alternate models that produced acceptable calibrations to the data did not produce contaminant transport more extensive than the base case, demonstrating that the models and parameter ranges considered in N-I (2013a) adequately bound the range of uncertainty.

Recommendations regarding unforeseen uncertainties (Section 2.8) were addressed by explaining that the current UGTA procedures are adequate for meeting the project goals.

Recommendations regarding location of RN plumes (Section 2.9) are being addressed by the continuing execution of the UGTA strategy (FFACO, 1996 as amended), and the NNSS Integrated Sampling Plan (NNSA/NFO, 2014). Sampling conducted since the completion of N-I (2013a) and sampling during the drilling of the three new wells supports the observation that ^{3}H contamination of the LCA is of limited areal extent and that simulations documented in N-I (2013a) adequately bound RN transport.

In conclusion, this document carefully addresses the uncertainties and associated recommendations identified in the PRC report (N-I, 2015), concluding that the drilling of three new wells, additional sampling of wells, and analysis of alternate flow and transport models conducted since the publication of the original report (N-I, 2013a) have adequately addressed all of the PRC concerns for the CAI stage, and further work is not warranted under these uncertainties and recommendations before moving into the CADD/CAP stage.

4.0 REFERENCES

BN, see Bechtel Nevada.

Barnes, H., F.N. Houser, and F.G. Poole. 1963. *Geologic Map of the Oak Spring Quadrangle, Nye County, Nevada,* Map GQ-214, scale 1:24,000. Washington, DC: U.S. Geological Survey.

Barnes, H., E.B. Ekren, C.L. Rodgers, and D.C. Hedlund. 1982. *Geologic and Tectonic Maps of the Mercury Quadrangle, Nye and Clark Counties, Nevada*, Miscellaneous Geologic Investigations Series Map I-1197, scale 1:24,000. Denver, CO: U.S. Geological Survey.

Bechtel Nevada. 2006. *A Hydrostratigraphic Model and Alternatives for the Groundwater Flow and Contaminant Transport Model of Corrective Action Unit 97: Yucca Flat-Climax Mine, Lincoln and Nye Counties, Nevada*, DOE/NV/11718--1119. Prepared for the U.S. Department of Energy, National Nuclear Security Administration Nevada Site Office. Las Vegas, NV.

Bedford, R.G., and D.D. Jackson. 1965. *Volatiles of the Fission Product and Uranium Oxides Chemistry,* 37th Edition, Report UC-4 TID-4500. Livermore, CA: University of California, Lawrence Radiation Laboratory.

Belcher, W.R., J.B. Blainey, F.A. D'Agnese, C.C. Faunt, M.C. Hill, R.J. Laczniak, G.M. O'Brien, C.J. Potter, H.M. Putnam, C.A. San Juan, and D.S. Sweetkind. 2004. *Death Valley Regional Ground-Water Flow System, Nevada and California—Hydrogeologic Framework and Transient Ground-Water Flow Model*, Scientific Investigations Report 2004-5205. Reston, VA: U.S. Geological Survey.

Boardman, C.R. 1970. "Engineering Effects of Underground Nuclear Explosives." In *Proceedings of Symposium on Engineering with Nuclear Explosives*, CONF-700101, 43–67. Las Vegas, NV, 14–16 January.

Borg, I.Y. 1975. "Radioactivity Trapped in Melt Produced by a Nuclear Explosion." In *Nuclear Technology*, Vol. 26(1): pp. 88–100.

Borg, I.Y., R. Stone, H.B. Levy, and L.D. Ramspott. 1976. *Information Pertinent to the Migration of Radionuclides in Ground Water at the Nevada Test Site, Part 1: Review and Analysis of Existing Information,* UCRL-52078. Livermore, CA: Lawrence Livermore Laboratory.

Bowen, S.M., D.L. Finnegan, J.L. Thompson, C.M. Miller, P.L. Baca, L.F. Olivas, C.G. Geoffrion, D.K. Smith, W. Goishi, B.K. Esser, J.W. Meadows, N. Namboodiri, and J.F. Wild. 2001. *Nevada Test Site Radionuclide Inventory, 1951–1992,* LA-13859-MS. Los Alamos, NM: Los Alamos National Laboratory.

Butkovich, T.R. 1976. *Cavities Produced by Underground Nuclear Explosions,* UCRL-52097. Livermore, CA: Lawrence Livermore Laboratory.

Byers, F.M., Jr., and H. Barnes. 1967. *Geologic Map of the Paiute Ridge Quadrangle, Nye and Lincoln Counties, Nevada,* Map GQ-577, scale 1:24,000. Washington, DC: U.S. Geological Survey.

CFR, see *Code of Federal Regulations.*

Carle, S.F., M. Zavarin, Y. Sun, and G.A. Pawloski. 2008. *Evaluation of Hydrologic Source Term Processes for Underground Nuclear Tests in Yucca Flat, Nevada Test Site: Carbonate Tests*, LLNL-TR-403485. Livermore, CA: Lawrence Livermore National Laboratory.

Carr, W.J., 1988. *Geology of the Devils Hole Area, Nevada,* Open-File Report 87-560. U.S. Geological Survey: Reston, VA.

Carroll, R.D. 1981. "Seismic Velocity and Postshot Properties in and near Chimneys." In *Proceedings of the Monterey Containment Symposium*, LA-9211-C, Vol. 1. Los Alamos, NM: Los Alamos National Laboratory.

Cashman, S., and K. Cashman. 2000. "Cataclasis and Deformation-Band Formation in Unconsolidated Marine Terrace Sand, Humboldt County, California." In *Geology*, Vol. 28(2): pp. 111–114.

Code of Federal Regulations. 2015. Title 40 CFR, Part 141, "National Primary Drinking Water Regulations." Washington, DC: U.S. Government Printing Office.

Cooper, C.A., R.L. Hershey, J.M. Healey, and B.F. Lyles. 2013. *Estimation of Groundwater Recharge at Pahute Mesa Using the Chloride Mass-Balance Method,* DOE/NV/0000939-09; Publication No. 45251. Reno, NV: Desert Research Institute, Water Resources Center.

Deutsch, C., and A. Journel. 1992. *GSLIB: Geostatistical Software Library and User's Guide by Clayton Deutsch and Andre Journel,* Oxford University Press.

Drellack, S., National Security Technologies, LLC. 2014. Written communication. Subject: *Water Penetration Depth in Yucca Flat Playa Following a 100-Year Storm.* Las Vegas, NV.

ESRI, see ESRI, i-cubed, USDA FSA, USGS, AEX, GeoEye, Getmapping, Aerogrid, and IGP.

Elliott, P.E., and J.M. Fenelon. 2013. *Database of Groundwater Levels and Hydrograph Descriptions for the Nevada Test Site Area, Nye County, Nevada.* Data Series 533, Version 4.0. Reston, VA: U.S. Geological Survey.

ESRI, i-cubed, USDA FSA, USGS, AEX, GeoEye, Getmapping, Aerogrid, and IGP. 2014. ArcGIS Online website. As accessed at http://www.arcgis.com/home/gallery.html on 23 December.

FFACO, see *Federal Facility Agreement and Consent Order*.

Faunt, C.C., D.S. Sweetkind, M.C. Hill, M.T. Pavelko, and W.R. Belcher. 2012. Written communication. Subject: *Update of the Death Valley Regional Groundwater Flow System Transient Model, Nevada and California*. U.S. Geological Survey.

Federal Facility Agreement and Consent Order. 1996 (as amended March 2010). Agreed to by the State of Nevada; U.S. Department of Energy, Environmental Management; U.S. Department of Defense; and U.S. Department of Energy, Legacy Management. Appendix VI, which contains the Underground Test Area Strategy, was last modified June 2014, Revision No. 5.

Fenelon, J.M., U.S. Geological Survey. 2015. Written communication. Subject: "Water-Filled Sump Near Well WW-3." Henderson, NV.

Fenelon, J.M., D.S. Sweetkind, and R.J. Laczniak. 2010. *Groundwater Flow Systems at the Nevada Test Site, Nevada: A Synthesis of Potentiometric Contours, Hydrostratigraphy, and Geologic Structures,* Professional Paper 1771. Reston, VA: U.S. Geological Survey.

Fenelon, J.M., D.S. Sweetkind, P.E. Elliott, and R.J. Laczniak. 2012. *Conceptualization of the Predevelopment Groundwater Flow System and Transient Water-Level Responses in Yucca Flat, Nevada National Security Site, Nevada*, Scientific Investigations Report 2012-5196. Reston, VA: U.S. Geological Survey.

Fenelon, J.M., K.J. Halford, and M.T. Moreo. 2016. *Delineation of the Pahute Mesa-Oasis Valley Groundwater Basin, Nevada,* Scientific Investigation Report 2015-5175. Reston, VA: U.S. Geological Survey.

Geldon, A.L. 2004. *Hydraulic Tests of Miocene Volcanic Rocks at Yucca Mountain and Pahute Mesa and Implications for Groundwater Flow in the Southwest Nevada Volcanic Field, Nevada and California,* GSA Special Papers Vol. 381. 93 pp. Boulder, CO: Geological Society of America.

Glynn, P.D., and L.N. Plummer. 2005. "Geochemistry and the Understanding of Ground-Water Systems." In *Hydrogeology Journal*, Vol. 13: pp. 263–287.

Grasso, D.N. 2000. *Geologic Surface Effects of Underground Nuclear Testing, Yucca Flat, Nevada Test Site, Nevada*, Open-File Report 00-176. Denver, CO: U.S. Geological Survey.

Halford, K., U.S. Geological Survey. 2009. Personal communication to A. Tompson (LLNL) regarding specified fluxes to lateral boundaries of the UGTA LCA model for Yucca Flat, 16 January. Carson City, NV.

Halford, K., U.S. Geological Survey. 2012. Personal communication to A. Tompson (LLNL) regarding groundwater flow estimates for the Yucca Flat/Climax Mine CAU, 9 October. Carson City, NV.

Halford, K., U.S. Geological Survey. 2016. Personal communication to S. Kelkar (Navarro/HGL) regarding UGTA-YF, MWAT analysis, 3 March. Carson City, NV.

Halford, K.J., R.J. Laczniak, and D.L. Galloway. 2005. *Hydraulic Characterization of Overpressured Tuffs in Central Yucca Flat, Nevada Test Site, Nye County, Nevada*, Scientific Investigations Report 2005-5211. Carson City, NV: U.S. Geological Survey.

Harrill, J.R., J.S. Gates, and J.M. Thomas. 1988. *Major Groundwater Flow Systems in the Great Basin Region of Nevada, Utah and Adjacent States*. Hydrological Investigation Atlas HA-694-C, scale 1:1,000,000. Denver, CO: U.S. Geological Survey.

Heynekamp, M.R., L.B. Goodwin, P.S. Mozley, and W.C. Haneberg. 1999. "Controls on Fault-Zone Architecture in Poorly Lithified Sediments, Rio Grande Rift, New Mexico: Implications for Fault-Zone Permeability and Fluid Flow," In *Geophysical Monograph*, "Faults and Subsurface Fluid Flow in the Shallow Crust," Vol. 113: pp. 27–48. Washington, DC: American Geophysical Union.

Hokett, S.L., D.R. Gillespie, G.V. Wilson, and R.H. French. 2000. *Evaluation of Recharge Potential at Subsidence Crater U10i, Northern Yucca Flat, Nevada Test Site*, DOE/NV/11508-53; Publication No. 45174. Las Vegas, NV: Desert Research Institute.

Hu, Q.H., T.P. Rose, M. Zavarin, D.K. Smith, J.E. Moran, and P.H. Zhao. 2008. "Assessing Field-Scale Migration of Radionuclides at the Nevada Test Site: 'Mobile' Species." In *Journal of Environmental Radioactivity*, Vol. 99(10): pp. 1617–1630.

IAEA, see International Atomic Energy Agency.

International Atomic Energy Agency. 1998a. *The Radiological Situation at the Atolls of Mururoa and Fangataufa, Technical Report, Volume 3: Inventory of Radionuclides Underground at the Atolls,* IAEA-MFTR-3. In "Proceedings of an IAEA Conference, Vienna, 30 June – 3 July." Vienna, Austria.

International Atomic Energy Agency. 1998b. *The Radiological Situation at the Atolls of Mururoa and Fangataufa, Technical Report, Volume 4: Releases to the Biosphere of Radionuclides from Underground Nuclear Weapons Tests at the Atolls*, IAEA-MFTR-4. In "Proceedings of an IAEA Conference, Vienna, 30 June – 3 July." Vienna, Austria.

International Atomic Energy Agency. 1998c. *The Radiological Situation at the Atolls of Mururoa and Fangataufa, Technical Report, Volume 6: Dose due to Radioactive Materials Present in the Environment or Released form the Atolls*, IAEA-MFTR-6. In "Proceedings of an IAEA Conference, Vienna, 30 June – 3 July." Vienna, Austria.

Kwicklis, E., Los Alamos National Laboratory. 2015. Technical memo titled "Recommendations for New Wells in Corrective Action Unit 97: Yucca Flat/Climax Mine, NNSS, following the Yucca Flat Peer Review," 20 March. Los Alamos, NM.

Kwicklis, E., and I. Farnham. 2014. "Testing the ^{14}C Ages and Conservative Behavior of Dissolved ^{14}C in a Carbonate Aquifer in Yucca Flat, Nevada (USA), Using ^{36}Cl from Groundwater and Packrat Middens." In *Hydrogeology Journal*, Vol. 22(6): pp. 1359–1381.

Laczniak, R.J., J.C. Cole, D.A. Sawyer, and D.A. Trudeau. 1996. *Summary of Hydrogeologic Controls on Ground-Water Flow at the Nevada Test Site, Nye County, Nevada*, Water-Resources Investigations Report 96-4109. Carson City, NV: U.S. Geological Survey.

Laczniak, R.J., G.A. DeMeo, S.R. Reiner, J.L. Smith, and W.E. Nylund. 1999. *Estimates of Ground-Water Discharge as Determined from Measurements of Evapotranspiration, Ash Meadows Area, Nye County, Nevada,* Water-Resources Investigations Report 99-4079. Carson City, NV: U.S. Geological Survey.

Landwehr, J.M., and I.J. Winograd. 2012. *Devils Hole, Nevada – A Primer*. Fact Sheet 2012-3021. 6 pp. Reston, VA: U.S. Geological Survey. Available at http://pubs.usgs.gov/fs/2012/3021.

Lyles, B.F. 1990. *Tritium Variations in Groundwater on the Nevada Test Site*, DOE/NV/10384-38; Publication No. 45086. Las Vegas, NV: Desert Research Institute, Water Resources Center.

Lyles, B.F. 1993. *Tritium Activities in Selected Wells on the Nevada Test Site,* DOE/NV/10845-20; Publication No. 45104. Las Vegas, NV: Desert Research Institute, Water Resources Center.

Miller, C.M., S.M. Bowen, D.L. Finnegan, J.L. Thompson, P.L. Baca, L.F. Olivas, C.G. Geoffrion, D.K. Smith, W. Goishi, B.K. Esser, J.W. Meadows, N. Namboodiri, and J.F. Wild. 2002. *Total Radionuclide Inventory Associated with Underground Nuclear Tests Conducted at the Nevada Test Site, 1951–1992*, LA-13989. Los Alamos, NM: Los Alamos National Laboratory.

Moore, J.E. 1962. *Selected Logs and Drilling Records of Wells and Test Holes Drilled at the Nevada Test Site Prior to 1960,* Open-File Report 62-87. 50 pp. Denver, CO: U.S. Geological Survey.

N-I, see Navarro-Intera, LLC.

N-I GIS, see Navarro-Intera Geographic Information Systems.

NNES, see Navarro Nevada Environmental Services, LLC.

NNSA/NFO, see U.S. Department of Energy, National Nuclear Security Administration Nevada Field Office.

NNSA/NSO, see U.S. Department of Energy, National Nuclear Security Administration Nevada Site Office.

Navarro. 2016a. Written communication. Subject: "UGTA Chemistry Database (UCDB)," UGTA Technical Data Repository Database Identification Number UGTA-4-1197. Las Vegas, NV.

Navarro. 2016b. Written communication. Subject: "UGTA Geochemistry Database," UGTA Technical Data Repository Database Identification Number UGTA-4-129. Las Vegas, NV.

Navarro-Intera Geographic Information Systems. 2012 and 2014. ESRI ArcGIS Software.

Navarro-Intera, LLC. 2012. *Pahute Mesa Well Development and Testing Analyses for Wells ER-20-8 and ER-20-4, Nevada National Security Site, Nye County, Nevada*, Rev. 0, N-I/28091-061. Las Vegas, NV.

Navarro-Intera, LLC. 2013a. *Phase I Flow and Transport Model Document for Corrective Action Unit 97: Yucca Flat/Climax Mine, Nevada National Security Site, Nye County, Nevada*, Rev. 1, N-I/28091-080. Las Vegas, NV.

Navarro-Intera, LLC. 2013b. Written communication. Subject: *Rainier Mesa/Shoshone Mountain CAU Flow and Transport Model, Nevada National Security Site, Nye County, Nevada.* Las Vegas, NV.

Navarro-Intera, LLC. 2015. *External Peer Review Team Report for Corrective Action Unit 97: Yucca Flat/Climax Mine, Nevada National Security Site, Nye County, Nevada*, Rev. 0, N-I/28091-091. Las Vegas, NV.

Navarro Nevada Environmental Services, LLC. 2010. *Phase II Transport Model of Corrective Action Unit 98: Frenchman Flat, Nevada Test Site, Nye County, Nevada*, Rev. 1, N-I/28091--004, S-N/99205--122. Las Vegas, NV.

OTA, see U.S. Congress, Office of Technology Assessment.

Pawloski, G.A. 1999. *Development of Phenomenological Models of Underground Nuclear Tests on Pahute Mesa, Nevada Test Site—BENHAM and TYBO*, UCRL-ID-136003. Livermore, CA: Lawrence Livermore National Laboratory.

Peterson, E., P. Lagus, and K. Lie. 1977a. *Summary of the DINING CAR Tracer-Gas Chimney Pressurization Studies,* SSS-R-77-3185. Prepared for the Defense Nuclear Agency. La Jolla, CA: Systems, Science and Software.

Peterson, E., P. Lagus, and K. Lie. 1977b. *Summary of the MING BLADE Tracer-Gas Chimney Pressurization Studies,* SSS-R-78-3535; DNA 4491T. Prepared for the Defense Nuclear Agency. La Jolla, CA: Systems, Science and Software.

Peterson, E., P. Lagus, and K. Lie. 1978. *Summary of the MIGHTY EPIC Tracer-Gas Pressurization Studies,* SSS-R-78-3542; DNA 4492T. Prepared for the Defense Nuclear Agency. La Jolla, CA: Systems, Science and Software.

Phelps, G.A., and E.H. McKee. 1999. *High-Angle Faults in the Basement of Yucca Flat, Nevada Test Site, Nevada, Based on Analysis of a Constrained Gravity Inversion Surface,* Open-File Report 99-383. Menlo Park, CA: U.S. Geological Survey.

Plummer, L.N., E. Busenberg, and A.C. Riggs. 2000. "In-Situ Growth of Calcite at Devils Hole, Nevada – Comparison of Field and Laboratory Rates to a 500,000-Year Record of Near-Equilibrium Calcite Growth." In *Aquatic Geochemistry*, Vol. 6(2): pp. 257–274.

Pohll, G.M., J.J. Warwick, and S.W. Tyler. 1996. "Coupled Surface–Subsurface Hydrologic Model of a Nuclear Subsidence Crater at the Nevada Test Site." *Journal of Hydrology,* Vol. 186(1–4): pp. 43–62.

Pohlmann, K., M. Ye, D. Reeves, D. Decker, J. Chapman, and M. Zavarin. 2007. *Modeling of Groundwater Flow and Radionuclide Transport at the Climax Mine Sub-CAU, Nevada Test Site*, DOE/NV/26383-06; Publication No. 45226. Las Vegas, NV: Desert Research Institute.

Powell, B.A., A. Kersting, M. Zavarin, and P. Zhao. 2011. *Development of a Composite Non-Electrostatic Surface Complexation Model Describing Plutonium Sorption to Aluminosilicates,* LLNL-TR-408276. Livermore, CA: Lawrence Livermore National Laboratory.

Prothro, L.B., S.L. Drellack, D.N. Haugstad, H.E. Huckins-Gang, and M.J. Townsend. 2009. *Observations on Faults and Associated Permeability Structures in Hydrogeologic Units at the Nevada Test Site*, DOE/NV/25946--690. Las Vegas, NV: National Security Technologies, LLC.

Rawling, G.C., L.B. Goodwin, and J.L. Wilson. 2001. "Internal Architecture, Permeability Structure, and Hydrologic Significance of Contrasting Fault-Zone Types." In *Geology*, Vol. 29(1): pp. 43–46.

Reimus, P.W., R.L. Hershey, D.L. Decker, E. Garcia, S. Earman, J. Ryu, R.C. Roback, and G. Pohll. 2008. *Laboratory Experiments of ^{14}C Uptake and Release on Calcite and Dolomite to Support Groundwater Radionuclide Transport Modeling for the Nevada Test Site Underground Test Area Program*, LA-UR-08-0427. Los Alamos, NM: Los Alamos National Laboratory.

Reiner, S. 2007. *Ground-Water Temperature Data, Nevada Test Site and Vicinity, Nye, Clark, and Lincoln Counties, Nevada, 2000–2006.* Data Series 269. Reston, VA: U.S. Geological Survey.

Rose, T.P., Q. Hu, P. Zhao, C.L. Conrado, R. Dickerson, G.F. Eaton, A.B. Kersting, J.E. Moran, G. Nimz, B.A. Powell, E.C. Ramon, F.J. Ryerson, R.W. Williams, P.T. Wooddy, and M. Zavarin. 2011. *Radionuclide Partitioning in an Underground Nuclear Test Cavity*, LLNL-TR-409817. Livermore, CA: Lawrence Livermore National Laboratory.

SNJV, see Stoller-Navarro Joint Venture.

Seager, R., M. Ting, I. Held, Y. Kushnir, J. Lu, G. Vecchi, H.-P. Huang, N. Harnik, A. Leetmaa, N.-C. Lau, C. Li, J. Velez, and N. Naik. 2007. "Model Projections of an Imminent Transition to a More Arid Climate in Southwestern North America." In *Science,* Vol. 316(5828): pp. 1181–1184.

Sigda, J.M., L.B. Goodwin, P.S. Mozley, and J.L. Wilson. 1999. "Permeability Alteration in Small-Displacement Faults in Poorly Lithified Sediments: Rio Grande Rift, Central New Mexico." In *Faults and Subsurface Fluid Flow in the Shallow Crust*, Geophysical Monograph Vol. 113: pp. 51–68. W.C. Haneberg, P.S. Mozley, J.C. Moore, and L.B. Goodwin eds. Washington, DC: American Geophysical Union.

Smith, D.K. 1995. *Challenges in Defining a Radiologic and Hydrologic Source Term for Underground Nuclear Test Centers, Nevada Test Site, Nye County, Nevada*, UCRL-JC-120389. Livermore, CA: Lawrence Livermore National Laboratory.

Smith, D.K. 1997. Private communication as referenced in IAEA (1998).

Smith, D.K., A.B. Kersting, T.P. Rose, J.M. Kenneally, G.B. Hudson, G.F. Eaton, and M.L. Davisson. 1998. *Hydrologic Resources Management Program and Underground Test Area FY 1997 Progress Report*, UCRL-ID-130792. Livermore, CA: Lawrence Livermore Laboratory.

Stoller-Navarro Joint Venture. 2005a. *Analysis of Hydraulic Responses from the ER-6-1 Multiple-Well Aquifer Test, Yucca Flat FY 2004 Testing Program, Nevada Test Site, Nye County, Nevada*, Rev. 0, S-N/99205--051. Las Vegas, NV.

Stoller-Navarro Joint Venture. 2005b. *Unclassified Source Term and Radionuclide Data for Corrective Action Unit 98: Frenchman Flat Nevada Test Site, Nevada,* S-N/99205--058. Las Vegas, NV.

Stoller-Navarro Joint Venture. 2006a. *Geochemical and Isotopic Evaluation of Groundwater Movement in Corrective Action Unit 97: Yucca Flat/Climax Mine, Nevada Test Site, Nevada,* Rev. 0, S-N/99205--070. Las Vegas, NV.

Stoller-Navarro Joint Venture. 2006b. *Phase I Hydrologic Data for the Groundwater Flow and Contaminant Transport Model of Corrective Action Unit 97: Yucca Flat/Climax Mine, Nevada Test Site, Nye County, Nevada*, Rev. 0, S-N/99205--077. Las Vegas, NV.

Stoller-Navarro Joint Venture. 2007. *Phase I Contaminant Transport Parameters for the Groundwater Flow and Contaminant Transport Model of Corrective Action Unit 97: Yucca Flat/Climax Mine, Nevada Test Site, Nye County, Nevada*, Rev. 0, S-N/99205--096. Las Vegas, NV.

Stoller-Navarro Joint Venture. 2009. *Phase I Transport Model of Corrective Action Units 101 and 102: Central and Western Pahute Mesa, Nevada Test Site, Nye County, Nevada*, Rev. 1, S-N/99205--111. Las Vegas, NV.

Sutton, M. 2009. *Review of Distribution Coefficients for Radionuclides in Carbonate Minerals.* LLNL-SR-415700. Livermore, CA: Lawrence Livermore National Laboratory.

Sweetkind, D.S., and R.M. Drake, II. 2007. *Characteristics of Fault Zones in Volcanic Rocks near Yucca Flat, Nevada Test Site, Nevada*, Open-File Report 2007-1293. Reston, VA: U.S. Geological Survey.

Szabo, B.J., P.T. Kolesar, A.C. Riggs, I.J. Winograd, and K.R. Ludwig. 1994. "Paleoclimatic Inferences from a 120,000-Yr Calcite Record of Water-Table Fluctuation in Browns Room of Devils Hole, Nevada." In *Quaternary Research*, Vol. 41(1): pp. 59–69.

Thompson, J.L., comp. and ed. 1992. *Laboratory and Field Studies Related to the Hydrology/Radionuclide Migration Project. October 1, 1990—September 30, 1991,* LA-12338-PR. Los Alamos, NM: Los Alamos National Laboratory.

Thompson, J.L 1996. "Radionuclide Distribution in a Nuclear Test Cavity: The Baseball Event." In *Radiochimica Acta*, Vol. 72: pp. 157–162.

Tompson, A.F.B., ed. 2008. *Evaluation of Hydrologic Source Term Processes for Underground Nuclear Tests in Yucca Flat, Nevada Test Site: Saturated Tests*, LLNL-TR-403429. Livermore, CA: Lawrence Livermore National Laboratory.

Tompson, A.F.B., M. Zavarin, W.W. McNab, S.F. Carle, D.E. Shumaker, C. Lu, Y. Sun, G.A. Pawloski, Q. Hu, and S.K. Roberts. 2011. Written communication. Subject: *Hydrologic Source Term Processes and Models for Underground Nuclear Tests at Rainier Mesa and Shoshone Mountain, Nevada National Security Site.* Livermore, CA: Lawrence Livermore National Laboratory.

Tyler, S.W., W.A. McKay, and T.M. Mihevc. 1992. "Assessment of Soil Moisture Movement in Nuclear Subsidence Craters." In *Journal of Hydrology,* Vol. 139(1–4): pp. 159–181. doi:10.1016/0022-1694(92)90200-F.

USGS and DOE, see U.S. Geological Survey and U.S. Department of Energy.

U.S. Department of Energy, National Nuclear Security Administration Nevada Field Office. 2014. *Nevada National Security Site Integrated Groundwater Sampling Plan,* Rev. 0, DOE/NV--1525. Las Vegas, NV.

U.S. Department of Energy, National Nuclear Security Administration Nevada Field Office. 2015. *United States Nuclear Tests, July 1945 through September 1992,* DOE/NV--209-REV 16. Las Vegas, NV.

U.S. Department of Energy, National Nuclear Security Administration Nevada Site Office. 2011. *Corrective Action Decision Document/Corrective Action Plan for Corrective Action Unit 98: Frenchman Flat Nevada National Security Site, Nevada*, Rev. 1, DOE/NV--1455. Las Vegas, NV.

U.S. Department of Energy, Nevada Operations Office. 2000. *Corrective Action Investigation Plan for Corrective Action Unit 97: Yucca Flat/Climax Mine, Nevada Test Site, Nevada,* DOE/NV--659. Las Vegas, NV.

U.S. Congress, Office of Technology Assessment. 1989. *The Containment of Underground Nuclear Explosions,* OTA-ISC-414. Washington, DC: U.S. Government Printing Office.

U.S. Geological Survey and U.S. Department of Energy. 2016. "USGS/U.S. Department of Energy Cooperative Studies in Nevada" web page. As accessed at http://nevada.usgs.gov/doe_nv on 9 March.

Wigley, T.M.L., L.N. Plummer and F.J. Pearson, Jr. 1978. "Mass Transfer and Carbon Isotope Evolution in Natural Water Systems." In *Geochimica et Cosmochimica Acta*, Vol. 42(8): pp. 117–1139.

Wilson, G.V., D.M. Ely, S.L. Hokett, and D.R. Gillespie. 2000. "Recharge from a Subsidence Crater at the Nevada Test Site." In *Soil Science Society of America Journal*, Vol. 64(5): pp. 1570–1581.

Winograd, I.J. 1965. Memorandum to "The Record" titled "Conference on the Distribution and Genesis of Solution Features in Carbonate Rocks at the Nevada Test Site," 3 August. Las Vegas, NV.

Winograd, I.J., and F.J. Pearson, Jr. 1976. "Major Carbon 14 Anomaly in a Regional Carbonate Aquifer: Possible Evidence for Megascale Channeling, South Central Great Basin." In *Water Resources Research,* Vol. 12(6): pp. 1125–1143. Washington, DC: American Geophysical Union.

Winograd, I.J., and W. Thordarson. 1975. *Hydrogeologic and Hydrochemical Framework, South-Central Great Basin, Nevada-California, with Special Reference to the Nevada Test Site*, Professional Paper 712-C. Washington, DC: U.S. Geological Survey.

Winograd, I.J., J.M. Landwehr, T.B. Coplen, W.D. Sharp, A.C. Riggs, K.R. Ludwig, and P.T. Kolesar. 2006. "Devils Hole, Nevada, $\delta^{18}O$ Record Extended to the mid-Holocene." In *Quaternary Research,* Vol. 66(2): pp. 202–212.

Zavarin, M., P. Zhao, C. Joseph, J. Begg, M. Boggs, Z. Dai, and A. B. Kersting. 2015. *Hydrothermal Alteration of Glass from Underground Nuclear Tests: Formation and Transport of Pu-Clay Colloids at the Nevada National Security Site,* LLNL-TR-671402. Livermore, CA: Lawrence Livermore National Laboratory.

Appendix A

Additional Model Simulations of the AA/VA System To Evaluate the Effects of Alternative Parameter Sets and Conceptual Models on RN Transport to the LCA

A.1.0 Additional Model Simulations of the AA/VA System To Evaluate the Effects of Alternative Parameter Sets and Conceptual Models on RN Transport to the LCA

The YF/CM PRC commented that insufficient documentation was provided pertaining to calibration of the SZ AA/VA model. The PRC requested additional hydrograph comparisons, maps of residuals, and plots of residuals versus time.

Response: The modeling team has provided the following:

- Detailed comparisons of simulated/measured hydrographs for all available wells with long-term data for 15 flow simulations
- Scatterplots and residual cumulative distribution plots for 26 simulations
- Maps of residuals by decade (1960s through 2005)

Important points to note include the following:

- None of the simulations match *all* head measurements well, for many reasons clearly documented in the final report (N-I, 2013) and supplemental material provided here. Essentially, the conditions at this site are much more complex than any numerical model will ever be able to capture.
- Many of the "what-if" scenarios used for sensitivity analysis as well as "alternative" conceptual models are poorly calibrated, but they are still useful because they illustrate the impact of the assumptions on transport.
- Comparison of transport results from a subset of relatively well-calibrated models and poorly calibrated models suggests that transport results are fairly insensitive to degree of calibration. Two possible exceptions:
    - The breaching scenarios, which are all very poorly calibrated (to head data) and which predict higher mass transport than all other scenarios.
    - The 0.1-mm/yr recharge cases, which are very poorly calibrated to the Interferometric Synthetic Aperture Radar (InSAR) dataset (N-I, 2013) and which predict lower mass transport than all other scenarios.

Figures A-1a through A-1c present comparisons of measured and simulated heads for 24 cases. Nineteen of these cases are described in N-I (2013, Section 4.5.2). For these cases, all the parameters are defined in Table 4-13 of N-I (2013). Case names correspond to the set number and row number beneath "set" divisions in the table. Two additional cases, Set3_6* and Set3_1*, are slight variations of Set3_6 and Set3_1 (defined in Table 4-13), which were developed during the Supplemental Analysis and Evaluation (SAE) phase, using minor adjustments to values of porosity (N-I, 2013, Table 4-6, Case 14) and specific storage (N-I, 2013, Table 4-5, Case 2) requested by the PER. Full transport results from these cases are presented in the final report (SAE_1 and SAE_2, respectively). The three breaching cases (LBB_Case1,2, and 3), also developed during the SAE phase, are defined in Table 4-35 and Figure 4-40 of N-I (2013).

New material developed in response to the PRC request for more documentation of the SZ AA/VA system model includes the following:

- Scatterplots (simulated vs measured heads, 575 measurements)
- Histogram plots of head residuals
- Measured vs simulated hydrographs for six wells
- An analysis of the relationship between quality of calibration and transport of RNs to the LCA

The quality of the calibration indicated by the coefficient of determination (r^2) values on the figure varies widely. The breaching scenarios (LBB_Case1, LBB_Case2, and LBB_Case3 in Figure A-1c) are poorly calibrated and have r^2 values less than 0.10. Histograms of error (measured minus simulated head, in meters) are shown in Figures A-2a through A-2c for the same 24 cases. The figures indicate that the quality of the fit is highly variable. Both figures indicate that heads in the branching models (LBB_Case1, 2, and 3) significantly underestimate the measured heads.

TW-7 was drilled in the early 1950s, and water levels have been monitored periodically for more than 50 years (Figures A-3a through A-3d). Water levels responded to detonations in the area beginning in the 1960s, and elevated water levels remain to this day as a result of pore compression associated with the detonations. Transient water levels from TW-7 are among the 575 water-level measurement used in the calibration and shown in scatterplots of simulated and measured heads in Figures A-1a through A-1c. In view of its long record, hydrographs from TW-7 constitute one of the most complete records of water-level responses to nuclear testing. Figures A-3a through A-3d show that different models have varying degrees of fit to the data.

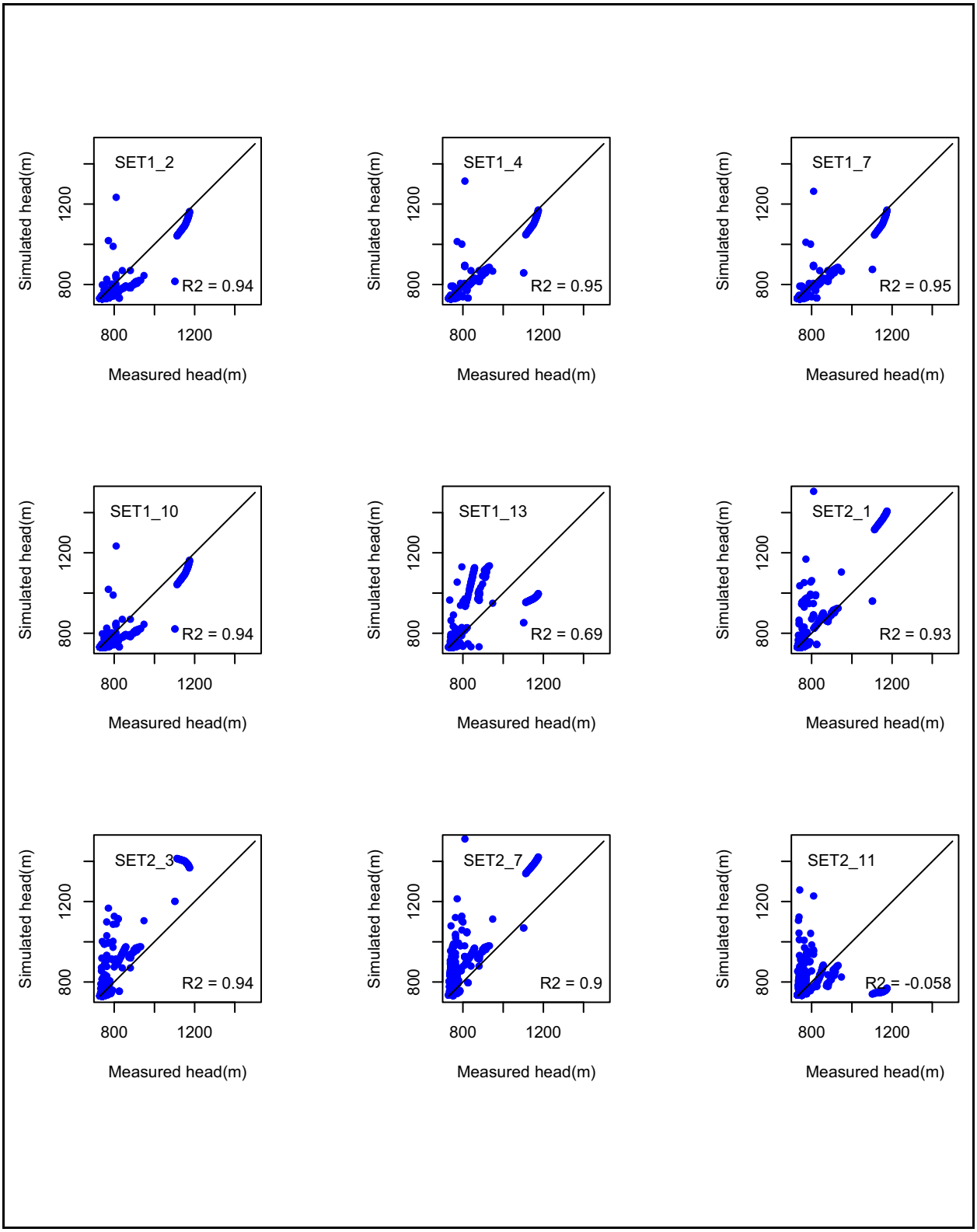

Figure A-1a
Scatterplots Showing Simulated versus Measured Heads along with the One-to-One Line and Calculated r^2 Values

Note: Case numbers correspond to case descriptions in Table 4-13 of N-I (2013).

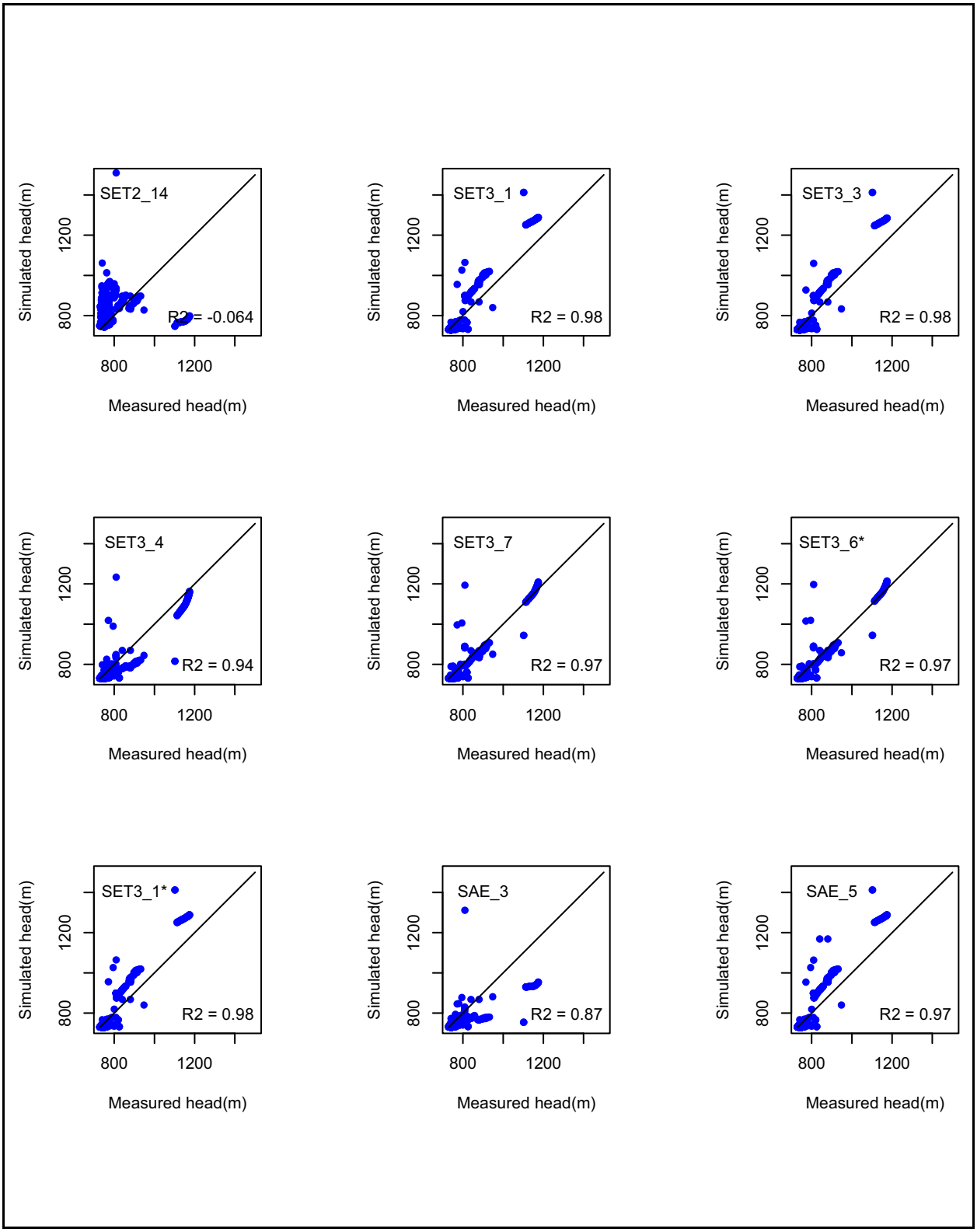

Figure A-1b
Scatterplots Showing Simulated versus Measured Heads along with the One-to-One Line and Calculated r^2 Values

Note: Case numbers correspond to case descriptions in Table 4-13 of N-I (2013).

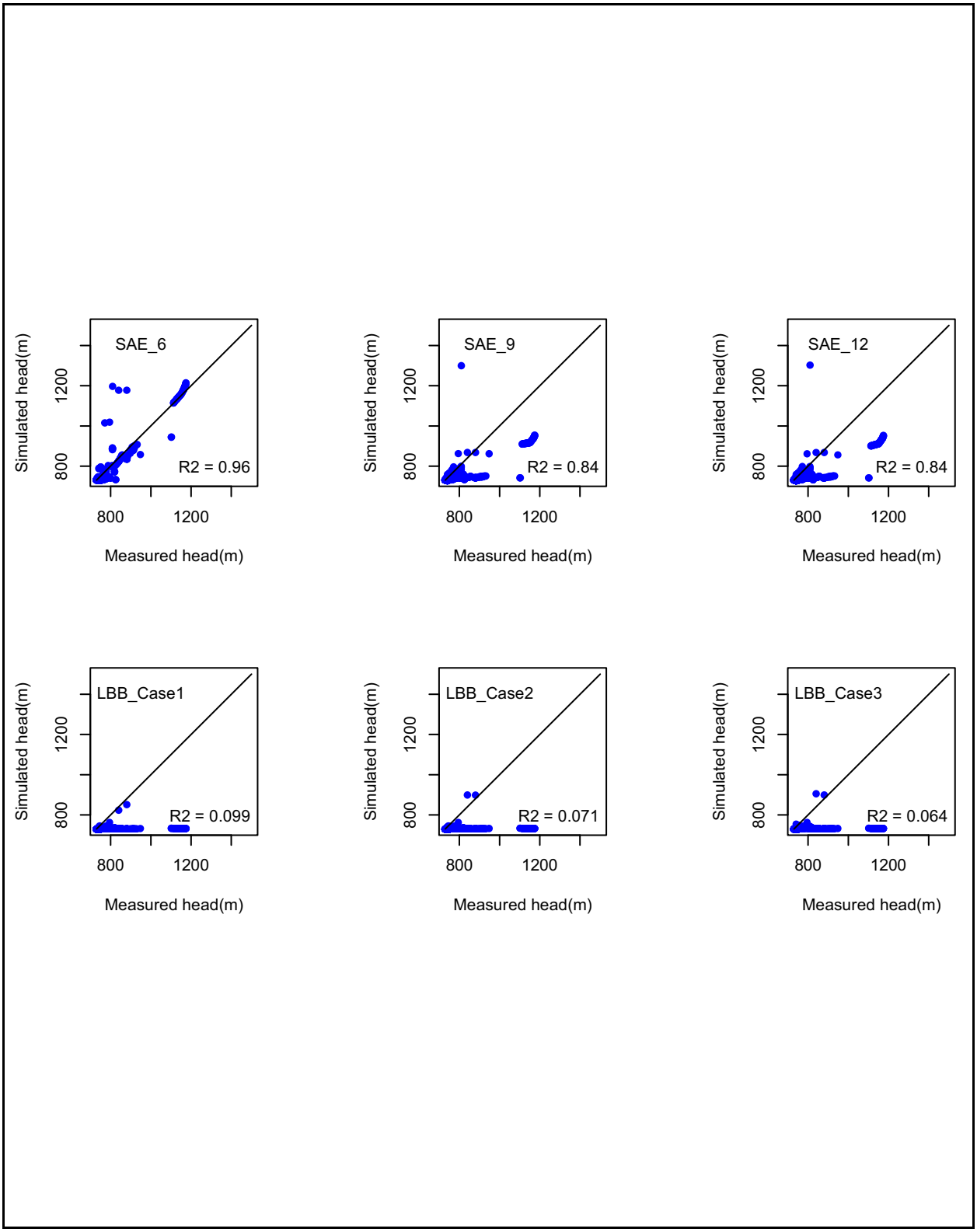

Figure A-1c
Scatterplots Showing Simulated versus Measured Heads along with the One-to-One Line and Calculated r^2 Values

Note: Case numbers correspond to case descriptions in Table 4-13 of N-I (2013).

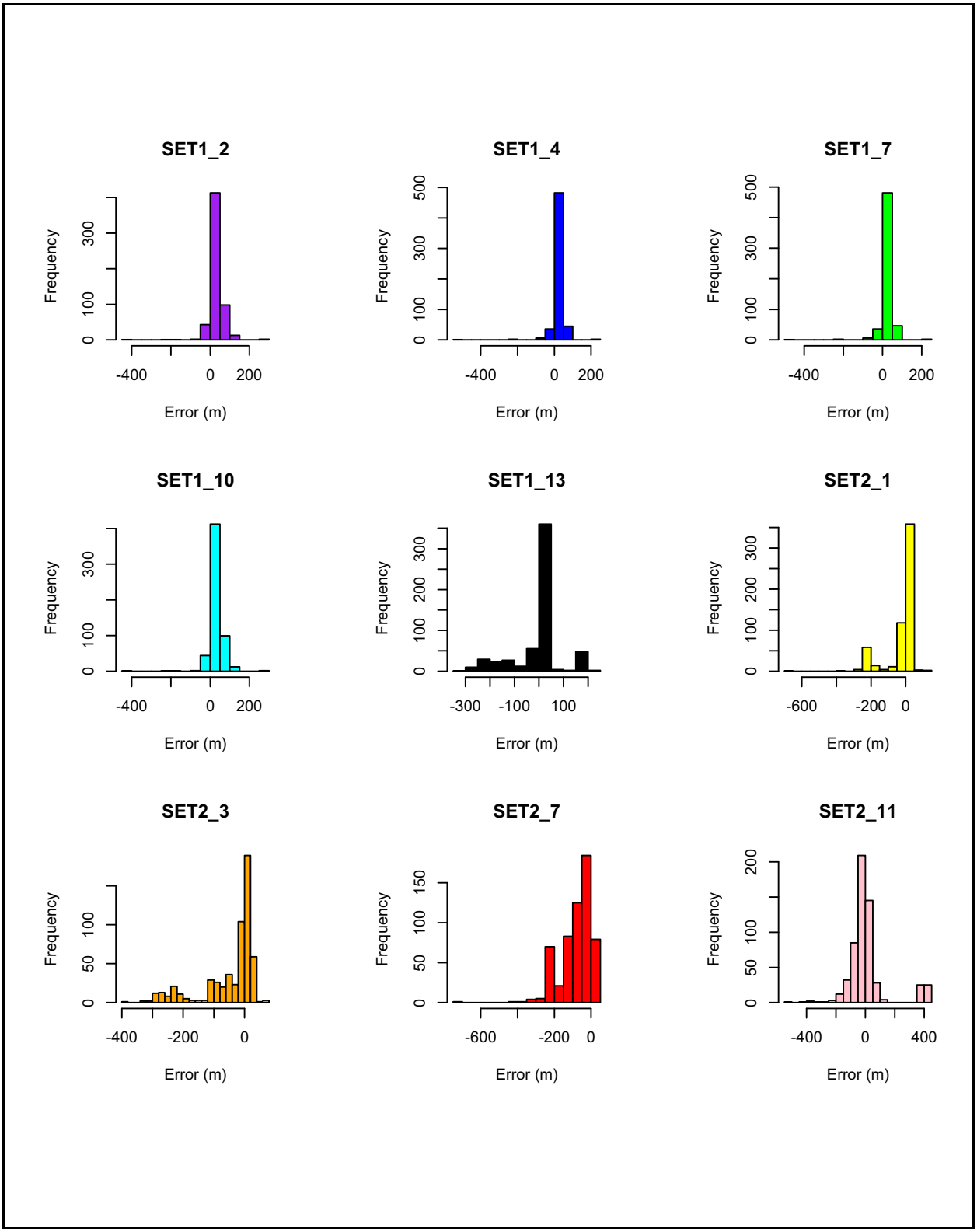

Figure A-2a
Histograms of Error (measured minus simulated heads, in meters) for 24 Simulations.
Note: Case numbers correspond to case descriptions in Table 4-13 of N-I (2013).

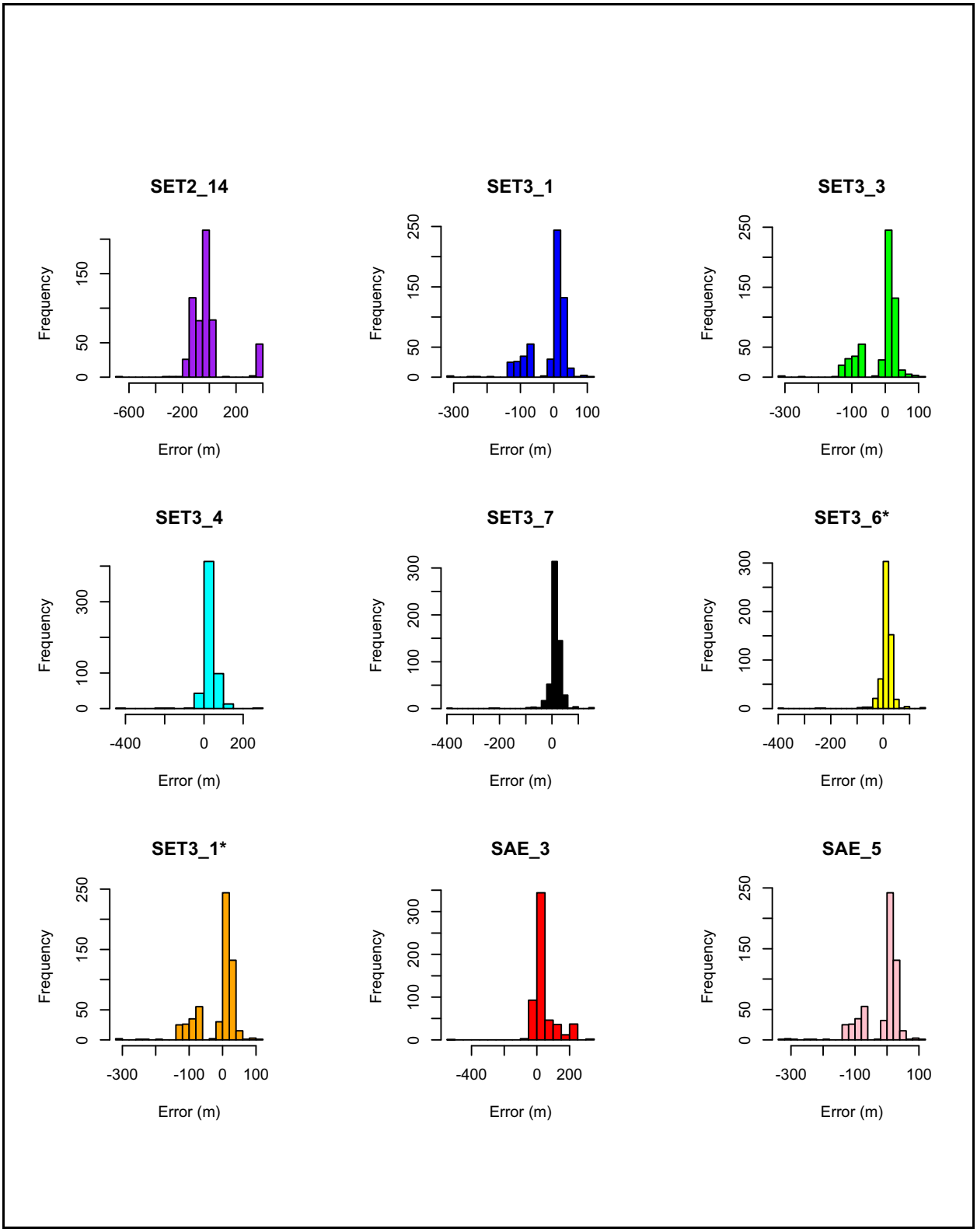

Figure A-2b
Histograms of Error (measured minus simulated heads, in meters) for 24 Simulations.
Note: Case numbers correspond to case descriptions in Table 4-13 of N-I (2013).

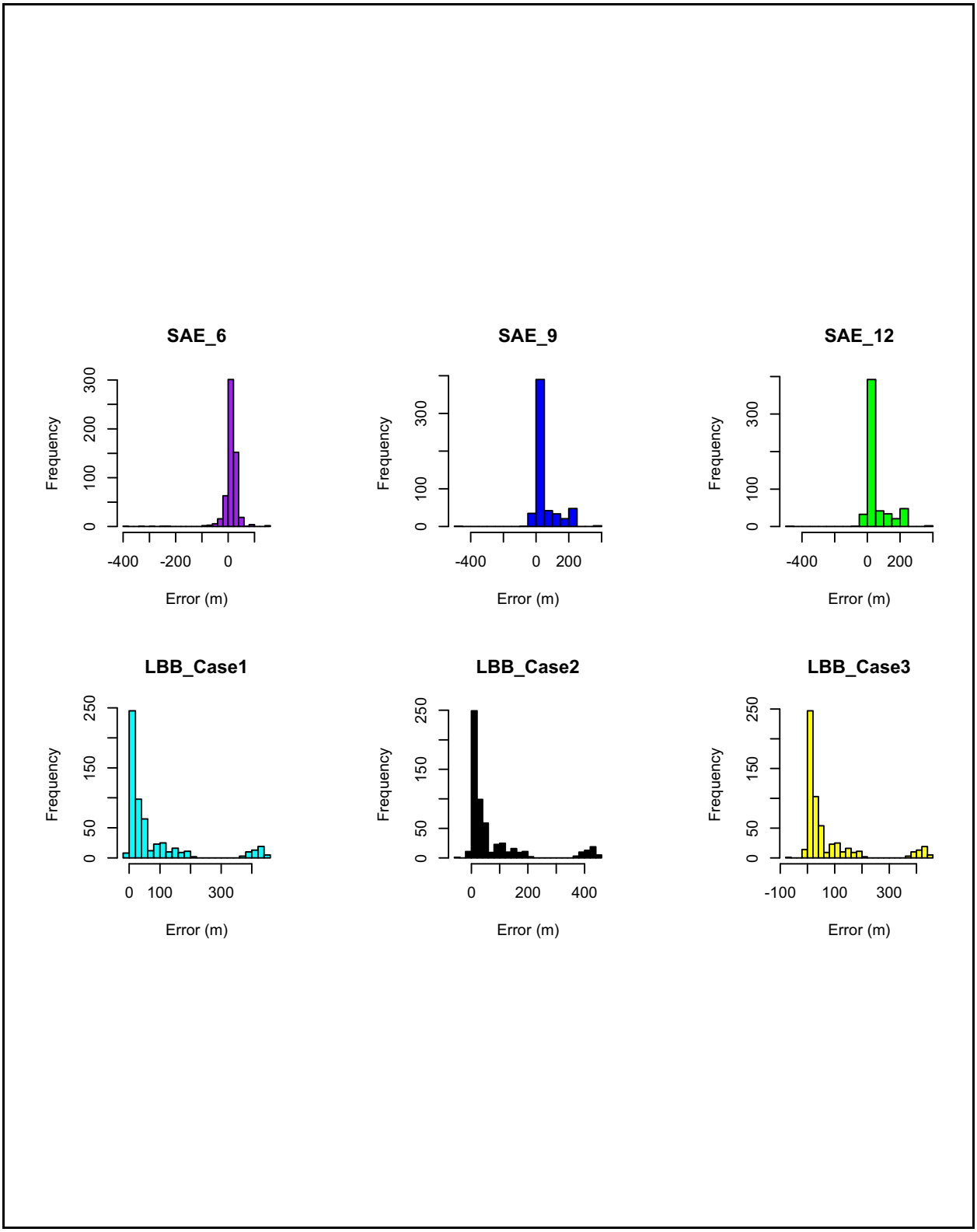

Figure A-2c
Histograms of Error (measured minus simulated heads, in meters) for 24 Simulations.
Note: Case numbers correspond to case descriptions in Table 4-13 of N-I (2013).

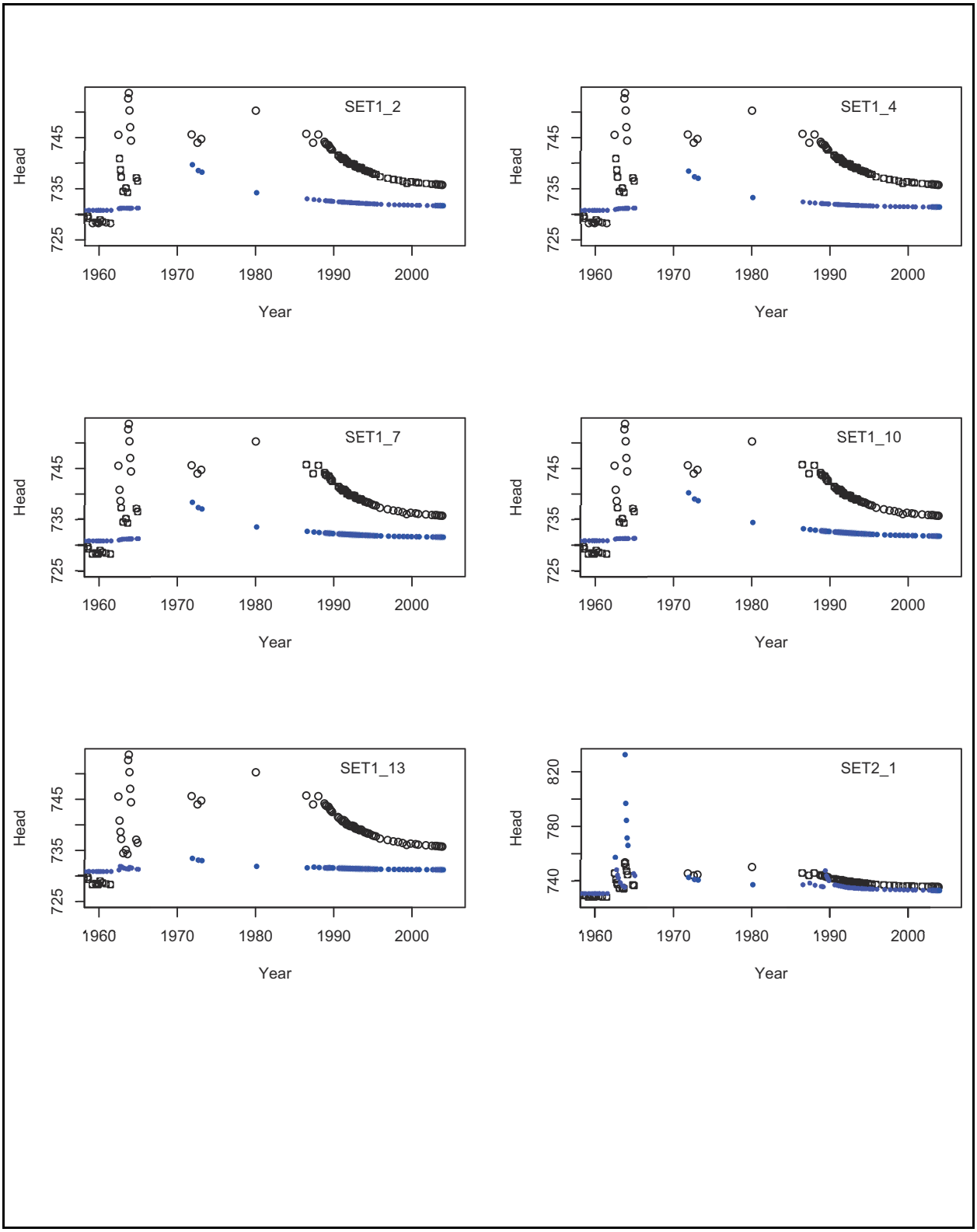

Figure A-3a
Simulated (blue circles) and Measured (black circles) Hydraulic Heads through Time at Well TW-7

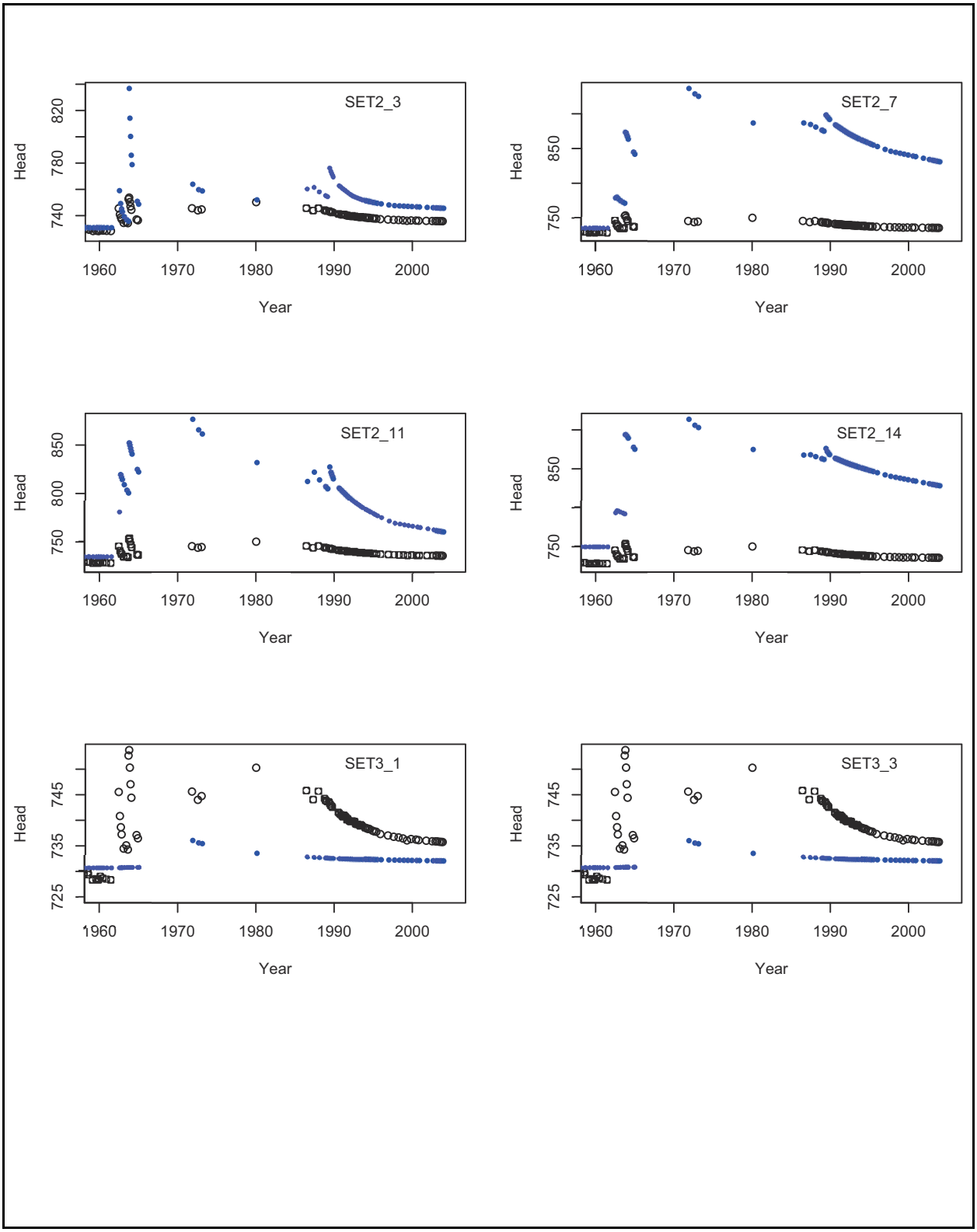

Figure A-3b
Simulated (blue circles) and Measured (black circles) Hydraulic Heads through Time at Well TW-7

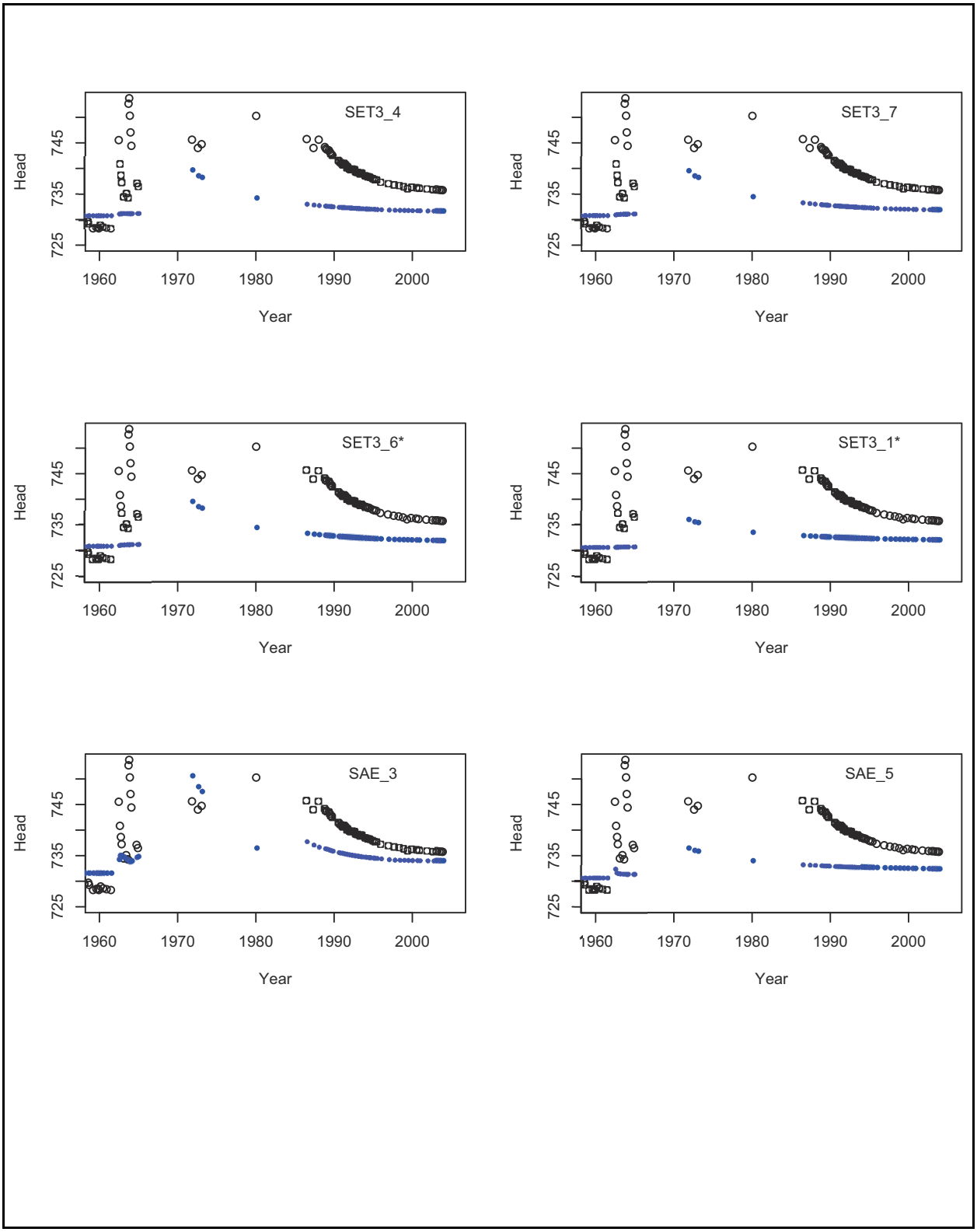

Figure A-3c
Simulated (blue circles) and Measured (black circles) Hydraulic Heads through Time at Well TW-7

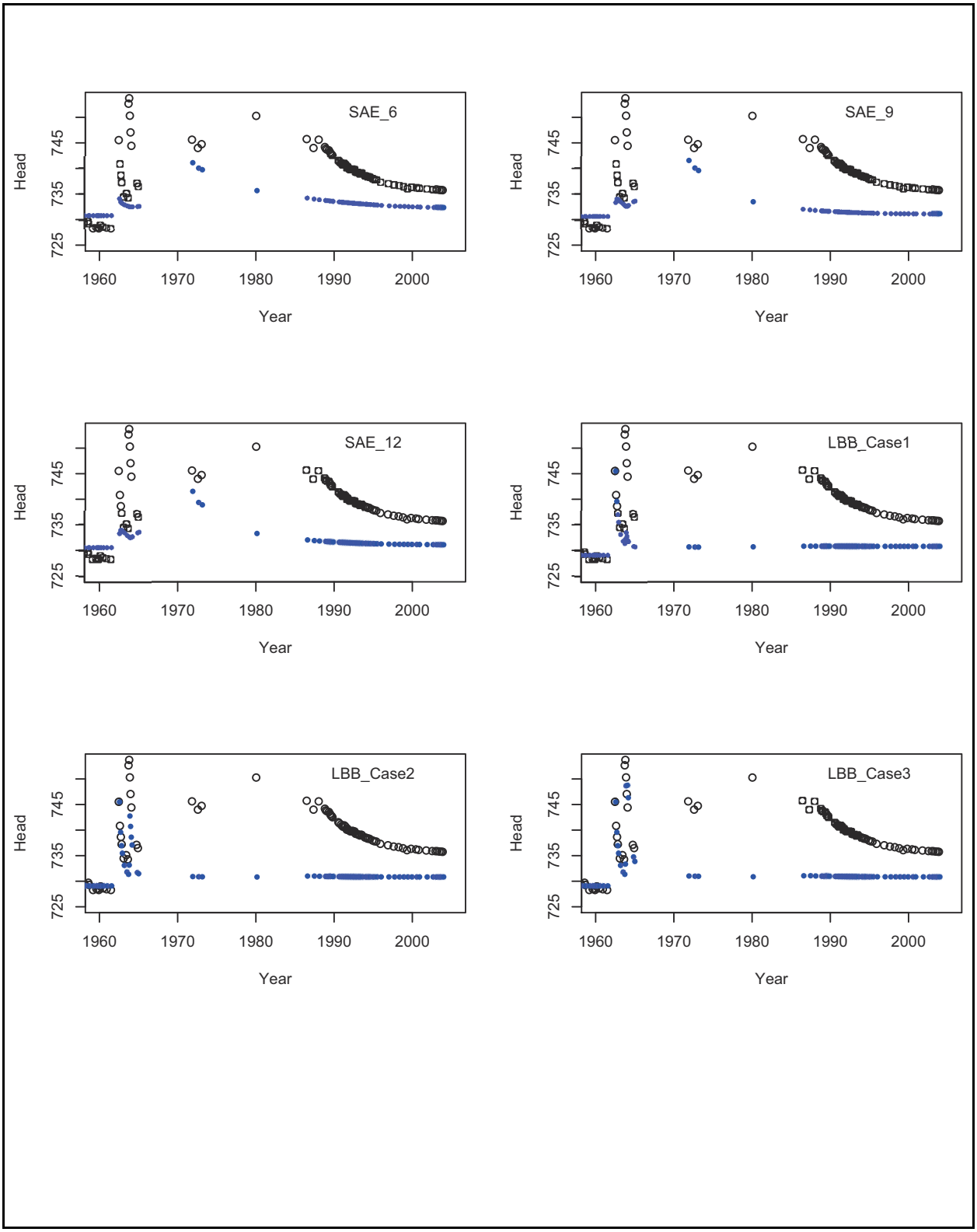

Figure A-3d
Simulated (blue circles) and Measured (black circles) Hydraulic Heads through Time at Well TW-7

Figure A-4 compares the fraction of particles reaching the LCA against the calibration correlation coefficient for all 45 cases listed in Table 4-13 of N-I (2013). The solid symbols show the percentage of particles associated with the SZ inventory that reach the LCA; the open symbols reflect the fraction of particles originally associated with the flux of UZ RNs into the model that reach the LCA. Figure A-4 indicates that the quality of the calibration indicated by the calibration correlation coefficients has very little influence on the fraction of the particles that leaves the SZ AA/VA model and reaches the LCA. It is not surprising that transport results are insensitive to the results of a calibration to hydraulic data because the parameters influencing transport (effective porosity for simple particle tracking; and effective porosity, matrix diffusion, sorption for contaminant transport) are independent of those affecting the match to the hydraulic calibration data (testing-effects model parameters, hydraulic conductivity, specific storage). Moreover, there were 178 SZ tests, each with their own testing-effects parameters, one of which (overpressurization) was assumed to be independent of other tests. Hydraulic data were available for only a relative handful of tests, leaving the testing-effects parameters relatively unconstrained for the overwhelming majority of the SZ AA/VA nuclear tests. Therefore, transport of either particles or contaminants to the LCA is dominated by assumptions regarding the nature of test-induced rock damage for the large number of unconstrained detonations. For both these reasons, the number of particles reaching the LCA from the SZ AA/VA tests was relatively independent of the quality of the calibration.

The flow and transport model was very computationally expensive (10 to 16 hours per forward run). It was also ill-posed, in the sense that model complexity exceeded the size of the dataset (hydraulic heads) available for calibration. This highly parameterized approach (Hunt et al., 2007) allowed the modeling team to effectively explore model uncertainty. However, it was impractical to calibrate all model scenarios of interest, and thus goodness of fit to model calibration data cannot be used to screen models to determine their feasibility. The results in Figure A-4 should be viewed primarily as a sensitivity analysis. An assessment of a model's plausibility would have to be made on the basis of other considerations not included in the calibration dataset, such as the presence of absence of ^{3}H in the LCA beneath the detonation, or the consistency of the models with InSAR data.

The InSAR dataset provided detailed measurements of ground surface subsidence related to depressurization of the saturated volcanic rocks during three discreet time periods, all after the end of testing. Transient flow simulations of the saturated volcanic systems have been able to reproduce the magnitude and spatial variability of the subsidence (Halford, 2005; Keating et al., 2010). The

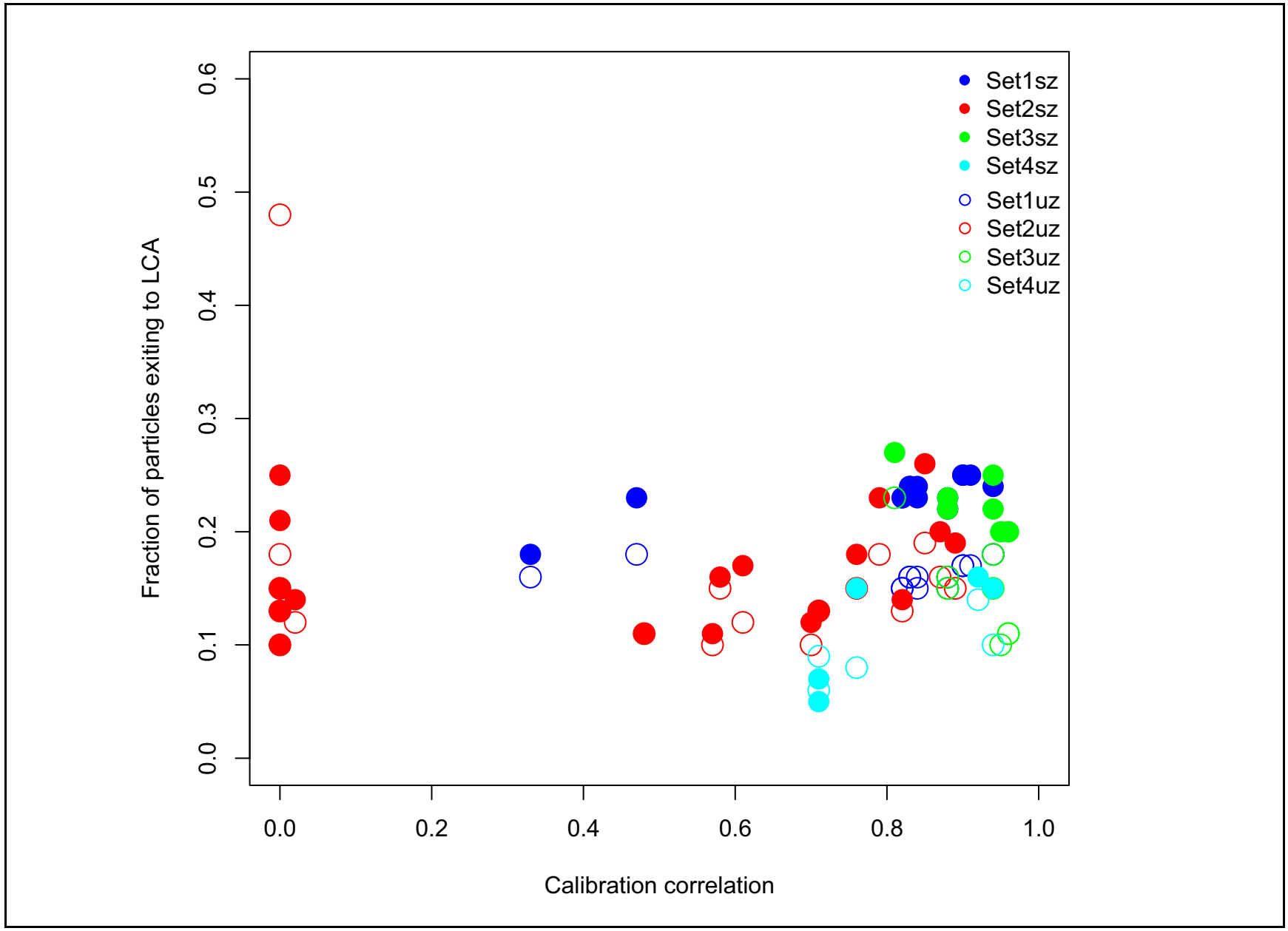

Figure A-4
Plot Showing the Fraction of Particles Reaching the LCA from SZ Sources (solid circles) and UZ Sources (open circles) as a Function of the Calibration Correlation Coefficient

subsidence data can also be used to directly calculate the amount of water leaving the system during post-testing depressurization. These estimates were reported for each of the three time periods in Table 4-2 (N-I, 2013), and were directly compared to outflow fluxes from all the volcanic flow models summarized in Figures A-3a through A-3d. The InSAR-based flux estimates were not used in the calibration process. The comparisons were presented in Table 4-12 (N-I, 2013). A number of the simulations were quite close to the measured values, easily within a factor of 2 or 3. A few of the simulations significantly overestimate the amount of testing-induced water charge by slightly more than an order of magnitude. These runs either are highly overpressurized (case C in Figure 4-13, N-I, 2013) or have reduced permeability of the fault zones, compared to the base case. The case C overpressurization runs were not propagated to the transport simulations. The "low fault" permeability runs were shown later to propagate very little radionuclide flux to the LCA, despite the apparent overestimate of testing-induced water flux. The very low background infiltration rates cases (0.1 mm/yr) all significantly underestimate testing-induced flux of water to the LCA. The very low permeabilities and the very low specific storage values required to calibrate the model for these very low infiltration rates are contributing factors.

Figure A-5 shows an example of how residuals change spatially over time for one of the better-calibrated models in the ensemble (SET3_7, $r^2 = 0.97$). Residual plots are shown by decade beginning in 1960 and extending until 2010.

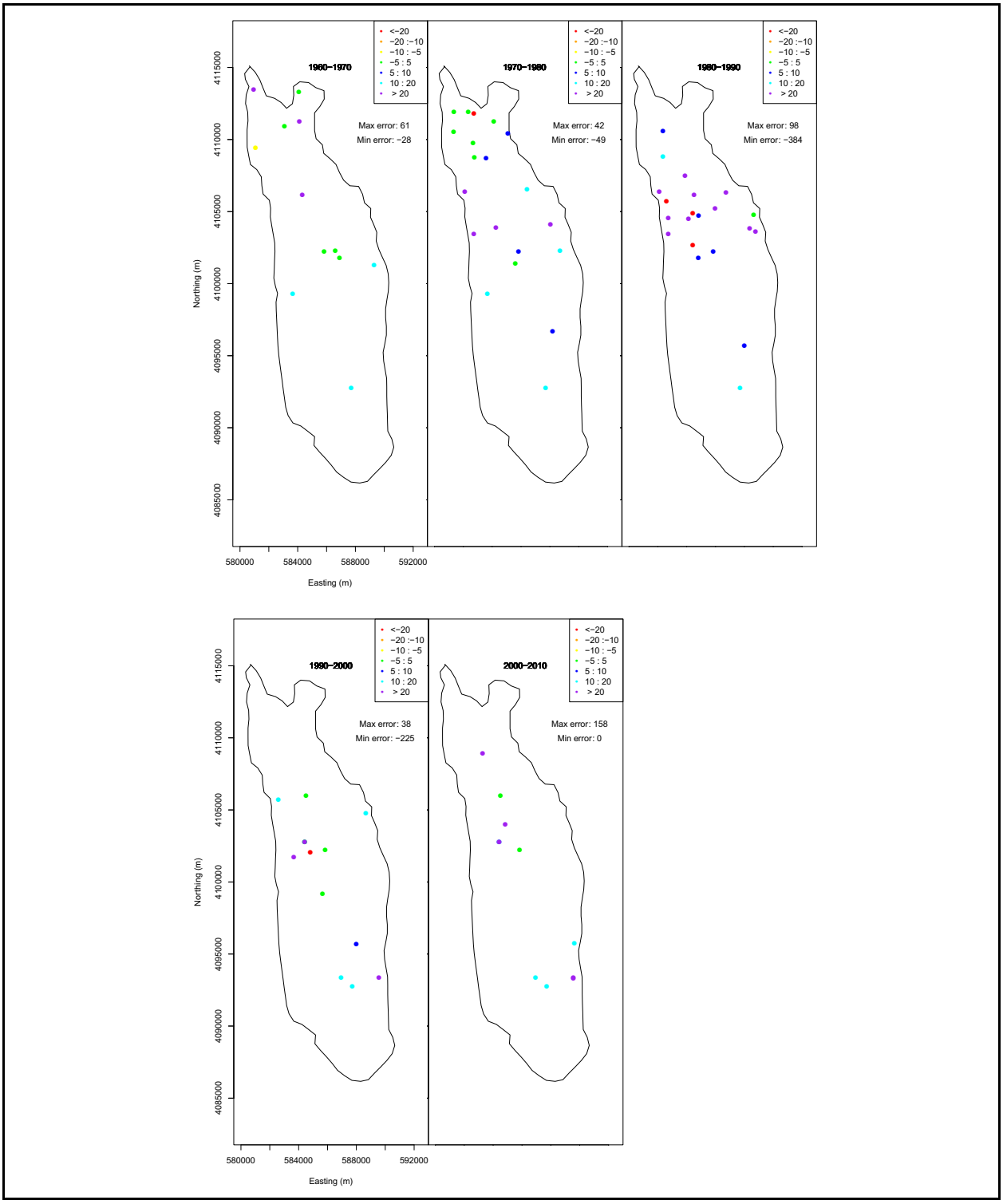

Figure A-5
Spatial Plot of Head Residuals (measured minus simulated) as a Function of Time for Model Run SET3_7 (r^2 = 0.97)

Note: The inset for the decade 1960 through 1970 shows the scatterplot of simulated versus measured heads for this case.

A.2.0 REFERENCES

Halford, K.J., R.J. Laczniak, and D.L. Galloway. 2005. *Hydraulic Characterization of Overpressured Tuffs in Central Yucca Flat, Nevada Test Site, Nye County, Nevada*, Scientific Investigations Report 2005-5211. Carson City, NV: U.S. Geological Survey.

Hunt, R.J., J. Doherty, and M.J. Tonkin. 2007. "Are Models Too Simple? Arguments for Increased Parameterization." In *Ground Water,* Vol. 45(3): pp. 254-262.

Keating, E.H., J. Doherty, J.A. Vrugt, and Q. Kang. 2010. "Optimization and Uncertainty Assessment of Strongly Nonlinear Groundwater Models with High Parameter Dimensionality." In *Water Resources Research,* Vol. 46: W10517. Washington, DC: American Geophysical Union.

N-I, see Navarro-Intera, LLC.

Navarro-Intera, LLC. 2013. *Phase I Flow and Transport Model Document for Corrective Action Unit 97: Yucca Flat/Climax Mine, Nevada National Security Site, Nye County, Nevada*, Rev. 1, N-I/28091-080. Las Vegas, NV.

Appendix B

Analysis of Low-Level ^{3}H Observations and Possible Sources

B.1.0 Analysis of Low-Level ^3H Observations and Possible Sources

In this appendix, ^3H and water-level data are discussed for Wells TW-B, WW-A, WW-3, UE-6d, and UE-6e. Possible sources of the low ^3H levels observed at each of these wells are discussed, and numerical models are presented to support the interpretations in the cases of WW-A and WW-3.

B.1.1 TW-B

TW-B is located at UTM North American Datum (NAD) 27 Easting of 587779.9 m and a UTM NAD 27 Northing of 4092815.9 m. It was drilled to a depth of 1,675 ft and completed on June 14, 1961, with four openings between 1,432 and 1,675 ft. The saturated part of the well is open to volcanic rocks including 170 ft of densely welded tuff. Five nuclear tests, all above the water table, were detonated within 1.6 km of TW-B. The nearest detonation to TW-B is PRESIDIO (UTM NAD 27 Easting = 588,591.4 m, UTM NAD 27 Northing = 4,093,261.8 m), which is 926 m away from TW-B. PRESIDIO was detonated in hole U6d on April 22, 1987 (NNSA/NFO, 2015) and had its working point in the TM-LVTA. The detonation has a 2 R_c exchange volume that comes within 64 m of the water table. More distant nuclear detonations took place above the tuffs in the overlying AA.

^3H has been measured at TW-B since 1976 (Lyles, 1990) (Figure B-1). The ^3H measurements prior to 1990 are well above zero given the small reported errors that average about 11 pCi/L. The TW-B pre-dates the PRESIDIO detonation by at least a decade, so PRESIDIO could not have been the source of the ^3H prior to 1987. No tests within 1 mi occurred before the first elevated ^3H measurements made in 1976.

Recent (May 20, 2015) measurements at TW-B showed that there was no ^3H in the well (<2.84 pC/L) which is consistent with the declining concentration trends since the late 1980s evident in Figure B-1. Lyles (1990) suggested that the ^3H at TW-B originated from surface water that infiltrated into the cracks that opened in Yucca Lake playa in 1969. The crack extended about 1.8 km, averaged about 2 to 5 centimeters wide, and was estimated to have extended 365 to 610 m deep (Lyles, 1990, p. 9). Doty and Rush (1985) estimated from flume experiments that about 140,000 cubic meters of water

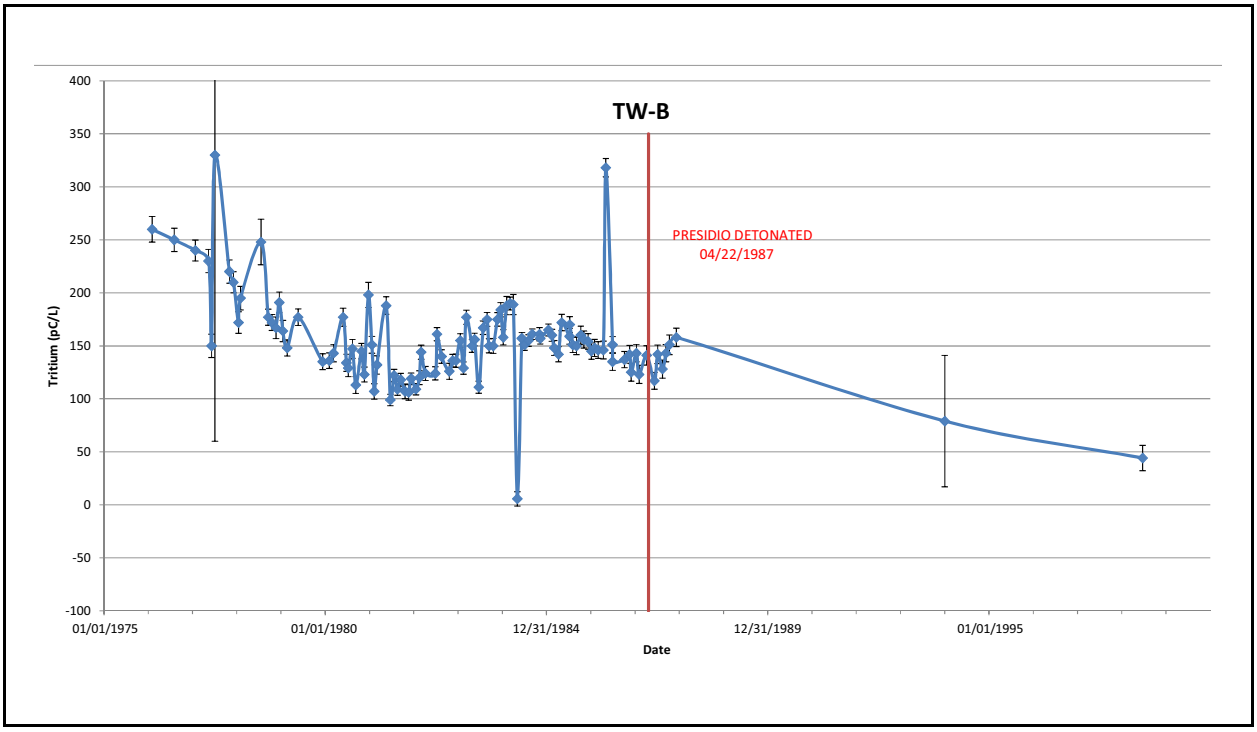

Figure B-1
^{3}H Measurements at TW-B Relative to the PRESIDIO Detonation
Note: Error bars represent the reported measurement errors.

flowed into the crack between October 1974 and August 1977. However, the amount of water that flowed into the crack in the years before the site was instrumented (1969 to 1974) is not known. Doty and Rush (1985, Figure 2) also indicate that between 1960 and 1966 an earlier crack existed north of the crack that developed in 1969. All the cracks have since filled with sediment, although open sinkholes along the projected extension of the 1969 crack exist northeast of the playa (Drellack, 2015). The fine-grained nature of the playa sediments suggests that deep infiltration does not occur through the playa after ponding events under normal conditions, when the playa does not have open cracks. This was verified when UGTA personnel penetrated the playa sediments with shovels on August 13, 2014 (following nine days of ponding after an August 4, 2014, rainfall event), and observed that the moisture front had penetrated only the playa sediments to a depth of about 4 inches (Drellack, 2014).

TW-B is about 0.75 km from the northern edge of the playa and could have been affected by subsurface flow originating from recharge into the cracks in Yucca Lake playa, which floods periodically following storms. Although data in this part of Yucca Flat are sparse, interpretations of pre-development hydraulic heads in the shallow AA/VA suggest that shallow groundwater moves

north from Yucca Lake playa (Fenelon et al., 2012, Plate 3). Even in the absence of local atmospheric ^3H sources at the NTS following atmospheric tests, which continued until mid-1962 with LITTLE FELLER I (July 17, 1962), global concentrations of ^3H at mid-latitudes in the 1960s would have been as high as 1,000 pCi/L (Rozanski et al., 1991). Thus, global atmospheric concentrations alone are sufficiently high to explain the groundwater ^3H concentrations of several hundred pCi/L measured at TW-B a decade later.

However, considerable doubt exists around this interpretation due to the fact that the well has low transmissivity (50 ft^2/day) and the cracks are not oriented in a way that would facilitate transport from the playa to TW-B. Flow from the playa 0.75 km north to TW-B would require velocities of about 150 m/yr, which is not supported by the low transmissivity of the well. Lyles (1993) discussed well conditions (well annulus cemented to the bottom of the casing at 510 m depth, mud diesel fuel, and drill bits at the bottom of the well) that make it clear that the well was never cleaned out and that the ^3H was probably introduced during drilling. The overall declines in ^3H concentrations over time are consistent with radioactive decay of a relatively immobile slug of tritiated groundwater near the well.

In conclusion, although no completely satisfactory explanation exists regarding the origin of ^3H at TW-B, recent (2015) samples indicate that the current ^3H levels are below detection and that the earlier detections were not the leading edge of a larger plume migrating toward TW-B.

B.1.2 WW-A

WW-A was completed in the AA on September 5, 1960, to a depth of 1,870 ft. It contains three openings between depths of 1,555 and 1,870 ft. WW-A was pumped for water supply between 1960 and 1988 (Figure B-2), with an estimated total withdrawal of 882 million gallons (Mgal). Many of the annual withdrawals, however, are estimates based on NTS activities being done at the time. Water levels were measured intermittently at WW-A (Figure B-3).

B.1.2.1 Hydraulic and Contaminant Data

Elliott and Fenelon (2010) described the water-level fluctuations as follows:

> *Well WW-A (1870 ft) represents hole WW-A after it had reached a total depth of 1,870 ft and was completed as a supply well. The saturated part of the well is open to about 270 ft of alluvium consisting of poorly sorted silt, sand and gravel. The well was used as*

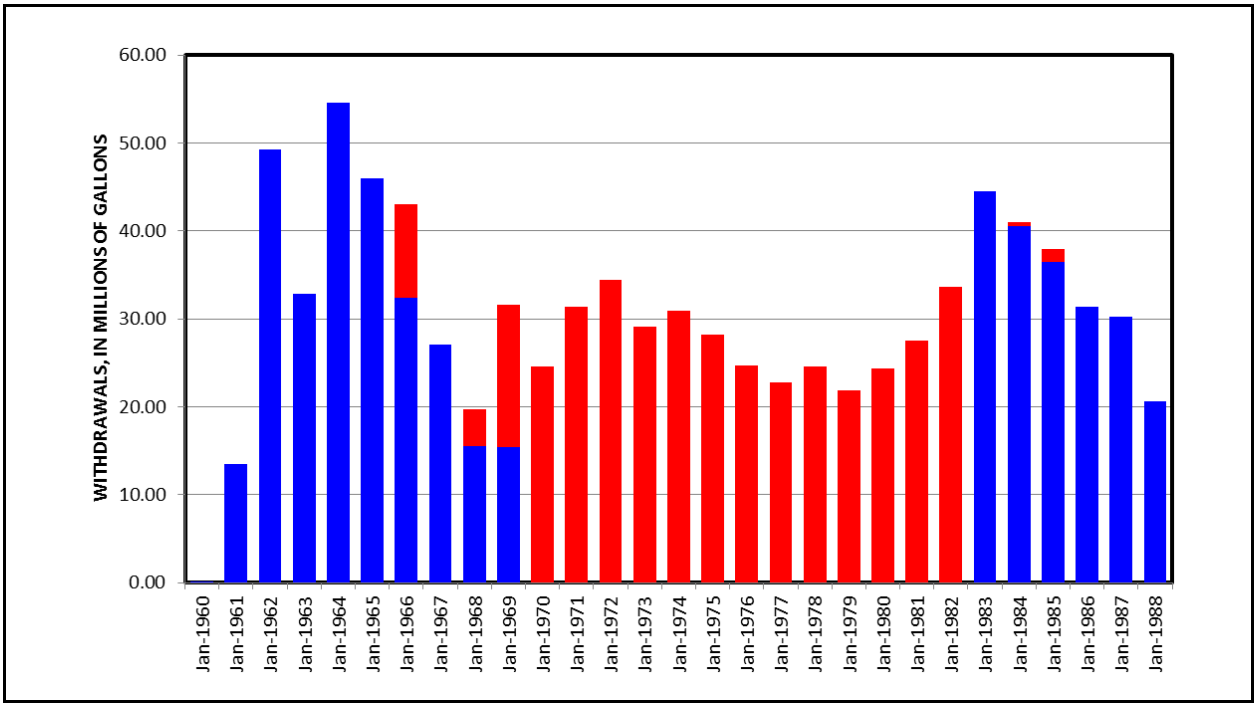

Figure B-2
Estimated Annual Water Withdrawals from WW-A in Gallons
(from Elliott and Moreo, 2011)

Note: Blue are measured values; red are estimated values.

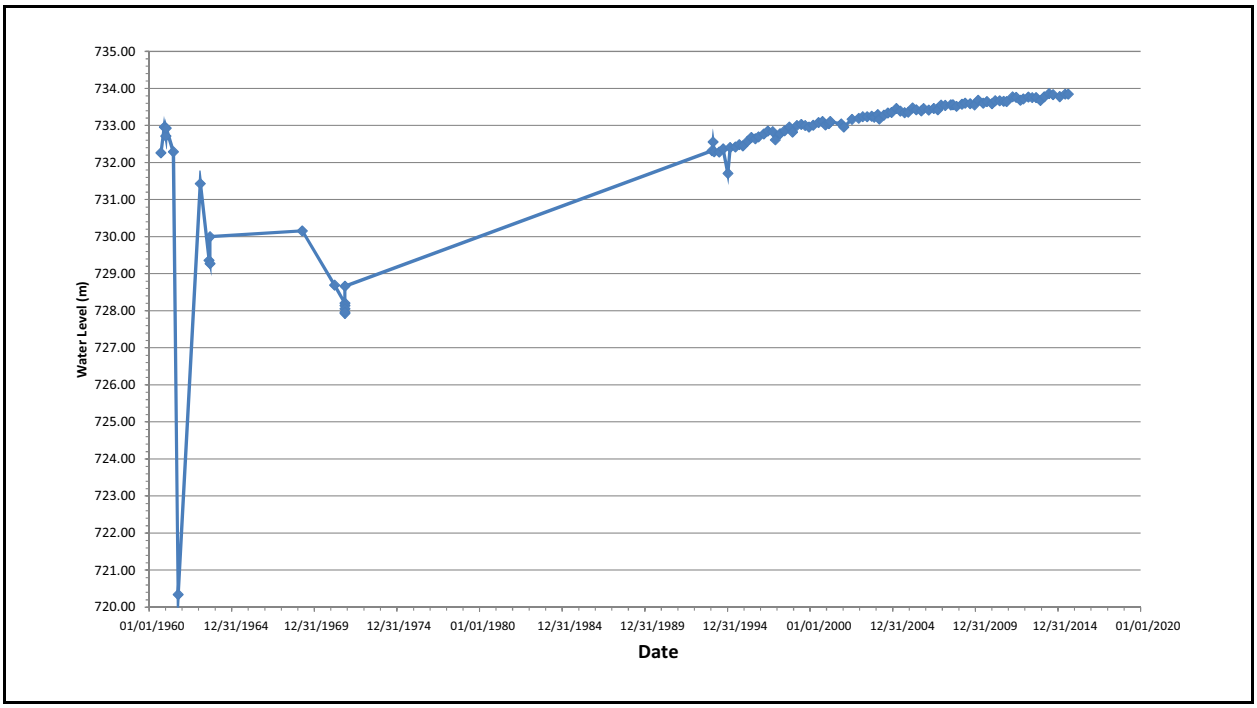

Figure B-3
Measured Water Levels at WW-A in Meters Above Mean Sea Level

a supply well beginning in October 1961 and was pumped through 1988, with an estimated total of about 880 Mgal of water withdrawn. The initial five water levels are pre-pumping levels and are considered representative of steady-state conditions in the alluvial aquifer. With the exception of one suspect measurement, water levels from 1994 to 2014 have been steadily rising and currently are about 3 to 5 ft higher than 1961 pre-pumping levels. Although higher, these rising water levels are interpreted as representative of transient conditions, as water levels equilibrate from past pumping. The reason that pre-pumping levels are lower than current transient levels is unknown, but might result from measurement inaccuracies, an undocumented measuring-point shift, or pre-pumping levels that were depressed as a result of well construction and development.

The rising trend and current (2014) water-level altitude (2,408 ft) are similar to water levels in the nearby Well ER-3-2-2 (middle). Seventy-two nuclear tests, two near or below the water table, were detonated within 1 mi of WW-A (1,870 ft). The closest test near or below the water table was 1,700 ft away. Water levels are corrected for borehole deviation.

^{3}H data from WW-A (Figure B-4) include data reported by Lyles (1990), sampled by Desert Research Institute between 1972 and 1987; and data collected by the UGTA Activity between 1994 and 2012. Reported errors are shown as error bars. The ^{3}H data from the 1970s and 1980s show a gradual increase in ^{3}H concentrations over that time period. Samples taken in 1994 and 2000 were below their detection thresholds of 297 and 9.9 pCi/L, whereas all samples taken since 2001 had ^{3}H values well above their detection thresholds. ^{3}H concentrations have showed an overall decline since the early 2000s.

Lyles (1990) noted the increase in ^{3}H at WW-A in the late 1980s and attributed it to RN migration from the HAYMAKER detonation induced by pumping from WW-A. HAYMAKER was detonated on June 27, 1962, in alluvium about 82 m above the water table approximately 530 m north of WW-A. However, with an R_c of 52 m, it had an estimated 2 R_c exchange volume that would extend about 22 m below the water table, thereby making it a plausible source for the ^{3}H measured at WW-A (cavity dimension based on maximum announced yield [NNSA/NFO, 2015] and Equation 1 in Pawloski [1999]).

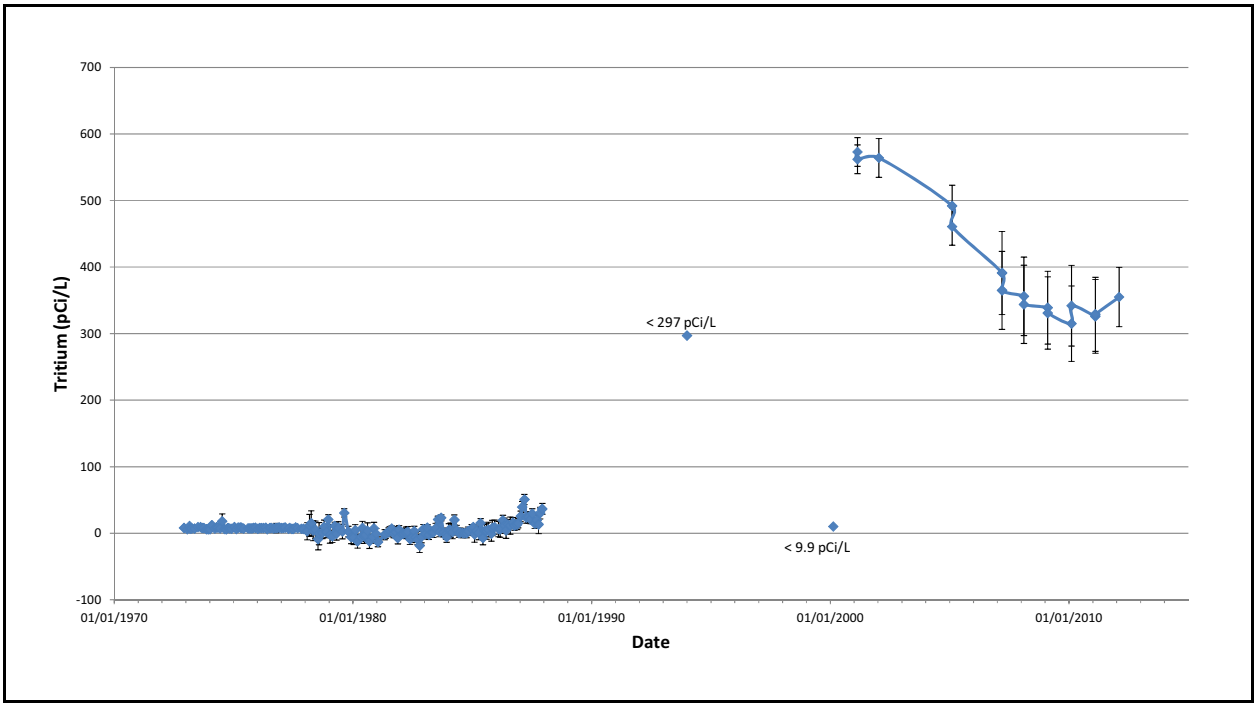

Figure B-4
Measured ^{3}H Concentrations at WW-A

A set of numerical simulations was performed to investigate whether pumping from WW-A could have induced RNs from the HAYMAKER detonation to migrate to WW-A within about 30 years and determine the combination of hydraulic and transport parameters that are consistent with this interpretation.

First, a calibration using PEST was performed to determine the hydraulic parameters using the pumping history as the driving mechanism for flow and observed water-level changes at WW-A as calibration targets. The hydraulic parameters were estimated with a two-dimensional (2-D) radially symmetric mesh centered on WW-A. Then, the estimated hydraulic parameters and their uncertainty are then assigned to the alluvium in a three-dimensional (3-D) mesh to determine whether particles from the intersection of the 2 R_c exchange volume and the water table could migrate to WW-A in under 30 years (approximately 1992).

B.1.2.2 WW-A Model Calibration

Attempts to calibrate a 2-D radially symmetric model of WW-A using the measured hydraulic heads at WW-A and the groundwater withdrawals at WW-A from Elliott and Moreo (2011) were unsuccessful because most of the pumping withdrawals were estimated and not measured

(Figure B-2). However, it was possible to use the recovery data from the post-1988 period along with the Cooper-Jacob graphical technique (Cooper and Jacob, 1946) to estimate a hydraulic conductivity (K) for the alluvium of 0.14 m/day (log K = -0.85 m/day) assuming an effective aquifer thickness of 119 m (Halford, 2016). This value of K corresponds to a permeability (k) of 1.7×10^{-13} m^2. The hydrologic data for Yucca Flat (SNJV, 2006, Table 6-1) indicate a mean pumping hydraulic conductivity for the alluvium of log K = -0.13 ±0.93 m/day, so the K value at WW-A estimated by Halford (2016) suggests a pocket of low-permeability material in the vicinity of the well.

B.1.2.3 WW-A Model Domain

A 3-D numerical model of the HAYMAKER detonation site and pumping well WW-A was built in order to determine whether elevated ^{3}H measured in WW-A can be explained by the introduction of ^{3}H into the groundwater flow system from the HAYMAKER test. Particle tracking with the *sptr* macro of FEHM was also used to simulate the movement of ^{3}H from HAYMAKER to WW-A.

A 2,000 m × 2,000 m × 298 m grid was built using GRIDDER software to simulate the local, 3-D groundwater flow system and particle transport at WW-A. The grid has 50-m grid spacing in most of the mesh, with increasing finer discretization in the 250 m in the x and y directions near the WW-A pumping well. The well is located at the center of the domain (1,000 m, 1,000 m). The grid has 10-m spacing between the bottom of the domain (435 m elevation) to 700m, and 3-m spacing between 700 m and the top of the model (733 m). The grid has 216,513 nodes and 204,800 elements.

The pumping well is screened from 650 m (above mean sea level [amsl]) to the water table surface (733.0 m amsl), with the pumping rate varying with the reported monthly average. Only the AA unit is pumped by the WW-A well, so it was the only hydrologic unit included in the model. The system is modeled as a confined aquifer with the top of the model equal to the water table elevation of 733 m. Because local flow gradients are uncertain in this data-sparse area, no regional gradient was assigned to the model. Fenelon et al. (2012, Plate 3) indicate a small northward hydraulic gradient exists near WW-A, which would offset the flow between WW-A and HAYMAKER induced by pumping. Conversely, the SZ AA/VA model uses heads mapped on to the base of the model from the LCA and has flow toward the south in this area (N-I, 2013).

A disk-shaped source area for the particles was used to simulate the area of ^{3}H release from the HAYMAKER test. The HAYMAKER detonation resulted in a cavity with an estimated radius (R_c) of

52 m. (Cavity dimension based on maximum announced yield [NNSA/NFO, 2015] and Equation 1 in Pawloski [1999].) The exchange volume for gas dispersal is approximated by a sphere with a radius of $r = 2.0\ R_c$. For this test, the $2.0\ R_c$ exchange volume extends 22 m below the water table, which could explain the introduction of elevated ^3H in the groundwater system. The part of the exchange volume beneath the water table was approximated by a disk of similar dimensions using Equation (B-1) to calculate the radius of the disk (Figure B-5):

$$a = [h(2r - h)]^{0.5} \qquad (B\text{-}1)$$

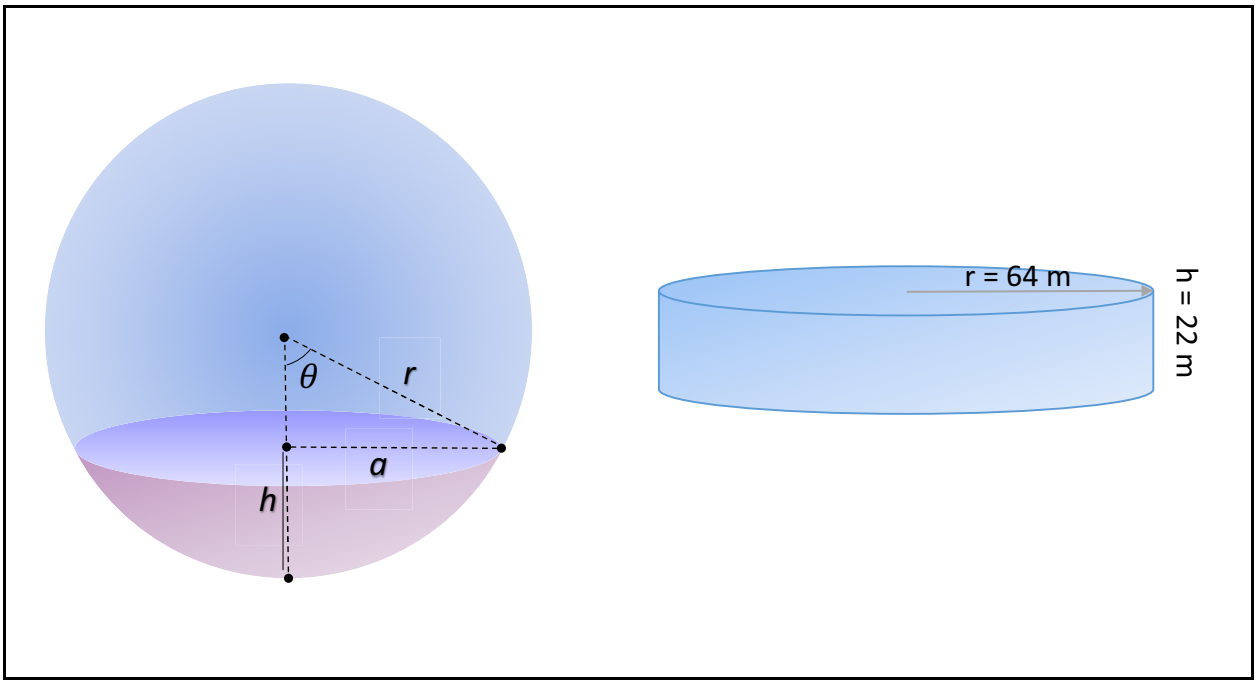

Figure B-5
Relation between the Cap of a Sphere and a Disk of an Equivalent Volume

Given that the radius of the exchange volume ($r = 2.0 * R_c = 104$ m) and the height of the cap ($h = 22$m) are known, it is straightforward to determine the radius of simplified disk ($a = 64.0$ m). The disk for releasing the particles is centered 513 m south of WW-A at local coordinate X = 1,000 m, Y = 487 m, and Z = 733 m (because no regional flow gradient is assumed, the location of HAYMAKER in the model either north or south of WW-A is not important).

B.1.2.4 3-D Transport Simulation with Particle Tracking

Elevated levels of ^3H were measured at WW-A between 1994 and 2005, after pumping at WW-A ceased. It is speculated that the ^3H is the result of the HAYMAKER test, the closest test to WW-A,

located about 531 m north of WW-A. The particle tracking capability in FEHM (sptr) was used to track particles emplaced in the groundwater flow system at the water table beneath the HAYMAKER test. In the discretized numerical model, 10,000 particles were released in a disk (discussed in Section B.1.2.3) with a radius of 64.0 m and thickness of 25 m. The initial gradient of the flow system was flat (head = 733 m) and was influenced only by the transient pumping rate; steady-state flow directions near WW-A were ambiguous, and steady-state flow was assumed to be negligibly small compared to flow rates induced during pumping. Particle breakthrough at pumping well WW-A was recorded for a qualitative comparison with the measured ^{3}H breakthrough.

Numerical simulations were run for three values (Table B-1) of permeability, porosity, and dispersivity, yielding a total of 27 transport model runs. All values are reasonable for alluvium in Yucca Flat based on data in SNJV (2006, Table 6-1), although the Halford (2016) analysis indicates that the permeability near WW-A is closer to the lower end of the permeability range used in this sensitivity analysis.

Table B-1
Parameter Values Used in Particle Tracking Simulations for WW-A

Parameter	Low	Mid	High
Permeability (m^2)	1.0×10^{-13}	1.0×10^{-12}	1.0×10^{-11}
Porosity (-)	0.2	0.3	0.4
Dispersivity (m)	25.0	50.0	100.0

A constant value of specific storage (approximately 1.0×10^{-06} m^{-1}) was assigned to all 27 simulations. This value may be on the low side based on summary data for alluvium specific storage values listed in SNJV (2006, Table 6-7).

The results from the particle tracking simulations show the importance of including an appropriate dispersivity (α) value in the simulations (Figure B-6). Initially, dispersion was not included in the particle tracking, and no particles arrived at the pumping well within the first 30 years. For α values of 50 m or 100 m, particles did arrive at the pumping well within the first 30 years, corresponding to a period in the late 1980s during which ^{3}H was actually observed to increase at WW-A (Figure B-4). Smaller values of dispersivity (α = 25 m) resulted in small numbers of particle breaking through at 40 years (roughly the year 2002) and beyond, but not during the initial rise in ^{3}H in the late 1980s noted by Lyles (1990).

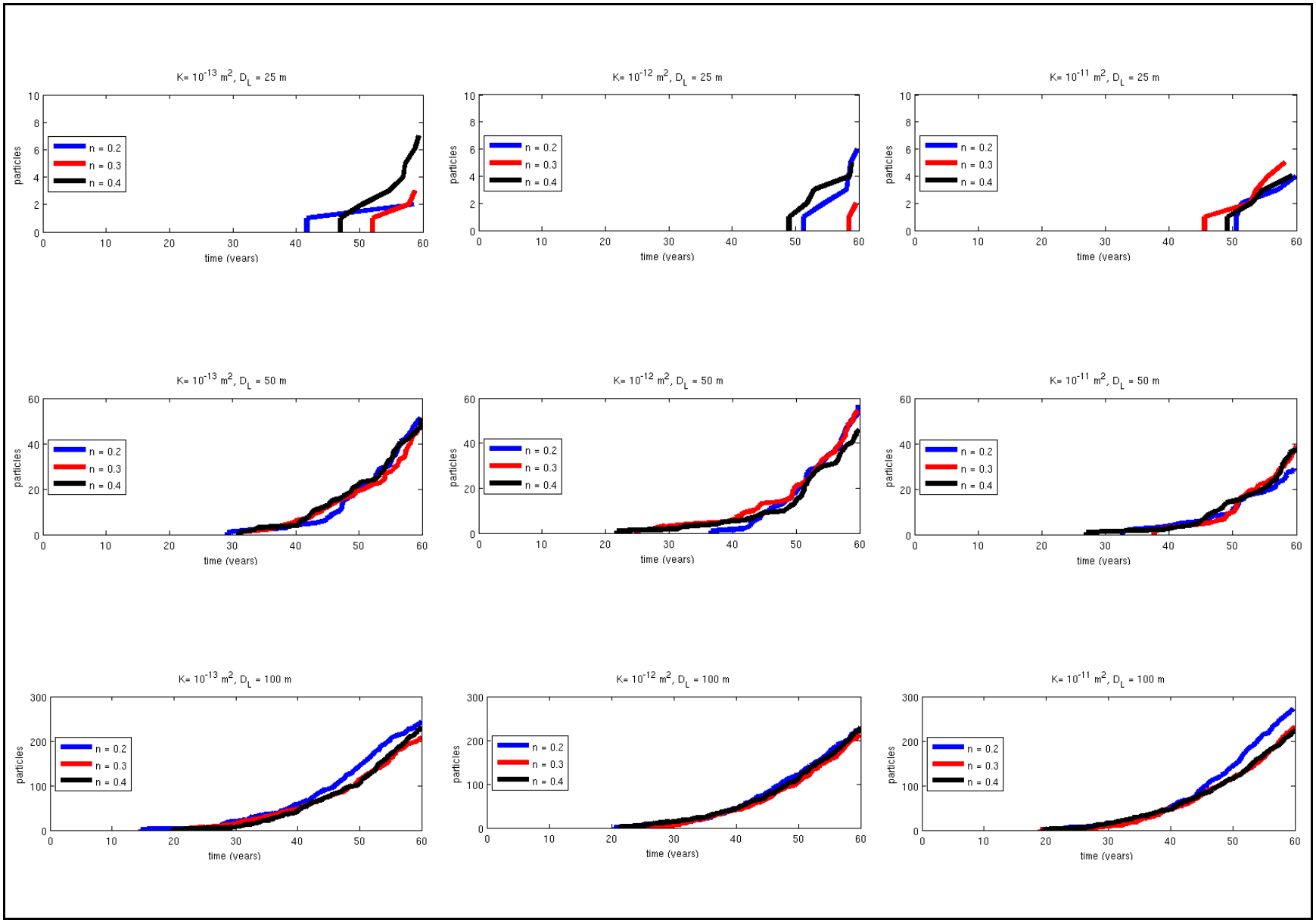

Figure B-6
Simulated Particle Breakthrough Curves at the Pumping Well (WW-A) as a Function of Elapsed Time since the HAYMAKER Detonation (June 27, 1962)
Note: Figures show a range of dispersivity values.

In conclusion, observed ^{3}H breakthrough at WW-A within the first 30 years after the HAYMAKER detonation could not be replicated with reasonable values of porosity and permeability in the absence of dispersion. While porosity and permeability do influence particle transport, with higher permeability and lower porosity resulting in more particles arriving at WW-A within the 60-year simulation time, the fact that different permeability and porosity values result in nearly identical breakthrough for a given dispersivity indicates the breakthrough curves are dominated by the chosen dispersivity values (Figure B-6).

B.1.3 WW-3

WW-3 was completed in alluvium on March 5, 1952, to a depth of 1,800 ft. It was pumped for about 18 years between 1952 and 1970 (Figure B-7) with an estimated total withdrawal of about 200 Mgal. WW-3 has three openings with the uppermost opening at 1,209.0 ft below ground surface (bgs) (841 m amsl), and the lowermost opening at 1,800 ft bgs (661 m amsl). Water-level measurements at WW-3 span more than 60 years (Figure B-8). Water-level records from WW-3 have lengthy periods with relatively sparse data.

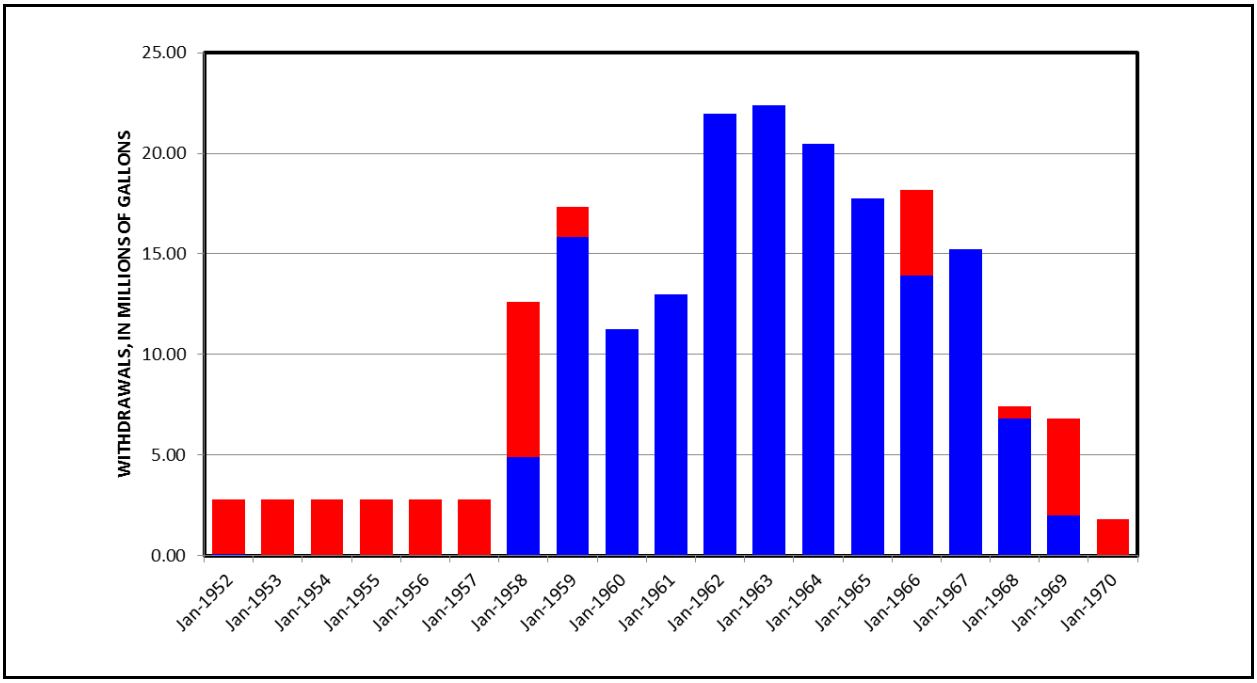

Figure B-7
Annual Water Withdrawals from WW-3 between 1952 and 1970
(from Elliott and Moreo, 2011)
Note: Blue are measured values; red are estimated values.

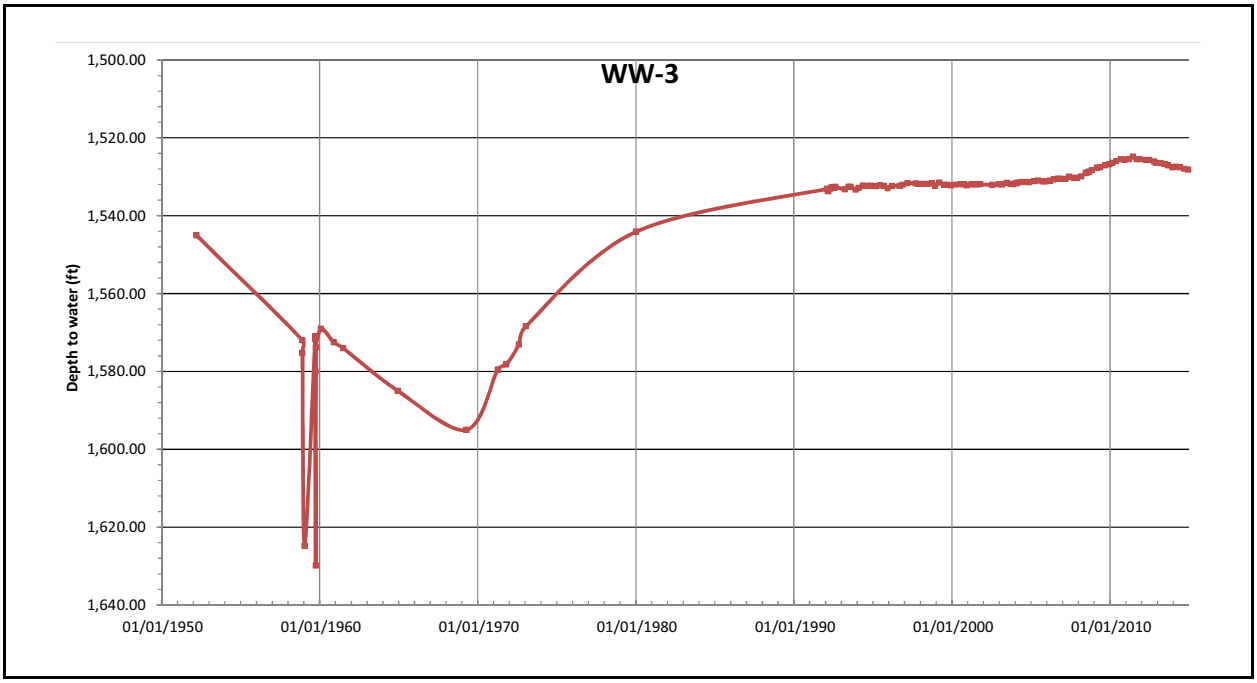

Figure B-8
Water-Level Changes at WW-3

B.1.3.1 WW-3 Pumping History and Water Levels

The water-level changes for WW-3 are described on the USGS website (USGS and DOE, 2016) as follows:

> *Well WW-3 (1800 ft) represents hole WW-3 when drilling had reached a total depth of 1,800 ft and after the well was completed for water supply. The well is open to about 155 ft of tuff overlying 80 ft of sandstone and 35 ft of conglomerate, which is assumed to be colluvial valley fill. The well was used for water supply from 1952 to 1970, with a total of about 203 Mgal withdrawn. Water levels show a declining trend through 1969 followed by a rising trend. These trends agree with the pumping history of the well. From 1997-2003, water levels are consistent and appear to have recovered from pumping; these levels are flagged as representative of steady-state conditions in the alluvial aquifer. Water levels show a rising trend of about 6 ft from 2004 through mid-2011. This rise, which is especially pronounced beginning in 2008, may be caused by seepage from a surface-water pond adjacent to WW-3. The pond had water in it from at least 2002 (and possibly much earlier) to April 2010 when it dried up; water was piped into the pond from WW-C-1 and was used to fill water trucks. Well UE-6d, about 0.7 miles south*

of WW-3, shows a similar overall water-level pattern to that in WW-3 (1800 ft); however, since 2004, the water-level rise in UE-6d of about 0.6 ft is much more subdued. This may indicate that seepage from the pond created a water-level mound centering on WW-3, and that this localized mound has little or no effect on water levels in nearby wells. Three nuclear tests, one near or below the water table, were detonated within 1 mi of WW-3 (1800 ft). The closest test near or below the water table was 4,700 ft away.

B.1.3.2 WW-3 Pond

WW-3 is located at UTM NAD 27 Easting (m) of 583827.5 and a Northing (m) 4094554.7. The center of the pond referred to on the USGS website (USGS and DOE, 2016) is at an Easting of 583847 and a Northing of 4094586, or approximately 37 m away. Based on a Geographic Information Systems analysis (N-I GIS, 2016), the elliptical basin is about 32.8 m by 15.3 m, for an area of about 394 m^2 (Figure B-9). A circular pond with an equivalent area ($A = \pi r^2$) would have a radius of 11.2 m. The depth of the pond based on the high-water mark is estimated to be a few meters.

Figure B-9
Elliptical Pond Near WW-3 That Was Used for Water Supply
Source: N-I GIS, 2016

B.1.3.3 ^3H Measurements at WW-3

Low levels of ^3H were measured at WW-3 in 2014 and 2015, but ^3H was not detected during previous sampling, a single sampling event on April 11, 1972 (Table B-2). The closest test near or below the water table was DUORO (June 20, 1984), with a maximum announced yield of 150 kt (NNSA/NFO, 2015). DUORO has an estimated R_c of 69 m and a 2 R_c exchange volume that extends about 45 m below the water table. (Cavity dimension based on maximum announced yield [NNSA/NFO, 2015] and Equation 1 in Pawloski [1999].) The DUORO working point is a lateral distance of 1,444 m from WW-3.

Table B-2
^3H Measurements at WW-3

Sample Date	Result	DL	Error
	(pCi/L)		
04/11/1972	ND	--	--
06/03/2014	7.28	1.97	2.56
06/09/2015	5.63	2.03	2.16
06/09/2015	6.27	2.25	2.4

-- = Not available

Given that the nearest test likely to have intersected the water table was over 1.4 km away, it is more likely that the low (<10 pCi/L) ^3H at WW-3 originated from water that is suspected to have infiltrated from the nearby pond. The water in the pond was piped from WW-C-1 in southern Yucca Flat, which is alleged to have been the site of an aborted cross-hole tracer test involving ^3H as a tracer in the early 1960s (Lyles, 1990). The low-levels of ^3H that have been detected in WW-C-1 groundwater samples (Table B-3) are attributed to that early tracer test rather than to groundwater migration from upgradient nuclear tests. Non-zero ^3H concentrations appear in WW-C-1 groundwater samples as early as 1973 and were reported above the DL as late as the February 15, 1995, and January 26, 2000, samples. So, it appears likely that the low ^3H concentration measured at WW-3 are associated with the infiltration of tritiated WW-C-1 groundwater at the nearby pond. However, ^3H was measured well above the DLs at UE-6d during both the January 1, 1994, and January 1, 1995, sampling events (Table B-4). These samples likely pre-date the operation of the WW-3 pond, but the history of the pond is not documented. Moreover, the measured ^3H concentration at WW-C-1 on April 6, 1992, was only half as high as measured at UE-6d in 1994 and 1995, and in any case, UE-6d is more than 1 km

Table B-3
^{3}H Measurements at WW-C-1
(Page 1 of 5)

Sample Date	Result	DL	Error
	(pCi/L)		
12/08/1966	<2,230	--	--
01/19/1973	96	--	12
07/02/1973	100	--	7.7
01/07/1974	38	--	7.0
07/10/1974	16	--	9.6
01/14/1975	70	--	9.3
07/07/1975	51	--	11
01/07/1976	45	--	7.7
07/11/1976	32	--	7.3
01/04/1977	22	--	8.9
06/12/1977	20	--	7.3
02/01/1978	23.6	--	8.8
07/18/1978	9.96	--	16.1
02/21/1979	14.2	--	5.76
02/06/1980	130	--	7.36
07/07/1980	3.17	--	9.28
01/20/1981	10.9	--	3.84
07/20/1981	10.1	--	3.92
01/20/1982	13.8	--	4.3
07/13/1982	6.6	--	7.43
01/19/1983	135	--	5.86
07/07/1983	13.9	--	5.09
09/27/1983	32.5	--	--
01/10/1984	10.7	--	10.8
07/16/1984	10.8	--	5.14
08/06/1984	14.6	--	4.26
02/04/1985	74.4	--	271
07/10/1985	0.252	--	10.2
02/04/1986	-148	--	283
07/02/1986	6.27	--	11.6
02/04/1987	73	--	326
07/07/1987	4.28	--	13.1
01/18/1989	<900	900	--

Table B-3
^{3}H Measurements at WW-C-1
(Page 2 of 5)

Sample Date	Result	DL	Error
	(pCi/L)		
02/15/1989	<900	900	--
03/17/1989	<900	900	--
04/11/1989	<900	900	--
05/17/1989	<900	900	--
06/20/1989	<900	900	--
07/11/1989	<900	900	--
08/09/1989	<900	900	--
09/11/1989	<900	900	--
10/16/1989	<900	900	--
11/06/1989	<900	900	--
12/12/1989	<900	900	--
02/07/1990	<900	900	--
03/05/1990	<900	900	--
05/16/1990	<900	900	--
06/07/1990	<900	900	--
07/10/1990	<900	900	--
08/16/1990	<900	900	--
09/10/1990	<900	900	--
10/04/1990	<900	900	--
11/21/1990	<900	900	--
12/10/1990	<900	900	--
01/07/1991	<500	500	--
02/08/1991	<500	500	--
03/11/1991	<500	500	--
04/11/1991	<500	500	--
05/09/1991	<500	500	--
06/04/1991	<500	500	--
07/11/1991	<500	500	--
08/07/1991	<500	500	--
09/07/1991	<500	500	--
10/08/1991	<500	500	--
11/13/1991	<500	500	--
12/09/1991	<500	500	--

Table B-3
^{3}H Measurements at WW-C-1
(Page 3 of 5)

Sample Date	Result	DL	Error
	(pCi/L)		
01/27/1992	<886	886	--
01/27/1992	<300	300	--
02/24/1992	<886	886	--
02/24/1992	<886	886	--
02/24/1992	<300	300	--
02/24/1992	<300	300	--
04/06/1992	<886	886	--
04/06/1992	<886	886	--
04/06/1992	320	300	260
04/06/1992	<300	300	--
05/12/1992	<886	886	--
05/12/1992	<300	300	--
06/02/1992	<886	886	--
06/02/1992	<300	300	--
07/13/1992	<886	886	--
07/13/1992	<886	886	--
07/13/1992	<300	300	--
07/13/1992	<300	300	--
08/04/1992	<886	886	--
08/04/1992	<300	300	--
09/01/1992	<886	886	--
09/01/1992	<300	300	--
10/05/1992	<886	886	--
10/05/1992	<300	300	--
10/05/1992	<300	300	--
11/09/1992	<886	886	--
11/09/1992	<300	300	--
12/02/1992	<886	886	--
12/02/1992	<300	300	--
02/04/1993	<500	500	--
03/10/1993	<500	500	--
04/04/1993	<500	500	--
07/12/1993	<500	500	--

Table B-3
^{3}H Measurements at WW-C-1
(Page 4 of 5)

Sample Date	Result	DL	Error
	(pCi/L)		
11/24/1993	<500	500	--
01/01/1994	12	12	--
01/01/1994	22	5.6	20
02/08/1994	<754	754	--
05/11/1994	<754	754	--
07/06/1994	<754	754	--
10/05/1994	<754	754	--
01/01/1995	<5.1	5.1	--
01/01/1995	17	16	--
02/15/1995	52	14.5	10.1
04/11/1995	<15.4	15.4	--
07/20/1995	<14.5	14.5	--
10/12/1995	<19	19	--
01/17/1996	<15	15	--
05/09/1996	<11	11	--
07/15/1996	<14	14	--
10/07/1996	<12	12	--
01/29/1997	<17.9	17.9	--
04/16/1997	<20	20	--
04/16/1997	<23.6	23.6	--
07/10/1997	<19.8	19.8	--
10/01/1997	<18.2	18.2	--
07/09/1998	<23.1	23.1	--
10/15/1998	<22.3	22.3	--
01/20/1999	<26.9	26.9	--
04/19/1999	<24.6	24.6	--
01/26/2000	27.4	9.94	6.33
07/19/2000	<10.9	10.9	--
10/25/2000	15.5	13.9	8.4
02/06/2001	<32.2	32.2	--
04/03/2001	<9.8	9.8	--
07/31/2001	<9.9	9.9	--
10/30/2001	<17.7	17.7	--

Table B-3
^{3}H Measurements at WW-C-1
(Page 5 of 5)

Sample Date	Result	DL	Error
	(pCi/L)		
07/20/2004	<21.3	21.3	--
10/12/2004	<17.9	17.9	--
01/18/2005	<20.2	20.2	--
04/12/2005	<25.9	25.9	--
07/12/2005	<23.6	23.6	--
10/04/2006	<11.6	11.6	--
01/23/2007	<27.8	27.8	--
04/10/2007	<22.6	22.6	--
07/17/2007	<22.5	22.5	--
10/16/2007	<18.2	18.2	--
01/16/2008	<23.3	23.3	--
04/29/2008	<21.0	21.0	--
07/15/2008	<20.6	20.6	--
10/21/2008	<23.8	23.8	--
01/27/2009	<27.5	27.5	--
06/09/2009	<27.4	27.4	--
10/27/2009	<19.8	19.8	--
01/19/2010	<27.9	27.9	--
05/11/2010	<24.7	24.7	--
07/14/2010	<28.8	28.8	--
10/19/2010	<27.3	27.3	--
01/11/2011	<28.4	28.4	--
01/11/2011	<28.5	28.5	--
04/26/2011	<20.2	20.2	--
07/19/2011	<24.8	24.8	--
10/18/2011	<28.2	28.2	--
01/18/2012	<23.1	23.1	--
01/18/2012	<23.3	23.3	--
04/17/2012	<27.1	27.1	--
04/17/2012	<25.4	25.4	--
07/17/2012	<20.1	20.1	--

-- = Not available

from WW-3. Therefore, it is very unlikely the ^3H measured at UE-6d in 1994 and 1995 originated from the WW-3 pond, even if the later water-level rises in the 2010 time frame can be associated with the pond, as suggested on the USGS website (USGS and DOE, 2016).

B.1.3.4 WW-3 Pond Model

To investigate whether the observed water-level rises and low levels of ^3H measured at WW-3 in the 2000s can be explained by infiltration of tritiated WW-C-1 water in the nearby pond, a radially symmetric, variably saturated model of the pond setting was created with the Los Alamos National Laboratory (LANL) code FEHM (Figure B-10). The model extends from land surface (1,210 m) to the water table (740 m) and from the center of the pond to a radial distance of 2 km. GRIDDER, a LANL-developed software package, was used to generate the mesh. The mesh coarsens outward with a radial spacing of about 2 m along the center to 20 m along the outward radial boundary. Vertical spacing is 5 m throughout the model domain, resulting in a grid with 38,095 nodes and 37,600 elements.

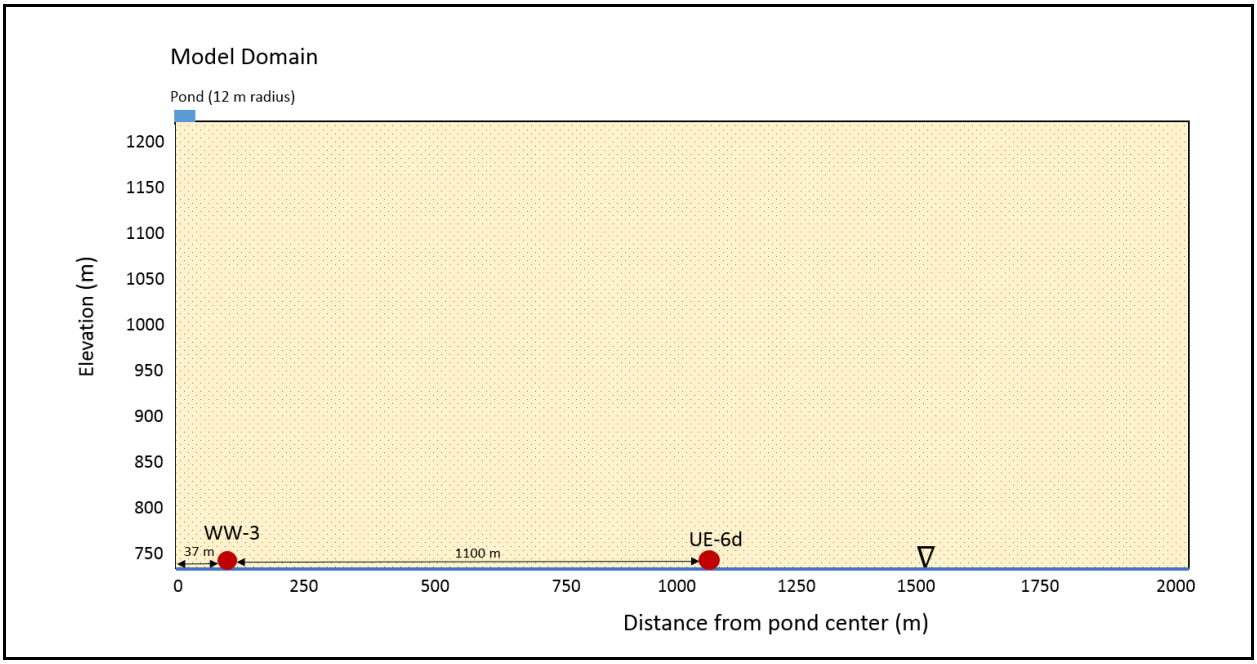

Figure B-10
Schematic of the Model Domain Showing Locations of Interest WW-3 and UE-6d

Although the well screen is open to tuff and sandstone, most of the unsaturated zone is alluvium. Alluvial properties were estimated from two sources: (1) the Area 3 low-level radioactive waste site investigation (BN, 1998) and (2) parameter estimation determined from hydrologic responses at

WW-3 and UE-6d due to groundwater pumping at WW-3. From these two sources, two permeability (K) values were chosen to represent the alluvium $K = 1.0 \times 10^{-12}$ m^2 and 5.0×10^{-13} m^2. The alluvium properties were assumed to be isotropic. The two values of permeability were used to determine whether the infiltration of tritiated pond water might explain the water table rise and low levels of ^{3}H at WW-3 in the 2002 to 2010 time frame.

Initial saturation and pressures in the alluvium before the pond was filled were determined by running the model to steady-state with a background flux of 1 mm/yr. A subsequent, 12-year transient simulation, beginning on January 1, 2002, included a ponded boundary condition along the top of the model of 3.0 m head of water (0.0294 megapascal [MPa] gage pressure or 0.1294 MPa absolute pressure assuming 0.1 MPa air pressure) out to a radius of 12 m. The additional head from the pond was imposed for a duration of eight years, between 2002 and 2010. The infiltrating water contained ^{3}H with an estimated input concentration of 20 pCi/L (9.17×10^{-13} moles ^{3}H/kg H_2O). Radioactive decay of ^{3}H (half-life $t_{1/2}$ = 12.3 years) was accounted for in the simulations.

B.1.3.5 WW-3 Pond Model Results

Overall, the results indicate that ponded water at the surface can explain the increase in water-table elevation and elevated ^{3}H measured at WW-3 for both scenarios tested. The two scenarios are identical with the exception of the alluvium permeability; permeability is assigned a value of $K_1 = 1.0 \times 10^{-12}$ m^2 for scenario 1 and $K_2 = 5.0 \times 10^{-13}$ m^2 for scenario 2. The resulting water pressures for the two cases are shown in Figure B-11 and discussed below. The model results show that alluvium permeability does affect the speed of the wetting front, and thus the ^{3}H-breakthrough time at the water table and WW-3. This is probably because twice as much water infiltrates in scenario 1 as in scenario 2.

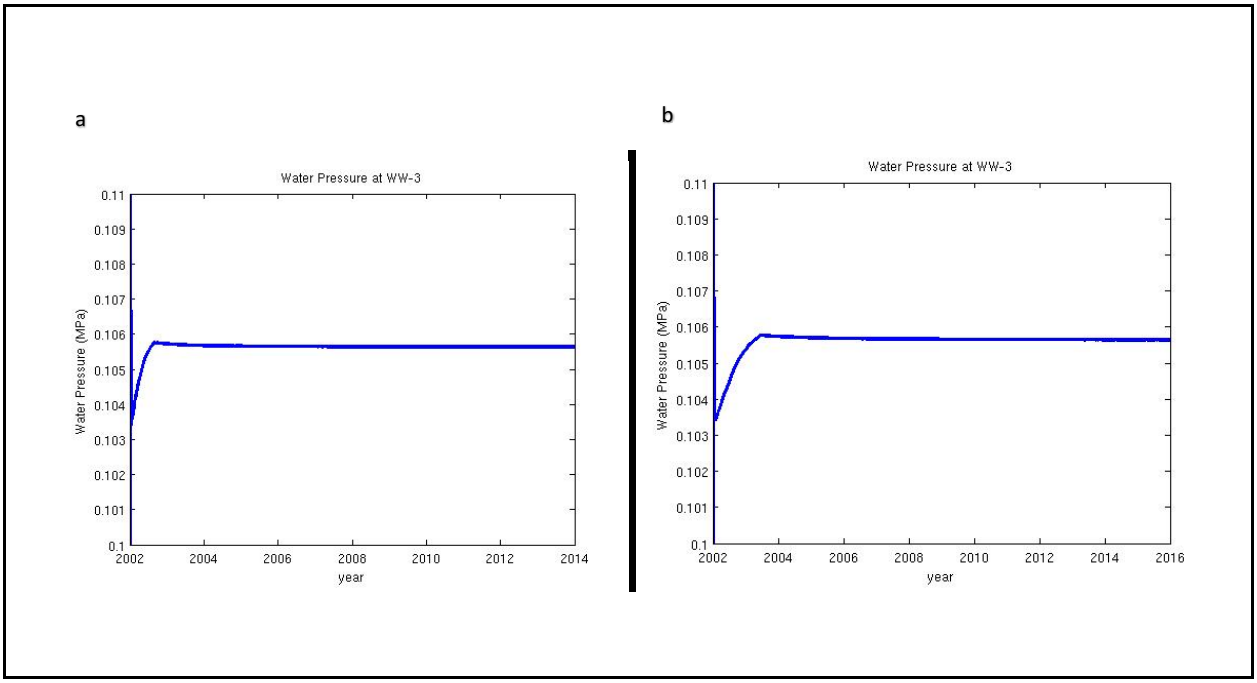

Figure B-11
Model Results of the Water Pressure at WW-3 for Scenarios 1 (a) and 2 (b)

The modeled water pressure change at WW-3 is similar for both simulations, with an overall increase from 0.1 MPa to approximately 0.106 MPa (Figure B-11):

$$\Delta h = \frac{\Delta p}{\rho g} \qquad (B\text{-}2)$$

where

h = head (m)

P = pressure (Pa)

ρ = density of water (1,000 $\frac{\text{kg}}{\text{m}^3}$)

g = acceleration due to gravity (9.81 $\frac{\text{m}}{\text{s}^2}$)

This corresponds to a groundwater head change, or a water-table elevation increase of about 0.6 m. A lower permeability does result in a slower migration of the wetting front and thus a slower rate of change of the water pressure at WW-3. A steady water pressure value is reached in less than one year for scenario 1 to about two years for the lower-permeability, scenario 2. WW-3 had a measured increase in water-table elevation of about 2 m (Elliott and Fenelon, 2011), which is underpredicted by the model but is on a similar order of magnitude.

The effect of alluvium permeability on the rate of water pressure increase is illustrated in Figure B-12 showing the saturated region below the pond. The alluvium is quick to saturate during scenario 1 (Figure B-12a); pond-water reaches the water table within the first year of ponding. In contrast, Figure B-12b shows slower infiltration for the lower permeability alluvium represented in scenario 2.

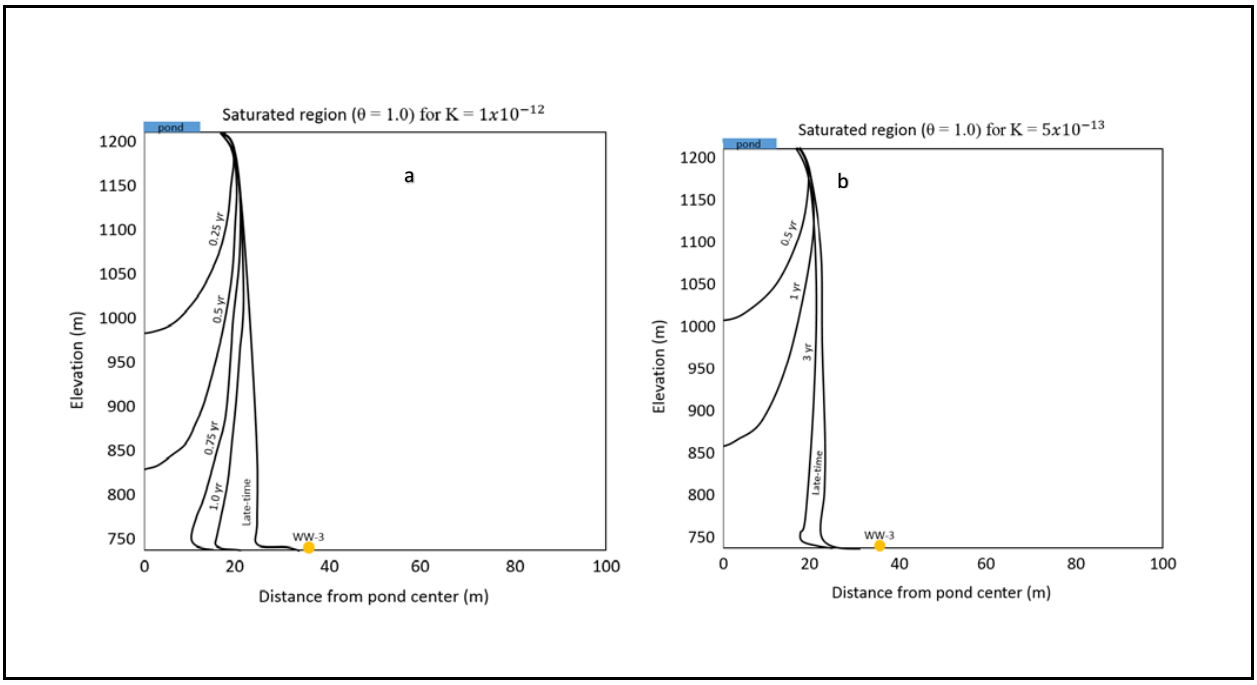

Figure B-12
Simulated Migration of the Wetting Front (θ = 1) for Scenarios 1 (a) and 2 (b)

The simulation results for both permeability scenarios bracket the observed ^3H concentrations at WW-3, indicating that it is possible that relatively recent infiltration and recharge of WW-C-1 groundwater with low ^3H concentration from the WW-3 pond is responsible for the ^3H in the groundwater at WW-3. The difference between ^3H concentration for scenarios 1 and 2 is the result of lower rates of infiltration in scenario 2 (Figure B-13). A model scenario with an alluvium permeability between 1.0×10^{-12} m^2 and 5.0×10^{-13} m^2 would likely pass through the ^3H data, although it would probably still underpredict the observed 2-m water table rise at WW-3, which may be due in part to other causes besides pond infiltration.

No change to the ^3H concentration or the water pressure at UE-6d was observed in the simulations. Due to the distance of UE-6d from the pond, this result is not surprising.

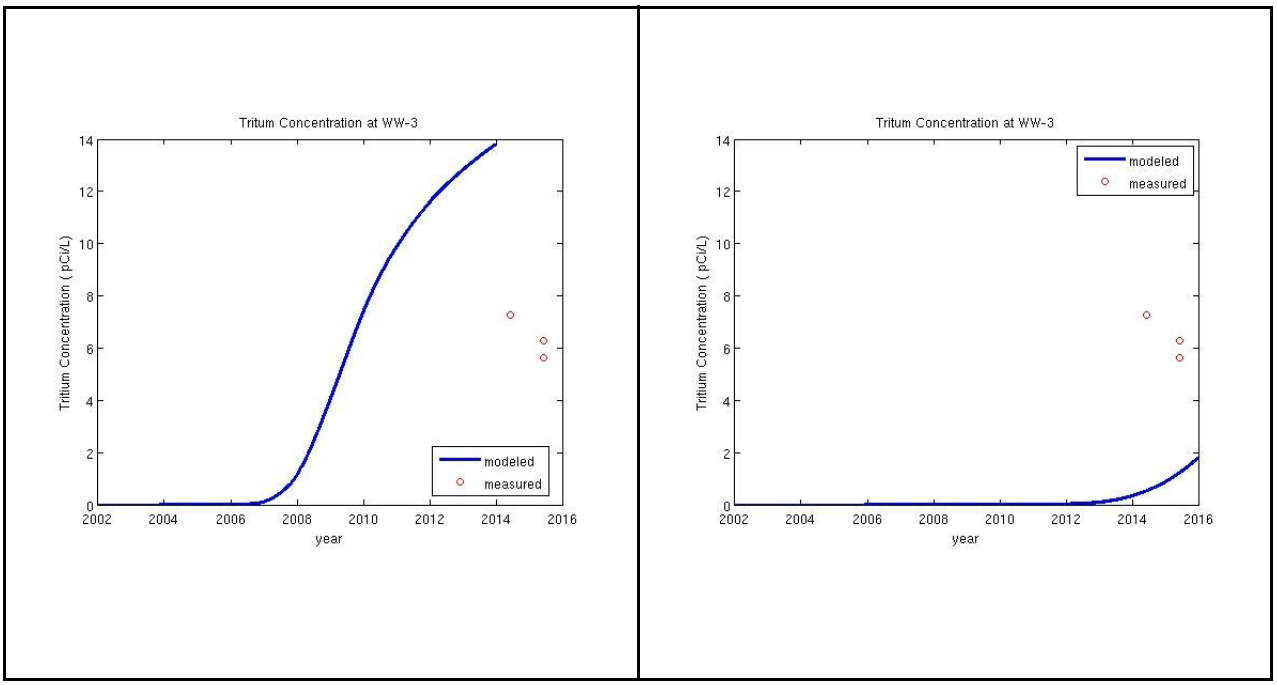

Figure B-13
Simulated Migration of ^3H to WW-3 for Scenario 1 (left) and Scenario 2 (right)

B.1.4 UE-6d

Additional water-level measurements spanning more than 45 years are also available from nearby UE-6d (Figure B-14) located about 1.1 km south of WW-3. This well was completed on May 7, 1968, to a depth of 3,896 ft with three open sections extending from 2,125.0 to 3,896.0 ft bgs (555.3 to 15.5 m amsl). UE-6d well is open between depths of 2,125 ft and 3,896 ft to conglomeratic alluvium overlying 90 ft of bedded and ash-fall tuff. Water-level records from UE-6d have lengthy periods with relatively sparse data.

The water-level changes for UE-6d are described on the USGS website (USGS and DOE, 2016) as follows:

> *The saturated part of Well UE-6d is open to about 1,500 ft of conglomeratic alluvium overlying 90 ft of bedded and ash-fall tuff. The first water-level measurement was made 1 day after the drill rig was used to clean out the well and 4 days after the total depth of the borehole was reached with the drill rig. The well is 0.7 mi south of WW-3, which ceased pumping in 1970. The rising trend in water levels in UE-6d through present (2014) is attributed primarily to equilibration following the cessation of pumping in*

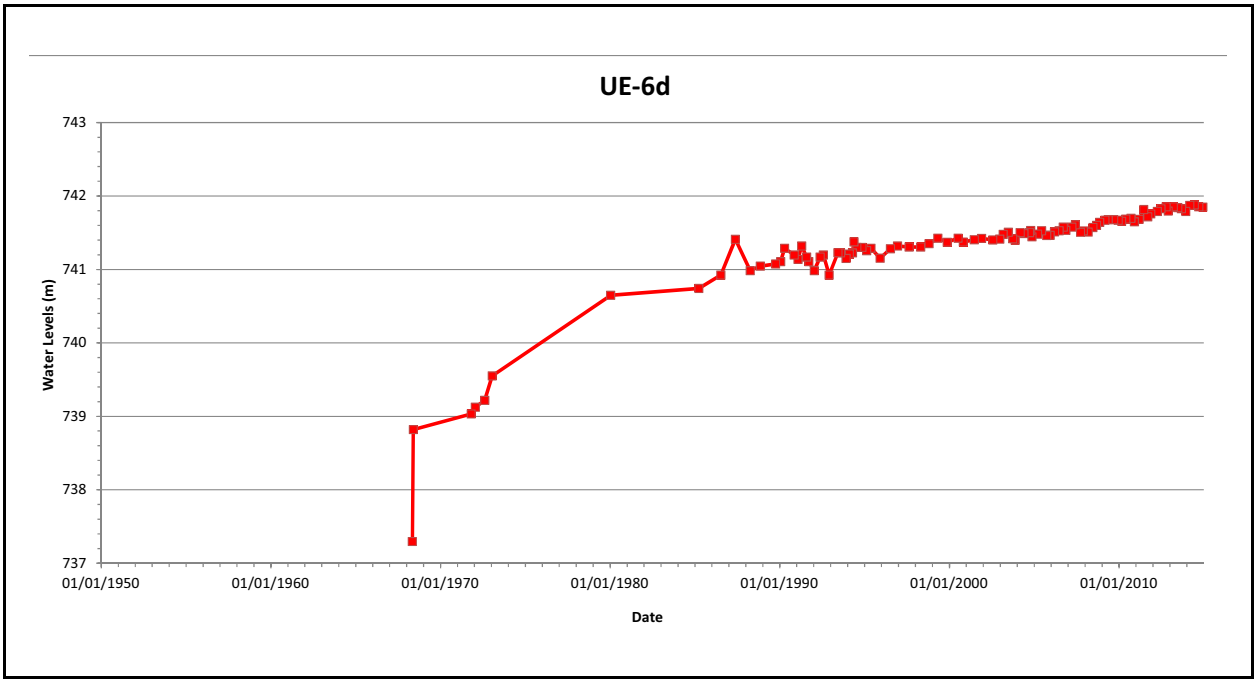

Figure B-14
Water-Level Changes at Well UE-6d

WW-3. Therefore, these rising water levels in UE-6d are flagged as representative of transient conditions in the alluvial aquifer. In general, the water-level trend in Well UE-6d is similar to the trend in well WW-3. However, water levels continue to slowly rise in UE-6d, whereas water levels in WW-3 appear to have equilibrated in 1997 from past pumping. Well UE-6d is interpreted to be open to alluvial and volcanic confining units, which might explain the slower recovery from past pumping. Since 2004, water levels rose about 1.0 ft in UE-6d, whereas water levels in WW-3 rose almost 7 ft through 2011, then began declining. The rise and subsequent decline in water levels in WW-3 is attributed to a water-level mound centered on WW-3 that was created by infiltration from a nearby pond. Although unlikely, the small rise in UE-6d also might be caused by infiltration from the pond, but could be less pronounced than in WW-3 because UE-6d is farther away from the source of the mound. No nuclear tests were detonated within 1 mi of UE-6d.

Groundwater samples from UE-6d on January 1, 1994, and January 1, 1995, had ^{3}H concentrations of 710 and 670 pCi/L (Table B-4), although these analyses are considered suspect. However, UE-6d groundwater was not analyzed again for ^{3}H until mid-2015, when ^{3}H for the May 18, 2015, sample was below detection (<2.44 pCi/L).

Table B-4
^{3}H Measurements at UE-6d

Sample Date	Result	DL	Error
	(pCi/L)		
01/01/1994	710	297	NA
01/01/1995	670	6.1	22
05/18/2015	<279	279	--
05/18/2015	<2.44	2.44	--
05/19/2015	<280	280	--
05/19/2015	<2.22	2.22	--

-- = Not applicable

NA = Not available

The nearest nuclear detonation to UE-6d is RUSSET, which was detonated in emplacement hole U6A in alluvium at a depth of 119.8 m on March 5, 1968. The RUSSET detonation had a maximum announced yield of 20 kt (NNSA/NFO, 2015) with an estimated radius based on maximum announced yield of 47 m. UE-6d lies roughly on a line between RUSSET and WW-3 (Figure B-15), so pumping from WW-3 may have induced groundwater to flow from the vicinity of RUSSET past UE-6d toward WW-3. However, the distance of RUSSET from UE-6d (1,675 m), the absence of a crater to focus recharge, and the considerable height of the RUSSET working point above the water table (339.1 m) make RUSSET an unlikely source of the ^{3}H that was reported for UE-6d in the mid-1990s.

Another potential source of the ^{3}H at UE-6d is the DUORO test, detonated above the water table in the VA (Ammonia Tanks tuff) on June 20, 1984. Although further (2,232 m) from UE-6d than RUSSET (Figure B-15), the 2 R_c exchange volume based on a maximum announced yield of 150 kt for DUORO (NNSA/NFO, 2015; Pawloski, 1999) extends almost 45 m below the water table. Moreover, unlike the RUSSET detonation, which produced no crater, the DUORO test has a large crater (88-m radius) that could capture surface runoff. However, DUORO was not detonated until long after WW-3 had stopped pumping (1970), so it is unlikely that WW-3 would have facilitated transport from DUORO to UE-6d.

In conclusion, none of the nearest detonations are likely to have contributed ^{3}H to UE-6d, and the low-level ^{3}H concentration measured at UE-6d in the mid-1990s remains unexplained. However,

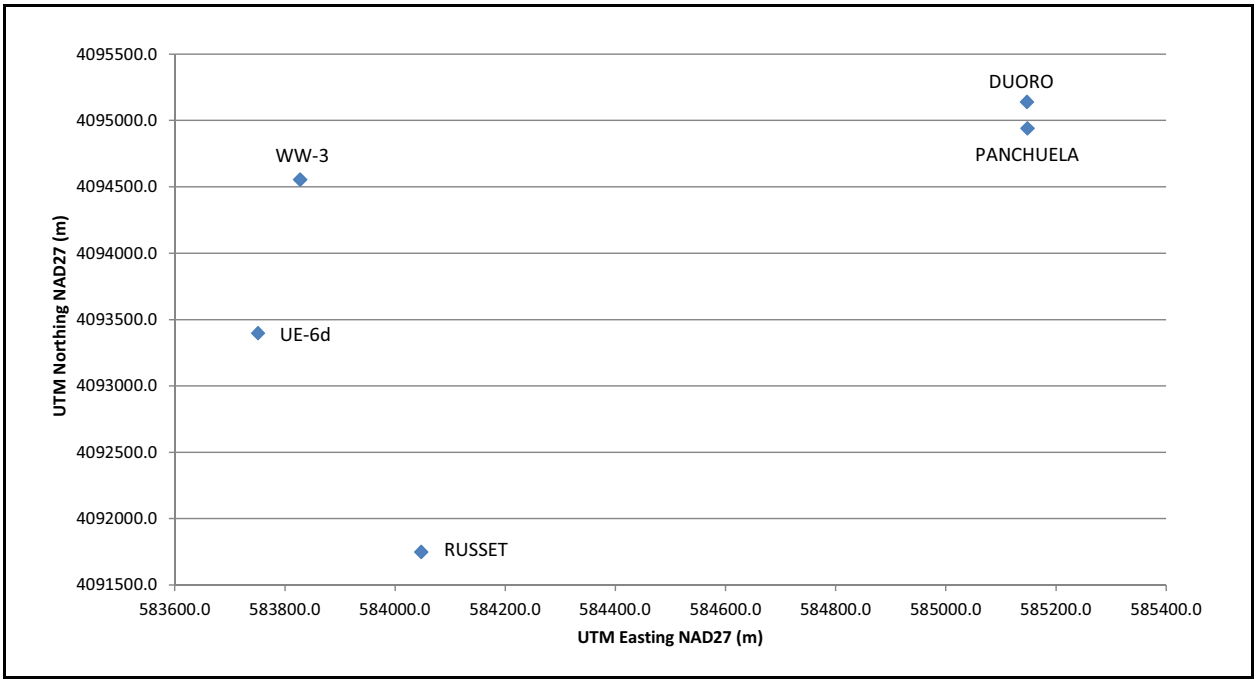

Figure B-15
Location of Nearby Nuclear Detonations to Wells UE-6d and WW-3

although there is no obvious explanation for the ^{3}H detected at UE-6d in 1994 and 1995, subsequent sampling and analysis have indicated that these samples were not a precursor to a contaminant plume of regulatory concern.

B.1.5 UE-6e

UE-6e (2,090 to 2,230 ft) is open to 140 ft of saturated volcanic rocks including the densely welded Topopah Spring aquifer (TSA) (Fenelon, 2005). ^{3}H measurements of groundwater samples taken from UE-6e showed low levels of ^{3}H in samples taken in 1994 and 1995 (Table B-5), although these analyses are considered suspect. Later samples taken in 1999 and 2015 were below their DLs, which were considerably higher than for the 1994 and 1995 samples. The sample collected in 2015 contained a large amount of solid material, and the commercial laboratory could not achieve the low DLs typical for other UGTA samples.

Well UE-6e has seven nuclear tests within 1 km, all of which had maximum announced yields of less than 20 kt and working points in alluvium at least 170 m above the water table. Each of the seven nearby detonations had estimated 2 R_c exchange volumes that were approximately 100 m or more

Table B-5
^{3}H Measurements from UE-6e

Sample Date	Result	DL	Error
	(pCi/L)		
01/01/1994	12.5	4.9	7.8
01/01/1995	16	6.4	4.2
03/31/1999	<55.3	55.3	--
05/19/2015	<281	281	--
05/19/2015	<102.5	102.5	--

-- = Not applicable

above the water table, so there are no obvious nearby sources for the low-levels of ^{3}H detected at UE-6e in 1994 and 1995.

Although there is no obvious explanation for the ^{3}H detected at UE-6e in 1994 and 1995, subsequent sampling and analysis have indicated that these samples were not a precursor to a contaminant plume of regulatory concern.

B.2.0 REFERENCES

BN, see Bechtel Nevada.

Bechtel Nevada. 1998. *Hydrogeologic Characterization of the Unsaturated Zone at the Area 3 Radioactive Waste Management Site*, DOE/NV/11718-210. Prepared for the U.S. Department of Energy, Nevada Operations Office. Las Vegas, NV.

Cooper, H.H., and C.E. Jacob. 1946. "A Generalized Graphical Method for Evaluating Formation Constants and Summarizing Well Field History." In *Eos, Transactions American Geophysical Union,* Vol. 27(4): pp. 526-534.

Doty, G.C., and F.E. Rush. 1985. *Inflow to a Crack in Playa Deposits of Yucca Lake, Nevada Test Site, Nye County, Nevada*, Water-Resources Investigations Report 84-4296. Denver, CO: U.S. Geological Survey.

Drellack, S.L., National Security Technologies, LLC. 2014. Written communication. Email and letter report to E. Kwicklis (LANL). Subject: "Recon trip after storm in YF," 21 August. Las Vegas, NV.

Drellack, S.L., National Security Technologies, LLC. 2015. "Report on the Evaluation of Cracks and Sinkholes near Yucca Lake." Letter report dated 18 March. Las Vegas, NV.

Elliott, P.E., and J.M. Fenelon. 2010. *Database of Groundwater Levels and Hydrograph Descriptions for the Nevada Test Site Area, Nye County, Nevada, 1941-2010,* Data Series 533. Reston, VA: U.S. Geological Survey. (Version 5.0 released in October 2014).

Elliott, P.E., and M.T. Moreo. 2011. *Groundwater Withdrawals and Associated Well Descriptions for the Nevada National Security Site, Nye County, Nevada*, *1951–2008,* Data Series 567. Reston, VA: U.S. Geological Survey.

Fenelon, J.M. 2005. *Analysis of Ground-Water Levels and Associated Trends in Yucca Flat, Nevada Test Site, Nye County, Nevada, 1951–2003*, Scientific Investigations Report 2005-5175. Carson City, NV: U.S. Geological Survey.

Fenelon, J.M., D.S. Sweetkind, P.E. Elliott, and R.J. Laczniak. 2012. *Conceptualization of the Predevelopment Groundwater Flow System and Transient Water-Level Responses in Yucca Flat, Nevada National Security Site, Nevada*, Scientific Investigations Report 2012-5196. Reston, VA: U.S. Geological Survey.

Halford, K., U.S. Geological Survey. 2016. Written communication. Subject: "Hydraulic Analysis of Transmissivity at WW-A and WW-3." Carson City, NV.

Lyles, B.F. 1990. *Tritium Variations in Groundwater on the Nevada Test Site*, DOE/NV/10384-38; Publication No. 45086. Las Vegas, NV: Desert Research Institute, Water Resources Center.

Lyles, B.F. 1993. *Tritium Activities in Selected Wells on the Nevada Test Site,* DOE/NV/10845-20; Publication No. 45104. Las Vegas, NV: Desert Research Institute, Water Resources Center.

N-I, see Navarro-Intera, LLC.

N-I GIS, see Navarro-Intera Geographic Information Systems.

NNSA/NFO, see U.S. Department of Energy, National Nuclear Security Administration Nevada Field Office.

Navarro-Intera Geographic Information Systems. 2016. ESRI ArcGIS Software.

Navarro-Intera, LLC. 2013. *Phase I Flow and Transport Model Document for Corrective Action Unit 97: Yucca Flat/Climax Mine, Nevada National Security Site, Nye County, Nevada*, Rev. 1, N-I/28091-080, Las Vegas, NV.

Pawloski, G.A. 1999. *Development of Phenomenological Models of Underground Nuclear Tests on Pahute Mesa, Nevada Test Site—BENHAM and TYBO*, UCRL-ID-136003. Livermore, CA: Lawrence Livermore National Laboratory.

Rozanski, K., R. Gonfiantini, and L. Araguas-Araguas. 1991. "Tritium in the Global Atmosphere: Distribution Patterns and Recent Trends." In *Journal of Physics G: Nuclear and Particle Physics,* Vol. 17: pp. S523–S536.

SNJV, see Stoller-Navarro Joint Venture.

Stoller-Navarro Joint Venture. 2009. *Unclassified Source Term and Radionuclide Data for Corrective Action Unit 97: Yucca Flat/Climax Mine, Nevada Test Site, Nevada,* Rev. 2, S-N/99205--114. Las Vegas, NV.

USGS and DOE, see U.S. Geological Survey and U.S. Department of Energy.

U.S. Department of Energy, National Nuclear Security Administration Nevada Field Office. 2015. *United States Nuclear Tests, July 1945 through September 1992,* DOE/NV--209-REV 16. Las Vegas, NV.

U.S. Geological Survey and U.S. Department of Energy. 2016. "USGS/U.S. Department of Energy Cooperative Studies in Nevada" web page. As accessed at http://nevada.usgs.gov/doe_nv on 9 March.

DISTRIBUTION

	Copies
W.R. Wilborn Environmental Management Operations U.S. Department of Energy National Nuclear Security Administration Nevada Site Office P.O. Box 98518, M/S 505 Las Vegas, NV 89193-8518	1 hard copy w/electronic media
Ed Kwicklis Los Alamos National Laboratory Hydrology, Geochemistry, and Geology Group, EES-6 Earth and Environmental Sciences Division SM-30 Bikini Atoll Rd., MS T003 Los Alamos, NM 87545	UGTA website
Elizabeth Keating Los Alamos National Laboratory Hydrology, Geochemistry, and Geology Group, EES-6 Earth and Environmental Sciences Division SM-30 Bikini Atoll Rd., MS T003 Los Alamos, NM 87545	UGTA website
Chris Andres State of Nevada Nevada Division of Environmental Protection 2030 E. Flamingo Road, Suite 230 Las Vegas, NV 89119-0818	1 hard copy w/electronic media
Joe Fenelon U.S. Geological Survey Water Resources Division 160 North Stephanie Street Henderson, NV 89074	UGTA website
Chuck Russell Desert Research Institute 755 E. Flamingo Las Vegas, NV 89119	UGTA website

	Copies
Ken Rehfeldt Navarro P.O. Box 98952, NSF 167 Las Vegas, NV 89193-8518	UGTA website
Sharad Kelkar Navarro P.O. Box 98952, NSF 167 Las Vegas, NV 89193-8518	UGTA website
Irene Farnham Navarro P.O. Box 98952, NSF 167 Las Vegas, NV 89193-8518	UGTA website
Pete Martian Navarro P.O. Box 98952, NSF 167 Las Vegas, NV 89193-8518	UGTA website
Jeff Wurtz Navarro P.O. Box 98952, NSF 167 Las Vegas, NV 89193-8518	UGTA website
Brian Haight Navarro P.O. Box 98952, NSF 167 Las Vegas, NV 89193-8518	UGTA website
Environmental Management Records U.S. Department of Energy National Nuclear Security Administration Nevada Field Office P.O. Box 98518, M/S 505 Las Vegas, NV 89193-8518	1 hard copy
Navarro Central Files P.O. Box 98952, NSF 156 Las Vegas, NV 89193-8518	1 hard copy